Institut für Theorie der Kondensierten Materie

Karlsruhe Institute of Technology

On the Majorana Representation for Spin 1/2

Zur Erlangung des akademischen Grades eines

DOKTORS DER NATURWISSENSCHAFTEN

von der Fakultät für Physik

am Karlsruher Institut für Technologie (KIT)

genehmigte

DISSERTATION

von

Dipl.-Phys. Pablo Schad

aus Bruchsal

Tag der mündlichen Prüfung: 22.04.2016

Referent: Prof. Dr. Alexander Shnirman

Korreferent: Priv.-Doz. Dr. Boris N. Narozhny

To my parents

Contents

1. Introduction

Many theses have been written, and this is one of them.

Spin physics lies at the heart of a wide range of topics of current condensed matter research. One of the rather prominent topics of this sort is the current quest for the quantum computer. Spin models play an important role in a range of different aspects in this research field. The basic building blocks of a quantum computer are so-called qubits, which can be realized using superconducting quantum interference devices (SQUIDs). The state of such a qubit is the quantum analogon to the state of a bit in a classical computer. One of the major obstacles on the route to the quantum computer is the problem of decoherence of the state of the qubit, i.e., the decay of the quantum properties of the state. To improve the understanding of decoherence effects, one studies dissipative spin models, which describe the dynamics of the qubit (Ref. [1]). In this case, the spin represents the qubit and the model couples the qubit to environmental degrees of freedom, which are generically described by bosonic environments. Beyond quantum computation, such scenarios are of paramount importance on a more fundamental level, namely, in the field of quantum foundations and the "quantum-to-classical" transition (Ref. [2]).

In recent years, the condensed matter community has seen huge advances in the area of electronic devices working at low temperatures (~ 1 K), for instance, superconducting devices. Like any other electronic devices, these devices are prone to noise. However, at low temperatures the standard sources of noise are different from noise at higher temperatures. At high temperatures noise is generally dominated by delocalized degrees of freedom, e.g. thermal motion of electrons or lattice vibrations (phonons). At low temperatures, noise is mostly generated by localized degrees of freedom (Ref. [2]). This can be, for example, two-level systems in the crystalline structure of a material in which an atom oscillates between two spatial locations. Another example are fluctuating magnetic moments of the spins of localized unpaired electrons. In order to understand the fluctuation dynamics both of these noise sources are described by spin models. If the noise sources fluctuate independently it is appropriate to use dissipative local spin models. If, on the other hand, interactions between the noise sources are relevant one rather has to use spin models that include spin-spin interactions. However, the detailed microscopic behavior of noise sources, e.g., whether interactions are relevant or not, is often difficult to find out, because these systems are mostly measured indirectly via fluctuations in the parameters of the devices. The standard way to characterize noise sources are noise measurement techniques. The outcomes of noise measurements are then related to correlation functions (or correlators)

1

of the noise sources.

Let us address one more area within condensed matter physics where spin physics are important. Namely, if properties of materials are governed by spin degrees of freedom, spin models play the role of effective theories. This can be the case in cuprates and heavy-fermion compounds Another example are quantum Heisenberg spin glasses, which can be described by an effectively local spin model on the mean-field level. In these cases, the spin models are often used to understand the low-energy properties of the systems (Ref. [3]).

Progress in our understanding of nature relies heavily on the interplay of experimental evidence with predictions from microscopic theories. Given a theoretical model, the derivation of reliable predictions for experimentally accessible quantities can be a challenging task. Many powerful methods that achieved vital progress in this direction have been developed. The possibly most important ones are the efficient tools of quantum field theory. Namely, these are the powerful Green's functions methods based on Wick's theorem, including diagrammatic perturbation theory. Unfortunately, these methods cannot be applied directly to the above-mentioned spin models. The reason for that are the complicated Lie-algebraic commutation relations of spin operators ($\alpha, \beta, \gamma = \{x, y, z\}$)

$$\left[\hat{S}_\alpha, \hat{S}_\beta\right] = i\hbar\epsilon_{\alpha\beta\gamma}\hat{S}_\gamma \ . \tag{1.1}$$

Due to these Lie-algebraic relations spin operators, unlike bosons and fermions, do not satisfy a Wick's theorem. In order to benefit from Green's functions methods, additional procedures have to be employed.

Many procedures that allow for the application of Green's functions methods to spin problems have been developed. Most of these techniques use bilinear combinations of auxiliary bosonic and fermionic operators to represent the spin, which then satisfy the conventional Wick's theorem and thus enable for Green's functions methods. One such technique is the Majorana representation for spin 1/2, which is the central topic of this thesis. Other, more widely used techniques include for example the Abrikosov-pseudofermion representation, the Holstein-Primakoff transformation, the Schwinger-boson representation as well as slave-fermion techniques. These techniques are essentially either limited to special cases or suffer from the following two types of complications. First, the auxiliary-particle Hilbert space is enlarged as compared to the original spin Hilbert space, mostly by unphysical states. In order to prevent that unphysical states affect physical quantities one has to introduce projection techniques. The need of projection techniques adds another technical step to the overall calculation and, besides that, projection techniques can suffer from additional limitations (Ref. [4]). The second complication is a rather natural consequence of the bilinear representations. Namely, any average of a number N of spin operators translates to an average of $2N$ auxiliary operators. This is annoying, since calculations generally become increasingly complicated with increasing numbers of operators. In perturbative calculations, this issue is related to outer spin vertices, thus it has been termed the "vertex problem" (Ref. [5]).

Do the above complications hamper the application of the Majorana representation? First, though the Majorana representation does enlarge the spin's Hilbert space, it is believed that it does not suffer from unphysical states. However, the Majorana representation has not been used very often, which points to a lack of trust in this respect. Therefore, we think that there is a need for clarification. Second, if applied in a straightforward fashion, the Majorana

representation indeed also suffers from the "vertex problem". However, rather recently a group of authors (Refs. [5, 6]) discovered identities between spin and Majorana correlation functions based on a particular property of the representation. These simplified relations establish correspondences between e.g. two-point spin correlation functions and two-point rather than four-point Majorana correlation functions, thus essentially avoiding the "vertex problem". This trick makes the Majorana representation a particularly promising candidate to enable the use of the Green's functions machinery for spin.

The early use of the rather powerful simplified identities led to partially wrong results in perturbation theory (Ref. [6]). The reason for these partially wrong results remained poorly understood. Furthermore, it is known that perturbative approaches using the Majorana technique are prone to divergencies. We suggest that this has been another factor that prevented the use of the Majorana representation.

This dissertation aims to validate the Majorana representation, to clarify the above-mentioned ambiguities, to understand and resolve previous failures of the method and to test the method against other techniques. Furthermore, we will elaborate the benefits of the Majorana method, in particular, it's ability to provide viable approaches to higher-spin correlation functions.

The Majorana representation uses the concept of Majorana fermions. Let us give a short historical account of the concept. Subsequently, we briefly introduce the technical details of the representation. The so-called Majorana fermions have originally been introduced by Ettore Majorana as real-valued solutions of the Dirac equation (with purely imaginary γ-matrices). When Dirac derived his famous equation in order to describe the relativistic dynamics of fermionic quantum mechanical particles, he only considered complex valued solutions. For the complex Dirac solutions the spinors $\hat{\Psi}^{\dagger}$ and $\hat{\Psi}$ can be interpreted as operators which create or annihilate a fermionic particles, respectively. In the framework of such an interpretation it appears natural to assume that creation and annihilation operators are different. Corresponding elementary particles that satisfy $\hat{\Psi}^{\dagger} \neq \hat{\Psi}$ are often called Dirac fermions. However, as Majorana pointed out, there are solutions to the Dirac equation which fulfill $\hat{\Psi}^{\dagger} = \hat{\Psi}$ and are therefore said to be their own antiparticles. These particles have been called Majorana fermions, a species of elementary particles which possibly exists in our universe. The most popular candidate for Majorana fermions are neutrinos; the nature of neutrinos, whether they are Dirac or Majorana fermions, is one of the major unresolved problems in particle physics and is of current research interest.

At this point we have to emphasize that this work is *not* dealing with actual Majorana fermions, rather, the concept of Majorana fermions is solely used at a technical level. The term "Majorana fermion" as used here refers to objects $\hat{\eta}_{\alpha}$ $(\alpha, \beta = \{x, y, z\})$ that satisfy fermionic commutation relations

$$\{\hat{\eta}_{\alpha}, \hat{\eta}_{\beta}\} = \hat{\eta}_{\alpha}\hat{\eta}_{\beta} + \hat{\eta}_{\alpha}\hat{\eta}_{\beta} = \delta_{\alpha\beta} \tag{1.2}$$

and obey $\hat{\eta}_{\alpha}^{\dagger} = \hat{\eta}_{\alpha}$, resembling the properties of the Majorana fermions in the original sense. Spin-1/2 operators can be expressed in terms of such Majorana fermion operators by ($\hbar = 1$)

$$\hat{S}_x = -i\hat{\eta}_y\hat{\eta}_z \ , \quad \hat{S}_y = -i\hat{\eta}_z\hat{\eta}_x \ , \quad \hat{S}_z = -i\hat{\eta}_x\hat{\eta}_y \ . \tag{1.3}$$

This representation was introduced by Martin (Ref. [7]). In addition to the above relations we introduce an alternative representation. The composite operator $\hat{\Theta} = -2i\hat{\eta}_x\hat{\eta}_y\hat{\eta}_z$, which

obeys $\hat{\Theta}^2 = \frac{1}{2}$ and commutes with $\hat{\eta}_\alpha$, allows to rewrite the Martin transformation Eqs. (1.3) as

$$\hat{S}_x = \hat{\Theta}\hat{\eta}_x \ , \quad \hat{S}_y = \hat{\Theta}\hat{\eta}_y \ , \quad \hat{S}_z = \hat{\Theta}\hat{\eta}_z \ . \tag{1.4}$$

The latter relations will be important for the derivation of the simplified identities between spin and Majorana correlation functions. In particular, we will show that these relations facilitate the computation of higher-spin correlation functions.

Let us now give an overview of the work presented in this dissertation. The thesis is divided into five chapters. In Chapter 2, we highlight the role of four-spin correlation functions in the context of noise measurements. We introduce the concept of noise of susceptibility on a general level and derive Wiener-Khinchin-like relations between the experimentally accessible quantity and a particular four-spin correlation function. Thanks to the Majorana representation and functional integral methods, we are able to give explicit results for the noise of susceptibility of a single dissipative spin. We generalize the single spin result to a model of independent spins and compare to experimental results that were obtained in the context of $1/f$ flux noise in SQUIDs. Furthermore, we discuss the role of second noise, another quantity related to four-spin correlation functions, in this context.

Chapter 3 introduces the Majorana representation itself and provides a brief overview over other techniques. We show explicitly that the Majorana representation does not suffer from Hilbert space complications and does not require projection procedures. Moreover, we review the derivation of the simplified relations between spin and Majorana correlators and extend these relations to pairwise spin correlation functions of arbitrary order. In addition, we outline the fundamentals needed for the calculations in subsequent chapters, namely, the path integral formalism for Majorana fermions, finite-temperature as well as real-time Green's functions.

Dissipative spin dynamics can be modeled by the Bose-Kondo model, in which a spin 1/2 is coupled to a bosonic bath with an Ohmic spectral density. In Chapter 4, we apply the Majorana representation to the Bose-Kondo model in order to compute spin correlation functions. To properly deal with divergencies encountered in perturbation theory, we formulate a path-integral approach. We use functional-integral methods to obtain an effective field theory and analyze the saddle point and fluctuations of the theory. Based on this analysis, we derive a simple and efficient approach to even-order diagonal spin correlators of arbitrary high order in the dissipative regime. This method justifies the results for the four-spin correlator relevant in the context of noise of susceptibility, presented in Ch. 2.

Chapter 5 focuses on the application of the Majorana representation to the spin-boson model, in which a spin 1/2 in a longitudinal magnetic field is coupled to an Ohmic bosonic bath in one transverse direction. Earlier work has found that a simple perturbative approach fails to reproduce the long-time behavior of longitudinal-spin correlations known from Bloch-Redfield theory. By computing the self-energy to second order in perturbation theory we confirm that this failure is caused by divergencies in higher orders in perturbation theory. Based on a path-integral approach similar to the Bose-Kondo case, we are able to identify the divergent second-order diagrams as fluctuations of the self-energy. We then formulate a prescription and, based on that, a generalized Wick's theorem for the efficient calculation of spin correlation functions in the spin-boson model. We demonstrate that this approach reproduces the correct longitudinal-spin correlations.

In the last chapter of the main part, Chapter 6, we employ the Majorana representation to present a renormalization group approach to the sub-Ohmic Bose-Kondo model. We perform the calculations up to two-loop order and compute renormalization group equations. Thus we confirm earlier results, which were obtained using the pseudofermion technique. The calculations in this chapter allow for a detailed comparison to the pseudofermion technique.

Finally, we review the findings of the thesis, in particular regarding general aspects of the Majorana representation, and add some concluding remarks.

In this thesis we use natural units, dimensionful physical quantities are measured in units of energy. That is, we use $\hbar = 1$ for the Planck constant, $k_B = 1$ for the Boltzmann constant, and $g\mu_B = 1$ for the gyromagnetic moment of the electron. Vectors are denoted by bold symbols, e.g. $\boldsymbol{S}$.

2. Higher-Order Correlations and Noise in Spin Systems

Noise is a virtually universal phenomenon in electronic circuits and is known to contain information about the microscopic physics of the devices. Standard measurements of noise power spectra, related to two-point correlation functions, are generally not sufficient to clarify microscopic mechanisms of noise, in particular for fluctuations of spin systems. In this chapter we discuss experimental approaches beyond standard noise measurements and relate outcomes of such measurement protocols to four-point correlation functions of the system. In particular, we consider noise of susceptibility, a measure for nonequilibrium spin flucuations that has been introduced in the context of $1/f$ flux noise in superconducting Josephson junction devices The present chapter underlines the importance of higher-spin correlation functions with regard to low-temperature noise. Thus, it emphasizes the need for theoretical approaches for the efficient computation of such higher-spin correlation functions from microscopic models. This, in turn, motivates the Majorana representation.

First, in Sec. 2.1, we provide an introduction to noise, traditional measurement protocols, the power spectrum and the second spectrum. In Sec. 2.2 we establish Wiener-Khinchin-like relations between the spectrum of noise of susceptibility and a four-spin correlation function, based on the measurement protocol. We anticipate results obtained in Ch. 4 using the Majorana representation, which allow us to compute the noise of susceptibility in a model of independent dissipative spins $1/2$. We conclude this chapter with a discussion of our results and their implications in the context of $1/f$ flux noise. The bulk of the work presented in this chapter has been published in[1]

> Pablo Schad, Boris N. Narozhny, Gerd Schön, and Alexander Shnirman
> "Nonequilibrium spin noise and noise of susceptibility"
> *Phys. Rev. B* 90, 205419 – Published 17 November 2014.

2.1. Introduction

In everyday life, noise refers to any kind of unwanted sound. In the context of electronic devices noise describes unwanted fluctuations in experimentally accessible quantities, e.g. voltage, current, resistance or magnetic flux. Noise is present in a wide range of electronic circuits. For some types of noise the origin is well-known, like so-called shot noise and Johnson-Nyquist noise. Shot noise has been discovered by Walter Schottky in 1918 and is

---

[1]Parts of this chapter are reprinted with permission from this article. Copyright 2014 by the American Physical Society.

a consequence of the discreteness of charge carriers. Johnson-Nyquist noise, also known as thermal noise, originates from thermal fluctuations. In contrast, there is no universal explanation for the phenomenon of $1/f$ or pink noise, which is present in a wide range of electronic circuits. Generally, pink noise depends on the microscopic structure of a system and, in turn, contains information about the microscopic processes.

The name of $1/f$ noise is inspired by the dependence of its power spectrum $S(f)$ on frequency f, for an introduction to noise spectra we refer to Section 2.1.2. $1/f$ noise is commonly used to summarize a wide class of noise spectra behaving like $1/f^\alpha$ with an exponent which can deviate from 1, $0 < \alpha < 2$. The $1/f$ noise is related to slow processes, e.g., slow rearrangements of impurities or internal dynamics of two-level systems, cf. Ref. [8]. This is different from e.g. thermal Johnson-Nyquist noise, which is intimately related to dissipative processes with typical time scales of the order of picoseconds. At low enough frequencies thermal noise is white, i.e. frequency-independent. The $1/f$ noise increases slowly for smaller frequencies and is therefore labeled as "pink" while noise which behaves like $\propto 1/f^2$ is called "red".

The problem of $1/f$ noise has attracted great interest in the field of superconducting quantum devices. Flux noise measurements initially reported in relatively large SQUIDs (Superconducting Quantum Interference Devices) in the 80's showed the $1/f$ behavior, reported e.g. in Ref. [9]. In the last decade similar observations were made in nanoscale quantum circuits, e.g. Refs. [10–21]. The $1/f$ flux noise has been identified as a limiting factor for coherence times of superconducting qubits in Refs. [10, 11]. Increasing coherence times is one of the major challenges on the route to the quantum computer, cf. Ref. [22], driving efforts to understand microscopic origins of the noise with the hope to find efficient ways for noise reduction.

As already pointed out by Wellstood *et al.* in Ref. [9] the magnitude of $1/f$ flux noise appears to be "universal", i.e., of the same order of magnitude across a wide spectrum of device sizes and materials. Meanwhile, this noise is believed to originate from a system of electronic spins which reside within surface or interface layers, cf. e.g. Refs. [21, 23–26]. Indeed evidence for surface spins was found in deliberately designed experiments, Refs. [27, 28]. The reported experimental findings are consistent with the surface spin density of $\sigma_S \sim 5 \cdot 10^{17}$ m^{-2} anticipated by the authors of Ref. [12] in order to account for the observed noise magnitude.

The information about a system obtained in a standard noise measurement is not complete. Basically, trying to classify fluctuations of a systems by its noise spectrum amounts to classifying a probability distribution only in terms of its second moment. Thus, this approach works for Gaussian systems but is strongly limited in cases where higher-order correlations are relevant. Experimental results in Refs. [27–29] suggest that higher-order correlations are relevant for $1/f$ flux noise.

2.1.1. Beyond Standard Noise Measurements

Early measurements of the electric resistance of a wide range of materials observed fluctuations in the voltage drop over resistors, cf. e.g. Ref. [30]. At zero bias voltage, the noise spectrum of the voltage fluctuations was found to be white, i.e. independent of frequency. The origin of this noise has been identified to be thermal fluctuation of charge

carriers and named after Johnson and Nyquist. The corresponding power spectrum is fully characterized by temperature and resistance, $S_v(f) = 4k_B T R(f)$. The frequency dependence of $R(f)$ is intimately related to dissipative processes with typical time scales of the order of picoseconds, e.g. Ref. [30]. Therefore, up to frequencies $f \gtrsim 10^{10}$ Hz the spectral density is frequency-independent, i.e. white.

At finite voltage bias the noise spectrum acquires additional contributions, in particular a part which has been found to increase like $1/f$ at low frequencies and is known as $1/f$ or flicker noise, cf. Ref. [30]. The spectral density of $1/f$ noise is commonly described by the Hooge's law, e.g. Refs. [31, 32], $S_V(f) \propto \overline{V}^2/f$, where $\overline{V}$ is the average observed voltage. Since the noise was only observed at finite current it was initially interpreted to be a nonequilibrium effect. As reported in Refs. [33, 34] Voss and Clarke adapted a novel noise measurement protocol which allowed them to measure the $1/f$-like low-frequency fluctuations at zero bias and thus to show that the $1/f$ noise is actually an equilibrium effect. Voss and Clarke measured fluctuations in the variance of Johnson-Nyquist noise, which are technically described by a four-point correlation function, cf. Refs. [35, 36]. To our knowledge, their approach is the first example of investigating noise properties beyond the two-point correlations described by the spectral density $S(f)$.

The measurement protocol used by Voss and Clarke was studied in detail by Beck and Spruit in Ref. [36]. The authors calculated the variance of the Johnson noise and showed that it comprised two contributions. The first one could be interpreted as arising from resistance fluctuations and had a $1/f$ spectrum. The second one has a white spectrum and is intrinsic to any Gaussian fluctuating quantity. Consequently the equilibrium $1/f$ noise could only be observed at very low frequencies.

Later, Restle *et al.*, cf. Refs. [37, 38], adopted a procedure similar to the one used by Voss and Clarke and introduced the term "second spectrum". They measured fluctuations in the noise power per octave of the spectral density. The concept allows to identify non-Gaussian contribution to the noise and was applied to a large variety of systems showing $1/f$ noise. As discussed in reviews by Weissman, Refs. [38, 39], the second spectrum was used as a test for microscopic models for $1/f$ noise, in particular diffusion models and spin glass models. For example, Weissman has attempted to distinguish the droplet and hierarchical models of spin glasses by the properties of the second spectrum. In this context, the experimentally measured second spectrum is related to a four-spin correlation function.

Sendelbach *et al.*, Ref. [29], recently developed an alternative method to measure properties of flux noise, by observing fluctuations in the inductance of SQUIDs. As the spin contribution to inductance is determined by the spin susceptibility, e.g. Ref. [13], this experiment essentially amounts to measuring noise of susceptibility.

Susceptibility describes the response properties of a system to external perturbations and corresponds, similar to the power spectrum, to a two-point correlation function. In turn, noise of susceptibility corresponds to a four-spin correlation function, which is however distinct from the second spectrum. There is no consensus in the literature on how to define noise of susceptibility. Some authors, Refs. [40, 41], employ the fluctuation-dissipation theorem (FDT) and, thus, relate the noise of noise and the noise of susceptibility. This relation seems to be justified in the case where the system is controlled by a slow fluctuating parameter and is always in quasi-equilibrium. At the same time it would be useful to establish a more general definition of the noise of susceptibility at the microscopic level.

2.1.2. Noise Measurement Protocols

The comparison of outcomes of experimental measurements with theoretical predictions requires a reasonable understanding of the experimental protocols. Here we recapitulate basic features of standard noise measurement protocols and their connection to theoretically accessible correlation functions. We also discuss some features of the so-called second spectrum, which is understood to be the "noise of noise". For more details, the reader is referred to the book by Kogan, Ref. [35].

Let $x(t)$ be a classical fluctuating quantity which is the signal to be measured. For simplicity let us assume that the signal fluctuates around some mean value, $x(t) = x_0 + \delta x(t)$. In case of resistance measurements like in Ref. [33] the fluctuating quantity is voltage, $x(t) = V(t)$. In a typical experimental protocol, the signal is bandwidth filtered and then squared, cf. Ref. [42]. On a qualitative level we can assume the filter output signal has a form

$$\delta x(\tau|\omega_0, \Delta\omega) = \frac{1}{T_s} \int\limits_{\tau-\frac{T_s}{2}}^{\tau+\frac{T_s}{2}} dt\, e^{i\omega_0 t} \delta x(t) \; . \tag{2.1}$$

The time T_s is the time of a single measurement of the spectral density. It defines the bandwidth $\Delta\omega = 2\pi/T_s$. Assuming fluctuations to be generated by stationary stochastic processes the spectral density or power spectrum $S(\omega)$ is related to the filter output signal via, cf. Ref. [35],

$$S(\omega_0) = 2 \lim_{T_s \to \infty} T_s |\delta x(\tau|\omega_0, \Delta\omega)|^2 \tag{2.2}$$

That is, the power spectrum $S(\omega_0)$ represents the continuum limit of the differential noise power per frequency bin $\delta\omega$. It is related to the stochastic two-point correlation function $C^{(2)}(t - t') = \langle x(t)x(t') \rangle$ via the Wiener-Khinchin theorem, cf. Ref. [35]. We introduce the classical two-point correlator and its Fourier transform by

$$C^{(2)}(t - t') = \langle x(t)x(t') \rangle \; , \quad C^{(2)}(\omega) = \int \frac{d\omega}{2\pi} e^{i\omega(t-t')} C^{(2)}(t - t') \; . \tag{2.3}$$

In stationary situations the correlator $C^{(2)}(t - t')$ depends on the time difference only. If the Fourier transform $C^{(2)}(\omega)$ is well-defined, the Wiener-Khinchin theorem relates the correlator and the power spectrum by

$$S(\omega_0) = 2C^{(2)}(\omega_0) \; . \tag{2.4}$$

The formula (2.2) implicitly assumes $S(\omega_0)$ is independent of τ, i.e., it does not capture fluctuations of the noise power $|\delta x(\tau|\omega_0, \Delta\omega)|^2$. In real situations the measurement time T_s is finite and the limit in (2.2) cannot be performed exactly. Thus, $|\delta x(\tau|\omega_0, \Delta\omega)|^2$ actually does fluctuate around its mean value, which is essentially given by $S(\omega)/(2T_s)$. The so-called second spectrum $S^{(2)}$ is a measure of fluctuations of the noise power. The definition given by Kogan, Ref. [35], is

$$S^{(2)}(\nu|\omega_0, \Delta\omega) = \frac{8}{T} \Big\langle \Big| \int_{-T/2}^{T/2} d\tau\, e^{i\nu\tau} \Big(|\delta x(\tau|\omega_0, \Delta\omega)|^2 - \langle |\delta x(\tau|\omega_0, \Delta\omega)|^2 \rangle \Big) \Big|^2 \Big\rangle. \tag{2.5}$$

The time T is the total measurement time and is assumed to be large, in particular $T \gg T_s$, such that one can safely use the limit $T \to \infty$.

Consider the right-hand side of Eq. (2.5). Using (2.1) the first term can be expressed as

$$\langle |\delta x(\tau_1|\omega_0, \Delta\omega)|^2 |\delta x(\tau_2|\omega_0, \Delta\omega)|^2 \rangle$$

$$= \frac{1}{T_s^4} \int_{\tau_1-\frac{T_s}{2}}^{\tau_1+\frac{T_s}{2}} dt_1 dt_1' \int_{\tau_2-\frac{T_s}{2}}^{\tau_2+\frac{T_s}{2}} dt_2 dt_2' \, e^{i\omega_0(t_1-t_1')} e^{i\omega_0(t_2-t_2')} \, C^{(4)}(t_1, t_1', t_2, t_2') \,, \quad (2.6)$$

in terms of the classical four-point correlation function

$$C^{(4)}(t_1, t_1', t_2, t_2') = \langle \delta x(t_1) \delta x(t_1') \delta x(t_2) \delta x(t_2') \rangle \,. \quad (2.7)$$

The two equations (2.5) and (2.6) establish the relation between the experimentally measurable second spectrum and the the four-point correlation function $C^{(4)}$, which can be calculated from microscopic models.

The four-point correlation function $C^{(4)}$ comprises a Gaussian contribution, which is obtained by pair-wise averaging, yielding three possible combinations,

$$C_G^{(4)}(t_1, t_1', t_2, t_2') = C^{(2)}(t_1, t_1') \, C^{(2)}(t_2, t_2') + C^{(2)}(t_1, t_2) \, C^{(2)}(t_1', t_2')$$
$$+ C^{(2)}(t_1, t_2') \, C^{(2)}(t_1', t_2) \,. \quad (2.8)$$

One can now use the Gaussian decomposition (2.8) to find the Gaussian contribution to the second spectrum. One finds that the first term on the right-hand side of (2.8) cancels the average $\langle |\delta x|^2 \rangle$ in (2.5). The remaining two terms contribute to the second spectrum. To proceed we assume stationarity and use the Fourier transform

$$C^{(2)}(\omega) = \int d\tau \, e^{i\omega\tau} C^{(2)}(\tau). \quad (2.9)$$

The Gaussian contribution to the second spectrum acquires the form

$$S_G^{(2)}(\nu|\omega_0, \Delta\omega) \quad = 8 \int \frac{d\Omega}{2\pi} \, C^{(2)}(\Omega) C^{(2)}(\Omega+\nu) f^2 \left(\frac{\pi(\omega_0 - \Omega)}{\Delta\omega} \right) f^2 \left(\frac{\pi(\omega_0 - \nu - \Omega)}{\Delta\omega} \right) \,. \quad (2.10)$$

The second spectrum measures slow fluctuations on long timescales $1/\nu$ of the noise power, measured in time intervals $T_s = 2\pi/\Delta\omega$. Therefore $\nu \ll \Delta\omega, \omega_0$ holds [35, 38] and the above formula simplifies to

$$S_G^{(2)}(\nu|\omega_0, \Delta\omega) \approx \frac{8\Delta\omega}{2\pi} \left(C^{(2)}(\omega_0) \right)^2 \,. \quad (2.11)$$

$S_G^{(2)}$ is a white Gaussian background and is understood as a consequence of the finite length T_s of single measurements of power spectra, cf. Refs. [36, 42].

With regard to the understanding of microscopic properties of physical systems the Gaussian background cannot provide information beyond the power spectrum. Therefore, measurements of second spectra focus on the non-Gaussian contributions, cf. Refs. [38, 39, 42]. However, the Gaussian part mostly dominates the second spectra and the non-Gaussian contributions are hard to observe, as e.g. in the context of spin glasses in Refs. [38, 39]. In this context, particularly, the insights of such measurements turned out to be limited.

In any case it is desirable to develop other experimental approaches to study microscopics of physical systems. In the context of fluctuating spin systems such a new approach is provided by the measurements of noise of susceptibility by Sendelbach *et al.*, Ref. [29]. Similar to the second spectrum, this quantity is related to a four-point correlation function. The discussion of the second spectrum provided here serves as the basis for a comparison of the two quantities.

2.2. Nonequilibrium Spin Fluctuations and Noise of Susceptibility

In order to gain information about microscopics of a fluctuating system, linear response transport measurements are a complementary approach to noise measurements, cf. Refs. [35, 43]. The linear response function of a spin system is the susceptibility. Both experimentally measurable quantities, the susceptibility and the noise spectrum, are related to two-spin correlation functions, albeit different ones. Above it was argued that the finite-time noise spectrum actually can fluctuate and that these fluctuations can help to understand microscopic processes. The same logic can be applied to the susceptibility.

The experimental protocol used in Ref. [29] measured fluctuations in the inductance of a SQUID that were dedicated to the fluctuations in the susceptibility of a spin system. So far, the definition of noise of susceptibility and its relation to four-point correlation functions is ambiguous, i.e., a general "Wiener-Khinchin theorem" is lacking. In Section 2.2.2 we solve this problem, i.e. we derive a general relation between experimentally accessible noise of susceptibility and a particular four-point correlation function based on the experimental protocol of Sendelbach *et al.*.

Thereafter, in Section 2.2.3, we present our results for the noise of susceptibility of a single spin 1/2. The technique used to obtain these results and the detailed calculation are presented in subsequent Chapters 3 and 4.

2.2.1. Qualitative Arguments

Before introducing the concept of noise of susceptibility thoroughly, we present qualitative arguments as a guide to noise of susceptibility from a statistical perspective. For simplicity we omit time dependence for the moment and take all quantities at equal times.

Let us illustrate the statistical concepts commonly used in the literature devoted to noise on a simple example. Consider a random quantity x with the probability distribution $P(x) = Z^{-1} \exp[-U(x)]$. It is well known that $P(x)$ provides the complete information about x, which can be expressed in terms of either all moments $\langle x^n \rangle$ or all cumulants $\langle\langle x^n \rangle\rangle$. Assuming the symmetry of the distribution $P(x) = P(-x)$, such that $\langle x \rangle = 0$, the noise of x, using Eq. (2.4), corresponds to

$$S = 2 \left\langle x^2 \right\rangle. \tag{2.12}$$

Thus, up to the factor of 2 the noise is equal to the second cumulant of x (which is also equal to the second moment since $\langle x \rangle = 0$).

At equal times, the definition of the second noise of x, Eq. (2.5), reduces to

$$S^{(2)} = 2 \left(\left\langle x^4 \right\rangle - \left\langle x^2 \right\rangle^2 \right), \tag{2.13}$$

which is neither a moment nor a cumulant. This particular definition is motivated by the measurement protocol, cf. Sec. 2.1.2 or Ref. [35], in which the time fluctuations of x^2 are recorded. For a Gaussian random quantity, i.e., $U(x)$ in $P(x)$ is quadratic in x, one finds

$$\left\langle\left\langle x^4\right\rangle\right\rangle = 0, \qquad \left\langle x^4\right\rangle = 3\left\langle x^2\right\rangle^2, \qquad S^{(2)} = 4\left\langle x^2\right\rangle^2. \tag{2.14}$$

Now we slightly perturb our system by a weak external field B, so that the new distribution function reads $P_B(x) = Z_B^{-1}\exp[-U(x) + Bx]$. Then the random quantity x acquires a nonzero average value

$$\langle x\rangle_B = Z_B^{-1}\frac{\partial Z_B}{\partial B} = \chi B + \mathcal{O}(B^3), \tag{2.15}$$

where $\chi = \langle x^2\rangle$ is the corresponding linear susceptibility. The second moment of x acquires an additional field dependence, i.e.,

$$\left\langle x^2\right\rangle_B = Z_B^{-1}\frac{\partial^2 Z_B}{\partial B^2} = \left\langle x^2\right\rangle + \chi^2 B^2 + aB^2 + \mathcal{O}(B^4), \tag{2.16}$$

where

$$a = \frac{1}{2}\left(\left\langle x^4\right\rangle - 3\left\langle x^2\right\rangle^2\right). \tag{2.17}$$

For the Gaussian distribution, $a = 0$. Therefore, the quantity (2.17) is a measure of non-Gaussian fluctuations. At the same time, a is proportional to the fourth cumulant of x and, therefore, is nonequivalent to the second noise $S^{(2)}$.

In laboratory experiments, e.g. in Refs. [29, 33, 34], the fluctuating quantity is time dependent and instead of the averages (2.16) one has to consider correlation functions and corresponding frequency dependent noise spectra in the presence of the external field. Such analysis of experimental data is typically performed over a reasonably long, but necessarily limited time interval. Repeating the analysis over a large number of such intervals one can find that the susceptibility χ may itself take different values when measured at different times as reported in Ref. [29]. Note that this averaging is no longer described by the distribution $P(x)$; within the above simple considerations the susceptibility defined in Eq. (2.15) does not fluctuate. Averaging over such fluctuations, one finds the mean value of the susceptibility. With regard to Eq. (2.16) it is then tempting to interpret χ as the averaged susceptibility and the quantity a as the noise of susceptibility measured in Ref. [29]. At this point one has to be careful, as there is no guarantee that a is positive. In fact, it is well-known in the theory of shot noise, cf. Refs. [43–45], that out of equilibrium the noise may be lower than the equilibrium noise at the same temperature.

As an example of such negative nonequilibrium contribution to noise, consider the simple problem of a single spin $1/2$ subjected to external magnetic field. If one is interested in equal-time correlators, then one can use the above arguments where x should be replaced by $\hat{S}_z$. Now, the square of the spin operator is simply proportional to the identity operator independently of whether the field is applied or not. Consequently, $\langle\hat{S}_z^2\rangle_B = \langle\hat{S}_z^2\rangle = 1/4$ and $a = -\chi^2 = -1/16$. Thus one might expect the nonequilibrium spin fluctuations to be described by the negative quantity (2.17) which appears to be inconsistent with its interpretation as noise of susceptibility. In what follows, we provide a proper microscopic definition of the noise of susceptibility corresponding to the experimental protocol used in Ref. [29].

2.2.2. Noise of Susceptibility

Instead of a simple stochastic variable x let us consider the case of a quantum spin system. Assume a coupling Hamiltonian $H_I = -\hat{\boldsymbol{S}}\boldsymbol{B}(t)$, where $\hat{\boldsymbol{S}}$ is the spin operator and $\boldsymbol{B}$ is a weak perturbing magnetic field. A traditional way of describing the response of the system to a weak external perturbation is the spin susceptibility, which relates the applied field to the resulting magnetization, $M_\alpha \equiv \langle \hat{S}_\alpha(t) \rangle = \int dt' \chi_{\alpha\beta}(t,t') B_\beta(t')$ with $\alpha,\beta = \{x,y,z\}$. In terms of spin operators, the susceptibility is given by the Kubo formula, cf. Ref. [46],

$$\chi_{\alpha\beta}(t,t') = i\theta(t-t') \left\langle \left[\hat{S}_\alpha(t), \hat{S}_\beta(t') \right] \right\rangle. \tag{2.18}$$

Here the spin operators must be in the Heisenberg representation with respect to the Hamiltonian of the system in the absence of the field. In isotropic systems, the susceptibility tensor is diagonal and isotropic $\chi_{\alpha\beta} = \chi \delta_{\alpha\beta}$.

Time-dependent magnetization fluctuations can be described by a spectrum $S_M(\omega)$ that in the simplest case can be related to the imaginary part of the susceptibility (2.18) with the help of the fluctuation-dissipation theorem (FDT), cf. Ref. [35]. The FDT states that

$$S_M(\omega) = 2 \coth \frac{\omega}{2T} \mathrm{Im}\chi(\omega). \tag{2.19}$$

Once the susceptibility is calculated, we can then use Eq. (2.19) to find the noise spectrum.

Practical calculations are often simplified by using field-theoretical techniques. Real-time fluctuations, especially in presence of external field, can be conveniently described within the Keldysh formalism, cf. Ref. [47]. The Keldysh formalism and the concept of generating functionals are outlined in Sec. 3.2. In this formalism, the spin susceptibility (2.18) has the form

$$\chi_{\alpha\beta}(t,t') = i\langle \mathcal{T}_K \hat{S}_\alpha^{cl}(t) \hat{S}_\beta^q(t') \rangle_0 = -i \left. \frac{\delta^2 \mathcal{Z}[\lambda^{cl},\lambda^q]}{\delta\lambda_\alpha^q(t)\delta\lambda_\beta^{cl}(t')} \right|_{\boldsymbol{\lambda}=0}, \tag{2.20}$$

where $\mathcal{T}_K$ denotes time ordering on the Keldysh contour and $\mathcal{Z}[\lambda^{cl},\lambda^q]$ is the Keldysh generating functional, Eq. (3.70), with the source terms $\lambda^{c(q)}$ included. The subscripts q and cl on both the spin operators and source fields refer to the so-called "quantum" and "classical" variables, which are related to the fields belonging to the upper (u) and the lower (d) branch of the Keldysh contour by a linear transformation

$$\hat{S}_\alpha^{cl} = \frac{1}{\sqrt{2}} \left(\hat{S}_\alpha^u + \hat{S}_\alpha^d \right), \quad \hat{S}_\alpha^q = \frac{1}{\sqrt{2}} \left(\hat{S}_\alpha^u - \hat{S}_\alpha^d \right)$$

$$\lambda_\alpha^{cl} = \frac{1}{\sqrt{2}} \left(\lambda_\alpha^u + \lambda_\alpha^d \right), \quad \lambda_\alpha^q = \frac{1}{\sqrt{2}} \left(\lambda_\alpha^u - \lambda_\alpha^d \right)$$

The source terms appear in an exponential form $e^{i \int dt' \lambda \hat{S}_z^q}$ in the generating functional. The "quantum" source term is only needed to construct the correlation function and always has to be set to zero at the end. In contrast, the "classical" source term describes the physical probing field, $\lambda_\alpha^{cl} \equiv \sqrt{2}B_\alpha$. For details on this technique we refer to Subs. 3.2.3 and the textbook by Kamenev, Ref. [47].

Fluctuations at Finite External Fields

Instead of using the susceptibility, as was done in Eq. (2.19), we can characterize fluctuations of the magnetization by directly evaluating the second moment of the spin in the presence of perturbation, generalizing Eq. (2.16). The time-dependent symmetric second moment within the Keldysh framework is the two-spin correlator

$$C_{\alpha\alpha}^{(2)}(t,t') = \langle \mathcal{T}_K \hat{S}_z^{cl}(t_1)\hat{S}_z^{cl}(t_2)\rangle = -\frac{1}{2}\left.\frac{\delta^2 \mathcal{Z}_K[\boldsymbol{\lambda}]}{\delta\lambda_\beta^q(t')\delta\lambda_\alpha^q(t)}\right|_{\boldsymbol{\lambda}=0}$$

$$= \frac{1}{2}\langle \hat{S}_\alpha(t)\hat{S}_\alpha(t') + \hat{S}_\alpha(t')\hat{S}_\alpha(t)\rangle \ , \tag{2.21}$$

which is the quantum spin analog to $C^{(2)}$ introduced in (2.3). Without loss of generality, we can assume that the external field is applied along z direction. Consider then the above second moment of the z-component of the physical spin in the presence of the field:

$$2\,C_{zz,B}^{(2)}(t_1,t_2) = -\left.\frac{\delta^2 \mathcal{Z}[\lambda_z^q,B]}{\delta\lambda_z^q(t_1)\delta\lambda_z^q(t_2)}\right|_{\lambda_z^q=0} = \langle \mathcal{T}_K \hat{S}_z^{cl}(t_1)\hat{S}_z^{cl}(t_2)e^{i\int dt'\sqrt{2}B\hat{S}_z^q}\rangle \ . \tag{2.22}$$

Notice that for the spin-1/2 operator the moment $2\,C_{zz,B}^{(2)}$ at equal times $t_1 = t_2$ is given by a B-independent constant which is equal to 1/2.

For weak external fields, we may expand the quantity (2.22) in a power series in B:

$$2\,C_{zz,B}^{(2)}(t_1,t_2) = 2\,C_{zz}^{(2)}(t_1,t_2) + \int dt_1'dt_2'\,C_\chi(t_1,t_1',t_2,t_2')B(t_1')B(t_2') + \mathcal{O}\left(B^4\right) \ . \tag{2.23}$$

The first term on the right-hand side above is the field-independent equilibrium term. By the relation (2.4) its Fourier transform corresponds to the equilibrium noise (2.19). This is consistent with the fact that the noise is characterized by the second cumulant of the fluctuating quantity in the absence of the applied field, similarly to Eqs. (2.12) and (2.19). For the spin 1/2 we find $C_{zz}^{(2)}(t=0) = 1/2$ for the equilibrium term in (2.23).

The second term in Eq. (2.23) contains the four-point correlation function

$$C_\chi(t_1,t_1',t_2,t_2') = -\left.\frac{\delta^4 \mathcal{Z}[\lambda^{cl},\lambda^q]}{\delta\lambda_z^q(t_1)\delta\lambda_z^{cl}(t_1')\delta\lambda_z^q(t_2)\delta\lambda_z^{cl}(t_2')}\right|_{\lambda=0}$$

$$= -\langle \mathcal{T}_K \hat{S}_z^{cl}(t_1)\hat{S}_z^q(t_1')\hat{S}_z^{cl}(t_2)\hat{S}_z^q(t_2')\rangle \ . \tag{2.24}$$

which can be split into the Gaussian and non-Gaussian parts

$$C_\chi = C_\chi^G + C_\chi^{NG} \ . \tag{2.25}$$

The Gaussian part is readily obtained by a pair-wise averaging of the spin operators:

$$C_\chi^G(t_1,t_1',t_2,t_2') = -\langle \mathcal{T}_K \hat{S}_z^{cl}(t_1)\hat{S}_z^q(t_1')\rangle\langle \mathcal{T}_K \hat{S}_z^{cl}(t_2)\hat{S}_z^q(t_2')\rangle$$

$$- \langle \mathcal{T}_K \hat{S}_z^{cl}(t_1)\hat{S}_z^q(t_2')\rangle\langle \mathcal{T}_K \hat{S}_z^{cl}(t_2)\hat{S}_z^q(t_1')\rangle$$

$$= \chi_{zz}(t_1,t_1')\chi_{zz}(t_2,t_2') + \chi_{zz}(t_1,t_2')\chi_{zz}(t_2,t_1'). \tag{2.26}$$

In contrast to the Gaussian four-point correlation function $C_G^{(4)}$ in (2.8), the third contribution is absent since the correlator of the two "quantum" fields is always zero.

For the spin 1/2, the moment (2.22) at equal times $t_1 = t_2 = t$ is equal to 1/2 independently of the magnetic field and therefore $C_\chi(t, t'_1, t, t'_2) = 0$. The Gaussian contribution (2.26) reduces to $2\chi_{zz}(t, t'_1)\chi_{zz}(t, t'_2)$, and hence does not satisfy this "sum rule". Thus, there must be a non-Gaussian contribution C_χ^{NG} as well which has to compensate for C_χ^G in this case. More generally, Wick's theorem does not hold for spin operators, reflecting the fact that their algebra is non-Abelian. The non-Gaussian contribution C_χ^{NG} cannot be expressed in terms of the averaged susceptibilities, in this sense it represents the connected part of C_χ. It can be written as

$$C_\chi^{NG}(t_1, t'_1, t_2, t'_2) = -\langle\langle \mathcal{T}_K \hat{S}_z^{cl}(t_1)\hat{S}_z^q(t'_1)\hat{S}_z^{cl}(t_2)\hat{S}_z^q(t'_2)\rangle\rangle . \tag{2.27}$$

Here, the double-angle brackets indicate the subtraction of the Gaussian contribution (2.26), i.e., the averaged susceptibility terms. The quantity C_χ^{NG} has to be evaluated specifically for each system.

Measurement Protocol and Correlation Functions

In laboratory experiments [29, 35], the system is typically probed with a harmonic perturbation,

$$B(t) = B_0 \cos(\omega_0 t) . \tag{2.28}$$

The susceptibility is then measured using the lock-in technique, i.e., by "asking the electronics" to obtain the average of the following operator (similar to (2.1)):

$$\hat{\chi}_\varphi(\tau_n|\omega_0, \Delta\omega) = \frac{1}{B_0 T_\chi} \int_{\tau_n - \frac{T_\chi}{2}}^{\tau_n + \frac{T_\chi}{2}} dt \cos(\omega_0 t - \varphi) \hat{S}_{z,B}(t). \tag{2.29}$$

The measurement is performed for a time period T_χ centered at τ_n, T_χ playing the role of T_s in (2.1). The measurement bandwidth $\Delta\omega \equiv 2\pi/T_\chi$ is assumed to be much smaller than ω_0. The phase delay φ allows for discriminating between the in-phase ($\varphi = 0$) and the out-of-phase ($\varphi = \pi/2$) response, corresponding to the real and the imaginary parts of the susceptibility, respectively. In practice, in every time bin one finds a different result and the average susceptibility is obtained after averaging over the time bins.

Treating the result of susceptibility measurements in each time bin as a fluctuating quantity (as it is in real experiment, cf. Ref. [29]), one can define the second moment or noise of susceptibility as follows

$$\chi_{\varphi_1, \varphi_2}^{(2)}(\tau_1, \tau_2|\omega_0, \Delta\omega) = \langle \hat{\chi}_{\varphi_1}(\tau_1)\hat{\chi}_{\varphi_2}(\tau_2) + \hat{\chi}_{\varphi_2}(\tau_2)\hat{\chi}_{\varphi_1}(\tau_1)\rangle - 2\langle\chi_{\varphi_1}(\tau_1)\rangle\langle\chi_{\varphi_2}(\tau_2)\rangle . \tag{2.30}$$

Using the explicit form (2.29), we find

$$\chi_{\varphi_1, \varphi_2}^{(2)}(\tau_1, \tau_2|\omega_0, \Delta\omega)$$

$$= \frac{1}{B_0^2 T_\chi^2} \int_{\tau_1 - \frac{T_\chi}{2}}^{\tau_1 + \frac{T_\chi}{2}} dt_1 \int_{\tau_2 - \frac{T_\chi}{2}}^{\tau_2 + \frac{T_\chi}{2}} dt_2 \cos(\omega_0 t_1 - \varphi_1)\cos(\omega_0 t_2 - \varphi_2)\, 2\, C_{zz,B}^{(2)}(t_1, t_2)$$

$$- 2\langle\chi_{\varphi_1}(\tau_1)\rangle\langle\chi_{\varphi_2}(\tau_2)\rangle . \tag{2.31}$$

In contrast to Eq. (2.29), the averaging in Eq. (2.31) has been already performed (as we are not interested in higher moments).

We now use the linear-response-like expansion (2.23) for the symmetric two-point correlator $C_{zz,B}^{(2)}(t_1, t_2)$ and decompose the second moment of susceptibility Eq. (2.31) into two parts

$$\chi^{(2)} = \chi_{eq}^{(2)} + \chi_{ne}^{(2)} \ . \tag{2.32}$$

The first term $\chi_{eq}^{(2)}$ describes the equilibrium magnetization noise S_M in the absence of the external field:

$$\chi_{eq,\varphi_1,\varphi_2}^{(2)}(\tau_1, \tau_2 | \omega_0, \Delta\omega)$$

$$= \frac{1}{B_0^2 T_\chi^2} \int_{\tau_1-\frac{T_\chi}{2}}^{\tau_1+\frac{T_\chi}{2}} dt_1 \int_{\tau_2-\frac{T_\chi}{2}}^{\tau_2+\frac{T_\chi}{2}} dt_2 \, \cos(\omega_0 t_1 - \varphi_1)\cos(\omega_0 t_2 - \varphi_2)\, 2\, C_{zz}^{(2)}(t_1 - t_2) \ . \tag{2.33}$$

The corresponding noise spectrum is given by the Fourier transform of $\chi_{eq}^{(2)}$

$$\chi_{eq,\varphi_1,\varphi_2}^{(2)}(\nu | \omega_0, \Delta\omega) = \frac{1}{4B_0^2} f^2 \left(\frac{\pi\nu}{\Delta\omega}\right) \Big(\cos(\varphi_1 - \varphi_2)\left[S_M(\omega_0 + \nu) + S_M(\omega_0 - \nu)\right]$$

$$- i\sin(\varphi_1 - \varphi_2)\left[S_M(\omega_0 + \nu) - S_M(\omega_0 - \nu)\right]\Big) + \mathcal{O}\left(\frac{\Delta\omega}{\omega_0}\right) \ , \tag{2.34}$$

where $f(x) = \sin(x)/x$ restricts the frequency ν to be small $\nu \lesssim \Delta\omega$. The appearance of the imaginary part in the noise spectrum (2.34) reflects the fact that cross-correlations between the real and imaginary parts of susceptibility do not possess any symmetry as functions of time. Indeed, according to the definition (2.30) the noise of susceptibility obeys the following symmetry

$$\chi_{\varphi_1,\varphi_2}^{(2)}(\tau_1, \tau_2) = \chi_{\varphi_2,\varphi_1}^{(2)}(\tau_2, \tau_1), \tag{2.35}$$

and is a symmetric function of the two times τ_i only if $\varphi_1 = \varphi_2$. Consequently, the noise of the real (or imaginary) part of susceptibility is characterized by the real spectrum, while the Fourier transform of the cross-correlator may contain an imaginary part.

The nonequilibrium contribution $\chi_{ne}^{(2)}$, which includes the correlator C_χ, is composed of the second term of the expansion (2.23) substituted into Eq. (2.31). We note that only the non-Gaussian part C_χ^{NG} contributes to $\chi_{ne}^{(2)}$. This is because the Gaussian part C_χ^{G}, Eq. (2.26), corresponds exactly to the subtracted product of the averages. Thus we obtain (assuming the harmonic form (2.28) for the external perturbation $B(t)$)

$$\chi_{ne,\varphi_1,\varphi_2}^{(2)}(\tau_1, \tau_2 | \omega_0, \Delta\omega) = \frac{1}{T_\chi^2} \int_{\tau_1-\frac{T_\chi}{2}}^{\tau_1+\frac{T_\chi}{2}} dt_1 \int_{\tau_2-\frac{T_\chi}{2}}^{\tau_2+\frac{T_\chi}{2}} dt_2 \, \cos(\omega_0 t_1 - \varphi_1)\cos(\omega_0 t_2 - \varphi_2)$$

$$\times \int dt_1' dt_2' \, C_\chi^{NG}(t_1, t_1', t_2, t_2')\cos(\omega_0 t_1')\cos(\omega_0 t_2') \ . \tag{2.36}$$

The time integrals in Eq. (2.36) can be simplified with the help of the Fourier transform defined as follows

$$C_\chi^{NG}(t_1, t_1', t_2, t_2') = \int \frac{d\nu d\omega_1 d\omega_2}{(2\pi)^3} C_\chi^{NG}(\nu, \omega_1, \omega_2) e^{-i\nu(t_1 - t_2)} e^{-i\omega_1(t_1 - t_1')} e^{-i\omega_2(t_2 - t_2')} \ . \tag{2.37}$$

According to the experimental protocol of Ref. [29] we are only interested in low-frequency noise $\nu \ll \Delta\omega \ll \omega_0$. Focusing on contributions that are slow functions of $\tau_1 - \tau_2$, we retain only the lowest harmonics and find

$$\chi^{(2)}_{ne,\varphi_1,\varphi_2}(\nu|\omega_0,\Delta\omega) = \frac{1}{16}f^2\left(\frac{\pi\nu}{\Delta\omega}\right)\left[\sum_{\epsilon_1,\epsilon_2=\pm 1} e^{-i\epsilon_1\varphi_1}e^{-i\epsilon_2\varphi_2}C^{NG}_\chi(\nu,\epsilon_1\omega_0,\epsilon_2\omega_0)\right.$$

$$\left. + \sum_{\epsilon=\pm 1} e^{i\epsilon(\varphi_1-\varphi_2)}C^{NG}_\chi(\nu-2\epsilon\omega_0,\epsilon\omega_0,-\epsilon\omega_0)\right] \ . \quad (2.38)$$

Thus the nonequilibrium contribution to the noise of susceptibility is a direct probe of non-Gaussian fluctuations in the system, in contrast to the second spectrum $S^{(2)}(\nu|\omega_0,\Delta\omega)$, cf. Eq. (2.5). Below, we will illustrate our general considerations by calculating C^{NG}_χ for the simplest model system, i.e. a single spin immersed in a dissipative environment.

2.2.3. Susceptibility Noise of a Single Spin

Having established a general relation between the experimentally accessible noise of susceptibility and a four-spin correlation function provides the basis for a comparison of experimentally obtained noise and the noise computed from microscopic spin models. The vast amount of literature concerned with the computation of two-spin correlation functions suggests that computation of a four-spin correlation is a hard task, naturally depending on the complexity of the microscopic model. In this regard it is natural to start with a simple model which at least allows to illustrate the above general arguments.

As a simple example we choose a single spin 1/2 coupled to an external bath and subjected to an externally applied magnetic field. The magnetic field is assumed to be much smaller than temperature, $B \ll T$, justifying the linear response-like expansion discussed in the preceding section. The technique developed in Chaps. 3 and 4 enables us to obtain analytic results for susceptibility noise in this model, which are presented here. Moreover, the calculation of the four-spin correlation function motivated the work presented in these chapters. Implications of the results in the context of $1/f$ flux noise are discussed in Section 2.3.

Calculating spin correlation functions can be greatly simplified by the long-known Majorana fermion representation of the spin operators:

$$\hat{s}_x = -i\hat{\eta}_y\hat{\eta}_z, \quad \hat{s}_y = -i\hat{\eta}_z\hat{\eta}_x, \quad \hat{s}_z = -i\hat{\eta}_x\hat{\eta}_y \ . \quad (2.39)$$

The Majorana method used here is discussed in great detail in Chap. 3. The properties of the spin can be obtained by the use of Green's functions of Majorana fermions, in the Keldysh formalism defined by

$$\hat{G}^{ab}_\alpha(t,t') = -i\langle\mathcal{T}_K\hat{\eta}^a_\alpha(t)\hat{\eta}^b_\alpha(t')\rangle \ , \qquad a,b \in \{cl,q\} \ . \quad (2.40)$$

In order to obtain the equilibrium and nonequilibrium noise of susceptibility, Eqs. (2.34) and (2.38), we need the symmetric spin correlator $C^{(2)}_{zz}$ as well as the four-spin correlation function C^{NG}_χ. Anticipating the results of Subs. 4.3, the Majorana method allows to compute these two correlators via

$$C^{(2)}_{zz}(t,t') = \frac{1}{2}\langle\mathcal{T}_K\hat{s}^{cl}(t)\hat{s}^{cl}(t')\rangle = \frac{1}{2}\langle\mathcal{T}_K[\eta_z m]^{cl}_t[\eta_z m]^{cl}_{t'}\rangle \quad (2.41)$$

Figure 2.1.: Diagrammatic representation of the two-spin correlator related to the noise spectrum (diagrams generated in Jaxodraw, Ref. [48]).

and

$$
\begin{aligned}
C_\chi^{NG}(t_1, t_1', t_2, t_2') &= -\langle\langle \mathcal{T}_K \hat{s}^{cl}(t_1)\hat{s}^q(t_1')\hat{s}^{cl}(t_2)\hat{s}^q(t_1')\rangle\rangle \\
&= -\langle\langle \mathcal{T}_K [\eta_x m]_{t_1}^{cl} [\eta_x m]_{t_1'}^q [\eta_x m]_{t_2}^{cl} [\eta_x m]_{t_2'}^q \rangle\rangle \; .
\end{aligned}
\tag{2.42}
$$

Here, m is an auxiliary, non-interacting Majorana m used only to establish the correct, spin-like, time ordering. The Green's functions of m in frequency space are given by Eqs. (3.81), i.e.,

$$
D^{R/A}(\omega) = (\omega \pm i0)^{-1} \; , \qquad D^K(\omega) = 0 \; .
\tag{2.43}
$$

Since the m-Majoranas do not interact, the knowledge of the full Majorana Green's functions $\hat{G}_\alpha$ allows for rather direct access to the spin correlation functions.

We first derive the full Majorana Green's functions $\hat{G}_\alpha$ within the chosen model. As a generic model to generate dissipative spin dynamics we consider the spin-isotropic Bose-Kondo model in Chapter 4. In this model, the external bath is realized by a continuum of bosonic modes with an Ohmic spectral density and a cutoff Λ. The bosonic modes described by $\hat{X}_\alpha$ are weakly coupled to the spin by the Hamiltonian $H = \hat{\boldsymbol{X}}\hat{\boldsymbol{S}}$, the weakness is controlled by a small coupling constant $g \ll 1$ (included in $\boldsymbol{X}$). Then, as long as the temperature is high, meaning $T \gg T_K$ with $T_K \equiv \Lambda \exp[-\pi/(2g)]$, the bosonic bath effectively provides a mechanism for thermal spin fluctuations, i.e., it allows for dissipative spin dynamics.

Based on the Majorana representation we develop a path-integral formulation of the model in Chapter 4. We integrate out the bosonic bath and obtain the effective action for the Majorana fermions. This action is formally expanded around the saddle-point solution and it is shown that in the high-temperature regime $T \gg T_K$ fluctuations around the saddle point are small. We find that the saddle-point solutions for Majorana Green's functions are

$$
G_\alpha^{R/A}(\omega) = \frac{1}{\omega \pm i\Gamma} \; , \qquad G_\alpha^K(\omega) = -\frac{2i\Gamma \tanh\frac{\omega}{2T}}{\omega^2 + \Gamma^2} \; .
\tag{2.44}
$$

Here, Γ is the Korringa relaxation rate $\Gamma = 2gT$, the inverse time scale associated with thermal fluctuations of the spin.

Spin correlators can now be computed through Majorana Green's functions Eqs. (2.44) and (3.81). In terms of diagrams the symmetric two-spin correlator needed for the equilibrium noise corresponds to Fig. 2.1. In this diagram, as well as in Figs. 2.2 and 2.3 below, double lines correspond to the saddle-point Green's functions (2.44) of Majorana fermions η_α, dashed lines refer to Green's function D of the non-interacting Majorana fermion m, see Eq. (3.81), and wavy lines represent the bosonic bath.
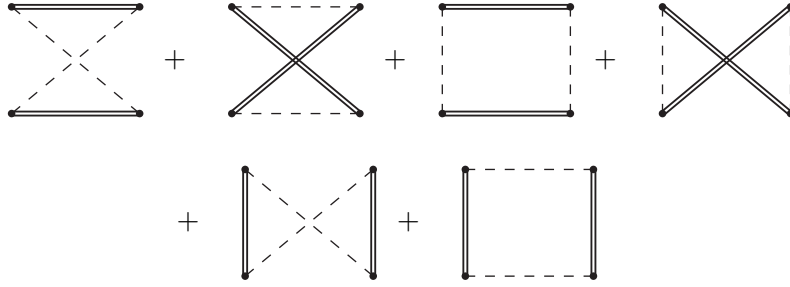
Figure 2.2.: The leading contributions to nonequilibrium noise of susceptibility.

First we focus on the equilibrium noise of susceptibility, Eq. (2.34). It turns out that the symmetric two-spin correlator basically corresponds to $G^R - G^A$, cf. Eq. (3.84). The noise spectrum of magnetic fluctuations $S_M = 2C_{zz}^{(2)}$ of a single spin 1/2 is found to be

$$S_{M,\Gamma}(\omega) = \frac{\Gamma}{\Gamma^2 + \omega^2} \tag{2.45}$$

For the equilibrium part, it turns out that the noise of the real part of susceptibility is identical with that of the imaginary part:

$$\chi_{eq,00}^{(2)}(\nu|\omega_0, \Delta\omega) = \chi_{eq,\frac{\pi}{2},\frac{\pi}{2}}^{(2)}(\nu|\omega_0, \Delta\omega) \tag{2.46a}$$

$$= \frac{1}{4B_0^2} f^2\left(\frac{\pi\nu}{\Delta\omega}\right) \left[\frac{\Gamma}{\Gamma^2 + (\omega_0 + \nu)^2} + \frac{\Gamma}{\Gamma^2 + (\omega_0 - \nu)^2}\right] \ .$$

The result is purely real and complies with the symmetry (2.35). In contrast, the cross-correlations are characterized by the purely imaginary noise spectrum

$$\chi_{eq,0,\frac{\pi}{2}}^{(2)}(\nu|\omega_0, \Delta\omega) = \frac{i}{4B_0^2} f^2\left(\frac{\pi\nu}{\Delta\omega}\right) \left[\frac{\Gamma}{\Gamma^2 + (\omega_0 + \nu)^2} - \frac{\Gamma}{\Gamma^2 + (\omega_0 - \nu)^2}\right]. \tag{2.46b}$$

The result is an odd function of ν. Integrating over the frequency would yield zero, reflecting the absence of cross-correlations between the real and imaginary parts of susceptibility at equal times.

Now we turn to the more interesting, nonequilibrium noise of susceptibility, Eq. (2.38). To compute this noise, we need to evaluate the four-spin correlation function (2.42). The diagrams depicted in Fig. 2.2 represent the saddle-point approximation for the non-Gaussian part of the four-spin correlation function. Higher-order diagrams of the type shown in Fig. 2.3 are closely related to fluctuations around the saddle point, which can be neglected in the high-temperature regime $T \gg T_K, \omega_1, \omega_2, \nu, \Gamma$. For details we refer to Ch. 4.

The leading diagrams, depicted in Fig. 2.2, produce the following result:

$$C_\chi^{NG}(\nu, \omega_1, \omega_2) = \frac{i\Gamma^2}{8T^2} \frac{\omega_1 + \omega_2 + 2i\Gamma}{(\omega_1 + i\Gamma)(\omega_2 + i\Gamma)(\omega_1 + \nu + i\Gamma)(\omega_2 - \nu + i\Gamma)} \ . \tag{2.47}$$

Substituting this result (2.47) into Eq. (2.38) yields the nonequilibrium noise spectrum of the spin susceptibility of the dissipative spin. For the noise of the real part of the

Figure 2.3.: An example of higher-order diagrams.

susceptibility we find

$$\chi_{ne,00}^{(2)}(\nu|\omega_0, \Delta\omega) = \frac{f^2\left(\frac{\pi\nu}{\Delta\omega}\right)}{32T^2} \frac{\Gamma^3\left[\omega_0^2 - 3(\Gamma^2 + \nu^2)\right]}{(\Gamma^2 + \omega_0^2)\left[(\Gamma^2 + \nu^2)^2 + 2(\Gamma^2 - \nu^2)\omega_0^2 + \omega_0^4\right]} \ . \qquad (2.48a)$$

Here, in contrast to the equilibrium contribution (2.46a), the noise of the imaginary part of the susceptibility is different from the noise of the real part. For noise of the imaginary part we obtain

$$\chi_{ne,\frac{\pi}{2},\frac{\pi}{2}}^{(2)}(\nu|\omega_0, \Delta\omega) = -\frac{f^2\left(\frac{\pi\nu}{\Delta\omega}\right)}{32T^2} \frac{\Gamma^3\left(\Gamma^2 + 5\omega_0^2 + \nu^2\right)}{(\Gamma^2 + \omega_0^2)\left[(\Gamma^2 + \nu^2)^2 + 2(\Gamma^2 - \nu^2)\omega_0^2 + \omega_0^4\right]} \ . \qquad (2.48b)$$

Finally, one can also compute the "cross-correlation" of the real and imaginary parts of the susceptibility:

$$\chi_{ne,0,\frac{\pi}{2}}^{(2)}(\nu|\omega_0, \Delta\omega) = -\frac{f^2\left(\frac{\pi\nu}{\Delta\omega}\right)}{32T^2} \frac{\omega_0\Gamma^2\left(3\Gamma^2 - \omega_0^2 + \nu^2 - 4i\Gamma\nu\right)}{(\Gamma^2 + \omega_0^2)\left[(\Gamma^2 + \nu^2)^2 + 2(\Gamma^2 - \nu^2)\omega_0^2 + \omega_0^4\right]} \ . \qquad (2.48c)$$

Note that (2.48b) is negative and (2.48a) also can take negative values. This is not a problem because these formulas have to be added to the equilibrium susceptibility noise (2.46a). For the linear response to a small external field B_0 in the high-temperature regime $1/B_0^2 \gg 1/T^2$ holds, thus the equilibrium noise is much larger than the nonequilibrium contributions and the sum of both is positive.

2.2.4. Discussion

Summarizing the findings in this section, we find that the four-spin correlation function corresponding to the noise of susceptibility vanishes if evaluated for any Gaussian fluctuating quantity. This implies that a system of harmonic oscillators (photons, phonons) would show no nonequilibrium fluctuations of susceptibility because C_χ would only contain Gaussian terms, which we have shown to be canceled exactly by the product of averages in (2.30).

As reviewed in 2.1.2, the second spectrum always contains a white Gaussian contribution, which can easily mask the interesting non-Gaussian noise. The noise of susceptibility comprises an equilibrium contribution but does not suffer from such Gaussian contributions. In experiments, the equilibrium part is distinguishable from non-Gaussian noise by its dependence on the external magnetic field (as was done in [29]). In this sense the noise of susceptibility constitutes a direct measure of non-Gaussian fluctuations.

Furthermore, we have computed the noise of susceptibility for the simple example of a single spin immersed into a dissipative bath. We find that the nonequilibrium noise tends to reduce equilibrium noise for the case of a single quantum spin 1/2.

Naturally, the concept of noise of a *single* spin might appear counter-intuitive in the context of noise problems, which usually deal with fluctuating systems composed of many degrees of freedom. Still, the connection to generic models for noise can be established simply by generalizing the results for a single spin to an ensemble of many spins which fluctuate independently.

2.3. Higher Correlations in $1/f$ Flux Noise

The main features of the experimental results on $1/f$ noise are often explained with the help of generic models of many independent fluctuators, e.g., two-level systems or paramagnetic spins [30, 38, 39]. This concept was also applied to the problem of $1/f$ flux noise in superconducting devices. There, a simple model of paramagnetic spins, discussed in Refs. [12, 13], yields for example the correct order of magnitude of the noise. Moreover, the required number of spins has been found to coincide with experimental findings of spin surface densities [27, 28].

The model consists of an ensemble of non-interacting spins, each coupled to a dissipative environment. It is assumed that the corresponding relaxation rates Γ vary with the distribution function in a certain interval between two cutoff scales Γ_L and Γ_H:

$$p(\Gamma) = \frac{1}{\ln(\frac{\Gamma_H}{\Gamma_L})} \frac{1}{\Gamma} \ . \tag{2.49}$$

This form of the distribution function can be motivated by a distribution of coupling strengths to the dissipative environments, discussed e.g. in Ref. [13].

As a single spin has the Lorentzian-shaped noise spectrum, averaging over $p(\Gamma)$ yields a $1/f$-noise spectrum of the whole system within the frequency range $\Gamma_L < f < \Gamma_H$. The resulting noise is roughly independent of temperature [13] and has the same order of magnitude as the experimental data. Weak deviations of the exponent α of the measured noise spectra $S_\phi \propto 1/f^\alpha$, as found e.g. in Refs. [9, 18, 19, 49], can be accounted for by changing the distribution function [38] to $p(\Gamma) \propto 1/\Gamma^\alpha$.

The paramagnetic model does not include any interactions between spins. As discussed in Ref. [26], typical interaction scales indeed seem to be small, of the order $J_{\text{typ}} \sim 50$ mK, justifying the approach of Refs. [12, 13] in the high-temperature regime $T > J_{\text{typ}}$. This is also consistent with the indications that the system of spins is in the classical high-temperature regime characterized by the Curie susceptibility, observed in Refs. [27, 50], and an Ohmic environment, cf. Ref. [51].

As we have argued above, the overall amount of information contained in noise spectra is strongly limited. In order to gain more information about the microscopic origin of $1/f$ flux noise, measurements of noise of susceptibility have been performed by Sendelbach *et al.*, Ref. [29], in a device specifically designed for this purpose. In Subs. 2.3.1 we derive the noise of susceptibility for the paramagnetic model from generalization of our results for a single spin presented in Subs. 2.2.3. This allows us to compare with the experimental results.

The second spectrum introduced in Subs. 2.1.2 is another tool to investigate higher correlations in the noise. In Subs. 2.3.2 we present an analysis of second spectra of $1/f$ flux

noise, which was done in collaboration with Steven Anton and John Clarke based on their extensive data on $1/f$ flux noise in SQUIDs, Ref. [52].

2.3.1. Noise of Susceptibility

A system of a large number of non-interacting spins is a natural generalization of our approach in 2.2.3. In this case, instead of the single spin 1/2 we need to consider the total spin of the system $\hat{\boldsymbol{S}} = \sum_i^N \hat{\boldsymbol{s}}_i$.

The corresponding four-point correlation function C_χ, Eq. (2.24), can be decomposed as follows:

$$C_\chi(t_1, t_1', t_2, t_2') = -\langle \mathcal{T}_K \hat{S}_z^{cl}(t_1) \hat{S}_z^q(t_1') \hat{S}_z^{cl}(t_2) \hat{S}_z^q(t_2') \rangle \tag{2.50}$$

$$= -\sum_i^N \langle \mathcal{T}_K \hat{s}_{z,i}^{cl}(t_1) \hat{s}_{z,i}^q(t_1') \hat{s}_{z,i}^{cl}(t_2) \hat{s}_{z,i}^q(t_2') \rangle$$

$$- \sum_{i \neq j}^N \langle \mathcal{T}_K \hat{s}_{z,i}^{cl}(t_1) \hat{s}_{z,i}^q(t_1') \rangle \langle \mathcal{T}_K \hat{s}_{z,j}^{cl}(t_2) \hat{s}_{z,j}^q(t_2') \rangle$$

$$- \sum_{i \neq j}^N \langle \mathcal{T}_K \hat{s}_{z,i}^{cl}(t_1) \hat{s}_{z,i}^q(t_2') \rangle \langle \mathcal{T}_K \hat{s}_{z,j}^{cl}(t_2) \hat{s}_{z,j}^q(t_1') \rangle \ .$$

Clearly, the last two lines of Eq. (2.50) do not contribute to Eq. (2.30) and therefore the noise of susceptibility of the system of independent spins is given by the sum of the individual noises of each spin

$$X_{\varphi_1, \varphi_2}^{(2)} = \sum_i \chi_{\varphi_1, \varphi_2}^{(2)}(\Gamma_i) \ . \tag{2.51}$$

Averaging over the distribution (2.49) one obtains [13, 23, 38]

$$X_{\varphi_1, \varphi_2}^{(2)} = N \int_{\Gamma_L}^{\Gamma_H} d\Gamma \, p(\Gamma) \, \chi_{\varphi_1, \varphi_2}^{(2)}(\Gamma) \ . \tag{2.52}$$

Using our single spin results (2.46) and (2.48) we can now obtain the noise of susceptibility in the model of non-interacting spins. In the limit, where the probing frequency ω_0 is much smaller than the slowest relaxation rate of the spins $\omega_0 \ll \Gamma_L$ we find

$$X_{0,0}^{(2)} \approx \frac{N}{4\Gamma_L} \left[\frac{2}{B_0^2} - \frac{3}{8T^2} \right] f^2 \left(\frac{\pi\nu}{\Delta\omega} \right) \ln^{-1} \frac{\Gamma_H}{\Gamma_L} \ , \tag{2.53}$$

$$X_{\frac{\pi}{2}, \frac{\pi}{2}}^{(2)} \approx \frac{N}{4\Gamma_L} \left[\frac{2}{B_0^2} - \frac{1}{8T^2} \right] f^2 \left(\frac{\pi\nu}{\Delta\omega} \right) \ln^{-1} \frac{\Gamma_H}{\Gamma_L} \ , \tag{2.54}$$

$$X_{0, \frac{\pi}{2}}^{(2)} \approx -\frac{N\omega_0}{4\Gamma_L^2} \left[\frac{3}{16T^2} + \frac{i\nu}{\Gamma_L} \left(\frac{4}{3B_0^2} - \frac{1}{6T^2} \right) \right] f^2 \left(\frac{\pi\nu}{\Delta\omega} \right) \ln^{-1} \frac{\Gamma_H}{\Gamma_L} \ . \tag{2.55}$$

That is, for $\omega_0 \ll \Gamma_L$ the noise of the real part and of the imaginary part are independent of the frequency ω_0.

In the opposite limit $\Gamma_L \ll \omega_0 \ll \Gamma_H$, which is the relevant limit for the paramagnetic model, we obtain

$$X_{0,0}^{(2)} \approx \frac{\pi N}{4\omega_0} \left[\frac{1}{B_0^2} - \frac{1}{16T^2} \right] f^2 \left(\frac{\pi\nu}{\Delta\omega} \right) \ln^{-1} \frac{\Gamma_H}{\Gamma_L} \; , \tag{2.56}$$

$$X_{\frac{\pi}{2},\frac{\pi}{2}}^{(2)} \approx \frac{\pi N}{4\omega_0} \left[\frac{1}{B_0^2} - \frac{1}{16T^2} \right] f^2 \left(\frac{\pi\nu}{\Delta\omega} \right) \ln^{-1} \frac{\Gamma_H}{\Gamma_L} \; , \tag{2.57}$$

$$X_{0,\frac{\pi}{2}}^{(2)} \approx -\frac{N}{4\omega_0} \left[\frac{1}{16T^2} + \frac{i\pi\nu}{\omega_0} \left(\frac{1}{B_0^2} - \frac{1}{16T^2} \right) \right] f^2 \left(\frac{\pi\nu}{\Delta\omega} \right) \ln^{-1} \frac{\Gamma_H}{\Gamma_L} \; . \tag{2.58}$$

These formulas show a $1/\omega_0$ behavior. For small fields and large temperatures $B_0 \ll T$ the equilibrium contributions always dominate, since $1/B_0^2 \gg 1/T^2$. The real part of the cross-correlation noise $X_{0,\frac{\pi}{2}}^{(2)}$ is purely given by nonequilibrium contributions. The results for noises of real and imaginary susceptibility show that the overall noise is reduced due to the nonequilibrium terms. Note that all of the above formulas are linear in the total number of spins N.

We may compare the above results with experimental observations by Sendelbach *et al.*, Ref. [29]. First of all, susceptibility noise spectra indeed showed the equilibrium contributions, easily identified by the $1/B_0^2$ behavior. Beyond this rather trivial observation, the authors reported nonequilibrium contributions to noise of susceptibility roughly proportional to $1/\nu$ at low frequencies. In the relevant low frequency regime $\nu \ll \Delta\omega$ it is $f^2 \left(\frac{\pi\nu}{\Delta\omega} \right) \approx 1$. Thus, results displayed above do not show $1/\nu$ behavior. Moreover, the experiment shows non-vanishing correlations between the fluctuations of flux and susceptibility. As the model of independent spins remains invariant under time reversal, such correlations are excluded in this theory. We conclude that the observations of Sendelbach *et al.* are inconsistent with the model of independent paramagnetic spins.

In Ref. [29], the magnitude of single jumps of the susceptibility was found to be comparable to or even larger than the thermal susceptibility average given by the Curie susceptibility $\chi \propto 1/T$. This is another feature in conflict with the simple model. In our results for the simple model above, the nonequilibrium noise scales as N/T^2. Thus the typical magnitude of fluctuations is $\sqrt{N}/T$. At the same time the average susceptibility itself scales as N/T, i.e., the fluctuations of the susceptibility in the simple model are small compared to the average value.

The authors of Ref. [29] interpreted the observed rich structure in fluctuations of the inductance in terms of complex, cooperative dynamics of spin clusters. The deliberately designed devices and the experimental setup were similar but slightly different to typical SQUID setups for flux noise measurements. Unfortunately, the results have never been reproduced by other groups and so far no conclusive microscopic picture has been developed.

2.3.2. Second Spectra of 1/f Flux Noise

The measurements by Sendelbach *et al.* naturally pose the question of similar $1/\nu$-like signatures in the second spectrum of flux noise. Here we address this issue in some detail and compare to experimental data on flux noise in SQUIDs obtained by Steven Anton and John Clarke at University of California, Berkeley. Steven Anton *et al.* carried out extensive

measurements of flux noise of a couple of different SQUIDs. Their data allowed to investigate the second spectra. For details of the measurement setup we refer to Refs. [53, 54]. This work was done in collaboration with Steven Anton and John Clarke, Ref. [52].

The second spectrum was introduced in Eqs. (2.5) and (2.6). To obtain the second spectrum of a spin system, we have to replace the classical four-point correlator $C_x^{(4)}$ related to the second spectrum by Eq. (2.6) with the corresponding symmetric four-spin correlator. The second spectrum of magnetization fluctuations $S_M^{(2)}(\nu|\omega_0, \Delta\omega)$ can be decomposed into the Gaussian and the non-Gaussian part

$$S_M^{(2)}(\nu|\omega_0, \Delta\omega) = S_{M,G}^{(2)}(\nu|\omega_0, \Delta\omega) + S_{M,NG}^{(2)}(\nu|\omega_0, \Delta\omega) \ . \tag{2.59}$$

According to Eqs.(2.11) and (2.19) the Gaussian contribution to the second spectrum of magnetization fluctuations is

$$S_{M,G}^{(2)}(\nu|\omega_0, \Delta\omega) \approx \frac{\Delta\omega}{\pi} \ (S_M(\omega_0))^2 \ . \tag{2.60}$$

In the model of independent paramagnetic spins the power spectrum $S_M(\omega_0)$ is easily obtained from $S_{M,\Gamma}(\omega)$ by integration with the distribution $p(\Gamma)$, Eqs. (2.45) and (2.49). Since $S_M(\omega_0) \propto N$, it is clear that $S_{M,G}^{(2)} \propto N^2$. Any non-Gaussian contributions $S_{M,NG}^{(2)}$ can be calculated similarly to the noise of susceptibility above, therefore $S_{M,NG}^{(2)} \propto N$. Thus, the Gaussian part dominates for large numbers N of spins and constitutes the only contribution that survives in the thermodynamic limit $N \to \infty$.

However, it is known that fluctuations in interacting spin systems can display non-Gaussian $1/\nu$-like behavior in the second spectrum, cf. Refs. [40, 55]. Nguyen and Girvin used second spectra to investigate non-Gaussian noise in quantum spin glass models in Ref. [55]. These authors demonstrate the existence of a model for which the non-Gaussian contribution $S_{M,NG}^{(2)}$ survives the limit $N \to \infty$, implying that $S_{M,NG}^{(2)} \propto N^2$ is generally possible. The special feature of this model is a "dilatation" term, which establishes infinite-range correlated fluctuations. In this sense non-Gaussian contributions $S_{M,NG}^{(2)}$ measure the degree of correlation amongst spin fluctuations.

In order to compare with experimental results of flux noise we switch from angular frequencies $\nu, \omega_0, \Delta\omega$ to ordinary frequencies $f_2, f_1, \Delta f_1$,

$$f_2 = 2\pi\nu \ , \quad f_1 = 2\pi\omega_0 \ , \quad \Delta f_1 = 2\pi\Delta\omega \ . \tag{2.61}$$

The plots of the experimental data show the second spectrum of flux noise, in units of $[(\Phi_0)^2/\text{Hz}]^2/\text{Hz}$ with the flux quantum Φ_0. The plotted second spectra are related to the magnetization noise defined above by

$$S_\Phi^{(2)}(f_2 \mid f_1, \Delta f_1) = \frac{c_{\Phi M}}{(\Delta f_1)^2} \ S_M^{(2)}(\nu \mid \omega_0, \Delta\omega) \ . \tag{2.62}$$

Here, $c_{\Phi M}$ is a constant which establishes the correct experimental units. The value of $c_{\Phi M}$ is not relevant here, details can be found e.g in Refs. [12, 56]. The Gaussian contribution to the second spectrum of flux noise is deduced to be

$$S_{\Phi,G}^{(2)}(f_2 \mid f_1, \Delta f_1) = 2\frac{(S_\Phi(f_1))^2}{\Delta f_1} \ , \tag{2.63}$$
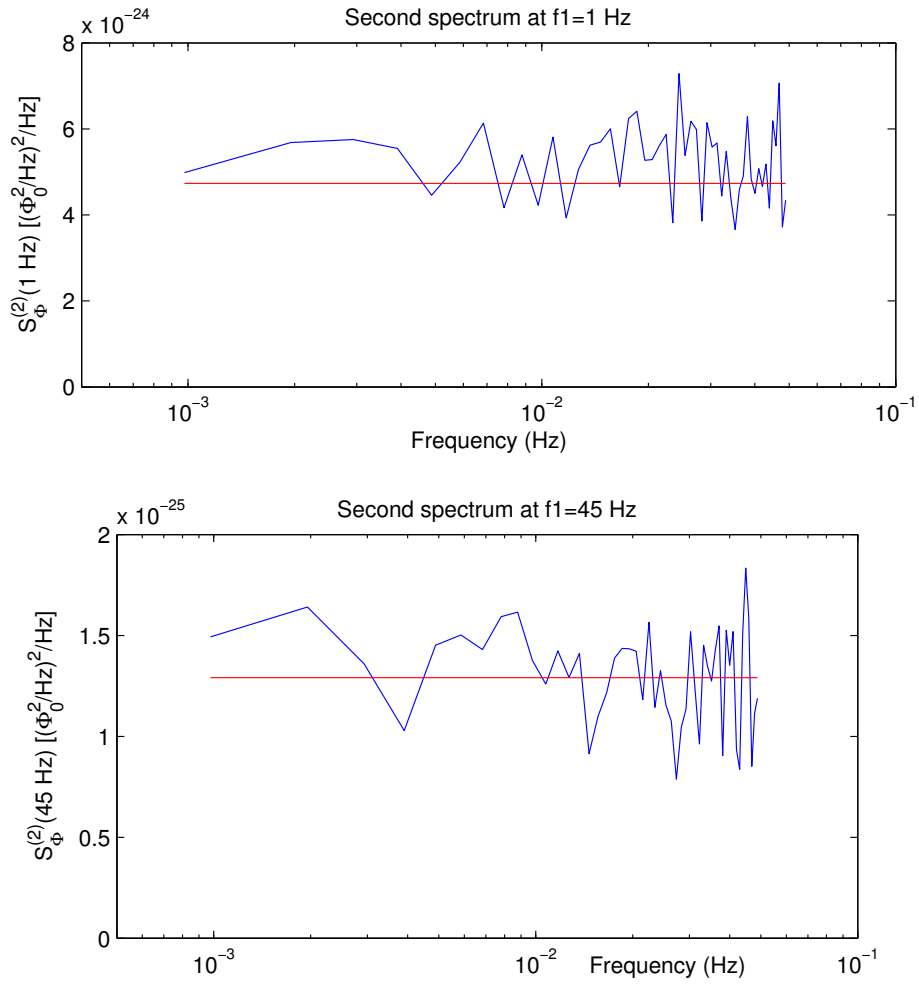
Figure 2.4.: Second spectra of SQUID flux noise measurements at $f_1 = 1$ Hz and $f_1 = 45$ Hz as a function of the slow frequency f_2. The constant red line indicates the Gaussian noise level given by Eq. (2.63). Courtesy of Steven Anton and John Clarke, UCB, Ref. [52].

its constant value is indicated by the red line in Figs. 2.4.

The second spectra of flux noise of ten different SQUIDs have been analyzed, for details on the devices and the experimental setup we refer to Refs. [53, 54]. As representative figures we show Figs. 2.4. The overall noise levels of obtained second spectra can be entirely explained in terms of the Gaussian contribution and signatures of $1/f_2$ have not been observed. This implies that in these samples spin-spin correlations between spins are rather weak. In this sense, the observed second spectra are consistent with the model of independent spins, in which spin fluctuations are completely uncorrelated.

2.3.3. Discussion

Recalling the discussion in Subs. 2.3.1 it is clear that the experimental results of Sendelbach *et al.*, Ref. [29], cannot be explained by the generic simple model of independent spins. In contrast, the second noise spectra obtained by the Clarke group are consistent with such a model.

The large fluctuations in Ref. [29] were interpreted in terms of fluctuations of spin clusters which show collective behavior. Such clusters can arise in the formation of spin glasses. Experiments in the 80's applied the concept of second spectra to measurements of materials showing spin glass behavior, cf. Refs. [38, 39] and references therein. Some of these experiments identified non-Gaussian contributions to the second spectra. It has been reported that the non-Gaussian contributions were only observed in material samples smaller than a certain size, cf. Ref. [39]. For larger samples, the second spectra were found to be dominated by the Gaussian contribution, similar to our observations for $1/f$ flux noise in Subs. 2.3.2. In turn, assuming that $1/f$ flux noise is related to spin glass physics, the size-dependence of second spectra in Ref. [39] suggests that non-Gaussian contributions could be observed in small-sized SQUIDs.

Clearly, for the case of spin glasses correlations are important and the model of independent spins is not applicable. However, a similar model, where independent spins are replaced by spin clusters or droplets, is indeed relevant in the context of spin glasses. In this model, spin droplets can effectively be described as two-level systems and still fluctuate independently, cf. Refs. [38, 39]. Thus, our results for noise of susceptibility in Subs. 2.3.1 imply that such a non-interacting droplet model cannot explain the susceptibility fluctuations observed in Ref. [29], too. Possible generalizations could include crystal fields as well as dynamics and temperature dependence of droplet formation, which is beyond the scope of this thesis.

Based on numerical analysis of two-dimensional Heisenberg spin glasses, Atalaya *et al.* in Ref. [57] studied the possible role of clusters for $1/f$ flux noise. The authors concluded that rarely occuring large clusters are responsible for low-frequency $1/f$ flux noise. The analysis also suggested that the contribution of rare large clusters to the overall susceptibility is small and that the susceptibility is dominated by the much larger number of small clusters. Within this rather phenomenological picture one could argue that fluctuations of susceptibility arise in a natural way. Namely, the small clusters are exposed to the slowly fluctuating crystal fields of the large clusters. The fluctuating crystal fields affect the susceptibilities of the small clusters, inducing fluctuations of the overall susceptibility on the slow time scale of the large clusters. It is unclear whether such a scenario would give rise to significantly large low-frequency susceptibility fluctuations, and, whether it

could account for the experimental results of Ref. [29]. This is an interesting problem for future studies.

2.4. Conclusion

In this chapter we have analyzed higher-order correlations in fluctuating spin systems. A long-known measure for higher-order correlations is the second spectrum, which is often dominated by a trivial Gaussian contribution. More recent experiments, Ref. [29], introduced the noise of susceptibility as an alternative measure of higher-order correlations. Based on the experimental measurement protocol, we have derived Wiener-Khinchin-like relations between the experimentally accessible noise of susceptibility and a particular four-spin correlation function in Subs. 2.2.2. These relations have not been existent in the literature so far. In contrast to the second spectrum, noise of susceptibility constitutes a direct measure of non-Gaussian fluctuations.

As a simple example, we have presented results for the noise of susceptibility of a single spin immersed into a dissipative bath. The calculation of the corresponding four-spin correlation function turned out to be a rather complicated task. We have been able to obtain controlled analytic results within a particular approach based on the Majorana representation for spin 1/2. The approach relies on two main ingredients. First, a special property of the Majorana representation, which will be introduced subsequently to the representation itself in Ch. 3. Second, the path-integral formulation presented in Ch. 6, which has allowed us to show that the results presented above are indeed a valid approximation for the four-spin correlator.

On the experimental side, the concept of noise of susceptibility was introduced as a new measure to study properties of $1/f$ flux noise in SQUIDs. Our results for a single spin have allowed us to obtain the noise of susceptibility of a generic, simple model of independent spins, which appears to be relevant in the context of $1/f$ flux noise. The discrepancy with experimental results confirms that the model of independent spins is unable to explain main features of $1/f$ flux noise. We also analyzed second spectra of $1/f$ flux noise, which we have found to be rather inconclusive due to the large Gaussian contributions.

3. Majorana Representation for Spin 1/2

This chapter introduces the Majorana method as a powerful approach to spin correlation functions, providing the basis for the studies in the remainder of the thesis. Crucial to this method is the Martin transformation, which expresses spin operators in terms of Majorana fermion operators. We show that, in contrast to other representations, the Majorana representation does not suffer from complications due to enlargement of the spin Hilbert space. Generally, auxiliary particle representations allow to express N-point spin correlation function in terms of $2N$-point correlation functions of the auxiliary particles. A crucial advantage of the Majorana representation is that a certain class of N-point spin correlation functions, pairwise correlation functions, can be reduced to N-point Majorana correlators.

We start this chapter by introducing the Majorana representation of spin operators. We show explicitly that spin-spin correlation functions can be directly calculated from Majorana correlation functions despite the enlargement of the Hilbert space. This is a significant advantage of the Majorana representation over other techniques. We discuss and generalize a particularly simple correspondence between pairwise spin correlation functions and Majorana correlation functions, which is another significant advantage of the Majorana representation. In Section 3.2 we recapitulate basic concepts required for the calculations in subsequent chapters and apply the findings of Section 3.1 to finite-temperature and real-time Green's functions within the path-integral framework. The findings presented in this chapter have been published in

> Pablo Schad, Yurij Makhlin, Boris N. Narozhny, Gerd Schön, and
> Alexander Shnirman
> "Majorana representation for dissipative spin systems"
> *Annals of Physics* 361, 401 – 422 (2015).

3.1. The Majorana Representation

To understand properties of microscopic models one has to calculate correlation functions. Usual fermionic and bosonic systems allow for direct application of field-theoretic methods on the basis of Wick's theorem. Wick's theorem reduces arbitrary products of bosonic or fermionic operators to sums of products of pairs. This is the starting point for Green's functions methods and Feynman diagram techniques in field theories as discussed in many textbooks, e.g. Ref. [46].

For spin operators, there is no Wick's theorem. The reason for that is the complicated,

non-Abelian nature of spin operators, which is reflected by the commutation relations of
the SU(2) algebra,

$$\left[\hat{S}_\alpha, \hat{S}_\beta\right] = i\epsilon_{\alpha\beta\gamma}\hat{S}_\gamma \, , \qquad \alpha, \beta, \gamma = \{x, y, z\} \, . \tag{3.1}$$

Thus, in contrast to fermionic or bosonic operators, the product of two spin operators
cannot be contracted to a c-number, which is equivalent to the statement that there is no
Wick's theorem. Generally, one can develop diagrammatic expansions for spin operators
on the basis of (3.1). However, such approaches are rather complicated, cf. Ref. [58] and
references therein.

The more successful recipe is to map the spins onto a system of auxiliary particles, either
bosons or fermions, enabling the application of Wick's theorem and the use of standard
field theory methods. There are a couple of options to construct such mappings, cf.
Refs. [58, 59], which primarily have to reproduce the spin commutation relations (3.1).
Mostly, these include the Jordan–Wigner transformation, Ref. [60], the Holstein–Primakoff
transformation, Ref. [61], the Martin Majorana–fermion representation, Ref. [7], the drone-
fermion representation, Refs. [62, 63], the Abrikosov–fermion representation, Ref. [4], the
semi-fermionic Popov–Fedotov representation, Ref. [64], as well as the Schwinger-boson
representation, cf. Refs. [65–68], and slave-fermion techniques, e.g. Refs. [69–74]. The
choice of a formulation often depends on the specific problem. For example, the Holstein-
Primakoff transformation is well-suited to describe spin-wave excitations in ferromagnetic
systems. The Jordan-Wigner transformation is a faithful fermionic representation as it
preserves the spin Hilbert space, though restricted to one-dimensional spin chains.[1]

Apart from the Jordan–Wigner transformation all representations express the spin operators
in terms of bilinears of fermionic or bosonic operators, cf. e.g. Refs. [58, 59]. This operator
"doubling" is connected to an enlargement of the target Hilbert space, i.e. the fermionic
or bosonic Hilbert space is larger than the original spin Hilbert space. Most of the
bilinear representations suffer from unphysical states in the target Hilbert space and require
additional constraints, cf. Refs. [68, 74], or projection procedures, cf. Ref. [4, 58], which
also complicate the calculations.

In this work we choose to use the Martin–Majorana representation for spin 1/2, which
bears significant advantages over other techniques. In Subs. 3.1.2 we show that the
Majorana representation does not suffer from Hilbert space complications. Furthermore,
in contrast to other bilinear representations the Majorana representation allows to avoid
the "vertex problem" as will be discussed in Subsections 3.1.3 and 3.1.4. In contrast to
other representations direct application of the Majorana representation is restricted to the
case of spin 1/2. In order to treat spins of quantum numbers larger than 1/2 within the
Majorana representation these have to be constructed from spins 1/2.

3.1.1. The Martin Transformation

The Majorana representation of the spin-1/2 operators was introduced by Martin in 1959
in Ref. [7] and has been applied to a wide range of condensed matter problems, e.g. Kondo
lattice models, Refs. [77–81] spin chains, Ref. [82], Kondo models, Refs. [5, 77, 83, 84],

---

[1]The Jordan-Wigner representation can be generalized to higher dimensions, but it then lacks the simplicity
of the original approach, cf. Refs. [75, 76]

as well as spin-boson models, Refs. [85, 86]. More recently, the representation has been used extensively in the context of spin lattice models, especially with regard to the search for solvable models as well as spin-liquid ground states, cf. Refs. [87, 88] and references therein.

Operators $\hat{S}_\alpha$ of spin 1/2 can be replaced by Majorana operators $\hat{\eta}_\alpha$ through the Martin transformation

$$\hat{S}_\alpha = -\frac{i}{2}\epsilon_{\alpha\beta\gamma}\hat{\eta}_\beta\hat{\eta}_\gamma \ . \tag{3.2}$$

The above equations were derived in the framework of generalized classical dynamics, in particular, the Grassmann variant of classical mechanics, cf. Refs. [7, 89, 90]. Grassmann variables are anticommuting variables, i.e., they obey fermionic anticommutation relations. The canonical quantization of canonical Grassmann phase-space variables replaces the Poisson brackets by the anticommutator of the corresponding operators, which is the Clifford algebra, Eq. (3.3). The Majorana operators above obey such a Clifford algebra,[2]

$$\{\hat{\eta}_\alpha, \hat{\eta}_\beta\} \equiv \hat{\eta}_\alpha\hat{\eta}_\beta - \hat{\eta}_\beta\hat{\eta}_\alpha = \delta_{\alpha\beta} \ , \qquad \hat{\eta}_\alpha^2 = 1/2 \ . \tag{3.3}$$

The above relations allow to recast Eq. (3.2) into

$$\hat{S}_x = -i\hat{\eta}_y\hat{\eta}_z \ , \quad \hat{S}_y = -i\hat{\eta}_z\hat{\eta}_x \ , \quad \hat{S}_z = -i\hat{\eta}_x\hat{\eta}_y \ . \tag{3.4}$$

The Majorana operators $\hat{\eta}_\alpha$ are real, cf. Ref. [59], in the sense that they satisfy

$$\hat{\eta}_\alpha^\dagger = \hat{\eta}_\alpha \ , \tag{3.5}$$

in contrast to usual complex or Dirac fermion operators. The above relation is often interpreted by saying creation and annihilation operators are equal. However, it prohibits the straightforward construction of a Fock space based on occupation numbers. The representation (3.2) exhibits a discrete Z_2 symmetry, which is seen by transforming $\hat{\eta}_\alpha \to -\hat{\eta}_\alpha$, cf. Ref [59].

The properties of spin 1/2 operators are exactly reproduced by the representation (3.2). It can be checked that the spin commutation relations are satisfied:

$$\left[\hat{S}_x, \hat{S}_y\right] = [-i\hat{\eta}_y\hat{\eta}_z, -i\hat{\eta}_z\hat{\eta}_x] = \hat{\eta}_x\hat{\eta}_y = i\hat{S}_z \ , \tag{3.6}$$

etc. The normalization (3.3) guarantees that $(\hat{S}_\alpha)^2 = 1/4$ and $\hat{\boldsymbol{S}}^2 = 3/4$ as required. The fact that $\hat{\boldsymbol{S}}^2 = 3/4$ directly implies that all Majorana states are physical, in contrast to other fermionic and bosonic representations. Furthermore, the Majorana representation (3.2) explicitly preserves the spin-rotation symmetry. This is an advantage of the Majorana representation over the similar drone-fermion representation, cf. Refs. [6, 62, 63, 91], which can be related to the Majorana representation by transforming Majorana fermions $\hat{\eta}_x, \hat{\eta}_y$ into one complex Dirac fermion. As a result spin projections are not treated on an equal footing which suggests that spin-rotation invariance is violated, cf. Ref. [82].

It is known from the theory of representations of the Clifford algebra (3.3) that, in case of an odd number of generators $2m + 1$, the irreducible matrix representation has the

---

[2]It is possible to use a different normalization of the Majorana operators, $\hat{\eta}^2 = 1$, as e.g. in Ref. [6]. This only changes some numerical prefactors at intermediate stages of the calculation.

dimensionality $d = 2^m$, cf. Refs. [59, 82, 90]. That is, the Hilbert space of three Majorana operators is at least four-dimensional and thus larger than the original spin space. The doubling of the original spin Hilbert space can be interpreted in terms of two copies of the original spin, cf. Refs. [6, 78, 82]. As a result, the spin states in the Majorana representation are degenerate, cf. Ref. [82]. However, this does not affect calculations since bilinear products of Majoranas do not switch between the spin copies. In Ref. [78], it is argued that the two copies reflect the Z_2 gauge symmetry.

The Hilbert space of Majorana fermions can be constructed explicitly by combining real Majorana fermions to complex Dirac fermions, as discussed e.g. in Ref. [92]. The Majorana Hilbert space then corresponds to the Fock space of Dirac fermions. This procedure is not unique as there are several options for such combinations. In order to combine the three Majorana fermions $\hat{\eta}_x$, $\hat{\eta}_y$ and $\hat{\eta}_z$ into Dirac fermions one has to add at least one more Majorana fermion to get an even number of Majorana fermions. If we add just one Majorana fermion $\hat{m}_0$ we can construct two Dirac fermions $\hat{c}_1, \hat{c}_2$ e.g. by

$$\hat{c}_1 = \frac{\hat{\eta}_x + i\hat{\eta}_y}{\sqrt{2}} \ , \qquad \hat{c}_2 = \frac{\hat{\eta}_z + i\hat{m}_0}{\sqrt{2}} \ . \tag{3.7}$$

This procedure is similar to the long-known drone fermion representation, cf. Refs. [62, 63, 91]. Within the construction (3.7) the "two-copy" concept can be demonstrated explicitly, cf. Ref. [6]. The Fock space of the two Dirac fermions $\hat{c}_1, \hat{c}_2$ is four-dimensional, larger than the original two-dimensional Hilbert space of the spin.

However, an alternative option is to construct three Dirac fermions, one out of each Majorana fermion, by adding three more Majorana fermions. This procedure explicitly preserves spin isotropy and yields an eight-dimensional Fock space. It can be shown, Ref. [93], that the eight-dimensional Hilbert space is spanned by eigenstates of spin operators, suggesting that the eight-dimensional Hilbert space can be interpreted as four copies of the original spin Hilbert space.

We conclude that the Hilbert space of Majorana fermions $\hat{\eta}_x, \hat{\eta}_y, \hat{\eta}_z$ is larger than the original spin Hilbert space, and, in addition, it is not unique but rather depends on the explicit construction. Now, one should check whether this issue complicates the calculation of spin correlation functions in the Majorana representation (3.2). Several authors have addressed this issue arguing that additional states factorize out, cf. Ref. [82], or that they are removed by fixing the above mentioned Z_2 gauge invariance, cf. Ref. [59]. At the same time, we find it more instructive to demonstrate the correspondence of spin and Majorana correlation functions directly.

3.1.2. Spin Correlation Functions in the Majorana Representation

Here we show explicitly that correlation functions of spin-1/2 operators are directly equivalent to correlation functions of Majorana operators, which are obtained through the Martin transformation (3.2). In particular, we find that this equivalence is independent of the Majorana Hilbert space dimension, that is, it is valid for any explicit construction of the Majorana Hilbert space.

As a starting point let us discuss a special relation of spin-1/2 operators central to our line of reasoning below. In a specific basis, the operators of a spin 1/2 can be represented by

Pauli matrices σ_α. Pauli matrices, in turn, obey anti-commutator relations $\{\sigma_\alpha, \sigma_\beta\} = 2\delta_{\alpha\beta}$, which is inherited by the spin operators. That is, the commutator and anti-commutator relations of spin 1/2 are

$$\left[\hat{S}_\alpha, \hat{S}_\beta\right] = \hat{S}_\alpha\hat{S}_\beta - \hat{S}_\beta\hat{S}_\alpha = i\epsilon_{\alpha\beta\gamma}\hat{S}^\gamma \quad \text{and} \tag{3.8}$$

$$\left\{\hat{S}_\alpha, \hat{S}_\beta\right\} = \hat{S}_\alpha\hat{S}_\beta + \hat{S}_\beta\hat{S}_\alpha = \frac{1}{2}\delta_{\alpha\beta} . \tag{3.9}$$

By adding the above two equations and dividing by a factor of 1/2 it becomes obvious that spin operators obey the relation

$$\hat{S}_\alpha\hat{S}_\beta = \frac{i}{2}\epsilon_{\alpha\beta\gamma}\hat{S}^\gamma + \frac{1}{4}\delta_{\alpha\beta} , \tag{3.10}$$

which reduces a product of two spin-1/2 operators to a linear expression of spin-1/2 operators. A product of three operators can be reduced by (3.10) to a product of two and, again by (3.10), to a linear expression. That is, by iterating (3.10) it follows that *any product of spin-1/2 operators is in fact a linear function.* Explicitly,

$$\hat{S}^{\alpha_1} \dots \hat{S}^{\alpha_n} = a_\alpha\hat{S}^\alpha + a_0, \qquad a_0, a_x, a_y, a_z \in \mathbb{C} . \tag{3.11}$$

The complex numbers a_0, a_x, a_y and a_z depend on the particular sequence $\{\alpha_i\}$. Since spin operators are traceless, the trace over the 2-dimensional ($d_S = 2$) spin Hilbert space Tr_S of (3.11) is given by the constant term a_0 multiplied by the dimension of the spin Hilbert space $d_S = 2$,

$$\text{Tr}_S\left\{\hat{S}^{\alpha_1} \dots \hat{S}^{\alpha_n}\right\} = d_S \, a_0(\alpha_1, ..., \alpha_n) . \tag{3.12}$$

As discussed in the preceding subsection 3.1.1, the Martin transformation (3.2) exactly reproduces the spin commutation relations. Hence, if spin operators in (3.10) and (3.11) are replaced by Majorana bilinears via (3.2), both equations remain valid. In particular, the coefficients a_α, a_0 remain the same. Irrespective of the explicit construction of the Majorana Hilbert space, the trace over Majorana bilinears vanishes due to (*a*) fermionic anti-commutation relations and (*b*) invariance of the trace under cyclic permutations, e.g.

$$\text{Tr}_M\{\hat{\eta}_y\hat{\eta}_z\} \overset{(a)}{=} -\text{Tr}_M\{\hat{\eta}_z\hat{\eta}_y\}$$
$$\overset{(b)}{=} +\text{Tr}_M\{\hat{\eta}_z\hat{\eta}_y\} \quad \Rightarrow \quad \text{Tr}_M\{\hat{\eta}_y\hat{\eta}_z\} = 0 . \tag{3.13}$$

Thus, the trace over Equation (3.11) in the Majorana representation (3.2) is given by

$$\text{Tr}_M\left\{\hat{S}^{\alpha_1} \dots \hat{S}^{\alpha_n}\right\} = d_M \, a_0(\alpha_1, ..., \alpha_n), \tag{3.14}$$

where d_M is the dimension of the Majorana Hilbert space and a_0 is the same complex number as in (3.12). Thus, *tracing an arbitrary product of the spin-1/2 operators over the spin and Majorana Hilbert spaces yields the same result up to a numerical factor, determined by the dimensionalities of the Hilbert spaces.*

The above statement can be readily generalized to an arbitrary ensemble of spins. Indeed, any function of spin operators is still linear in the components of each spin. If the operators on the left-hand side of Eq. (3.11) describe more than one spin, then on the right-hand side additional terms appear, which contain all possible products of operators related to

different spins. For example, in the case of two spins the right-hand side of Eq. (3.11) is replaced by

$$a_0 + a_\alpha \hat{S}_1^\alpha + b_\alpha \hat{S}_2^\alpha + c_{\alpha\beta} \hat{S}_1^\alpha \hat{S}_2^\beta \ . \tag{3.15}$$

However, all such additional terms are still traceless, and hence the only change in Equations (3.12) and (3.14) will be in the constants d_S and d_M.

Generally, we are interested in the dynamics of spins which couple to other systems. The spin dynamics is described by auto-correlation functions

$$\langle \hat{S}^{\alpha_1}(t_1) \dots \hat{S}^{\alpha_n}(t_n) \rangle \equiv \frac{\mathrm{Tr}\left\{\hat{S}^{\alpha_1}(t_1) \dots \hat{S}^{\alpha_n}(t_n)\hat{\rho}\right\}}{\mathrm{Tr}\left\{\hat{\rho}\right\}}, \tag{3.16}$$

where $\hat{\rho} = \exp(-\beta\hat{H})$ is the non-normalized Gibbs density matrix. The Hamiltonian $\hat{H}[\hat{\boldsymbol{S}}, X]$ can contain terms which couple the spin to degrees of freedom of other systems, denoted collectively by X (In Chapters 4, 5 and 6 we consider the case of a spin coupled to bosonic degrees of freedom).

The density matrix exponential can be reduced by (3.11), which allows us to write $\hat{\rho} = \hat{\rho}_0(X) + \hat{S}^\alpha\hat{\rho}_\alpha(X)$, where $\hat{\rho}_0(X)$ and $\hat{\rho}_\alpha(X)$ are matrices in the X space. Moreover, $\hat{\rho}_0(X)$ is the reduced density matrix describing the rest of the system, i.e., the X-degrees of freedom. The general expression $Z = \mathrm{Tr}\{\hat{\rho}\}$ for the partition function Z can be simplified by separating the traces and decomposing the density matrix,

$$\mathrm{Tr}\left\{\hat{\rho}\right\} = \mathrm{Tr}_\mathrm{X}\mathrm{Tr}_\mathrm{S}\left\{\hat{\rho}\right\} = \mathrm{Tr}_\mathrm{X}\mathrm{Tr}_\mathrm{S}\left\{\hat{\rho}_0(X) + \hat{S}^\alpha\hat{\rho}_\alpha(X)\right\} = d_s\mathrm{Tr}_\mathrm{X}\left\{\hat{\rho}_0(X)\right\} \ . \tag{3.17}$$

Time-dependent spin operators $\hat{S}^{\alpha_i}(t_i)$ are operators in the Heisenberg picture. They are related to the time-independent Schrödinger operators (i.e., the Pauli matrices) by the time evolution operator $\hat{U}(t, t') = \exp[-i\int_{t'}^t d\tau \hat{H}(\tau)]$. Similarly to the density matrix, the exponentials in the time evolution operator can be converted to a linear expression of spin operators by (3.11). As a result, we obtain a generalized version of (3.11),

$$\hat{S}^{\alpha_1}(t_1) \dots \hat{S}^{\alpha_n}(t_n)\hat{\rho} = \hat{A}_0(X) + \hat{S}^\alpha\hat{A}_\alpha(X) \ , \tag{3.18}$$

where $\hat{A}_0(X)$ and $\hat{A}_\alpha(X)$ are matrices in X-space. With the use of Equations (3.17) and (3.18), we can formally perform the trace over the spin variables in the auto-correlation function (3.16). We find

$$\langle \hat{S}^{\alpha_1}(t_1) \dots \hat{S}^{\alpha_n}(t_n) \rangle_\mathrm{S} = \frac{\mathrm{Tr}_\mathrm{X}\mathrm{Tr}_\mathrm{S}\left\{\hat{A}_0(X) + \hat{S}^\alpha\hat{A}_\alpha(X)\right\}}{d_\mathrm{S}\mathrm{Tr}_\mathrm{X}\left\{\hat{\rho}_0(X)\right\}} = \frac{\mathrm{Tr}_\mathrm{X}\left\{\hat{A}_0(X)\right\}}{\mathrm{Tr}_\mathrm{X}\left\{\hat{\rho}_0(X)\right\}} \ , \tag{3.19}$$

and observe that the dimension $d_\mathrm{S} = 2$ of the spin Hilbert space cancels out.

In the Majorana representation, where spin operators are replaced by Majorana bilinears according to (3.2), the trace over the density can be evaluated analogously to (3.17), only the Hilbert space dimension d_S has to be replaced by d_M as in Eq. (3.14). Also, Equation (3.18) holds. Therefore, spin auto-correlation functions in the Majorana representation can be formally calculated by

$$\langle \hat{S}^{\alpha_1}(t_1) \dots \hat{S}^{\alpha_n}(t_n) \rangle_\mathrm{M} = \frac{\mathrm{Tr}_\mathrm{X}\mathrm{Tr}_\mathrm{M}\left\{\hat{A}_0(X) + \hat{S}^\alpha\hat{A}_\alpha(X)\right\}}{d_M\mathrm{Tr}_\mathrm{X}\left\{\hat{\rho}_0(X)\right\}} = \frac{\mathrm{Tr}_\mathrm{X}\left\{\hat{A}_0(X)\right\}}{\mathrm{Tr}_\mathrm{X}\left\{\hat{\rho}_0(X)\right\}} \ , \tag{3.20}$$

which is identical to Eq. (3.19). As discussed above, the generalization to the case of multi-spin correlation functions is straightforward.

Thus, we have demonstrated that

$$\langle \hat{S}^{\alpha_1}(t_1) \ldots \hat{S}^{\alpha_n}(t_n)\rangle_{\mathrm{S}} = \langle \hat{S}^{\alpha_1}(t_1) \ldots \hat{S}^{\alpha_n}(t_n)\rangle_{\mathrm{M}} \ . \tag{3.21}$$

We conclude that spin correlation functions can be calculated with the help of the Majorana representation (3.2) without any projection onto "physical" states.

We note that a similar discussion was provided by Spencer and Doniach in Ref. [91] in the context of the drone-fermion representation.

3.1.3. Simple Correspondence of Pairwise Spin and Majorana Correlation Functions

Here we discuss a particular feature of the Majorana representation discovered independently by Mao, Coleman, Hooley and Langreth in Ref. [5] and Shnirman and Makhlin in Ref. [6], which is the second significant advantage of the Majorana representation. We review and generalize the findings of these authors.

As discussed above, most fermionic or bosonic techniques use bilinears of auxiliary fermionic or bosonic operators to represent the spin operators. In turn, N-point spin correlation functions can be obtained through $2N$-point correlation functions of auxiliary operators, which also applies to the Majorana representation through Eq. (3.21). In diagrammatic terms, one spin operator can be understood to split into a vertex of two auxiliary particles. In perturbative approaches the treatment of such vertices can be complicated. This fact is known as the "vertex problem", cf. Ref. [5]. In the Majorana representation a simple trick allows to establish the correspondence of N-point spin correlation functions to N-point Majorana correlation functions for a certain class of correlation functions. Thus, the "vertex problem" can be avoided.

To begin with, we consider the composite Majorana operator $\hat{\Theta}$, cf. Refs. [5, 6, 80, 83],

$$\hat{\Theta} = -2i\hat{\eta}_x \hat{\eta}_y \hat{\eta}_z, \qquad \hat{\Theta}^2 = \frac{1}{2} \ . \tag{3.22}$$

Due to fermionic anti-commutation and $\hat{\eta}_\alpha^2 = 1/2$ the operator $\hat{\Theta}$ commutes with all three Majorana operators $\hat{\eta}_\alpha$,

$$[\hat{\Theta}, \hat{\eta}_\alpha] = 0 \ , \tag{3.23}$$

and thus with any spin operator and Hamiltonian expressed in terms of $\hat{\eta}_\alpha$. The operator $\hat{\Theta}$ allows us to rewrite the Martin transformation Eqs. (3.2) as

$$\hat{S}_\alpha = \hat{\Theta}\hat{\eta}_\alpha \ , \tag{3.24}$$

effectively replacing one Majorana in the bilinear expressions. Since $\hat{\Theta}$ commutes with all other operators, the corresponding Heisenberg operator is time-independent. In particular, it commutes with other Heisenberg operators.

The power of (3.24) becomes apparent if we consider e.g. a two-spin correlation function and take advantage of the commutation properties of $\hat{\Theta}$:

$$\langle \hat{S}_\alpha(t)) \hat{S}_\beta(t') \rangle_{\mathrm{M}} = \langle \hat{\Theta} \hat{\eta}_\alpha(t) \hat{\Theta} \hat{\eta}_\beta(t') \rangle = \frac{1}{2} \langle \hat{\eta}_\alpha(t) \hat{\eta}_\beta(t') \rangle \ . \tag{3.25}$$

Thereby a two-point spin correlation function reduces to a two-point, rather than four-point, Majorana-fermion correlation function. In fact, the concept can be used for any correlation function containing an even number N of spin operators of a spin $1/2$,

$$\langle \hat{S}_{\alpha_1}(t_1) \dots \hat{S}_{\alpha_N}(t_N) \rangle_{\mathrm{M}} = \frac{1}{2^{N/2}} \langle \hat{\eta}_{\alpha_1}(t_1) \dots \hat{\eta}_{\alpha_N}(t_N) \rangle \ , \tag{3.26}$$

since $\hat{\Theta}^N = (1/2)^{N/2}$ for N even.

So far, the discussion was restricted to the case of a single spin $1/2$. If we consider a system of N_s spins $\hat{S}_{k,\alpha}$, $k = 1, \dots N_s$, the straight-forward generalization of (3.24) is to introduce an operator $\hat{\Theta}_k$ for each spin,

$$\hat{S}_{k,\alpha} = \hat{\Theta}_k \hat{\eta}_{\alpha,k} \ . \tag{3.27}$$

Since operators $\hat{\Theta}_k$ of different spins are different, $\hat{\Theta}_k \neq \hat{\Theta}_j$ for $k \neq j$, they cannot cancel each other. As a consequence, some spin-spin correlation functions, for example

$$\langle \hat{S}_{\alpha,1}(t) \hat{S}_{\beta,2}(t') \rangle_{\mathrm{M}} \ , \tag{3.28}$$

cannot be simplified similarly to (3.26) by (3.27). Mao *et al.* in Ref. [5] address this issue, suggesting that objects $Z_{ij} = 2 \langle \hat{\Theta}_k \hat{\Theta}_j \rangle$ are constants of motion, acting as Z_2 gauge fields in lattice theories. Here we continue on a simpler route, we restrict ourselves to cases with even products of any $\hat{\Theta}_k$.

Since $\hat{\Theta}_k$ commutes with any spin operator and $\hat{\Theta}_k^2 = 1/2$, the representation (3.27) can be used to simplify spin correlation functions comprised of pairs of operators for each spin such as

$$\langle \hat{S}_{\alpha,1}(t) \hat{S}_{\beta,2}(t') \hat{S}_{\gamma,1}(t'') \hat{S}_{\delta,2}(t''') \rangle_{\mathrm{M}} = \langle \hat{\Theta}_1 \hat{\eta}_{\alpha,1}(t) \hat{\Theta}_2 \hat{\eta}_{\beta,2}(t') \hat{\Theta}_1 \hat{\eta}_{\gamma,1}(t'') \hat{\Theta}_2 \hat{\eta}_{\delta,2}(t''') \rangle$$

$$= \frac{1}{4} \langle \hat{\eta}_{\alpha,1}(t) \hat{\eta}_{\beta,2}(t') \hat{\eta}_{\gamma,1}(t'') \hat{\eta}_{\delta,2}(t''') \rangle \ . \tag{3.29}$$

We identify these types of spin correlation functions as pairwise correlators. Auto-correlation functions of an even number of spin operators of the same spin constitute a subgroup thereof. We conclude that the modified Majorana representation (3.24) can be used to demonstrate that any N-point pairwise spin correlation function is equal to the corresponding N-point Majorana correlation function up to constant factor $(1/2)^{N/2}$.

In Subs. 3.1.1 we mentioned the Z_2 symmetry of the Majorana representation (3.2) under the transformation $\hat{\eta}_\alpha \to -\hat{\eta}_\alpha$. With regard to this symmetry the above relations (3.26) and (3.29) have to be treated with care, as was done in Ref. [6]. Consider the case of a time-dependent gauge transformation

$$\hat{\eta}_\alpha \to (-1)^{\phi(t)} \hat{\eta}_\alpha \ , \quad \text{with} \quad \phi \in \{0,1\} \ . \tag{3.30}$$

Spin operators are invariant under such a transformation because they are even products of Majorana operators. Thus the spin correlators on the left-hand side of Eq. (3.26) are

invariant. In contrast, the Majorana correlators on the right-hand side of Eq. (3.26) are not invariant since they transform by

$$\langle \hat{\eta}_\alpha(t) \hat{\eta}_\beta(t') \rangle \to (-1)^{\phi(t)+\phi(t')} \langle \hat{\eta}_\alpha(t) \hat{\eta}_\beta(t') \rangle , \qquad (3.31)$$

cf. Refs. [6, 59, 83]. Due to an additional term $\propto \dot{\phi}(t)$ the Hamiltonian is not invariant as well under such transformations. The problem is solved by fixing the gauge to be explicitly time-independent: $\dot{\phi}(t) = 0$. This is the gauge in that the above relations (3.26) and (3.29) are written. However, in particular situations, as in Ref. [83], the gauge fixing has to be reconsidered. Namely, one could define objects $\sim \langle \eta_\alpha \ldots \rangle$ which include an odd number of Majorana fermions. At a saddle points where such objects are finite the Z_2-symmetry is broken and gauge fluctuations have to be reconsidered. In the present thesis we do not deal with such situations, therefore we can safely fix $\dot{\phi}(t) = 0$ for the remainder of this thesis.

3.1.4. Equivalence of Time-Ordered Correlation Functions

Time-ordered Green's functions are a particular type of correlation functions which play an important role in the field-theoretical Green's functions formalism. Products of time-dependent operators can be ordered in time by the time-ordering operator $\mathcal{T}$, which acts on spin operators and Majorana operators by

$$\mathcal{T}\hat{S}_\alpha(t)\hat{S}_\beta(t') \equiv \begin{cases} \hat{S}_\alpha(t)\hat{S}_\beta(t'), & t > t' \\ \hat{S}_\beta(t')\hat{S}_\alpha(t), & t < t' , \end{cases}$$

$$\mathcal{T}\hat{\eta}_\alpha(t)\hat{\eta}_\beta(t') \equiv \begin{cases} \hat{\eta}_\alpha(t)\hat{\eta}_\beta(t'), & t > t' \\ -\hat{\eta}_\beta(t')\hat{\eta}_\alpha(t), & t < t' . \end{cases} \qquad (3.32)$$

Due to the additional fermionic sign in the lower line of the above equation, $\mathcal{T}$ acts differently on spin and Majorana operators, preventing direct generalization of the result (3.26) to time-ordered correlators.

Here we introduce a recipe that effectively generalizes the correspondence of N-point spin and N-point Majorana correlation functions to time-ordered functions. In order to compensate for the "wrong" sign in (3.32), we add an auxiliary Majorana fermion $\hat{m}$ which satisfies

$$\hat{m}^2 = 1/2 , \qquad \{\hat{\eta}_\alpha, \hat{m}\} = 0 . \qquad (3.33)$$

The Majorana $\hat{m}$ commutes with any spin operator and any Hamiltonian expressed in the Majorana representation (3.2), i.e., in terms bilinears of Majorana operators $\hat{\eta}_\alpha$. Thus, $\hat{m}$ is time-independent, in particular $\hat{m}(t)\hat{m}(t') = \hat{m}^2 = 1/2$. Keeping the formal time-argument $\hat{m}(t)$, the correct "spin-like" time order in (3.32) can now be established by

$$\langle \mathcal{T} i\hat{m}(t)\hat{\eta}_\alpha(t) i\hat{m}(t')\hat{\eta}_\beta(t') \rangle \equiv \begin{cases} \langle i\hat{m}(t)\hat{\eta}_\alpha(t) i\hat{m}(t')\hat{\eta}_\beta(t') \rangle, & t > t' \\ \langle i\hat{m}(t')\hat{\eta}_\beta(t') i\hat{m}(t)\hat{\eta}_\alpha(t) \rangle, & t < t' \end{cases}$$

$$= \frac{1}{2} \begin{cases} \langle \hat{\eta}_\alpha(t)\hat{\eta}_\beta(t') \rangle, & t > t' \\ \langle \hat{\eta}_\beta(t')\hat{\eta}_\alpha(t) \rangle, & t < t' . \end{cases} \qquad (3.34)$$

Thus we arrive at the identity

$$\langle \mathcal{T}\hat{S}_\alpha(t)\hat{S}_\beta(t') \rangle_{\mathrm{M}} = \langle \mathcal{T} i\hat{m}(t)\hat{\eta}_\alpha(t) \, i\hat{m}(t')\hat{\eta}_\beta(t') \rangle . \qquad (3.35)$$

Similarly, we can use the auxiliary operator $\hat{m}(t)$ to express higher-order correlation functions. For a 4-point spin correlator we find

$$\langle \mathcal{T} \hat{S}_\alpha(t_1) \hat{S}_\beta(t'_1) \hat{S}_\delta(t_2) \hat{S}_\gamma(t'_2) \rangle_{\mathrm{M}}$$
$$= \langle \mathcal{T} \hat{m}(t_1) \hat{\eta}_\alpha(t_1) \hat{m}(t'_1) \hat{\eta}_\beta(t'_1) \hat{m}(t_2) \hat{\eta}_\delta(t_2) \hat{m}(t'_2) \hat{\eta}_\gamma(t'_2) \rangle \ . \quad (3.36)$$

In Eqs. (3.35) and (3.36) N-point spin correlators are again expressed in terms of $2N$-point Majorana correlation functions However, the auxiliary Majorana operators $\hat{m}(t)$ and $\hat{m}(t')$ do not appear in the Hamiltonian. Therefore the $\hat{m}$-propagator lines are not broadened and $\hat{m}\hat{\eta}_\alpha$-vertices do not suffer from vertex corrections. In this sense the relations (3.35) and (3.36) are similar to the N to N spin Majorana correspondence relations (3.26) and (3.29) and constitute a powerful approach for efficient calculation of spin correlation functions.

We note that Cabrera Cano and Florens used an alternative method to circumvent the time-ordering problem in Ref. [84]. These authors directly introduced Green's functions of the operator $\hat{\Theta} = -2i\hat{\eta}_x\hat{\eta}_y\hat{\eta}_z$ used in the preceding Subsection 3.1.3. However, $\hat{\Theta}$ is a function of Majorana operators $\hat{\eta}_\alpha$ and does commute with $\hat{\eta}_\alpha$ instead of anti-commuting. The approach presented here is simpler and more straightforward as the auxiliary Majorana fermion $\hat{m}$ is independent of Majorana operators $\hat{\eta}_\alpha$.

3.2. Basic Concepts for the Application of the Majorana Representation

In order to provide the basics for all subsequent chapters we outline the construction of the Majorana path integral and the concept of generating functionals in the frameworks of Matsubara and Keldysh formalism. In these techniques spin correlators can be calculated with the use of finite-temperature and real-time Majorana Green's functions.

3.2.1. The Path Integral for Majorana Fermions

The preceding Section 3.1 treated the Majorana representation on the operator level. On this level, given the Hamiltonian of a problem, the Majorana representation allows to apply standard perturbative approaches, discussed in many textbooks on condensed matter theory, e.g. Ref. [46]. That is, switching to some interaction picture, expanding the exponentials of the time evolution operator in the observable of interest in orders of the interacting Hamiltonian and suitable resummation.

The path integral framework can be considered as a complementary approach, which often proves more flexible, cf. e.g. textbook [94]. The Majorana representation has already been used within path integral approaches by some authors, e.g. Refs. [58, 59, 81, 83, 85]. We will use the path integral formalism in subsequent chapters, therefore we briefly recapitulate the construction of the Majorana path integral here.

In order to construct the Majorana fermion path integral one has to represent the Majorana fermions in terms of complex fermions.[3] This is achieved either by combining two Majorana fermions into one Dirac fermion, so-called fermion halving, or by combining each Majorana fermion with a new, additional Majorana fermion into one Dirac fermion, so-called fermion

---

[3]The author of Refs. [58, 77] establishes an operator to path integral correspondence without the use of coherent states and a Fock space, based on Refs. [7, 90].

doubling, cf. Refs. [81, 92, 95]. For an odd number of Majorana fermions $\hat{\eta}_x, \hat{\eta}_y, \hat{\eta}_z$ one has to use the fermion doubling procedure. A detailed discussion can be found in Bastianelli and van Nieuwenhuizen, Ref. [92, Chap. 2] and references therein.

In order to introduce the concept of a "path" one can consider transition probabilities $\langle \Psi_f | e^{-iHt} | \Psi_i \rangle$ from an initial state $| \Psi_i \rangle$ to a final state $| \Psi_f \rangle$, with the evolution operator e^{-iHt}. The Hamiltonian $H = H[\hat{\Psi}^\dagger, \hat{\Psi}]$ is written in second quantization and has to be Weyl ordered, i.e., creation operators $\hat{\Psi}^\dagger$ to the left and annihilation operators $\hat{\Psi}$ to the right. Now, the time evolution in the time interval t can be divided into N small time slices of length t/N. Between each time slice a complete set of so-called coherent states $|\bar{\Psi}\rangle$, a particular superposition of Fock states, can be inserted. Coherent states are eigenstates of the annihilation operator,

$$\hat{\Psi} | \bar{\Psi}(t_i) \rangle = \Psi(t_i) | \bar{\Psi}(t_i) \rangle \ , \quad \langle \bar{\Psi}(t_i) | \hat{\Psi} = \langle \bar{\Psi}(t_i) | \Psi^*(t_i) \ . \tag{3.37}$$

Thus, by acting on the coherent states creation and annihilation operators generate complex numbers $\Psi(t_i), \Psi^*(t_i)$ in each time slice t_i (creation operators acting to the left and annihilation to the right). For fermionic systems, these complex numbers inherit the properties of fermionic operators, thus they are so-called Grassmann numbers which obey fermionic commutation relations, $\{\Psi_1, \Psi_2\} = 0$.

The obtained complex Grassmann numbers are time dependent, therefore left and right values in each time step differ, leading to differences of the form $(\Psi(t_i) - \Psi(t_{i-1})/N$. In the limit of infinitely small time slices, $N \to \infty$, and assuming that $\Psi(t_i)$ change smoothly in time, these differences can be rewritten as time-differentials. Terms of order $1/N^2$ can be neglected. This procedure, known as Suzuki-Trotter decomposition, allows to reformulate the transition probability in terms of an integral over possible values of complex Grassmann numbers, "paths",

$$\langle \Psi_f | e^{-i\hat{H}t} | \Psi_i \rangle = c(\Psi_f, \Psi_i) \int D[\Psi, \Psi^*] e^{-\int_0^t dt' \Psi^* \partial_{t'} \Psi - i \int_0^t dt' \hat{H}[\Psi^*, \Psi] dt'} \tag{3.38}$$

Here, $c(\Psi_f, \Psi_i)$ is a constant depending on initial and final state. Complex Grassmann numbers Ψ, Ψ^* are implicitly time-dependent and can be treated as independent, instead of treating the real and imaginary part as independent. The integration measure $D[\Psi]$ has to be understood as integration over all possible values of Ψ at each time and is normalized.

To rewrite the obtained Dirac fermion path integral expression in terms of real Majorana Grassmann variables, complex Grassmann variables are again decomposed into real and imaginary part, i.e., two real Majorana Grassmann variables. We started with three Majorana fermions $\hat{\eta}_x, \hat{\eta}_y, \hat{\eta}_z$, thus the fermion doubling added another three Majorana fermions $\hat{m}_x, \hat{m}_y, \hat{m}_z$ and the path integral expressions take the form

$$\int D[\boldsymbol{\eta}, \boldsymbol{m}] \ \exp\left\{ -\frac{1}{2} \int_0^t dt' \ \eta_\alpha \partial_{t'} \eta_\alpha - \frac{1}{2} \int_0^t dt' \ m_\alpha \partial_{t'} m_\alpha - i \int_0^t dt' \ H[\boldsymbol{\eta}] \right\} \ . \tag{3.39}$$

Any Grassmann variables which do not appear in the Hamiltonian are quadratic can be integrated out again, using rules for Gaussian integration of Grassmann variables in Ref. [92]. In the construction of the path integral Majorana fermion operators translate to real Grassmann variables. The operators fulfill $\hat{\eta}_\alpha^2 = 1/2$ in contrast to the Grassmann variables which satisfy $\eta_\alpha^2 = 0$ by definition. The latter reflects normal ordering of Majorana fermions in the path integral.

3.2.2. Green's Functions at Finite Temperatures

The properties of systems at finite temperatures are conveniently described by the use of finite temperature Green's functions, so-called Matsubara Green's functions, cf. Ref. [94] or other textbooks on condensed matter theory. Here we briefly review the concept of Matsubara Green's functions for the example of one spin 1/2 using the Majorana representation for spin described above.

The partition function of a system described by the Hamiltonian H is given by the trace over the finite temperature (Gibbs) density matrix $e^{-\beta H}$,

$$\mathcal{Z} = \text{Tr}\left\{e^{-\beta H[\hat{\eta}]}\right\} \tag{3.40}$$

$\beta = 1/T$ is the inverse temperature, the index M indicates that we are concerned with the finite temperature (Matsubara) partition function. Based on the similarity of $e^{-\beta H}$ with the time evolution operator e^{-itH}, the former can be interpreted as the time evolution of $\tau = it$ from 0 to β in imaginary time space. In the Majorana representation the corresponding path integral expression is

$$\mathcal{Z} = \int D[\boldsymbol{\eta}] \exp\left\{-\frac{1}{2}\int_0^\beta d\tau\, \eta_\alpha(\tau)\partial_\tau\eta_\alpha(\tau) - \int_0^\beta d\tau H[\boldsymbol{\eta}]\right\}. \tag{3.41}$$

The exponent above is identified to be the action $\mathcal{S}$ of the system, which is a functional of the fields. Here we define the Matsubara action by

$$i\mathcal{S}[\boldsymbol{\eta}] = -\frac{1}{2}\int_0^\beta d\tau\, \eta_\alpha(\tau)\partial_\tau\eta_\alpha(\tau) - \int_0^\beta d\tau H[\boldsymbol{\eta}]\,, \qquad \mathcal{Z} = \int D[\boldsymbol{\eta}]\, e^{i\mathcal{S}[\boldsymbol{\eta}]}\,. \tag{3.42}$$

Let us turn to physical observables, for example two-point correlation functions. On the operator level, the two-point Matsubara Green's function $\mathcal{G}_\alpha$ is defined by

$$\mathcal{G}_\alpha(\tau, \tau') = -\langle \mathcal{T}_\tau \hat{\eta}_\alpha(\tau)\hat{\eta}_\alpha(\tau')\rangle \equiv -\frac{\text{Tr}\left\{\mathcal{T}_\tau \hat{\eta}_\alpha(\tau)\hat{\eta}_\alpha(\tau')\right\}}{\mathcal{Z}}\,, \tag{3.43}$$

with imaginary time Heisenberg operators $\hat{\eta}_\alpha(\tau) = e^{-\tau H}\hat{\eta}_\alpha e^{\tau H}$. In the path integral formalism, Green's functions can be obtained by derivation with respect to so-called source fields. Here, Grassmann source fields ξ_α can be introduced by

$$\mathcal{Z}[\boldsymbol{\xi}] = \int D[\boldsymbol{\eta}] \exp\left\{-\frac{1}{2}\int_0^\beta d\tau\, \eta_\alpha(\tau)\partial_\tau\eta_\alpha(\tau) - \int_0^\beta d\tau H[\boldsymbol{\eta}] - \int_0^\beta d\tau\, \xi_\alpha(\tau)\eta_\alpha(\tau)\right\}, \tag{3.44}$$

where $\mathcal{Z}[\boldsymbol{\xi}]$ is understood as the generating functional. The Matsubara Green's functions $\mathcal{G}_{\alpha\beta}$ are obtained by

$$\mathcal{G}_{\alpha\beta}(\tau, \tau') = -\langle \mathcal{T}_\tau \eta_\alpha(\tau)\eta_\beta(\tau')\rangle \equiv -\frac{1}{\mathcal{Z}}\int D[\boldsymbol{\eta}]\, \eta_\alpha(\tau)\eta_\beta(\tau')\, e^{i\mathcal{S}[\boldsymbol{\eta}]}$$
$$= \frac{\delta^2 \log \mathcal{Z}[\boldsymbol{\xi}]}{\delta\xi_\beta(\tau')\delta\xi_\alpha(\tau)}\bigg|_{\boldsymbol{\xi}=0}. \tag{3.45}$$

The sole purpose of source fields is to generate physical observables from the generating functional, they do not have a physical meaning and are therefore set to 0 at the end of a

calculation, as indicated in the above formula. One can rewrite the action in (3.44) with the use of the Green's function (3.45),

$$
i\mathcal{S}[\boldsymbol{\eta}] = \frac{1}{2} \int_0^\beta d\tau d\tau' \, \eta_\alpha(\tau) \mathcal{G}^{-1}_{\alpha\beta}(\tau,\tau') \eta_\beta(\tau') - \int_0^\beta d\tau \, \xi_\alpha(\tau) \eta_\alpha(\tau) \ , \tag{3.46}
$$

It can be checked that the $\mathcal{G}$ appearing in the exponent above indeed coincides with the Matsubara Green's function (3.45). To do so, the source term $\xi_\alpha(\tau)\eta_\alpha(\tau)$ is absorbed into the quadratic term in the action (3.42) by completing the square. Then, Majorana fields can be integrated out, leaving an exponential quadratic in source fields, like $\exp(\xi\mathcal{G}\xi)$, for $\mathcal{Z}$. By derivation with respect to source fields according to (3.45) one finds that both $\mathcal{G}$'s are identical.

For the case of $H = 0$ the Majorana Green's function at finite temperatures is diagonal in spin space, its inverse is given by

$$
\mathcal{G}^{-1}_{f\alpha}(\tau,\tau') = -\delta(\tau - \tau')\partial_{\tau'} \ . \tag{3.47}
$$

In Matsubara frequency space, it is

$$
\mathcal{G}^{-1}_{f\alpha}(i\nu) = \int_0^\beta d(\tau - \tau') \mathcal{G}^{-1}_{f\alpha}(\tau,\tau') \, e^{i\nu(\tau-\tau')} = i\nu \ , \tag{3.48}
$$

with fermionic Matsubara frequencies $\nu = (2n+1)\pi/\beta$ and an integer number $n \in \mathbb{Z}$. In the following, we refer to $\mathcal{G}_{f\alpha}$ as the free Majorana Green's function.

Spin Correlators at Finite Temperatures

In order to obtain spin Green's functions one can use source terms that couple to spin fields. Spin fields can be introduced as composite fields of Majorana Grassmann fields, Ref. [77],

$$
S_\alpha = -\frac{i}{2} \, \epsilon_{\alpha\beta\gamma} \eta_\beta \eta_\gamma, \tag{3.49}
$$

which is the field analogue of the Martin transformation (3.2) on the operator level. The generating functional for spin correlation functions at finite temperatures is then

$$
\mathcal{Z}[\boldsymbol{\lambda}] = \int D[\boldsymbol{\eta}] \, \exp\left\{ i\mathcal{S}[\boldsymbol{\eta}] - \int_0^\beta d\tau \, \lambda_\alpha(\tau) S_\alpha(\tau) \right\} \ . \tag{3.50}
$$

Physical observables are obtained by derivation with respect to λ_α. For example, the spin Matsubara Green's function $\mathcal{G}^S_\alpha$ is

$$
\mathcal{G}^S_\alpha(\tau,\tau') = -\langle \mathcal{T}_\tau S_\alpha(\tau) S_\alpha(\tau') \rangle \equiv -\frac{1}{\mathcal{Z}} \int D[\boldsymbol{\eta}] \, S_\alpha(\tau) S_\alpha(\tau') \, e^{i\mathcal{S}[\boldsymbol{\eta}]}
$$
$$
= -\left. \frac{\delta^2 \log \mathcal{Z}[\boldsymbol{\lambda}]}{\delta\lambda_\alpha(\tau')\delta\lambda_\alpha(\tau)} \right|_{\boldsymbol{\lambda}=0} \ . \tag{3.51}
$$

To reformulate the simplified correspondences between time-ordered pairwise spin and Majorana correlators discussed in Subs. 3.1.4 we have to add an additional Majorana fermion m. One can use a generating functional similar to (3.50),

$$
\tilde{\mathcal{Z}}[\boldsymbol{\lambda}] = \int D[\boldsymbol{\eta}]D[m] \, \exp\left\{ i\mathcal{S}[\boldsymbol{\eta},m] - i\int_0^\beta d\tau \, \lambda_\alpha(\tau) m(\tau)\eta_\alpha(\tau) \right\} \ . \tag{3.52}
$$

According to Eq. (3.35) in Subs. (3.1.4) the two-spin correlator can also be obtained by

$$
\begin{aligned}
\mathcal{G}^S_{\alpha\beta}(\tau, \tau') &= \langle \mathcal{T}_\tau m(\tau) \eta_\alpha(\tau) m(\tau') \eta_\beta(\tau') \rangle \\
&= - \left. \frac{\delta^2 \log \tilde{\mathcal{Z}}[\boldsymbol{\lambda}]}{\delta \lambda_\beta(\tau') \delta \lambda_\alpha(\tau)} \right|_{\boldsymbol{\lambda}=0} .
\end{aligned}
\tag{3.53}
$$

Similar formulas can be derived for auto-correlators of even numbers of spin fields and pairwise spin-spin correlators.

3.2.3. Real-Time Green's Functions in the Keldysh Formalism

Real-time correlation functions can be conveniently computed within the so-called Keldysh formalism, treated in textbooks, e.g. Refs. [47, 94]. On a qualitative level the Keldysh formalism can be considered as a generalization of time-dependent perturbation theory, based on a "double" time evolution forth and back in time. The so-called Schwinger-Keldysh time contour $\mathcal{C}$ evolves from $-\infty$ to $+\infty$ and back. In order to introduce generating functionals one can use, similar to the imaginary time formulas (3.42), cf. Ref. [47], [4]

$$
\mathcal{Z}_K = \mathrm{Tr} \left\{ e^{-i \int_\mathcal{C} dt\, \hat{H}[\hat{\eta}]} \right\} = \int D[\boldsymbol{\eta}]\, e^{i \mathcal{S}_K[\boldsymbol{\eta}]}
\tag{3.54}
$$

with the action

$$
i\mathcal{S}_K[\boldsymbol{\eta}] = \int D[\boldsymbol{\eta}] \exp \left\{ -\frac{1}{2} \int_\mathcal{C} dt\, \eta_\alpha(t) \partial_t \eta_\alpha(t) - i \int_\mathcal{C} dt\, H[\boldsymbol{\eta}] \right\} .
\tag{3.55}
$$

However, $\mathcal{Z}$ is the finite temperature partition function while in Keldysh $\mathcal{Z}_K$ is equal to $\mathcal{Z}_K = 1$. Still, $\mathcal{Z}_K$ is called the Keldysh generating function, cf. Ref. [47], and it provides the basis to define the generating functional.

First we briefly review common Keldysh notation, refering to the book by Kamenev, Ref. [47]. Similar to Eq. (3.46) above, any quadratic action can be rewritten with the use of Green's functions,

$$
\mathcal{Z}_K = \int D[\boldsymbol{\eta}^u, \boldsymbol{\eta}^d] \exp \left\{ \frac{i}{2} \int_C dt dt'\, \eta_\alpha(t) (G^{-1}(t, t'))_{\alpha\beta} \eta_\beta(t') \right\} .
\tag{3.56}
$$

The Schwinger-Keldysh double-time path can be decomposed into upper and lower contour, which allows to separate Majorana fields into fields on the upper and fields on the lower time contour and to write

$$
\mathcal{Z}_K = \int D[\boldsymbol{\eta}^u, \boldsymbol{\eta}^d] \exp \left\{ \frac{i}{2} \int_{-\infty}^{\infty} dt dt'\, \eta_\alpha^a(t) (G^{-1}(t, t'))_{\alpha\beta}^{ab} \eta_\beta^b(t') \right\} .
\tag{3.57}
$$

Here, Keldysh-indices $a, b \in u, d$ denote the time branch. The index u is chosen to denote the earlier, "upper", time branch while d denotes the later, "lower", time branch.[5] The

---

[4] Real and imaginary time are related via $t = -i\tau$, $\partial_t = i\partial_\tau$.

[5] On the lower time branch time evolves in "negative" direction resulting in an additional negative sign of t, which is included in the inverse Green's function. If the negative sign for the backward contour is included explicitly, the free Majorana term in the action is

$$
\frac{i}{2} \int_{-\infty}^{\infty} dt\, \eta^a(t) i\tau_z^a \partial_t \eta^a(t) .
\tag{3.58}
$$

Majorana Green's function $G(t, t')$ in (3.57) acquires a 2×2 matrix structure in Keldysh space, it is given by

$$G_{\alpha\beta}(t, t') = \begin{pmatrix} G^T(t, t') & G^<(t, t') \\ G^>(t, t') & G^{\tilde{T}}(t, t') \end{pmatrix}_{\alpha\beta} , \tag{3.59}$$

The time-ordered Green's function G^T, the anti-time-ordered Green's function $G^{\tilde{T}}$, $G^>$ and $G^<$ defined by, cf. Ref. [47],

$$G_{\alpha\beta}^T(t, t') = -i\langle \mathcal{T}\eta_\alpha^u(t)\eta_\beta^u(t')\rangle , \quad G_{\alpha\beta}^{\tilde{T}}(t, t') = -i\langle \tilde{\mathcal{T}}\eta_\alpha^d(t)\eta_\beta^d(t')\rangle , \tag{3.60}$$

$$G_{\alpha\beta}^>(t, t') = -i\langle \eta_\alpha^d(t)\eta_\beta^u(t')\rangle , \quad G_{\alpha\beta}^<(t, t') = -i\langle \eta_\alpha^u(t)\eta_\beta^d(t')\rangle . \tag{3.61}$$

The operator $\tilde{\mathcal{T}}$ arranges fields in inverse time order, opposite to $\mathcal{T}$.

Due to the additional 2×2 matrix structure, the Keldysh formalism is considered to be a more complex approach compared to the finite temperature formalism in the preceding Subs. 3.2.2. Still, it is a more natural approach to real-time dynamics and also allows for calculations in non-equilibrium situations.

It is known, cf. Ref. [47], that the four entries of the above defined 2×2 Green's function $G_{\alpha\beta}(t, t')$ only contain three independent functions. It is therefore common to use a rotated picture in which one of the entries vanishes. Here we use the bosonic-like rotation. Defining new variables and a rotation matrix

$$\eta_\alpha^{cl} = \frac{1}{\sqrt{2}}\left(\eta_\alpha^u + \eta_\alpha^d\right) , \qquad \eta_\alpha^q = \frac{1}{\sqrt{2}}\left(\eta_\alpha^u - \eta_\alpha^d\right) , \qquad L = \frac{1}{\sqrt{2}}\begin{pmatrix} 1 & 1 \\ 1 & -1 \end{pmatrix} = L^{-1} , \tag{3.62}$$

the object (3.57) can be rewritten as

$$\mathcal{Z}_K = \int D[\boldsymbol{\eta}^{cl}, \boldsymbol{\eta}^q] \exp\left\{i\mathcal{S}_K[\boldsymbol{\eta}^{cl}, \boldsymbol{\eta}^q]\right\} , \tag{3.63}$$

$$i\mathcal{S}_K[\boldsymbol{\eta}^{cl}, \boldsymbol{\eta}^q] = \frac{i}{2}\int_{-\infty}^{\infty} dt dt' \, \eta_\alpha^a(t)(\hat{G}^{-1}(t, t'))_{\alpha\beta}^{ab}\eta_\beta^b(t') , \qquad a, b \in \{cl, q\}$$

$$= \frac{i}{2}\int_{-\infty}^{\infty} dt dt' (\eta_\alpha^{cl}, \eta_\alpha^q)_t (\hat{G}(t, t'))_{\alpha\beta}^{-1}\begin{pmatrix} \eta_\beta^{cl} \\ \eta_\beta^q \end{pmatrix}_{t'} , \tag{3.64}$$

with the Keldysh-rotated Majorana Green's function

$$\hat{G}_{\alpha\beta}^{ab}(t, t') = -i\langle \mathcal{T}_K \eta_\alpha^a(t)\eta_\beta^b(t')\rangle = \begin{pmatrix} G_{\alpha\beta}^K(t, t') & G_{\alpha\beta}^R(t, t') \\ G_{\alpha\beta}^A(t, t') & 0 \end{pmatrix}^{ab} = (LG_{\alpha\beta}(t, t')L)^{ab} . \tag{3.65a}$$

For $H = 0$ the Fourier transformed free Majorana Green's functions, $\int dt e^{i\omega t}(\dots)$, are given by

$$G_{f\alpha}^R(\omega) = (\omega + i0)^{-1} , \qquad G_{f\alpha}^A(\omega) = (\omega - i0)^{-1} , \qquad G_{f\alpha}^K(\omega) = 0 , \tag{3.65b}$$

which are the Keldysh equivalents to the free Matsubara Green's function $\mathcal{G}(i\nu) = 1/i\nu$, Eq. (3.48). $i0$ denotes an infinitesimal imaginary part. In general, $G^{R/A}$ contain information about particle propagation and the energy spectrum of a system while G^K also contains the distribution function, i.e., average occupation numbers of single-particle states.

Spin Correlation Functions in Keldysh Formalism

As above, Eq. (3.49), spin fields S_α can be described as composite fields of Majorana Grassmann fields $\eta_\alpha^{cl/q}$. It is convenient to define c/q-components of spin variables

$$S_\alpha^{cl} = \frac{1}{\sqrt{2}}\left(S_\alpha^u + S_\alpha^d\right)\ , \qquad S_\alpha^q = \frac{1}{\sqrt{2}}\left(S_\alpha^u - S_\alpha^d\right)\ . \tag{3.66}$$

By introducing vectors $\check{\eta}_\alpha^T = (\eta_\alpha^{cl}, \eta_\alpha^q)$ and matrices $\gamma^{cl/q}$ in Keldysh space, the Majorana representation (3.2) for fields can be written as

$$S_\alpha^{cl} = -\frac{i}{2\sqrt{2}}\,\epsilon_{\alpha\beta\gamma}[\check{\eta}_\beta\gamma^{cl}\check{\eta}_\gamma], \qquad S_\alpha^q = -\frac{i}{2\sqrt{2}}\,\epsilon_{\alpha\beta\gamma}[\check{\eta}_\beta\gamma^q\check{\eta}_\gamma] \tag{3.67}$$

$$\text{with}\qquad \check{\eta}_\alpha = \begin{pmatrix} \eta_\alpha^{cl} \\ \eta_\alpha^q \end{pmatrix}\ , \qquad \gamma^{cl} = \begin{pmatrix} 1 & 0 \\ 0 & 1 \end{pmatrix}\ , \qquad \gamma^q = \begin{pmatrix} 0 & 1 \\ 1 & 0 \end{pmatrix}\ . \tag{3.68}$$

Here, the parentheses $[\dots]$ indicate a scalar product in Keldysh space. Note that γ-matrices and scalar products are symmetric, hence e.g. $[\check{\eta}_\alpha\gamma^a\check{\eta}_\beta] = -[\check{\eta}_\beta\gamma^a\check{\eta}_\alpha]$. Using source fields

$$\lambda^{cl} = \frac{1}{\sqrt{2}}\left(\lambda_\alpha^u + \lambda_\alpha^d\right)\ , \qquad \lambda^{cl} = \frac{1}{\sqrt{2}}\left(\lambda_\alpha^u + \lambda_\alpha^d\right) \tag{3.69}$$

the generating functional for spin may be defined as follows, similar to Eq. (3.50),

$$\mathcal{Z}_K[\boldsymbol{\lambda}] = \int D[\boldsymbol{\eta}^{cl}, \boldsymbol{\eta}^q]\exp\left\{i\mathcal{S}_K + i\int_{-\infty}^{\infty} dt\left(\lambda_\alpha^{cl}S_\alpha^q + \lambda_\alpha^q S_\alpha^{cl}\right)\right\}\ . \tag{3.70}$$

In the first source term $\lambda_\alpha^{cl}S_\alpha^q$ the "classical" source field λ_α^{cl} could be identified with a physical probing field $\lambda_\alpha^{cl} \equiv \sqrt{2}B_\alpha$. This can be seen by including a magnetic field into the action by $H = -\boldsymbol{BS}$. For a physical magnetic field it is $B_\alpha = B^u = B^d$, thus magnetic field generates a term $i\int dt\,\sqrt{2}B_\alpha S_\alpha^q$ which resembles the λ_α^{cl}-term above. Here, we prefer to include magnetic field explicitly in $i\mathcal{S}_K$, such that all source fields $\boldsymbol{\lambda}^{cl}$ and $\boldsymbol{\lambda}^q$ can be set to zero .

Taking the derivative of the functional $\mathcal{Z}_K$ in (3.70) with respect to the source fields $\lambda_\alpha^{cl(q)}$, one finds the spin correlation functions, as was done in Subsection 2.2.2. The spin magnetization is defined by the one-point function

$$\sqrt{2}\,M_\alpha = \langle S_\alpha^{cl}(t)\rangle = -i\,\frac{\delta\mathcal{Z}_K[\boldsymbol{\lambda}]}{\delta\lambda_\alpha^q(t)}\bigg|_{\boldsymbol{\lambda}=0}\ . \tag{3.71}$$

For the sake of completeness we repeat the two-point functions susceptibility χ, Eq. (2.20), and the symmetric correlator $C_{\alpha\beta}^{(2)}$, Eq. (2.21),

$$\chi_{\alpha\beta}(t,t') = i\langle \mathcal{T}_K S_\alpha^{cl}(t)S_\beta^q(t')\rangle = -i\,\frac{\delta^2\mathcal{Z}_K[\boldsymbol{\lambda}]}{\delta\lambda_\beta^{cl}(t')\delta\lambda_\alpha^q(t)}\bigg|_{\boldsymbol{\lambda}=0} = i\langle[S_\alpha(t),S_\beta(t')]\rangle\ , \tag{3.72}$$

$$C_{\alpha\beta}^{(2)}(t,t') = \frac{1}{2}\langle \mathcal{T}_K S_\alpha^{cl}(t)S_\alpha^{cl}(t')\rangle = -\frac{1}{2}\,\frac{\delta^2\mathcal{Z}_K[\boldsymbol{\lambda}]}{\delta\lambda_\beta^q(t')\delta\lambda_\alpha^q(t)}\bigg|_{\boldsymbol{\lambda}=0} = \frac{1}{2}\langle\{S_\alpha(t),S_\beta(t')\}\rangle\ , \tag{3.73}$$

denoting the commutator by $[.,.]$ and the anti-commutator by $\{.,.\}$. As discussed in Section 2.2.2, the Fourier transform $C_{zz}^{(2)}(\omega)$ determines the noise spectrum in Eq. (2.19). In Chapter 2 we introduced the spin correlator $C_\chi(t_1, t_1', t_2, t_2')$, Eq. (2.24), which is related to noise of susceptibility.

Simplified Equivalence of Auto-Correlation Functions

To take advantage of the simplified equivalence formulas between spin and Majorana correlators derived in Subs. 3.1.4, we define another generating functional $\tilde{\mathcal{Z}}_K[\boldsymbol{\lambda}]$, including the auxiliary m-Majorana. Similar to Eqs. (3.52) and (3.70),

$$\tilde{\mathcal{Z}}_K[\boldsymbol{\lambda}] = \int D[\boldsymbol{\eta}^{cl}, \boldsymbol{\eta}^q] D[m^{cl}, m^q]$$
$$\times \exp\left\{ i\mathcal{S}_K[\boldsymbol{\eta}, m] - \frac{i}{\sqrt{2}} \int_{-\infty}^{\infty} dt \left(\lambda_\alpha^{cl}[\check{m}\gamma^q\check{\eta}_\alpha] + \lambda_\alpha^q[\check{m}\gamma^{cl}\check{\eta}_\alpha] \right) \right\} , \quad (3.74)$$

with

$$\check{m} = \begin{pmatrix} m^{cl} \\ m^q \end{pmatrix} , \qquad m^{cl} = \frac{m^u + m^d}{\sqrt{2}} , \qquad m^q = \frac{m^u - m^d}{\sqrt{2}} . \qquad (3.75)$$

Now, the equivalence formulas of spin and Majorana correlators, (3.35) and (3.36), imply that correlators obtained through the generating functional $\tilde{\mathcal{Z}}_K$ are equivalent to the ones obtained through $\mathcal{Z}_K$. For the susceptibility one finds

$$\chi_{\alpha,\beta}(t, t') = -i \left. \frac{\delta^2 \mathcal{Z}_K[\boldsymbol{\lambda}]}{\delta\lambda_\beta^{cl}(t')\delta\lambda_\alpha^q(t)} \right|_{\boldsymbol{\lambda}=0} = i\langle \mathcal{T}_K S_\alpha^{cl}(t) S_\beta^q(t') \rangle = -i \left. \frac{\delta^2 \tilde{\mathcal{Z}}_K[\boldsymbol{\lambda}]}{\delta\lambda_\beta^{cl}(t')\delta\lambda_\alpha^q(t)} \right|_{\boldsymbol{\lambda}=0}$$

$$\Rightarrow \chi_{\alpha,\beta}(t, t') = -\frac{i}{2}\langle \mathcal{T}_K [\check{m}(t)\gamma^{cl}\check{\eta}_\alpha(t)][\check{m}(t')\gamma^q\check{\eta}_\beta(t')] \rangle . \qquad (3.76)$$

For the four-spin correlator C_χ,

$$C_\chi(t_1, t_1', t_2, t_2') = -\langle \mathcal{T}_K S_\alpha^{cl}(t_1) S_\alpha^q(t_1') S_\alpha^{cl}(t_2) S_\alpha^q(t_1') \rangle$$

$$= - \left. \frac{\delta^4 \mathcal{Z}_\lambda}{\delta\lambda_\alpha^{cl}(t_2')\delta\lambda_\alpha^q(t_2)\delta\lambda_\alpha^{cl}(t_1')\delta\lambda_\alpha^q(t_1)} \right|_{\boldsymbol{\lambda}=0} , \qquad (3.77)$$

which appeared in the discussion of susceptibility noise in Chapter 2, this implies

$$C_\chi(t_1, t_1', t_2, t_2') = - \left. \frac{\delta^4 \tilde{\mathcal{Z}}_\lambda}{\delta\lambda_\alpha^{cl}(t_2')\delta\lambda_\alpha^q(t_2)\delta\lambda_\alpha^{cl}(t_1')\delta\lambda_\alpha^q(t_1)} \right|_{\boldsymbol{\lambda}=0}$$

$$= -\langle \mathcal{T}_K [\check{\eta}_\alpha\gamma^{cl}\check{m}]_{t_1} [\check{\eta}_\alpha\gamma^q\check{m}]_{t_1'} [\check{\eta}_\alpha\gamma^{cl}\check{m}]_{t_2} [\check{\eta}_\alpha\gamma^q\check{m}]_{t_2'} \rangle . \qquad (3.78)$$

Similar identities can be easily derived for all pairwise spin correlation functions in the same fashion.

We briefly demonstrate the power of the simplified relations derived in Subsection 3.1.4 within the Keldysh framework and for the example of two-spin correlation functions. As we have shown above in (3.76) the susceptibility is

$$\chi_{\alpha\beta}(t, t') = -\frac{i}{2}\langle \mathcal{T}_K [\check{m}(t)\gamma^{cl}\check{\eta}_\alpha(t)][\check{m}(t')\gamma^q\check{\eta}_\beta(t')] \rangle . \qquad (3.79)$$

The auxiliary m-Majorana is absent from the Hamiltonian and can therefore readily be contracted. The remaining average of Majorana fields η_α and η_β is recognized as the Majorana Green's function $\hat{G}_{\alpha\beta}$. Thus, introducing the auxiliary Green's function $\hat{D}^{ab}(t, t') = -i\langle \mathcal{T}_K m^a(t) m^b(t') \rangle$ with $a, b \in \{cl, q\}$, the susceptibility is found to be

$$\chi_{\alpha\beta}(t, t') = \frac{i}{2} \text{Tr}\left\{ \gamma^{cl}\hat{G}_{\alpha\beta}(t, t')\gamma^q\hat{D}(t', t) \right\} . \qquad (3.80)$$

Here In frequency space Green's functions of the non-interacting auxiliary Majorana, similarly to Eqs. (3.65a) and (3.65), are simply given by

$$\hat{D}(\omega) = \begin{pmatrix} D^K(\omega) & D^R(\omega) \\ D^A(\omega) & 0 \end{pmatrix} \ ,$$

$$D^R(\omega) = (\omega + i0)^{-1} \ , \quad D^A(\omega) = (\omega - i0)^{-1} \ , \quad D^K(\omega) = 0 \ . \tag{3.81}$$

To obtain the susceptibility in frequency space one assumes a stationary situation, i.e., one assumes that quantities depend on the time-difference only. Using the above formulas for $\hat{D}$ and performing the Keldysh trace one finds

$$\chi_{\alpha\beta}(\omega) = \frac{i}{2} \int \frac{d\Omega}{2\pi} \operatorname{Tr} \left\{ \gamma^{cl} \hat{G}_{\alpha\beta}(\Omega + \omega) \gamma^q \hat{D}(\Omega) \right\} = \frac{i}{2} \int \frac{d\Omega}{2\pi} G_{\alpha\beta}^K(\Omega + \omega) D^A(\Omega)$$

$$\Rightarrow \quad \chi_{\alpha\beta}(\omega) = \frac{i}{2} \int \frac{d\Omega}{2\pi} \frac{G_{\alpha\beta}^K(\Omega + \omega)}{\Omega - i0} \ . \tag{3.82}$$

The susceptibility is the retarded spin correlator, whereas the Keldysh component of the Majorana Green's function is the symmetric Majorana correlator. Thus we recognize that Eq. (3.82) relates the retarded spin correlator to the symmetric Majorana correlator. For the imaginary part of susceptibility χ'', defined by $\chi = \chi' + i\chi''$, (3.82) implies the relation $\chi'' = iG^K/4$, which was also obtained in Ref. [5].

With the action (3.74) one finds that the the symmetric two-spin correlator $C_{\alpha\beta}^{(2)}(t,t')$ (3.73) equals to

$$C_{\alpha\beta}^{(2)}(t,t') = \frac{1}{4} \langle \mathcal{T}_K [\check{m}(t) \gamma^{cl} \check{\eta}_\alpha(t)][\check{m}(t') \gamma^{cl} \check{\eta}_\beta(t')] \rangle \ . \tag{3.83}$$

Along the lines above for the susceptibility it follows that

$$C_{\alpha\beta}^{(2)}(\omega) = \frac{1}{4} \int \frac{d\Omega}{2\pi} \operatorname{Tr} \left\{ \gamma^{cl} \hat{G}_{\alpha\beta}(\Omega + \omega) \gamma^{cl} \hat{D}(\Omega) \right\}$$

$$= \frac{i}{4} \left(G_{\alpha\beta}^R(\omega) - G_{\alpha\beta}^A(\omega) \right) + \frac{1}{4} \mathcal{P} \int \frac{d\Omega}{2\pi} \frac{G_{\alpha\beta}^R(\Omega) + G_{\alpha\beta}^A(\Omega)}{\Omega - \omega} \ . \tag{3.84}$$

Thus the symmetric spin correlator is related to retarded and advanced Majorana correlators. We note that for spin-diagonal symmetric correlators $\alpha = \beta$ the second term on the right-hand side above exactly vanishes.

The above Eqs. (3.82) and (3.84) show that the knowledge of the Majorana Green's function $\hat{G}_{\alpha\beta}(\omega)$ fully determines the two-spin correlators. It is neither necessary to consider complicated vertices nor to apply subspace projection procedures in order to obtain two-spin correlators from the Majorana Green's functions, demonstrating the advantage of the Majorana representation against many other techniques.

3.3. Conclusion

In this chapter we have analyzed the Majorana representation (3.2). We have shown that the Majorana representation is a faithful representation of spin 1/2 which directly allows to calculate spin correlation functions. In Subs. 3.1.2 we have demonstrated that the

equivalence of spin and corresponding Majorana correlators is directly connected to the fact that any product of spin operators can be reduced to an expression linear in the spin operators.

In Subs. 3.1.3 we have reviewed the identities between N-point spin and N-point Majorana correlation functions introduced in Refs. [5, 6]. We have generalized these identities to all pairwise spin-spin correlation functions. With regard to practical applications we have developed a scheme in Subs. 3.1.4 that allows to treat time-ordered spin correlators on an equal footing. Due to the simplified relations the Majorana representation is a particularly powerful tool with regard to higher-spin correlation functions.

Sec. 3.2 introduced basic concepts for the calculations in subsequent chapters, i.e., the path integral formalism for Majorana fermions as well as finite-temperature and real-time Green's functions. The benefits of the Majorana representation will become evident by application on the Bose-Kondo model, in Chapters 4 and 6, and on the spin-boson model in Chapter 5.

4. Majorana Representation for Dissipative Spin Dynamics in the Bose-Kondo Model

In this chapter we study the zero-field Bose-Kondo model within the Majorana representation. That is, a spin 1/2 isotropically coupled to a bosonic environment with the Ohmic spectral density. This model exemplifies a general situation of the dissipative spin dynamics. Our goal is to calculate the higher-order spin correlators related to noise, which requires to consider higher orders in perturbation theory. In the zero-magnetic field case higher-order diagrams show divergencies. To provide a thorough investigation of the problem we resort to the path-integral technique. Through a sequence of transformations we derive the effective theory that produces the spin relaxation rate from the saddle-point solution. We justify the solution by considering fluctuations around the saddle point and report on a curious gauge freedom in our model. Finally, we show that certain higher-order spin correlators can be safely calculated in the saddle-point approximation, substantiating the results for noise of susceptibility presented in Chapter 2.

In Section 4.1 we motivate the model, provide details of the bosonic bath and present the diagrammatic perturbation theory. The path-integral approach is developed in Sections 4.2 and 4.3, using both Matsubara and Keldysh techniques. In Section 4.4 we demonstrate the efficient calculation of spin correlation functions within our approach. The work presented in this chapter has been published in

4.1. Introduction

In this chapter we consider a spin 1/2 coupled to a bosonic bath. The interaction is described by the Hamiltonian

$$H_{int} = \hat{\boldsymbol{X}} \hat{\boldsymbol{S}} = \hat{X}_x \hat{S}_x + \hat{X}_y \hat{S}_y + \hat{X}_z \hat{S}_z \ . \tag{4.1}$$

The operators $\hat{X}_\alpha$ represent the bosonic bath and include the spin-bath coupling strength g. The spectral density ρ of the bosonic bath is assumed to have an Ohmic form $\rho(\omega) \propto \omega$ up to a large cutoff Λ.

The isotropic form of the spin-environment coupling in (4.1) resembles the well-known Kondo model, motivating the "Kondo" in the Bose-Kondo model. "Bose" refers to the bosonic degrees of freedom used to describe the environment. The term "Bose-Kondo" presumably dates back to Sengupta, Ref. [96], who introduced the term in the context of the spin 1/2 coupled to fluctuating magnetic fields. The fluctuating fields can be described in terms of bosonic degrees of freedom, therefore we think that the term "Bose-Kondo" is appropriate here. Based on the notion of spin-boson models in the general sense, the model described by the Hamiltonian above could also be understood as a zero-field isotropic spin-boson model.

Below, we provide the physical context for the model and recapitulate the relevant details of the bosonic bath. Then, we discuss the perturbative approach to spin correlation functions, which serves as a motivation for the path integral formulation in subsequent sections.

4.1.1. Motivation of the Model

The zero-field Bose-Kondo model appears in many physical contexts, including spin glasses and liquids, cf. Refs. [3, 96–99] and references therein. In Sec. 2.3, we have reported that the model of many independent paramagnetic spins 1/2 is discussed in the framework of $1/f$ flux noise in SQUIDs, cf. Refs. [12, 13]. Assuming that each spin is coupled to its own bath, we use the Bose-Kondo model as a generic approach to the dissipative dynamics of an ensemble of independent spins.

The Bose-Kondo model can be viewed as a generic model in the context of open quantum systems, the spin 1/2 representing the central quantum system and the bosonic bath assuming the role of the environment. According to Ref. [2] and references therein, virtually any environment can be described by harmonic oscillators, i.e. bosons, as long as the system-environment couplings are weak enough[1]. In particular, this has been demonstrated for environments of two-level systems in Ref. [100]. In this sense the concept of a bosonic bath is generic. Still, the dissipative spin dynamics depend on the form of the spectral density of the bosonic environment. The linear, Ohmic form chosen here is widely discussed in literature, e.g. Refs. [2, 101].

As a specific example, we can motivate the zero-field Bose-Kondo model by the extensively studied original Kondo model. The Kondo model describes a spin 1/2 impurity immersed into the electronic conduction sea of a metal. It displays highly interesting features at low temperatures, i.e., at temperatures on the scale of the so-called Kondo temperature $T_K \equiv \Lambda \exp[-\pi/(2g)]$ and below. At high temperatures $T \gg T_K$ the physics of the electronic system are dominated by bosonic excitations around the Fermi surface, which interact with the spin. The spectral densities of these bosonic excitations exhibit an Ohmic form at low energies, cf. Ref. [102]. Since in a rotationally invariant three-dimensional metal the conduction sea has to be isotropic, the Bose-Kondo model can serve as an effective high-temperature description for this scenario.

The spin in the above introduced Bose-Kondo model is treated by the Majorana representation introduced in the preceding Chapter 3. Using Eq. (3.2), the full Hamiltonian in

---

[1]There are exceptions to this statement, for instance the fermionic environment at low temperatures. Though the bare spin-environment coupling may be weak the effective coupling becomes strong at low temperatures $T \sim T_K \equiv\equiv \Lambda \exp[-\pi/(2g)]$ and the above statement becomes invalid.

terms of Majorana operators is

$$H = H_B + \hat{\boldsymbol{S}}\hat{\boldsymbol{X}} = H_B - \frac{i}{2}\hat{X}_\alpha \epsilon_{\alpha\beta\gamma}\hat{\eta}_\beta\hat{\eta}_\gamma \ , \qquad \alpha, \beta, \gamma \in \{x, y, z\} \ . \tag{4.2}$$

Here, H_B is the Hamiltonian of the bosonic bath, controlling the free dynamics of $\hat{\boldsymbol{X}}$. The coupling strength parameters are included in bosonic operators $\hat{X}_\alpha$ and appear in the bosonic correlator Π.

4.1.2. Bosonic Bath

Bosonic environments are widely discussed in textbooks, e.g. Refs. [2, 47, 94]. The bosonic Matsubara correlator used here is defined by

$$\langle \mathcal{T}_\tau \hat{X}_\alpha(\tau)\hat{X}_\beta(\tau')\rangle = \delta_{\alpha\beta}\Pi(\tau - \tau') \ , \tag{4.3}$$

the Keldysh versions are introduced below. In Matsubara frequency space Π can be expressed in terms of the spectral density of bosonic modes $\rho(|x|)$ at energy x by

$$\Pi(i\omega_m) = \int\limits_{-\Lambda}^{\Lambda} \frac{dx}{\pi}\,\frac{\rho(|x|)\,\mathrm{sign}\,x}{x - i\omega_m} \ , \tag{4.4}$$

where $\rho(|x|)$ is the bath spectral density and $\omega_m = 2\pi m T$ a bosonic Matsubara frequency, $m \in \mathbb{Z}$. We assume that the bosonic bath exhibits a continuous spectral density ρ of bosonic modes, which grows linearly with frequency,

$$\rho(|x|) = g|x| \ , \tag{4.5}$$

called an "Ohmic" spectral density. Naturally, the linear growth of ρ has to be cut off at some high-energy scale Λ. Here, we use a sharp cutoff, i.e. $\rho(|x|) = 0$ for $|x| > \Lambda$, which is implemented by the integral representation (4.4). In the low-frequency limit $\omega_m \ll \Lambda$ Eq. (4.4) simplifies to

$$\Pi(i\omega_m) \approx -g|\omega_m| + \frac{2g\Lambda}{\pi} \ . \tag{4.6}$$

The energy scales in our model are temperature T and the large cutoff $\Lambda > T$. We are interested in real-time dynamics, therefore frequency plays the role of a third energy scale. Throughout the present chapter the largest relevant energy scale is assumed to be temperature T. Thus, it is useful to perform a renormalization procedure for the problem, which allows to integrate out energies of the bath between $\sim T$ and Λ, effectively reducing the high-energy cutoff Λ to a new cutoff Λ' on the level of temperature, $\Lambda' \gtrsim T$.

Such a renormalization group approach is applied to the Bose-Kondo model in Chapter 6. The reduction of the cutoff Λ to Λ' leads to a rescaled coupling constant g' as well as rescaled Majorana Green's functions $\mathcal{G}'_\alpha$. Similar to the original Kondo model, the renormalization effects only become important for temperatures on the scale of the Kondo temperature T_K. That is, as long as the initial coupling g is sufficiently small, $g \ll 1$, and temperature sufficiently high, the condition $T \gg T_K$ is satisfied and renormalization effects can be neglected. Here we assume this to be the case. We therefore set $\mathcal{G}'_\alpha = \mathcal{G}_\alpha$, $g' = g$ and consider Λ to be of order of temperature for the remainder of the present chapter.

Here we are mostly concerned with real frequencies, therefore the crucial calculations are carried out within the Keldysh formalism, cf. Sec. 3.2 or Ref. [47]. Superscripts u, d on operators $\hat{X}_\alpha^u$ and $\hat{X}_\alpha^d$ denote the forward and the backward part of the Schwinger-Keldysh contour, respectively. The standard rotation to "classical" and "quantum" operators is, cf. Ref. [47],

$$\hat{X}_\alpha^{cl} = \frac{1}{\sqrt{2}} \left(\hat{X}_\alpha^u + \hat{X}_\alpha^d \right) , \qquad \hat{X}_\alpha^q = \frac{1}{\sqrt{2}} \left(\hat{X}_\alpha^u - \hat{X}_\alpha^d \right) . \tag{4.7}$$

The matrix-valued bosonic correlator $\hat{\Pi}$ is defined by

$$\langle \mathcal{T}_K \hat{X}_\alpha^a(t) \hat{X}_\beta^b(t') \rangle = \delta_{\alpha\beta} \hat{\Pi}^{ab}(t, t') , \qquad \hat{\Pi}(t, t') = \begin{pmatrix} \Pi^K(t, t') & \Pi^R(t, t') \\ \Pi^A(t, t') & 0 \end{pmatrix} , \tag{4.8a}$$

with $a, b = \{cl, q\}$. The retarded component $\Pi^R(\omega)$ in frequency space can be obtained by analytic continuation from the Matsubara formula, Eq. (4.4), by $-i\Pi(i\omega_m \to \omega + i0)$. For $|\omega| < \Lambda$ one finds

$$\Pi^R(\omega) = g\omega - iD, \qquad \Pi^A(\omega) = -g\omega - iD, \tag{4.8b}$$

with $D \approx (2g/\pi)\Lambda$. In equilibrium, the Keldysh component follows from the bosonic fluctuation-dissipation theorem

$$\Pi^K(\omega) = \coth\left(\frac{\omega}{2T}\right) \left(\Pi^R(\omega) - \Pi^A(\omega)\right) = 2g\omega \coth\left(\frac{\omega}{2T}\right) . \tag{4.8c}$$

The Ohmic behavior appears in the linear frequency terms in Π^R and Π^A in (4.8b).

4.1.3. Perturbation Theory

We proceed by developing the perturbative approach to Majorana Green's functions of the Bose-Kondo model, based on the expansion in small spin-bath coupling, $g \ll 1$. The full Hamiltonian (4.2) is $H = H_{int} + H_B$, since we expand in orders of H_{int} the zeroth-order Hamiltonian consists of the bath part H_B only. We find the perturbative approach leads to divergent contributions and numerous cancellations, which motivate us to use the path-integral formalism in the subsequent Sections 4.2 and 4.3. The path integral approach allows for an efficient reformulation of the perturbative expansion, cf. Ref. [94].

Elements of the perturbation theory are constructed by the free Majorana Green's function $\hat{G}(\omega)$ and the bosonic propagator $\hat{\Pi}(\omega)$. For the former we recall Eqs. (3.65),

$$\hat{G}_{f\alpha} = \begin{pmatrix} G_{f\alpha}^K & G_{f\alpha}^R \\ G_{f\alpha}^A & 0 \end{pmatrix} , \qquad G_{f\alpha}^{R/A}(\omega) = (\omega \pm i0)^{-1} , \qquad G_{f\alpha}^K(\omega) = 0 , \tag{4.9}$$

while the latter is given by Eqs. (4.8) above. In perturbation theory, the aim is to construct the full Majorana Green's function $\hat{G}_\alpha$ from these elements in perturbative approximations. The dressed, or full, Green's function can be constructed by means of the so-called self energy $\hat{\Sigma}$ and the free Green's function. The formula can be found in standard textbooks, e.g. Ref. [47], and is known as the Dyson equation. Here, in a time translation-invariant and zero-dimensional system the Dyson equation for the dressed retarded Majorana Green's function is given by

$$G_\alpha^R(\omega) = \left(\omega - \Sigma_\alpha^R(\omega) \right)^{-1} . \tag{4.10}$$

Figure 4.1.: The leading contribution to the self-energy. Solid and wavy lines represent Majorana propagators and bosonic bath propagators, respectively.

Given the self-energy in some approximation, the Dyson equation effectively sums up corresponding perturbative contributions up to infinite order for the dressed Green's function.

As an example we calculate self-energy Σ_α^R in lowest order, depicted by the diagram in Fig. 4.1. For the x-projection Σ_x^R one finds

$$\Sigma_x^R(\omega) = -\frac{1}{2} \sum_\alpha^{y,z} \int \frac{d\Omega}{2\pi} \left(\Pi^K(\omega+\Omega) G_{f\alpha}^A(\Omega) + \Pi^R(\omega+\Omega) G_{f\alpha}^K(\Omega) \right) \tag{4.11}$$

$$= -2igT \left(1 + \mathcal{O}\left(\frac{\omega}{T}\right) \right) , \tag{4.12}$$

The factor $2gT$ is recognized to be the Korringa rate $\Gamma = 2gT$. In the isotropic case considered here the above formula applies to all spin projections x, y, z. Thus, the spin sum in (4.11) merely adds a factor of two. The Dyson equation (4.10) implies that

$$G_\alpha^R(\omega) = (\omega + i\Gamma)^{-1} . \tag{4.13a}$$

The dressed advanced Green's function can be obtained by complex conjugation, $G_\alpha^A(\omega) = (G_\alpha^R(\omega))^*$. Since coupling to the bath relaxes the (spin) Majorana system to equilibrium the dressed Keldysh component G_α^K is easily deduced by the use of the fermionic fluctuation-dissipation theorem,

$$G_\alpha^K(\omega) = \tanh \frac{\omega}{2T} \left(G_\alpha^R(\omega) - G_\alpha^A(\omega) \right) = \frac{-2i\Gamma \tanh \frac{\omega}{2T}}{\omega^2 + \Gamma^2} . \tag{4.13b}$$

In the high-temperature regime $T \gg T_K, \omega, \Gamma$ the results (4.13) can be corroborated as follows. If the free Majorana Green's functions $G_{f\alpha}^{A(K)}$ in the approximation (4.11) for the the self-energy are replaced by the dressed ones, Eqs. (4.13), the results (4.12) and (4.13) remain the same. In this sense the Majorana Green's functions (4.13) are self-consistent. Now, the two-spin correlation functions can be directly deduced from Majorana Green's functions by the method discussed in Chapter 3.

Figure 4.2.: Examples of higher-order diagrams that include connected Majorana propagators.

Typically, the above method is used to calculate 1- or 2-point spin correlation functions, e.g., magnetization or susceptibility. In lower orders, for instance in the self-energy diagram 4.1, Majorana propagators are never connected by a bosonic line. Such an element only appears in higher orders or in higher correlation functions. An example was already mentioned in Sec. 2.2 and is shown in Fig. 4.2. These two diagrams in Fig. 4.2 include an inner loop composed of two Majorana propagators and two bosonic lines. At high temperatures, the bosonic line is dominated by the frequency independent part $\Pi^K(0) \sim 2gT = \Gamma$. In the perturbative approach using free Green's functions G_f, Eqs. (4.9), the inner loops are dominated by contributions of the type

$$\left(\Pi^K(0)\right)^2 \int \frac{d\Omega}{2\pi} \, G_f^R(\Omega + \omega_1) G_f^A(\Omega - \omega_2) \, , \tag{4.14}$$

which diverge. The divergency can be dealt with by using dressed Majorana Green's functions (4.13). However, the existence of this divergency implies that there is no small parameter which controls the perturbative expansion. In turn, to compute more complex higher-order diagrams or correlation functions one has to sum up series of diagrams including ladders of bosonic propagators. Below we demonstrate how this can be achieved within diagrammatic perturbation theory, for the case of one particular component of the dressed bosonic Majorana-Majorana interaction line. Subsequently we resort to the path integral technique, a method which combines functional integral techniques and perturbation theory, cf. e.g. Ref. [94], and hence allows for a more general treatment of complex higher-order diagrams.

One example of more complex structures is the type of dressed bosonic interaction line that is obtained by summing up ladders of bosonic propagators. This dressed interaction carries four times (or frequencies), the Keldysh indices $a, b, c, d = \{cl, q\}$, and the spin indices $\alpha, \beta, \gamma, \delta = \{x, y, z\}$; diagrammatically it is depicted by

$$\hat{\Gamma}^{ab,cd}_{\alpha\beta,\gamma\delta} = \quad \begin{array}{c} a,\alpha \quad\rule{2cm}{0.4pt}\quad b,\beta \\[-2pt] \boxed{\hat{\Gamma}} \\[-2pt] c,\gamma \quad\rule{2cm}{0.4pt}\quad d,\delta \end{array} \quad . \tag{4.15}$$

For demonstration, we pick one of several possible components of $\hat{\Gamma}$ that carries identical spin indices on the left (as well as on the right) and the Keldysh indices (qc, qc), which corresponds to the retarded-retarded component, that is $\Gamma^{RR}_{\alpha\beta}$. The bare bosonic interaction line can be constructed from the interacting Hamiltonian (4.2), it carries the bosonic correlator (4.8) and corresponds to

$$^{(0)}\Gamma^{RR}_{\alpha\beta}(\nu) = \quad \begin{array}{c} \alpha \quad\rule{1cm}{0.4pt}\quad \beta \\ \nu \\ \alpha \quad\rule{1cm}{0.4pt}\quad \beta \end{array} \quad = \Pi^K(\nu) M_{\alpha\beta} \, . \tag{4.16}$$

The spin structure is encapsulated in the fully off-diagonal matrix M, which is defined by

$$M = \begin{pmatrix} 0 & 1 & 1 \\ 1 & 0 & 1 \\ 1 & 1 & 0 \end{pmatrix} \tag{4.17}$$

and will also appear in the path integral approach below.
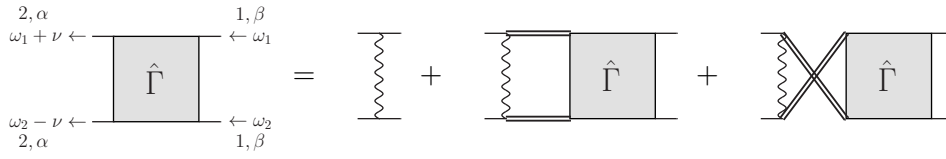
Figure 4.3.: Bethe-Salpeter-like equation for the partially dressed bosonic interaction. Thick solid lines are dressed Majorana propagators, wavy lines correspond to the bosonic bath.

The partially dressed interaction $\Gamma_{\alpha,\beta}^{RR}$, which includes the sum of divergent contributions up to all orders, can be obtained from the Bethe-Salpeter-like equation depicted in Fig. 4.3, cf. Ref. [94].[2] At high temperatures the two right-most diagrams in Fig. 4.3 are dominated by terms comprising $\Pi^K \sim 2gT = \Gamma$ combined with Green's functions $G^R G^A$, such that the upper and lower halves of the complex plane each contain one of the Green-functions poles. A simple analysis shows that these leading contributions are of the same order in g as the bare bosonic line. Thus, we might suspect a strong renormalization of the interaction line. This is, however, not the case due to a cancellation.

Taking into account all contributions depicted in Fig. 4.3 we obtain

$$
\begin{aligned}
\Gamma_{\alpha\beta}^{RR}(\omega_1, \omega_2, \nu) = {}& \Pi^K(\nu) M_{\alpha\beta} \\
& + \int \frac{d\Omega}{2\pi} \Pi^K(\nu - \Omega) M_{\alpha\gamma} G_\gamma^R(\Omega + \omega_1) G_\gamma^A(\Omega - \omega_2) \Gamma_{\gamma\beta}^{RR}(\omega_1, \omega_2, \Omega) \\
& - \int \frac{d\Omega}{2\pi} \Pi^K(\nu - \Omega) M_{\alpha\gamma} G_\gamma^R(\Omega + \omega_1) G_\gamma^A(\Omega - \omega_2) \Gamma_{\gamma\beta}^{RR}(\omega_1, \omega_2, -\Omega - \omega_1 + \omega_2)
\end{aligned}
\tag{4.18}
$$

The Green's functions are calculated within the approximation (4.12) for Σ^R in the high-temperature regime $T \gg T_K, \nu, \omega_1, \omega_2, \Gamma$. Let us assume that the leading term in Γ_0^{RR} does not depend on the third frequency, split $\Gamma^{RR} = \Gamma_0^{RR} + \Gamma_\nu^{RR}$ and suggest that Γ_ν^{RR} is sub-leading. If this is the case, the integrals in the second and third term become equal, and we find that the renormalized interaction coincides with the bare one,

$$
\Gamma_{\alpha\beta}^{RR}(\omega_1, \omega_2) = \Pi^K(0) M_{\alpha\beta} \ .
\tag{4.19}
$$

For the case considered here, the above result shows that large, leading contributions cancel. The basic reason for this cancellation is the different sign of the two additional terms in Eq. (4.18). The corresponding diagrams in Fig. 4.3 suggest that the sign change is related to the interchange of two Majorana fermions, i.e., an underlying symmetry of Majorana fermions. The path integral approach pursued in Section 4.3.3 will indeed show that such cancellations are connected to this symmetry.

The fact that leading contributions can be of the same order as the bare bosonic line can be attributed to the fact that the non-perturbed spin Hamiltonian is zero, $H_0 = 0$, corresponding to zero or weak magnetic fields. In this case, the energy scale given by some interaction cannot directly assumed to be weak, that is, perturbations are not weak in

---

[2]Due to the self-annihilating nature of Majorana operators there are two contributions to the Bethe-Salpeter equation, in contrast to the standard fermionic case as discussed in Ref. [94]. There, the right-most diagram in Fig. 4.3 does not appear.

terms of the unperturbed scale over interaction scale. Nevertheless it is possible to sum up the leading contributions in a weak coupling limit, which is done for example by Paaske et al. in [102], using Abrikosov fermions.

4.2. Path-Integral Approach using Matsubara Technique

The perturbative approach in the preceding section can be understood as an expansion around the saddle point of free Majorana Green's functions. The functional integral techniques that are available within the path integral framework enable to transform to other saddle points. Different saddle points provide alternative starting points for the perturbative analysis, which often prove more suitable, cf. e.g. Ref. [94]. In the path integral formulation the perturbative analysis amounts to the analysis of fluctuations around the saddle points.

Here we perform the path integral transformations and the saddle-point analysis in the framework of the more transparent Matsubara technique, demonstrating the main features of our approach. This is followed by a thorough treatment of low real frequencies in the framework of the Keldysh formalism in Section 4.3.

The Matsubara imaginary-time technique, $t = -i\tau$, $\partial_\tau = -i\partial_t$ and inverse temperature $\beta = 1/T$, was briefly discussed in Sec. 3.2 for Majorana fermions. Here, in addition to the Majorana fermions representing the spin, the bosonic bath has to be included. The bosonic part of the path integral can be constructed from the Hamiltonian in a similar way, i.e., by time-slicing and the use of coherent states, for details we refer to textbooks, e.g. Refs. [47, 94]. The integration measures $D[\dots]$ are normalized. Omitting the source fields, cf. Sec. 3.2, the partition function of the Bose-Kondo model, Eq. (4.2), in the Matsubara formalism reads

$$\mathcal{Z} = \int D[\boldsymbol{X}]D[\boldsymbol{\eta}] \exp\left\{i\,\mathcal{S}_B + i\int_0^\beta d\tau \left[\frac{1}{2}\,\eta_\alpha(\tau)i\partial_\tau\eta_\alpha(\tau) + \frac{1}{2}\,X_\alpha(\tau)\epsilon_{\alpha\beta\gamma}\eta_\beta(\tau)\eta_\gamma(\tau)\right]\right\} . \tag{4.20}$$

Here $\mathcal{S}_B$ is the free bosonic action, given by, cf. Ref. [47]

$$i\mathcal{S}_B = -\frac{1}{2}\int_0^\beta d\tau d\tau' \, X_\alpha(\tau)\,\Pi^{-1}(\tau-\tau')X_\alpha(\tau') . \tag{4.21}$$

For the Gaussian integral over the bosonic fluctuations $\boldsymbol{X}$ to be well-defined, the bosonic correlator $\Pi(\tau-\tau')$, defined in (4.3) has to be positive and non-zero. The standard Ohmic form in imaginary time space reads, cf. Ref. [94],

$$\Pi(\tau-\tau') = \frac{g\pi T^2}{\sin^2(\pi T(\tau-\tau'))} . \tag{4.22}$$

At short times $|\tau - \tau'| < 1/\Lambda$ the formula (4.22) has to be cut off, i.e. its maximal value is of order $g\Lambda^2$. The cutoff Λ already appeared in the $\Pi(\omega_m)$, Eq. (4.4), related by $\Pi(\tau) = T\sum_m \Pi(\omega_m)$. Here, we use the divergent form (4.22) keeping the regularization and renormalization in mind, cf. Subs. (4.1.2).

4.2.1. Path-Integral Transformations

The first step in our treatment is to average over the bosonic fluctuations of $\boldsymbol{X}$. To do so we complete the square in the exponent of (4.20). Introducing the shifted variable $X'_\alpha = X_\alpha + \frac{i}{2}\Pi\epsilon_{\alpha\beta\gamma}(\eta_\beta\eta_\gamma)$ we can write symbolically

$$-\frac{1}{2}X_\alpha \cdot \Pi^{-1} \cdot X_\alpha + \frac{i}{2}X_\alpha\epsilon_{\alpha\gamma\delta}\eta_\gamma\eta_\delta = -\frac{1}{2}X'_\alpha \cdot \Pi^{-1} \cdot X'_\alpha - \frac{1}{4}\sum_{\alpha,\gamma}^{\alpha\neq\gamma}(\eta_\alpha\eta_\gamma) \cdot \Pi \cdot (\eta_\alpha\eta_\gamma)$$

$$= -\frac{1}{2}X'_\alpha \cdot \Pi^{-1} \cdot X'_\alpha - \frac{1}{4}M_{\alpha\gamma}(\eta_\alpha\eta_\gamma) \cdot \Pi \cdot (\eta_\alpha\eta_\gamma) \ . \quad (4.23)$$

In the above equation we imply that each term is summed over $\alpha, \gamma, \delta = \{x, y, z\}$ separately, and M is the symmetric off-diagonal matrix

$$M = \begin{pmatrix} 0 & 1 & 1 \\ 1 & 0 & 1 \\ 1 & 1 & 0 \end{pmatrix} \ . \quad (4.24)$$

The normalized Gaussian integrals over shifted variables $\boldsymbol{X}'(\tau)$ in (4.20) are readily evaluated to unity, leaving the last term in (4.23) which is quartic in Majorana variables. Thus, we arrive at

$$\mathcal{Z} = \int D[\boldsymbol{\eta}] \exp\left\{ -\frac{1}{2}\int_0^\beta d\tau\, \eta_\alpha(\tau)\, \partial_\tau\, \eta_\alpha(\tau) \right.$$

$$\left. -\frac{1}{4}\int_0^\beta d\tau d\tau' M_{\alpha\gamma}\, \eta_\alpha(\tau)\eta_\gamma(\tau)\, \Pi(\tau - \tau')\ \eta_\alpha(\tau')\eta_\gamma(\tau') \right\} \ . \quad (4.25)$$

Next we decouple the quartic Majorana-interaction in a different channel. To this end we rearrange the Majorana variables in the quartic term

$$i\mathcal{S}_{int}[\boldsymbol{\eta}] = -\frac{1}{4}\int_0^\beta d\tau d\tau' M_{\alpha\gamma}\, \Pi(\tau - \tau')\, \eta_\alpha(\tau)\eta_\gamma(\tau)\, \eta_\alpha(\tau')\eta_\gamma(\tau')$$

$$= +\frac{1}{4}\int_0^\beta d\tau d\tau'\, \Pi(\tau - \tau')\, [\eta_\alpha(\tau)\eta_\alpha(\tau')]\, M_{\alpha\gamma}\, [\eta_\gamma(\tau)\eta_\gamma(\tau')] \ . \quad (4.26)$$

We now employ the Hubbard-Stratonovich transformation by introducing fields Σ_α. The new path integral runs over all configurations of the Σ_α fields,

$$\mathcal{Z} = \int D[\boldsymbol{\eta}]D[\boldsymbol{\Sigma}]\, e^{i\mathcal{S}[\boldsymbol{\eta},\boldsymbol{\Sigma}]} \ . \quad (4.27)$$

The fields $\Sigma(\tau, \tau')$ are non-local in τ-space and inherit the symmetry of Majorana propagators, therefore $\Sigma_\alpha(\tau, \tau') = -\Sigma_\alpha(\tau', \tau)$. The new effective action reads

$$i\mathcal{S}[\boldsymbol{\eta}, \boldsymbol{\Sigma}] = \int_0^\beta d\tau d\tau'\left(\frac{1}{2}\, \eta_\alpha(\tau)\, (\mathcal{G}_\alpha^{-1})_{\tau\tau'}\, \eta_\alpha(\tau') - \frac{1}{4}\frac{\Sigma_\alpha(\tau, \tau')\, (M^{-1})_{\alpha\gamma}\, \Sigma_\gamma(\tau, \tau')}{\Pi(\tau - \tau')} \right) \ , \quad (4.28)$$

with the Majorana Green's function

$$(\mathcal{G}_\alpha^{-1})_{\tau\tau'} = -\delta(\tau - \tau')\partial_{\tau'} - \Sigma_\alpha(\tau, \tau') \ , \quad (4.29)$$

which is a functional of the fields $\mathcal{G}_\alpha = \mathcal{G}_\alpha[\Sigma_\alpha]$.

At this point we have to ensure that the functional $\boldsymbol{\Sigma}$- integrals in (4.27) indeed converge. The inverse matrix M^{-1} has the positive eigenvalue $(1/2)$ and the double degenerate negative eigenvalue (-1). The function $\Pi(\tau - \tau')$, Eq. (4.22), is positive and non-zero. We choose the eigenmode with the positive eigenvalue to be real and eigenmodes with negative eigenvalues to be imaginary, such that the overall sign of the action term in the exponent is negative, and the functional integral over Σ_α converges. In particular, we choose $\boldsymbol{\Sigma} = \boldsymbol{\Sigma}' + i\boldsymbol{\Sigma}_1'' + i\boldsymbol{\Sigma}_2''$, where the real part represents the eigenvector corresponding to the eigenvalue $(1/2)$, whereas the imaginary parts incorporate the eigenvectors to the eigenvalues (-1),

$$\boldsymbol{\Sigma}' = \Sigma' \cdot \begin{pmatrix} 1 \\ 1 \\ 1 \end{pmatrix} , \qquad \boldsymbol{\Sigma}_1'' = \Sigma_1'' \cdot \begin{pmatrix} 1 \\ 0 \\ -1 \end{pmatrix} , \qquad \boldsymbol{\Sigma}_2'' = \Sigma_2'' \cdot \begin{pmatrix} 1 \\ -2 \\ 1 \end{pmatrix} . \qquad (4.30)$$

With this choice the three-dimensional integral over the fields Σ', Σ_1'' and Σ_2'' indeed converges.

The redecoupled action (4.28) is again quadratic in Majorana Grassmann variables η_α, which allows us to integrate them out by the rules of Grassmann Gaussian integration as described in Ref. [94]. In case of real Grassmann variables one obtains the Pfaffian, i.e. the square root of the determinant, cf. Ref. [90],

$$\int D[\boldsymbol{\eta}] \exp\left\{ \int_0^\beta d\tau d\tau' \frac{1}{2} \eta_\alpha(\tau) \, (\mathcal{G}_\alpha^{-1})_{\tau\tau'} \, \eta_\alpha(\tau') \right\} = \sqrt{\det \frac{1}{2} (\mathcal{G}_\alpha^{-1})_{\tau\tau'}} . \qquad (4.31)$$

The matrix argument in the determinant above has to be interpreted as a matrix in imaginary-time space. We remind that the Green's function $\mathcal{G}$ is a functional of fields $\Sigma(\tau, \tau')$, cf. Eq. (4.29).

The determinant in (4.31), in turn, can be recast into the exponential of a $\mathrm{Tr}\log$-expression. In this way, we obtain

$$i\mathcal{S}[\boldsymbol{\Sigma}] = \frac{1}{2} \sum_\alpha^{x,y,z} \mathrm{Tr}\log\left(\mathcal{G}_\alpha^{-1} \right) - \frac{1}{4} \sum_{\alpha,\gamma}^{x,y,z} \int_0^\beta d\tau d\tau' \frac{\Sigma_\alpha(\tau,\tau') \, (M^{-1})_{\alpha\gamma} \, \Sigma_\beta(\tau,\tau')}{\Pi(\tau - \tau')} , \qquad (4.32)$$

which is the effective action of Σ_α-fields. The trace Tr denotes the trace over imaginary-time space.

4.2.2. Saddle-Point Solution

We can now identify the saddle point and fluctuations of the effective Σ-action. The saddle-point solution is found by expanding $\Sigma_\alpha = \Sigma_{0\alpha} + \delta\Sigma_\alpha$. Through

$$\log\left(\mathcal{G}_\alpha^{-1} \right) = \log\left(\mathcal{G}_{0\alpha}^{-1} \cdot (1 - \mathcal{G}_{0\alpha}\delta\Sigma_\alpha) \right) \qquad (4.33)$$

the $\mathrm{Tr}\log$-term is expanded to

$$\frac{1}{2} \sum_\alpha \mathrm{Tr}\log\left(\mathcal{G}_\alpha^{-1} \right) = \frac{1}{2} \sum_\alpha \mathrm{Tr}\log\left(\mathcal{G}_{0\alpha}^{-1} \right) - \frac{1}{2} \sum_\alpha \int_0^\beta d\tau d\tau' \, \mathcal{G}_{0\alpha}(\tau' - \tau)\delta\Sigma_\alpha(\tau', \tau)$$
$$+ \mathcal{O}(\delta\Sigma^2) . \qquad (4.34)$$

Comparing the linear terms $\delta\Sigma$ in (4.32), the linear order vanishes for

$$\Sigma_{0\alpha}(\tau - \tau') = \Pi(\tau - \tau')M_{\alpha\beta}\mathcal{G}_{0\beta}(\tau - \tau') . \tag{4.35}$$

This saddle-point solution is stationary, i.e., the Green's function $\mathcal{G}_{0\alpha}(\tau - \tau')$ and the self-energy $\Sigma_{0\alpha}(\tau - \tau')$ only depend on the time difference. In Matsubara frequency space, the Green's function, Eq. (4.29), assumes the form

$$(\mathcal{G}_{0\alpha}(i\epsilon_n))^{-1} = i\epsilon_n - \Sigma_{0\alpha}(i\epsilon_n) . \tag{4.36}$$

Eqs. (4.35) and (4.36) require the saddle-point solutions $\mathcal{G}_{0\alpha}$ and $\Sigma_{0\alpha}$ to be computed in a self-consistent fashion.

As a starting point, we calculate the self-energy (4.35) by the use of the free Majorana Green's function $\mathcal{G}_{f\alpha}$, leading to

$$\Sigma_{0\alpha}(i\epsilon_n) = -\int\limits_{-\Lambda}^{\Lambda} \frac{dx}{\pi} \frac{gx \coth\left(\frac{x}{2T}\right)}{x - i\epsilon_n} . \tag{4.37}$$

At high temperatures $T \gg T_K$ it turns out that the saddle-point self-energy remains unchanged if the broadening by $\Sigma_{0\alpha}$ is included in the calculation. This can be seen from the Keldysh calculation in Subs. 4.3.2. The retarded self-energy can be obtained from (4.37) by analytic continuation $i\epsilon_n \to \epsilon + i0$. For $\epsilon \to 0$ we find

$$\Sigma_{0\alpha}^R(\epsilon \to 0) = -2igT = -i\Gamma . \tag{4.38}$$

The solution (4.38) coincides with the perturbative result (4.12) in Subs. 4.1.3 and we again recognize the Korringa relaxation rate $\Gamma = 2gT$. With regard to the eigenmodes (4.30) the solution (4.38) means that $\Sigma_{1,0}'' = \Sigma_{2,0}'' = 0$, whereas $\Sigma_0'(i\epsilon_n) = \Sigma_{0\alpha}(i\epsilon_n)$. Having obtained the saddle-point solution we can turn to the fluctuations around the saddle point.

4.2.3. Fluctuations

To study the fluctuations we expand the trace-log term in (4.32) to second order in $\delta\Sigma_\alpha$. The action reads

$$iS_{\delta\Sigma} = -\frac{1}{4}\sum_\alpha \int_0^\beta d\tau_1 d\tau_2 d\tau_3 d\tau_4 \, \mathcal{G}_{0\alpha}(\tau_1 - \tau_2)\,\delta\Sigma_\alpha(\tau_2, \tau_3)\mathcal{G}_{0\alpha}(\tau_3 - \tau_4)\,\delta\Sigma_\alpha(\tau_4, \tau_1)$$

$$-\frac{1}{4}\int_0^\beta d\tau d\tau' \frac{\delta\Sigma_\alpha(\tau, \tau')\,(M^{-1})_{\alpha\beta}\,\delta\Sigma_\beta(\tau, \tau')}{\Pi(\tau - \tau')} . \tag{4.39}$$

The analysis of the fluctuations is most easily done in Matsubara frequency space. The Fourier transform of fields $\delta\Sigma$ is introduced via

$$\delta\Sigma_\alpha(\epsilon_n, \nu_m) = \int_0^\beta d\tau d\tau' \, e^{i\nu_m(\tau + \tau')} \, e^{i\epsilon_n(\tau - \tau')} \delta\Sigma_\alpha(\tau, \tau') . \tag{4.40}$$

In this Fourier transform ϵ_n and ν_m are fermionic and bosonic Matsubara frequencies, respectively. In Matsubara frequency space we obtain for the action

$$iS_{\delta\Sigma} = -\frac{T^2}{4}\sum_\alpha \sum_{\epsilon_n, \nu_m} \mathcal{G}_{0\alpha}(\epsilon_n + \nu_m)\,\mathcal{G}_{0\alpha}(\epsilon_n - \nu_m)\,\delta\Sigma_\alpha(\epsilon_n, \nu_m)\,\delta\Sigma_\alpha(\epsilon_n, -\nu_m)$$

$$-\frac{T^3}{4}\sum_{\alpha\beta}\sum_{\epsilon_1, \epsilon_2, \nu} A(\epsilon_1 + \epsilon_2)\,\delta\Sigma_\alpha(\epsilon_1, \nu)\,(M^{-1})_{\alpha\beta}\,\delta\Sigma_\beta(\epsilon_2, -\nu) . \tag{4.41}$$

Here, $A(i\omega_m)$ includes Π, Eq. (4.22), and is given by

$$
\begin{aligned}
A(i\omega_m) &= \int_0^\beta d\tau \, \frac{e^{i\omega_m\tau}}{\Pi(\tau)} = \frac{1}{g\pi T^2} \int_0^\beta d\tau \, e^{i\omega_m\tau} \, \sin^2(\pi T\tau) \\
&= \frac{1}{2g\pi T^3} \left(\delta_{m,0} - \frac{1}{2}\delta_{m,1} - \frac{1}{2}\delta_{m,-1} \right) \; .
\end{aligned}
\tag{4.42}
$$

At this point we can argue that the second term in the action (4.41) dominates. The fermionic Matsubara Green's functions satisfy $|\mathcal{G}_{0\alpha}| < 1/(\pi T)$. Thus the first term is estimated to be of order one, whereas the second term is much larger due to the inverse of the small coupling constant $1/g$ contained in $A(i\omega_m)$. Therefore the first term cannot compete with the second but can rather describes a small correction of order $g \ll 1$. This important observation allows us to disregard the first term of (4.41), which originated in second order from the trace-log term in (4.32). Above that, the argument applies to higher-order terms in the trace-log expansion. Thus, concerning the action of fluctuations, the trace-log term in the original action (4.32) can be neglected.

Within the Majorana representation, the insights above can facilitate the calculation of spin correlators significantly. The saddle-point solution for Majorana Green's functions (4.35) provides a new starting point for a perturbative treatment in terms of fluctuations $\delta\Sigma$. The propagator of fluctuations $\langle\delta\Sigma\delta\Sigma\rangle$ can be obtained by inverting the prefactor of the quadratic action. The second term in (4.41) was found to be dominating, thus the prefactor to be inverted is $M^{-1}A(i\omega_m)$. In turn, the propagator of fluctuations is $\propto M_{\alpha\beta}$. As a consequence, the diagonal parts of the propagator vanish:

$$
\langle\delta\Sigma_\alpha(\dots)\delta\Sigma_\alpha(\dots)\rangle \propto M_{\alpha\alpha} = 0 \; .
\tag{4.43}
$$

That is, for all Majorana correlation functions which include only one spin component α, corrections due to fluctuations can be safely omitted.

The argument above for the smallness of the first term of (4.41) is based on the discreteness of the Matsubara fermionic frequencies. Ultimately, we are interested in real times and the behavior in various frequency ranges, including low frequencies $\omega \ll T$. The line of reasoning above suggests that the Green's functions $\mathcal{G}_{0\alpha}$ in the first term of (4.41) might become of order $1/\Gamma = 1/(2gT)$ for real frequencies $\epsilon \to 0$. Then, it seems that the first term could take values of order g^{-2} and dominate over the second term $\propto g^{-1}$. To clarify the situation in the low-frequency range we perform a direct Keldysh calculation in Sec. 4.3. Anticipating the results, we find that the arguments presented above hold.

4.3. Path-Integral Approach Using Keldysh Technique

To be able to treat also low real frequencies not covered by the discussion above, we provide here the Keldysh version of the path-integral calculation. The path-integral transformations can be done similarly to the Matsubara case in Subs. 4.2.1. Prior to the thorough analysis of the effective action we present qualitative arguments supporting that the trace-log term remains negligible on the low-frequency range, which was not covered by the Matsubara discussion. The Keldysh analysis of the saddle-point solution and fluctuations of the final effective action is performed in Subsections 4.3.2 and 4.3.3. Thereafter, we analyze a curious gauge freedom of the model.

A short description of the Keldysh formalism was provided in Section 3.2, for details we refer to the textbook Ref. [47]. For the Bose-Kondo model considered here, Eq. (4.2), the partition function reads

$$\mathcal{Z} = \int D[\boldsymbol{X}]D[\boldsymbol{\eta}] \exp\left\{\frac{i}{2}\int_C dt\left(\eta_\alpha(t)i\partial_t\eta_\alpha(t) + iX_\alpha(t)\epsilon_{\alpha\beta\gamma}\eta_\beta(t)\eta_\gamma(t)\right) + i\mathcal{S}_B\right\}$$

$$= \int D[\boldsymbol{X}]D[\boldsymbol{\eta}] \exp\left\{\frac{i}{2}\sum_a^{u,d}\int_{-\infty}^{\infty} dt\left(\eta^a(t)i\tau_3^a\partial_t\eta^a(t) + i\tau_3^a X_\alpha^a(t)\epsilon_{\alpha\beta\gamma}\eta_\beta^a(t)\eta_\gamma^a(t)\right)\right.$$

$$\left. + i\mathcal{S}_B\right\}, \qquad (4.44)$$

where the Keldysh index a takes the value u at the forward part of the contour and d on the backward part of the contour. The Pauli matrix τ_3 accounts for the negative sign on the backward contour. $\mathcal{S}_B$ denotes the internal action of the bosonic bath.

At the first step we average over the fluctuations of $\boldsymbol{X}$, in full analogy to the Matsubara discussion above. This yields, dropping the integration boundaries $\{-\infty, \infty\}$ for the remainder,

$$\mathcal{Z} = \int D[\boldsymbol{\eta}] \exp\left\{-\frac{1}{2}\int dt\, \eta_\alpha^a(t)\,\tau_3^{ab}\partial_t\,\eta_\alpha^b(t)\right.$$

$$\left. + \frac{1}{4}\int dtdt' M_{\alpha\beta}\tau_3^a\,\Pi^{ab}(t,t')\,\tau_3^b\,\eta_{t,\alpha}^a\eta_{t,\beta}^a\,\eta_{t',\alpha}^b\eta_{t',\beta}^b\right\}. \qquad (4.45)$$

Here $\langle TX_\alpha^a(t)X_\beta^b(t')\rangle = \delta_{\alpha\beta}\Pi^{ab}(t - t')$ is the bosonic Keldysh correlator given in Eqs. (4.8), and $a, b \in \{u, d\}$ are the Keldysh contour indices over which summation is implied. As in Subs. 4.2.1, we decouple the quartic term in a different channel

$$i\mathcal{S}_{int}[\boldsymbol{\eta}] = \frac{1}{4}\int dtdt' M_{\alpha\beta}\tau_3^a\,\Pi^{ab}(t,t')\,\tau_3^b\,\eta_{t,\alpha}^a\eta_{t,\beta}^a\,\eta_{t',\alpha}^b\eta_{t',\beta}^b$$

$$= -\frac{1}{4}\int dtdt' \tau_3^a\,\Pi^{ab}(t,t')\,\tau_3^b\,(\eta_{t,\alpha}^a\eta_{t',\alpha}^b)\,M_{\alpha\beta}(\eta_{t,\beta}^a\eta_{t',\beta}^b). \qquad (4.46)$$

In contrast to the Matsubara case the Keldysh bath correlator $\Pi^{ab}(t,t')$ is not necessarily positive and non-zero, we will therefore use slightly different Hubbard-Stratonovich fields below. However, we are again aiming at an analysis of the effective action of these fields.

4.3.1. Qualitative Considerations

Before turning to the full-fledged Keldysh analysis, we provide here a qualitative argument based on the locality of the bath correlation function $\Pi^{ab}(t - t')$ on the relevant time scale of order $1/\Gamma$. The time scale $1/\Gamma$ corresponds to the low-frequency range $\omega \sim \Gamma \ll T$, which was not covered by the Matsubara discussion of $\mathcal{S}[\delta\Sigma]$, Eq. (4.39), in Subs. 4.2.3. On this long time scale the bosonic environment is time-local and we can safely replace all components of $\Pi^{ab}(t - t')$ by its classical (Keldysh) part, i.e.,

$$\Pi^{ab}(t - t') \approx \tilde{\Pi}(t - t') = (1/2)\Pi^K(t - t'). \qquad (4.47)$$

which is positive and non-zero. This is allows us to proceed similarly to the treatment in the Matsubara case in Subs. 4.2.1. That is, we can consider an action of the form Eq. 4.32,

$$i\mathcal{S}[\boldsymbol{\Sigma}] = \frac{1}{2}\sum_\alpha^{x,y,z}\mathrm{Tr}\log\left(G_\alpha^{-1}\right) - \frac{1}{4}\int dtdt'\frac{\Sigma_\alpha^{ab}(t,t')\,\tau_3^a\tau_3^b(M^{-1})_{\alpha\beta}\,\Sigma_\beta^{ab}(t,t')}{\tilde{\Pi}(t - t')}, \qquad (4.48)$$

where

$$(G_\alpha^{-1})_{tt'}^{ab} = i\tau_3^{ab}\delta(t - t')\partial_{t'} - \Sigma_\alpha^{ab}(t, t') . \tag{4.49}$$

One can find the saddle point and again obtain the relaxation rate $\Gamma = 2gT$. This is done below in the full Keldysh calculation. Here we concentrate on the fluctuations $\delta\Sigma^{ab}$. On the relevant time scales ($\sim \Gamma^{-1}$) the function $\tilde{\Pi}$ is local, $\tilde{\Pi}(t - t') \sim 2gT\delta(t - t')$.[3] This locality means, in turn, that the fluctuating self-energies $\delta\Sigma^{ab}$ are local. On the other hand they are anti-symmetric, $\Sigma^{ab}(t, t') = -\Sigma^{ba}(t', t)$. This strong constraint implies that only off-diagonal (in Keldysh indices) components of $\delta\Sigma$ fluctuate: $\delta\Sigma^{ud}(t, t') = -\delta\Sigma^{du}(t', t) \sim \delta(t - t')$, whereas $\delta\Sigma^{uu} = \delta\Sigma^{dd} = 0$. Upon the Keldysh rotation (see Eq. (4.53) below), this means that only the retarded and advanced components $\delta\Sigma^{R/A}$ fluctuate.

Keeping the above arguments in mind, we expand the trace-log term of (4.48) and check whether it contributes to the fluctuations. Terms including the Keldysh component of the Majorana Green's function G_α^K can be neglected against those including $G_\alpha^{R/A}$, since the Keldysh component is smaller on the relevant time scale. Thus the only terms that remain are of the type $\text{Tr}[G_\alpha^R\delta\Sigma^R G_\alpha^R\delta\Sigma^R G_\alpha^R\delta\Sigma^R \dots]$ and $\text{Tr}[G_\alpha^A\delta\Sigma^A G_\alpha^A\delta\Sigma^A G_\alpha^A\delta\Sigma^A \dots]$. Since $\delta\Sigma^{R/A}$ are local in time and $G^{R/A}$ are causal functions, these terms vanish. This strongly suggests that we are allowed to disregard the trace-log term of (4.48). (Notice that this argument is not valid at moderate magnetic fields $B \geq \Gamma$, see below).

4.3.2. Effective Keldysh Action and Saddle-Point Solution

We now turn to the full Keldysh version of (4.48) keeping all Keldysh components of Π^{ab}. One can decouple the quartic Majorana interaction with the help of complex bosonic fields Q_α via a Hubbard-Stratonovich transformation. The fields Q_α inherit the symmetry of the Majorana propagators, therefore $Q_\alpha^{ab}(t, t') = -Q_\alpha^{ba}(t', t)$. Since the correlator $\Pi^{ab}(t - t')$ may have a complicated time-dependent structure, we choose to keep it in the numerator:

$$i\mathcal{S}[\boldsymbol{\eta}, \boldsymbol{Q}] = \int dtdt' \left(\frac{i}{2}\eta_\alpha^a(t)\,(G_\alpha^{-1})_{tt'}^{ab}\,\eta_\alpha^b(t') - \frac{1}{4}\tau_3^a\tau_3^b\Pi^{ab}(t, t')\,Q_\alpha^{ab}(t, t')\,(M^{-1})_{\alpha\beta}Q_\beta^{ab}(t, t')\right).$$
$$\tag{4.50}$$

Within the Matsubara discussion in Subs. 4.2.1 we have addressed the issue of convergence in the integrals over the Hubbard-Stratonovich fields Σ. Namely, we have presented a particular choice of the complex fields in order to establish the negative signs required for well-defined Gaussian integration. Here we only note that similar arguments can be applied to the complex fields Q above, that is, an appropriate combination of real and imaginary modes is sufficient to ensure the convergence of Q-integrals.

The Majorana Green's function in (4.50) reads

$$(G_\alpha^{-1})_{tt'}^{ab} = i\tau_3^{ab}\delta(t - t')\partial_{t'} - \Sigma_\alpha^{ab}(t, t') , \tag{4.51}$$

with the self-energy

$$\Sigma_\alpha^{ab}(t, t') = \tau_3^a\tau_3^b Q_\alpha^{ab}(t, t')\Pi^{ab}(t, t') . \tag{4.52}$$

---

[3]Note that the delta-function should be understood as such only at relatively long time scales. For instance, it does not force us to take the Grassmann variables in (4.46) at coinciding times.

By the use of the standard Keldysh rotation, cf. Ref. [47],

$$\hat{G} = LGL = \begin{pmatrix} G^K & G^R \\ G^A & 0 \end{pmatrix}, \qquad \hat{\Pi} = L\Pi L = \begin{pmatrix} \Pi^K & \Pi^R \\ \Pi^A & 0 \end{pmatrix},$$

$$\hat{\Sigma} = L\Sigma L = \begin{pmatrix} 0 & \Sigma^A \\ \Sigma^R & \Sigma^K \end{pmatrix}, \qquad L = \frac{1}{\sqrt{2}} \begin{pmatrix} 1 & 1 \\ 1 & -1 \end{pmatrix}, \tag{4.53}$$

the above equations transform to

$$(\hat{G}_\alpha^{-1})_{tt'} = i\tau_1 \delta(t - t')\partial_{t'} - \hat{\Sigma}_\alpha(t, t') \tag{4.54}$$

and

$$\hat{\Sigma}_\alpha^{ab}(t, t') = -\frac{1}{2}\text{Tr}\left\{ \bar{\gamma}^a \hat{\Pi}(t, t') \bar{\gamma}^b \hat{Q}_\alpha(t', t) \right\} . \tag{4.55}$$

Depending on the value of indices a, b, the matrices $\bar{\gamma}$ are given by $\bar{\gamma}^{cl} = \mathbb{1}$ and $\bar{\gamma}^q = \tau_1$ with the Pauli matrix τ_1.

The re-decoupled action (4.50) is again quadratic in Majorana Grassmann variables η_α. This enables us to integrate them out as described in the Matsubara case in Subs. 4.2.1, and to obtain an effective action for the Q-fields:

$$iS[\boldsymbol{Q}] = \frac{1}{2}\text{Tr}_t \sum_\alpha^{x,y,z} \log\left(\hat{G}_\alpha(\hat{Q}_\alpha)\right)^{-1}$$
$$+ \frac{1}{8}\int dt dt' \hat{\Pi}^{ab}(t, t')(M^{-1})_{\alpha\beta}\text{Tr}\left\{\bar{\gamma}^a \hat{Q}_\alpha(t, t')\bar{\gamma}^b \hat{Q}_\beta(t', t)\right\} . \tag{4.56}$$

Here Tr_t denotes the trace in the Keldysh and time space and Tr is the trace in the Keldysh space.

To find the saddle point we substitute $\hat{Q}_\alpha = \hat{Q}_{0\alpha} + \delta\hat{Q}_\alpha$ and expand in fluctuations $\delta\hat{Q}_\alpha$. The saddle-point solution $\hat{Q}_{0\alpha}$ is found by demanding the linear order in the $\delta\hat{Q}$-expansion to vanish. The solution must be stationary, depending only on the time difference: $\hat{G}_{0\beta}(t, t') = \hat{G}_{0\beta}(t - t')$. We obtain the equation

$$\hat{Q}_{0\alpha}(t - t') = M_{\alpha\beta}\hat{G}_{0\beta}(t - t') , \tag{4.57}$$

which again has to be solved self-consistently since $\hat{G}_{0\alpha}$ itself depends on the saddle-point value $\hat{Q}_{0\alpha}$.

In the high-temperature regime, $T \gg T_K$, it is easy to obtain the self-consistent solution for the self-energy. In frequency space, one finds

$$\Sigma_{0\alpha}^R(\omega) = -\frac{1}{2}M_{\alpha\beta}\int \frac{d\Omega}{2\pi}\left(\Pi^K(\omega + \Omega)G_{0\beta}^A(\Omega) + \Pi^R(\omega + \Omega)G_{0\beta}^K(\Omega)\right) \tag{4.58}$$

Using the ansatz of a constant self-energy with $\text{Im}\Sigma_{0\alpha}^R \ll T$ in $\hat{G}_0$ we obtain at low frequencies $\omega \ll T$

$$\Sigma_{0\alpha}^R(\omega) = -2igT\left(1 + \mathcal{O}\left(\frac{\omega}{T}\right)\right) , \tag{4.59}$$

This coincides with the saddle-point result (4.38) and the results of the perturbation theory (4.12) and (4.13). That is, the rate $\Gamma = 2gT$ is corresponds to the physical Korringa rate. This suggests that the saddle-point Majorana Green's functions $\hat{G}_{0\alpha}(\omega)$ coincide with the physical Green's function $\hat{G}_\alpha(\omega)$, which describes the dissipative dynamics of the spin 1/2 the high-temperature regime. Moreover, due to the result (4.59) the saddle-point Green's functions are well-approximated by the results obtained in first-order perturbation theory in Subs. 4.1.3, namely,

$$ G_{0\alpha}^{R/A}(\omega) = \frac{1}{\omega \pm i\Gamma} \ , \qquad G_{0\alpha}^{K}(\omega) = \frac{-2i\Gamma \tanh \frac{\omega}{2T}}{\omega^2 + \Gamma^2} \ . \tag{4.60} $$

However, so far we did not include fluctuations δQ around the saddle point. In principle we would have to average the saddle-point results obtained above over δQ-fluctuations in order to get the physical quantities. Below we discuss the fluctuations in detail and find that the leading-order saddle-point solution is stable against fluctuations.

4.3.3. Fluctuations Around the Saddle Point

To analyze the fluctuations $\delta \hat{Q}$, we expand the trace-log term in (4.56) up to the second order in $\delta \hat{Q}$. With the help of the Fourier transform of $\delta \hat{Q}$, introduced as

$$ \delta \hat{Q}_\alpha(\omega, \nu) = \int dt dt' \, e^{-i\frac{\nu}{2}(t+t')} \, e^{-i\omega(t-t')} \delta \hat{Q}_\alpha(t, t') \,, \tag{4.61} $$

we rewrite the action in the form $i\mathcal{S}_{\delta Q} = i\mathcal{S}_{\delta Q}^{(1)} + i\mathcal{S}_{\delta Q}^{(2)}$. The first term $i\mathcal{S}_{\delta Q}^{(1)}$ arises from the expansion of the trace-log term of (4.56):

$$ \begin{aligned} i\mathcal{S}_{\delta Q}^{(1)} &= \frac{1}{2} \int dt dt' dt_1 dt_1' \, \mathrm{Tr} \left\{ \hat{G}_{0\alpha}(t, t_1') \, \delta\hat{\Sigma}_\alpha(t_1', t_1) \hat{G}_{0\alpha}(t_1, t') \, \delta\hat{\Sigma}_\alpha(t', t) \right\} \ , \\ &= \frac{1}{2} \int \frac{d\nu d\Omega}{(2\pi)^2} \, \mathrm{Tr} \left\{ \hat{G}_{0\alpha}(\Omega - \nu/2) \, \delta\hat{\Sigma}_\alpha(\Omega, \nu) \hat{G}_{0\alpha}(\Omega + \nu/2) \, \delta\hat{\Sigma}_\alpha(\Omega, -\nu) \right\} \ . \end{aligned} \tag{4.62} $$

Here, for brevity, we expressed $i\mathcal{S}_{\delta Q}^{(1)}$ via the self-energy fluctuations

$$ \delta\hat{\Sigma}_\alpha^{ab}(\Omega, \nu) = -\frac{1}{2} \int \frac{d\omega}{2\pi} \mathrm{Tr} \left\{ \bar{\gamma}^a \hat{\Pi}(\Omega + \omega) \bar{\gamma}^b \delta\hat{Q}_\alpha(\omega, -\nu) \right\} \ . \tag{4.63} $$

The second term $i\mathcal{S}_{\delta Q}^{(2)}$ resulted from the Hubbard-Stratonovich transformation:

$$ \begin{aligned} i\mathcal{S}_{\delta Q}^{(2)} &= \frac{(M^{-1})_{\alpha\beta}}{8} \int dt dt' \hat{\Pi}^{ab}(t, t') \mathrm{Tr} \left\{ \bar{\gamma}^a \delta\hat{Q}_\alpha(t, t') \bar{\gamma}^b \delta\hat{Q}_\beta(t', t) \right\} \\ &= \frac{(M^{-1})_{\alpha\beta}}{8} \int \frac{d\nu d\omega d\omega'}{(2\pi)^3} \hat{\Pi}^{ab}(\omega' - \omega) \mathrm{Tr} \left\{ \bar{\gamma}^a \delta\hat{Q}_\alpha(\omega, \nu) \bar{\gamma}^b \delta\hat{Q}_\beta(\omega', -\nu) \right\} \ . \end{aligned} \tag{4.64} $$

In order to simplify the analysis of fluctuations around the saddle point we parametrize fluctuations in terms of modes $R^{(i)}$,

$$ \delta\hat{Q}_\alpha(\omega, \nu) = \begin{pmatrix} R_\alpha^{(3)}(\omega, \nu) + R_\alpha^{(4)}(\omega, \nu) & iR_\alpha^{(1)}(\omega, \nu) + R_\alpha^{(2)}(\omega, \nu) \\ -iR_\alpha^{(1)}(\omega, \nu) + R_\alpha^{(2)}(\omega, \nu) & R_\alpha^{(3)}(\omega, \nu) - R_\alpha^{(4)}(\omega, \nu) \end{pmatrix} \ . \tag{4.65} $$

The parametrization is chosen in a way such that the anti-symmetry condition $\delta Q_\alpha^{ab}(t,t') = -\delta Q_\alpha^{ba}(t',t)$ in Keldysh time space is satisfied. In time space the modes $R^{(i)}$ obey

$$R_\alpha^{(1)}(t,t') = R_\alpha^{(1)}(t',t) \ , \qquad\qquad\qquad R_\alpha^{(2)}(t,t') = -R_\alpha^{(2)}(t',t) \ ,$$

$$R_\alpha^{(3)}(t,t') = -R_\alpha^{(3)}(t',t) \ , \qquad\qquad R_\alpha^{(4)}(t,t') = -R_\alpha^{(4)}(t',t) \ . \qquad (4.66)$$

That is, the mode $R^{(1)}$ is symmetric with respect to time, whereas the three modes $R^{(2)}, R^{(3)}$ and $R^{(4)}$ are anti-symmetric in time.

Fluctuations: Trace-Log Term

First we focus on the first term $i\mathcal{S}_{\delta Q}^{(1)}$, Eq. (4.62), which emerged in the expansion of the trace-log term. We give a detailed discussion of this term on the basis of a small-g expansion and conclude that it may be neglected as compared to the second term (4.64), as suggested in Subs. 4.2.3 and 4.3.1. The second term $i\mathcal{S}_{\delta Q}^{(2)}$ is analyzed in more detail in Subs. 4.3.4 below.

Clearly, the second term (4.64) is proportional to g originating from the bath correlation function $\hat{\Pi}$. In the first term $i\mathcal{S}_{\delta Q}^{(1)}$, Eq. (4.62), each $\delta\hat{\Sigma}$ contains a factor of $\hat{\Pi}$, therefore the whole term appears to be of at least second order in g unless the Green's functions yield an inverse factor g^{-1}. The only combination of Green's functions yielding g^{-1} is $G^A(\Omega + \nu/2)G^R(\Omega - \nu/2)$ (or vice versa, $R/A \to A/R$). For example, one type of contributions to (4.62) which occurs including arbitrary combinations of $R^{(3)}$ and $R^{(4)}$ has the form

$$\int \frac{d\omega d\omega' d\nu d\Omega}{(2\pi)^4} \, G^A(\Omega + \nu/2)G^R(\Omega - \nu/2)\Pi^K(\Omega + \omega)\Pi^K(\Omega + \omega')R_\alpha^{(3)}(\omega,\nu)R_\alpha^{(3)}(\omega',-\nu) \ .$$
$$(4.67)$$

In this term, assuming $\Pi^K \approx 4gT$ to be constant (at low frequencies), the Ω integration of $G^R G^A$ yields an inverse factor of g since $1/\Gamma = (2gT)^{-1}$. The structure of this term resembles the structure of the contributions to the Bethe-Salpeter-like equation discussed in Subs. 4.1.3. However, in writing (4.67) we did not take into account the anti-symmetry of $R^{(3)}$ and $R^{(4)}$ as explained in (4.66). Due to this anti-symmetry terms of the kind (4.67) cancel out. This is the same cancellation which we encountered in perturbation theory in Eq. (4.18). Hence, we conclude that the above mentioned divergent terms also cancel out in perturbation theory if symmetries are respected during the resummation.

To substantiate our claim we provide a rigorous analysis of the first term $i\mathcal{S}_{\delta Q}^{(1)}$. For this purpose we decompose $\delta\hat{\Sigma}_\alpha(\Omega,\nu)$, use the explicit form of $\Pi^{R/A}$ and take advantage of the symmetry relations (4.66) of $R^{(i)}$. We find (Keldysh superscripts $1 = cl$, $2 = q$)

$$\delta\Sigma_\alpha^{11}(\Omega,-\nu) = -\frac{1}{2}\int \frac{d\omega}{2\pi}\left(2ig\Omega\, R_\alpha^{(1)}(\omega,\nu)\right.$$

$$\left. + \frac{\Pi^K(\omega+\Omega) - \Pi^K(-\omega+\Omega)}{2}\left(R_\alpha^{(3)}(\omega,\nu) - R_\alpha^{(4)}(\omega,\nu)\right)\right), \quad (4.68a)$$

$$\delta\Sigma_\alpha^{12}(\Omega, -\nu) = -\frac{1}{2} \int \frac{d\omega}{2\pi} \left(\frac{\Pi^K(\omega + \Omega) + \Pi^K(-\omega + \Omega)}{2} \, iR_\alpha^{(1)}(\omega, \nu) \right.$$

$$\left. + \frac{\Pi^K(\omega + \Omega) - \Pi^K(-\omega + \Omega)}{2} \, R_\alpha^{(2)}(\omega, \nu) - 2g\omega \, R_\alpha^{(4)}(\omega, \nu) \right). \quad (4.68b)$$

The remaining two components are related to the ones above by

$$\delta\Sigma_\alpha^{21}(\Omega, -\nu) = \delta\Sigma_\alpha^{12}\left(\Omega, -\nu; R_\alpha^{(1)} \to -R_\alpha^{(1)}; R_\alpha^{(4)} \to -R_\alpha^{(4)}\right), \quad (4.68c)$$

$$\delta\Sigma_\alpha^{22}(\Omega, -\nu) = \delta\Sigma_\alpha^{11}\left(\Omega, -\nu; R_\alpha^{(1)} \to -R_\alpha^{(1)}; R_\alpha^{(4)} \to -R_\alpha^{(4)}\right). \quad (4.68d)$$

We recall the bosonic correlator in frequency space, Eqs. (4.8),

$$\Pi^{R/A}(\Omega + \omega) = \pm g\,(\Omega + \omega) - iD, \qquad \Pi^K(\Omega + \omega) = 2g(\Omega + \omega)\coth\left(\frac{\Omega + \omega}{2T}\right). \quad (4.69)$$

At low frequencies $\Omega \ll T$ the terms containing the 'classical' contribution $\Pi^K \approx 4gT$ dominate over those containing $\Pi^{R/A}$. Indeed $\Pi^{R/A}$ are important only in the 'quantum' region $\Omega \gtrsim T$, then $\Pi^{R/A/K} \propto g\Omega$. Here we recall the discussion about the RG in Subsection 4.1.2. We can disregard most of the 'quantum' domain $\Omega \gtrsim T$ because these frequencies could be integrated out in the initial RG procedure.

Regarding the Ω-integration in $i\mathcal{S}_{\delta Q}^{(1)}$, Eq.4.62, we may ask where large contributions can arise. In the region $\Omega \sim T$ Green's functions generate a factor of $1/T^2$, the expression as a whole scales as g^2 and can therefore be neglected as compared with $i\mathcal{S}_{\delta Q}^{(2)}$, which scales as g. The remaining region to consider is $\Omega \sim \Gamma \ll T$. There, terms containing the Keldysh Green's function

$$G_{0\alpha}^K(\Omega) = \frac{-2i\Gamma \tanh\frac{\Omega}{2T}}{\Omega^2 + \Gamma^2} \quad (4.70)$$

get another order of g due to the hyperbolic tangent in the small g expansion: $\tanh\Omega/2T \sim \Gamma/T = 2g$. Neglecting G^K-terms we observe that the remaining terms of $i\mathcal{S}_{\delta Q}^{(1)}$ can be written as (omitting the spin index α for the moment)

$$G_0^R \delta\Sigma^{21} G_0^R \delta\Sigma^{21} + G_0^R \delta\Sigma^{22} G_0^A \delta\Sigma^{11} + G_0^A \delta\Sigma^{11} G_0^R \delta\Sigma^{22} + G_0^A \delta\Sigma^{12} G_0^A \delta\Sigma^{12}. \quad (4.71)$$

In the limit $\Omega \ll T$, except for $\alpha\omega R^{(4)}$ in (4.68b) all prefactors of $\delta\Sigma^{ab}$ in (4.68) are linear in Ω. Concerning the region $\Omega \sim \Gamma = 2gT$ the linear prefactor Ω yields another order of g, and therefore the corresponding terms can also be neglected. Finally, the Ω-independent term $\alpha\omega R^{(4)}$ in $\delta\Sigma^{(12)}$ only appears combined with $G^R G^R$ and $G^A G^A$, having both poles on the same side of the real axis. The integration by residue theorem yields zero. We conclude that all terms of $i\mathcal{S}_{\delta Q}^{(1)}$ are of higher order in g than those of $i\mathcal{S}_{\delta Q}^{(2)}$, Eqs. (4.62) and (4.64). This line of reasoning still holds if a magnetic field B is included in the problem provided that $B \lesssim \Gamma$. For larger fields, which are however still smaller than the temperature, the frequency in the hyperbolic tangent would essentially be replaced by B and thus yield a factor $\tanh\frac{B}{2T} \approx \frac{B}{T} > g$. Thus the trace-log term can no longer be neglected at intermediate fields.

As a result we have confirmed the argument in Subs. 4.2.3 and 4.3.1, that is, it is justified to neglect the first term in the action (4.62), which was obtained from the expansion of the trace-log term around the saddle point. The action of δQ-fluctuations around the saddle point is governed by second term $i\mathcal{S}_{\delta Q}^{(2)}$.

Fluctuations: Hubbard-Stratonovich Term

Building on the insights above, the fluctuations around the saddle point can be analyzed purely in terms of the dominating second term, generated in the Hubbard-Stratonovich decoupling of the quartic Majorana term with Q-fields. That is, the propagator of fluctuations is fully determined by the second term $i\mathcal{S}^{(2)}_{\delta Q}$, Eq. (4.64). To simplify the discussion we recall the parametrization (4.65) of δQ in terms of symmetric, $R^{(1)}(\omega, \nu)$, and anti-symmetric modes $R^{(2)}(\omega, \nu)$, $R^{(3)}(\omega, \nu)$ and $R^{(4)}(\omega, \nu)$ and define

$$R^{(1)}_\alpha(\nu) = \int_0^\infty \frac{d\omega}{2\pi} R^{(1)}_\alpha(\omega, \nu), \qquad R^{(i)}_\alpha(\nu) = \int_0^\infty \frac{d\omega}{2\pi} \frac{\omega}{T} R^{(i)}_\alpha(\omega, \nu) \quad \text{for } i = 2, 3, 4. \quad (4.72)$$

Introducing vectors $(R^{(1)}_\alpha, R^{(2)}_\alpha, R^{(3)}_\alpha, R^{(4)}_\alpha)$, the leading terms in the high-temperature regime can be written in the matrix form

$$i\mathcal{S}^{(2)}_{\delta Q} = 2g(M^{-1})_{\alpha\beta} \int \frac{d\nu}{2\pi} \int_0^\infty \frac{d\omega d\omega'}{(2\pi)^2} R^{(i)}_\alpha(\omega, \nu) \begin{pmatrix} 2T & 0 & 0 & i\omega' \\ 0 & \frac{\omega\omega'}{3T} & 0 & 0 \\ 0 & 0 & \frac{\omega\omega'}{3T} & 0 \\ i\omega & 0 & 0 & -\frac{\omega\omega'}{3T} \end{pmatrix}_{ij} R^{(j)}_\beta(\omega', -\nu),$$

$$= -\frac{1}{2} \int \frac{d\nu}{2\pi} R^{(i)}_\alpha(\nu) \left(K^{-1}\right)^{(ij)}_{\alpha\beta} R^{(j)}_\beta(-\nu), \qquad i, j = \{1, 2, 3, 4\}. \quad (4.73)$$

Here we define the propagator of fluctuations by

$$\langle R^{(i)}_\alpha(\nu_1) R^{(j)}_\beta(\nu_2) \rangle = K^{(ij)}_{\alpha\beta} 2\pi \delta(\nu_1 + \nu_2), \quad (4.74)$$

and find

$$K^{(ij)}_{\alpha\beta} = \frac{M_{\alpha\beta}}{4gT} \begin{pmatrix} 1 & 0 & 0 & 3i \\ 0 & -3 & 0 & 0 \\ 0 & 0 & -3 & 0 \\ 3i & 0 & 0 & -6 \end{pmatrix}_{ij}. \quad (4.75)$$

$$(4.76)$$

As expected, the propagator of fluctuations is proportional to M and thus diagonal fluctuations vanish. However, due to the inverse g^{-1} the magnitude of off-diagonal fluctuations is large.

4.3.4. Gauge Freedom

In this subsection we observe that the effective quartic Majorana action exhibits an interesting gauge freedom. The saddle-point solution acquires an explicit gauge-field dependence and becomes unphysical. We demonstrate that the problem is resolved by taking δQ-fluctuations into account.

We recall the quartic Majorana action (4.46), before the Q-fields were introduced,

$$i\mathcal{S}_{int}[\boldsymbol{\eta}] = -\frac{1}{4} \int dt dt' \tau_3^a \Pi^{ab}(t, t') \tau_3^b \left(\eta^a_{t,\alpha} \eta^b_{t',\alpha}\right) M_{\alpha\beta}(\eta^a_{t,\beta} \eta^b_{t',\beta}). \quad (4.77)$$

Grassmann variables obey the fundamental property $\eta_{t,\alpha}^2 = 0$ at equal times. Let us suppose that the matrix M is replaced by the matrix $\bar{M}$, which is similar to M but comprises finite entries A_α on the diagonal,

$$\bar{M} \equiv \begin{pmatrix} A_x & 1 & 1 \\ 1 & A_y & 1 \\ 1 & 1 & A_z \end{pmatrix} . \tag{4.78}$$

Then, due to the property $\eta_{t,\alpha}^2 = 0$ additional terms in the action vanish, i.e., both actions are equivalent, $i\mathcal{S}[M] = i\mathcal{S}[\bar{M}]$. The range of possible values A_α is limited by the constraints that $\bar{M}$ is invertible (or equivalently, $\det \bar{M} \neq 0$) and has real-valued eigenvalues. We interpret the A_α as gauge fields, which may be fixed by some condition.

The transformations, i.e., decoupling in terms of $\hat{Q}$-fields and integration of Majorana fields, are not affected by the modified matrix $\bar{M}$. In order to obtain the new effective Keldysh action of the $\hat{Q}$ fields, we only have to replace matrices M by $\bar{M}$ in (4.56), yielding

$$iS[\boldsymbol{Q}] = \frac{1}{2}\mathrm{Tr}_t \sum_\alpha^{x,y,z} \log\left(\hat{G}_\alpha(\hat{Q}_\alpha)\right)^{-1}$$
$$+ \frac{1}{8}\int dt\,dt'\,\hat{\Pi}^{ab}(t,t')(\bar{M}^{-1})_{\alpha\beta}\mathrm{Tr}\left\{\bar{\gamma}^a\hat{Q}_\alpha(t,t')\bar{\gamma}^b\hat{Q}_\beta(t',t)\right\} . \tag{4.79}$$

Similarly, the modified saddle-point equation is obtained from (4.57),

$$\hat{Q}_{0\alpha}(t,t') = \bar{M}_{\alpha\beta}\hat{G}_{0\beta}(t,t') . \tag{4.80}$$

We emphasize that this saddle-point equation now depends on the gauge fields A_α, suggesting that there is a whole set of saddle-point solutions characterized by the values of $\{A_x, A_y, A_z\}$.

The explicit dependence on gauge can be illustrated by recalculating the self-consistent solution for Σ^R, Eq. (4.59). In the high-temperature regime we find

$$\Sigma_{0\alpha}^R(\omega) = -\frac{1}{2}\bar{M}_{\alpha\beta}\int \frac{d\Omega}{2\pi}\left(\Pi^K(\omega+\Omega)G_{0\beta}^A(\Omega) + \Pi^R(\omega+\Omega)G_{0\beta}^K(\Omega)\right)$$
$$= -2igT\left(1 + \frac{A_\alpha}{2} + \mathcal{O}\left(\frac{\omega}{T}\right)\right) . \tag{4.81}$$

As the imaginary part of Σ^R now depends on the gauge fields, we can no longer identify it as a physically observable rate. Thus, for any finite $\{A_x, A_y, A_z\}$ the saddle-point Green's function and the physical Green's function do not coincide. In order to find the physical Green's function, we have to reconsider fluctuations around the saddle points.

The fluctuation propagator (4.75) enables us to compute the fluctuation-averaged Green's function. As a starting point we use the self-consistent Dyson equation,

$$\int dt'\left(\hat{G}_{f\alpha}^{-1}(t,t') - \hat{\Sigma}_\alpha(t,t')\right)\hat{G}_\alpha(t',t'') = \mathbb{1}\,\delta(t-t'') . \tag{4.82}$$

which has to be satisfied by the Green's function $\hat{G}_\alpha$. Before the average is actually performed causality does not necessarily apply, and we have to allow for a finite "anti-Keldysh" 22 component of the fluctuating self-energy. For the 12-component of the Green's function, which will become retarded after the averaging, we obtain the equation

$$i\partial_t\hat{G}_\alpha^{12}(t,t') = \delta(t-t') + \int dt_1\hat{\Sigma}_\alpha^{21}(t,t_1)\hat{G}_\alpha^{12}(t_1,t') + \int dt_1\hat{\Sigma}_\alpha^{22}(t,t_1)\hat{G}_\alpha^{22}(t_1,t') . \tag{4.83}$$

We have found that the propagator of fluctuations (4.76) does not depend on the frequency ω corresponding to the time difference $t - t_1$. Therefore, we assume that $\Sigma^{21}(t, t_1) = \delta(t - t_1)\Sigma^{21}(t)$ is local in time, but keep the dependence on total time for the fluctuation average later on. We also neglect $\Sigma^{22}G^{22}$, which is of higher order because $\Sigma^{22} \sim \Pi^{R/A}G^{R/A} + \Pi^K G^K$ is smaller than the 'big' combination $\Pi^K G^{R/A}$.

$$i\partial_t G^{12}_\alpha(t, t') = \delta(t - t') + \Sigma^{21}_\alpha(t)G^{12}(t, t') \tag{4.84}$$

The above equation is solved by the following ansatz:

$$G^{12}_\alpha(t, t') = -i\Theta(t - t') \exp\left\{-i\int_{t'}^t dt_1 \Sigma^{21}_\alpha(t_1)\right\} \tag{4.85}$$

Here, the self-energy Σ^{21} includes the constant saddle-point contribution and fluctuations. The saddle-point contribution is $\Sigma^R_{0\alpha}$, Eq. (4.81). Separating the saddle-point part of the exponential, the resulting prefactor can be identified with the saddle-point Green's function:

$$G^{12}_\alpha(t, t') = -i\Theta(t - t')e^{-i\Sigma^R_{0\alpha}(t-t')} \exp\left\{-i\int_{t'}^t dt_1 \delta\Sigma^{21}_\alpha(t_1)\right\}$$

$$= G^R_0(t, t') \exp\left\{-i\int_{t'}^t dt_1 \delta\Sigma^{21}_\alpha(t_1)\right\} \tag{4.86}$$

The $\delta\hat{Q}$-fluctuations can be treated using the Gaussian averaging procedure based on the Gaussian action of fluctuations, Eq. (4.73). To keep the discussion simple we encode the fluctuations into a "self-energy correlator" that encodes the propagation of fluctuations,

$$\left\langle G^{12}_\alpha(t, t') \right\rangle_{\delta Q} = G^R_{0\alpha}(t, t') \left\langle \exp\left\{-i\int_{t'}^t dt_1 \delta\Sigma^{21}_\alpha(t_1)\right\} \right\rangle_{\delta Q}$$

$$= G^R_{0\alpha}(t - t') \exp\left\{-\frac{1}{2}\int_{t'}^t dt_2 dt_3 \left\langle \delta\Sigma^{21}_\alpha(t_2)\delta\Sigma^{21}_\alpha(t_3) \right\rangle_{\delta Q}\right\} . \tag{4.87}$$

The 21-component of the 'self-energy correlator' is comprised of the bath correlator and fluctuating modes according to Eq. (4.63). Taking into account the symmetry of modes $R^{(i)}$, Eqs. (4.66), and the symmetries of the bosonic correlator, $\Pi^K(t) = \Pi^K(-t)$ and $\Pi^R(t) = \Pi^A(-t)$, the 21-component is

$$\delta\Sigma^{21}_\alpha(t, t') = \frac{i}{2}\Pi^K(t - t')R^{(1)}_\alpha(t', t) - \frac{1}{2}\left(\Pi^R(t - t') - \Pi^A(t - t')\right)R^{(4)}_\alpha(t', t) . \tag{4.88}$$

Based on the locality $\delta\Sigma(t, t') \propto \delta(t - t')$ we can use the Fourier transform

$$\delta\Sigma^{21}_\alpha(\nu) = \int_{-\infty}^\infty \frac{d\omega}{2\pi} \int dt dt' e^{-i\frac{\nu}{2}(t+t')} e^{-i\omega(t-t')} \delta\Sigma^{21}_\alpha(t, t') , \tag{4.89}$$

similar to (4.61). Applying the above Fourier transform to (4.88) we obtain

$$\delta\Sigma^{21}_\alpha(\nu) = \int_0^\infty \frac{d\omega}{2\pi} \left(4igTR^{(1)}_\alpha(\omega, -\nu) - 2g\omega R^{(4)}_\alpha(\omega, -\nu)\right) . \tag{4.90}$$

Then, we use the redefined modes $R^{(i)}(\nu)$ (4.72) and rewrite the expression above in terms of a scalar product

$$\delta\Sigma^{21}_\alpha(\nu) = \int_0^\infty \frac{d\omega}{2\pi} \left(4igTR^{(1)}_\alpha(\omega, -\nu) - 2g\omega R^{(4)}_\alpha(\omega, -\nu)\right) \tag{4.91}$$

$$= 4igTR^{(1)}_\alpha(-\nu) - 2gTR^{(4)}_\alpha(-\nu)) = 2gT\left(2i, 0, 0, -1\right)\begin{pmatrix} R^{(1)}_\alpha(-\nu) \\ R^{(2)}_\alpha(-\nu) \\ R^{(3)}_\alpha(-\nu) \\ R^{(4)}_\alpha(-\nu) \end{pmatrix} , \tag{4.92}$$

This form directly allows to insert the fluctuation propagator $K_{\alpha\beta}^{(ij)}$, Eq. (4.75), into the average below. We note that for finite $\{A_x, A_y, A_z\}$ the fluctuations propagator acquires finite diagonal entries. With the use of (4.92) the exponent of (4.87) can now be evaluated:

$$-\frac{1}{2}\int_{t'}^{t} dt_2 dt_3 \left\langle \delta\Sigma_\alpha^{21}(t_2)\delta\Sigma_\alpha^{21}(t_3)\right\rangle_{\delta Q}$$

$$= -\frac{1}{2}\int_{t'}^{t} dt_2 dt_3 \int \frac{d\nu_2}{2\pi}\int \frac{d\nu_3}{2\pi}\left\langle \delta\Sigma_\alpha^{21}(\nu_2)\delta\Sigma_\alpha^{21}(\nu_3)\right\rangle_{\delta Q} e^{-i\nu_2 t_2 - i\nu_3 t_3}$$

$$= -\frac{(2gT)^2}{2}(t-t')\,(2i,0,0,-1)^{(i)}\,K_{\alpha\alpha}^{(ij)}\begin{pmatrix}2i\\0\\0\\-1\end{pmatrix}^{(j)} = -gT\,(t-t')\,A_\alpha\,. \quad (4.93)$$

At the saddle point the imaginary part of the self-energy (4.81) was found to depend on the arbitrary constants A_α. Hence it cannot correspond to the physical decay rate. To provide a valid definition of physical decay rates we use the physical, fluctuation-averaged 12-component of the Green's function. The latter corresponds to the physical retarded Green's function $G_\alpha^R(t,t')$ in time space:

$$iG_\alpha^R(t,t') \equiv i\left\langle G_\alpha^{12}(t,t')\right\rangle_{\delta Q}\,. \quad (4.94)$$

The time-dependence of the physical retarded Green's function can be used to identify the physical rates Γ_α. The result (4.93) allows us to rewrite (4.87):

$$iG_\alpha^R(t,t') = G_{0\alpha}^R(t-t')\exp\left\{-\frac{1}{2}\int_{t'}^{t} dt_2 dt_3 \left\langle \delta\Sigma_\alpha^{21}(t_2)\delta\Sigma_\alpha^{21}(t_3)\right\rangle_{\delta Q}\right\}$$

$$= \Theta(t-t')e^{-\Gamma_\alpha(t-t')}\,, \quad (4.95)$$

which defines the rates Γ_α. With (4.81) and (4.93) we find

$$\Gamma_\alpha = -\operatorname{Im}\Sigma_{0\alpha}^R - gTA_\alpha = 2gT. \quad (4.96)$$

Fortunately, this result is indeed independent of $\{A_\alpha\}$, confirming that for arbitrary A_α the physical decay rate is not given by the self-energy at the saddle point but rather by the decay rate Γ_α of the fluctuation-averaged Green's function.

We have found that finite diagonal entries $\{A_\alpha\}$ can be added to the matrix M without changing the quartic Majorana action. However, the saddle-point solution (4.80) of the effective action of Q-fields is modified. As a consequence, the allowed values of $\{A_\alpha\}$ span a manifold of saddle-point solutions. Additionally, the finite diagonal entries $\{A_\alpha\}$ lead to large diagonal fluctuations $\langle\delta Q_\alpha\delta Q_\alpha\rangle$. We have shown that the the gauge dependence of the saddle-point self-energy is exactly canceled by the average over diagonal fluctuations. Thus, concerning physical quantities, diagonal fluctuations are understood to compensate for the gauge dependence of results obtained from the saddle-point approximation.

Having identified A_α as kind of an arbitrary gauge, we can now choose $A_\alpha = 0$. Then, the diagonal part $K_{\alpha\alpha}$ of the propagator of fluctuations vanishes. In turn, any Majorana correlators only involving a single projection α can be safely computed within the saddle-point approximation.

4.4. Spin Correlators in the Bose-Kondo Model

The knowledge of the propagator of the $\delta \hat{Q}$-fluctuations allows one to construct a new perturbative series, starting at the fixed-point solution where the Green's function and the self-energy are given by the saddle-point values Eqs. (4.59) and (4.60). The new perturbative expansion for the Green's function is based on the following series:

$$\hat{G}_\alpha(\tau, \tau') = \hat{G}_{0\alpha}(\tau, \tau') + \int d\tau_1 d\tau_2 \hat{G}_{0\alpha}(\tau, \tau_1) \delta \hat{\Sigma}_\alpha(\tau_1, \tau_2) \hat{G}_{0\alpha}(\tau_2, \tau')$$

$$+ \int d\tau_1 d\tau_2 d\tau_3 d\tau_4 \hat{G}_{0\alpha}(\tau, \tau_1) \delta \hat{\Sigma}_\alpha(\tau_1, \tau_2) \hat{G}_{0\alpha}(\tau_2, \tau_3) \delta \hat{\Sigma}_\alpha(\tau_3, \tau_4) \hat{G}_{0\alpha}(\tau_4, \tau') + ... \quad (4.97)$$

This series is to be averaged over the fluctuations to obtain $\left\langle \hat{G}_\alpha(t, t') \right\rangle_{\delta\Sigma}$. However, on the right-hand side the spin index α is the same in all the terms, essentially because the saddle-point Green's function is diagonal in spin space. Taking into account the dominance of the second term (4.73) in the action $i\mathcal{S}_{\delta Q}$, we conclude that

$$\langle \delta \hat{\Sigma}_\alpha(\dots) \delta \hat{\Sigma}_\alpha(\dots) \rangle \propto M_{\alpha\alpha} = 0 \;, \quad (4.98)$$

since the diagonal entries of the matrix M vanish (corresponding to the gauge $A_\alpha = 0$ in Subs. 4.3.4). Thus, the fluctuation-averaged Green's function coincides with the saddle-point solution

$$\left\langle \hat{G}_\alpha(t, t') \right\rangle_{\delta\Sigma} = \hat{G}_{0\alpha}(t, t') \;. \quad (4.99)$$

Any "diagonal" Majorana correlator $\langle \eta_\alpha(t_1) \dots \eta_\alpha(t_n) \rangle$ can be decomposed into averages of Majorana Green-function products with the same spin index α. Due to the relation (4.98), such correlators can be calculated by substituting all $\hat{G}_\alpha$ with their saddle-point values, i.e., through application of Eq. (4.99).

The Majorana representation allows for the calculation of spin correlation functions. The direct application of the representation $\hat{S}_\alpha = -\frac{i}{2}\epsilon_{\alpha\beta\gamma}\hat{\eta}_\beta \hat{\eta}_\gamma$ to spin correlator leads to Majorana correlators of different spin indices $\beta \neq \gamma$ and the arguments above do not apply. Therefore, the special relations (3.26) that connect 'diagonal' N-spin correlators to 'diagonal' N Majorana correlators are crucial. On the basis of these relations the calculation of 'diagonal' spin correlators is considerably simplified. We note that the method is restricted to the high-temperature regime $T \gg T_K, \omega, \Gamma$. Below, we employ the method on some examples.

4.4.1. Two-Spin Correlation Functions: Susceptibility

As an example we calculate the diagonal spin susceptibility. The susceptibility can be calculated from Eq. (3.79) derived in the course of Ch. 3:

$$\chi(t, t') = i\langle \mathcal{T}_K S_\alpha^{cl}(t) S_\alpha^q(t') \rangle = -i\langle \mathcal{T}_K [\check{m}(t)\gamma^{cl}\check{\eta}_\alpha(t)][\check{m}(t')\gamma^q\check{\eta}_\alpha(t')] \rangle \;. \quad (4.100)$$

Employing the approach developed above, the only contribution to $\chi(t, t')$ is given by the diagram in Fig. 4.4, which includes the saddle-point Green's function $\hat{G}_{0\alpha}$. We immediately arrive at the standard result

$$\chi''(\omega) = \frac{1}{2}\frac{\Gamma \tanh\frac{\omega}{2T}}{\omega^2 + \Gamma^2} \overset{\omega \ll T}{\approx} \frac{1}{4T}\frac{\omega\Gamma}{\omega^2 + \Gamma^2} \;. \quad (4.101)$$

The absence of vertex corrections in Fig. 4.4 demonstrates the benefit of the formulas discussed in Ch. 3. Due to the absence of vertex corrections the precision of this calculation rests solely on the precision with which the self-energy is evaluated.

Figure 4.4.: The diagram for spin susceptibility. Double lines represent the saddle-point Green's functions of η_α-Majoranas, dashed lines indicate the propagators of auxiliary m-Majoranas.

4.4.2. Four-Spin Correlation Functions

The power of our approach becomes more evident with regard to higher-order spin correlators. Here we demonstrate that by calculating one of the fourth-order spin correlators. In Ch. 2 we introduced the spin correlation function C_χ, Eq. (2.24), which is related to noise of spin susceptibility. Namely, as we have shown in Subs. (2.2.2), Eq. (2.38), the non-Gaussian contribution

$$C_\chi^{NG}(t_1, t_1', t_2, t_2') = -\langle\langle \mathcal{T}_K S_\alpha^{cl}(t_1) S_\alpha^q(t_1') S_\alpha^{cl}(t_2) S_\alpha^q(t_2')\rangle\rangle \tag{4.102}$$

determines the non-equilibrium contribution to the experimentally accessible noise of susceptibility, cf. Ref. [29]. In the discussion in Subs. 2.2.2 it turned out that the disconnected Gaussian part of C_χ does not contribute to noise of susceptibility, therefore we omit this part here.

According to Eq. (3.78), the Majorana representation allows to reexpress the above correlator by

$$C_\chi^{NG}(t_1, t_1', t_2, t_2') = -\langle\langle \mathcal{T}_K [\check{\eta}_x \gamma^{cl} \check{m}]_{t_1} [\check{\eta}_x \gamma^q \check{m}]_{t_1'} [\check{\eta}_x \gamma^{cl} \check{m}]_{t_2} [\check{\eta}_x \gamma^q \check{m}]_{t_2'}\rangle\rangle \ . \tag{4.103}$$

Since the above correlator is of the 'diagonal' type, self-energy fluctuations vanish, cf. Eq. (4.98), and we can readily employ the approach developed in Sec. 4.4. That is, we compute (4.103) by decomposition into products of saddle-point Green's functions in a Wick-theorem-like fashion. In this way we obtain six contributions, which correspond to the diagrams depicted in Fig. 4.5.

With the help of Mathematica, we obtain the following result from the diagrams in Fig. 4.5:

$$C_\chi^{NG}(\nu, \omega_1, \omega_2) = \frac{i\Gamma^2}{8T^2} \frac{\omega_1 + \omega_2 + 2i\Gamma}{(\omega_1 + i\Gamma)(\omega_2 + i\Gamma)(\omega_1 + \nu + i\Gamma)(\omega_2 - \nu + i\Gamma)} \ . \tag{4.104}$$

As argued in Subs. 2.2.3, this allows to compute the noise of susceptibility of a single spin. For the discussion and the implications of the result we refer to Ch. 2, in particular Subs. 2.2.3 and 2.3.1.

The fact that the diagrams in Fig. 4.5 provide a valid approximation for the four-spin correlator (4.103) demonstrates the power of the method. In contrast to the perturbative approach in Subs. 4.1.3, one does not have to deal with series of diagrams of the type shown in Fig. 4.2, i.e., diagrams that arise by connecting the saddle-point Green's functions in Fig. 4.5 by additional bosonic lines. We recognize that such structures are related to fluctuations of susceptibility. Thus the path-integral approach has equipped us with an
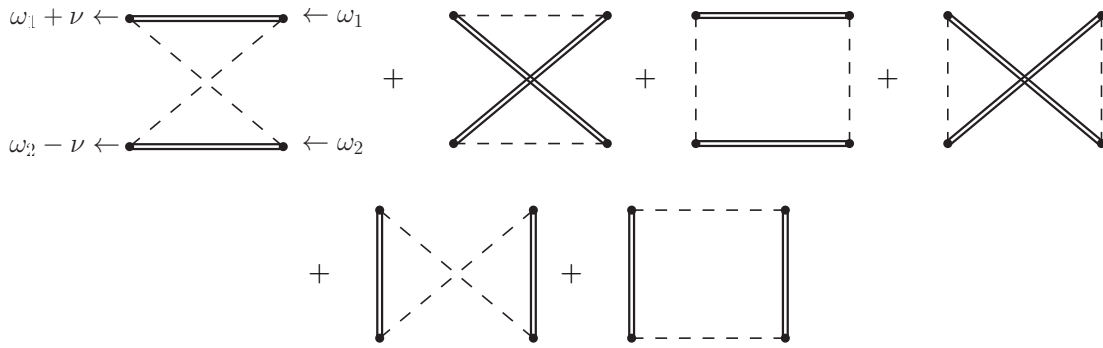
Figure 4.5.: The leading contributions to non-equilibrium noise of susceptibility.

efficient tool to treat complicated series of diagrams on a more general level and to produce controlled results for higher 'diagonal' spin correlation functions.

If a spin correlation function involves different spin components, one can no longer rely on the saddle-point contributions. One example is the correlator

$$\langle \mathcal{T}_K S_\alpha^{cl}(t_1) S_\alpha^q(t_1') S_\beta^{cl}(t_2) S_\beta^q(t_2') \rangle \;, \tag{4.105}$$

related to the correlations of susceptibilities in different ($\alpha \neq \beta$) directions. Thus, off-diagonal fluctuations $\langle \delta \hat{\Sigma}_\alpha \delta \hat{\Sigma}_\beta \rangle$ appear in the calculation. We have found that the off-diagonal part $\langle \delta \hat{Q}_\alpha \delta \hat{Q}_\beta \rangle$ of the correlator of fluctuations is large, therefore fluctuations contribute to the above correlator. In such calculations, the physical result may be obtained by averaging over fluctuations, similarly to Subs. (4.3.4). However, the simple saddle-point approximation fails in such cases.

We may compare the above Majorana approach to 'diagonal' four-spin correlators with other spin representations, e.g., the Abrikosov pseudo-fermion representation. Using the latter, any of the four lines in the diagrams shown in Fig. 4.5 would be replaced by the fermionic propagator. Now, each of these four propagators has to be dressed and may connect, via bosonic lines, to each other. In particular, due to increased number of four outer vertices, the "vertex problem" becomes even more obvious. This demonstrates that, concerning higher-order spin correlators, the Majorana method is superior to other methods.

4.5. Conclusion

In this chapter we have discussed the zero-field Bose-Kondo model as a generic model for the dissipative spin $1/2$ within the Majorana representation, assuming an Ohmic spectrum for the bosonic bath. In the standard perturbative approach higher-order contributions appear to be badly controlled. As a more systematic approach to higher orders we have employed the path integral formalism, presented in Secs. 4.2 and 4.3. A sequence of transformations allowed us to derive an effective action of auxiliary fields. We have analyzed the saddle point of the effective action and identified the relevant contributions to fluctuations around the saddle point, which can be understood as fluctuations of the self-energy. The problem possesses a curious gauge dependence. For a suitable choice of the gauge the saddle-point

solution allows to directly obtain the physical Majorana Green's functions. We have found that fluctuations that only contain one single spin index can be safely neglected and have concluded that the saddle-point approximation is accurate as long as off-diagonal fluctuations do not appear.

In Section 4.4 we have employed our approach to compute spin correlators, taking advantage of the simplified relations between spin and Majorana correlators discussed in Chapter 3. We have shown that the longitudinal spin relaxation and susceptibility are efficiently described within the saddle-point approximation. Moreover, we have demonstrated that arbitrary spin correlation functions containing a single spin index can be efficiently calculated within the saddle-point approximation. As an example, we have evaluated a particular four-spin correlation function which, as we have shown in Chapter 2, is directly related to the noise of susceptibility.

Finally, we mention possible future applications of our approach. One option would be to consider sub- or super-Ohmic bath spectra. The former, in particular, appears to be relevant in the context of mean-field theories of Heisenberg spin glasses, cf. e.g. Refs. [96–98]. Thinking of the bosonic bath correlator Π as "mean field" generated by the spins, that is $\Pi = \Pi[G]$, the saddle-point equation (4.57) connects the single-spin behavior with collective physics. That is, the saddle-point equation corresponds to the self-consistency equation of the mean-field theory. It would be exciting to reanalyze the saddle-point equation in this regard.

5. The Spin-Boson Model in the Majorana Representation

Spin-boson models are relevant in a wide range of physical contexts and have been investigated by a variety of numerical and analytic methods. The rather simple Majorana method developed in Ch. 3 provides a valuable tool to understand the rich spin dynamics of such models. A prominent example for such models is the "standard" spin-boson model, i.e., a spin 1/2 exposed to a static external magnetic field and coupled to an Ohmic bosonic bath perpendicular to the field. The Majorana representation has been applied to this model in Refs. [6, 86]. In Ref. [6], Shnirman and Makhlin found that the standard perturbative approach easily produces correct transversal-spin correlations but fails to reproduce the longitudinal-spin correlations in the long-time limit. The purpose of this chapter is to indicate the reason for this failure and, beyond that, to develop a more accurate approach to the dynamics of the spin-boson model within the Majorana technique.

In this chapter we apply the Majorana representation to the spin-boson model. We review the well-established Bloch-Redfield results and the failure of the first-order perturbative approach within the Majorana representation. In Section 5.2 we compute the second order to demonstrate that higher-order contributions to the longitudinal self-energy account for the failure. We then develop a path-integral approach for the spin-boson model in Section 5.3, which is similar to the procedure presented in the preceding chapter. The path-integral formulation improves our understanding of the above-mentioned failure. In Sec. 5.4 we present a prescription for efficient calculation of spin correlation functions, which circumvents the problems associated with the mentioned failure and allows to reproduce the Bloch-Redfield results. Finally, we demonstrate that the method indeed produces the correct longitudinal dynamics. The work presented in this chapter has been submitted to *Phys. Rev. B* and is available on arXiv.org as

> Pablo Schad, Alexander Shnirman, Yurij Makhlin
> "Using Majorana spin-1/2 representation for the spin-boson model"
> arXiv:1510.05838 [cond-mat.mes-hall].

5.1. Introduction

In Ch. 4 we have been concerned with the spin-boson-like Bose-Kondo model in zero magnetic field. Here, in contrast, we include a finite longitudinal field, and consider a spin-boson model where the Ohmic bosonic bath only couples to the x-component of the spin. Within the Majorana representation (3.2) for the spin 1/2, the Hamiltonian assumes

the form

$$H = B\hat{S}_z + \hat{X}\hat{S}_x + H_B = -iB\hat{\eta}_x\hat{\eta}_y - i\hat{X}\hat{\eta}_y\hat{\eta}_z + H_B \ . \qquad (5.1)$$

Here, H_B is the internal Hamiltonian of the bosonic bath. We again assume that the bosonic modes of the bath are described by the Ohmic spectral density with a sharp high-energy cutoff as outlined in Subs. 4.1.2. The bosonic operator $\hat{X}$ implicitly carries the dimensionless coupling constant g, which appears in the bosonic correlator Π, Eq. (4.6). The magnetic field term in (5.1) induces coherent oscillations of the spin around the z-axes, the transversely coupled bath causes transitions between the z-spin eigenstates and thus allows the spin to dissipate energy to the bath. The model (5.1) covers both effects in a minimal form.

The spin-boson model (5.1) and extensions thereof have been studied extensively over the last decades. In particular, the dynamical properties were discussed by Leggett *et al.* in Ref. [101] in great detail. In the limit of weak spin-bath coupling bosonic descriptions of the environment are generic, cf. Ref. [2], thus the spin-boson model is a standard approach to spin-environment models. For example, the model (5.1) is used to describe relaxation and decoherence in Josephson junction based qubits, cf. Ref. [1, 103]. The model Hamiltonian can be derived from the physical setups.

Depending on the strength of the dissipative coupling, the spin-boson model (5.1) undergoes a quantum phase transition between a localized and a delocalized state, cf. e.g. Refs. [86, 101, 104]. On the qualitative level, the localized state can be understood from the zero-field limit $B \to 0$. Since the bath cannot induce transitions between x-eigenstates, the spin component $\hat{S}_x$ commutes in this limit with the Hamiltonian (5.1), that is, $\hat{S}_x$ is conserved. Then, $\langle \hat{S}_x \rangle$ can be interpreted as an order parameter, and the system is said to be localized in a state characterized by the value of $\langle \hat{S}_x \rangle$. However, in the Ohmic version of the model the phase transition to the localized state only occurs at the strong critical coupling $g_c = 1$ below a certain temperature and at small non-zero field. At intermediate couplings $g \lesssim 1$ and small temperatures the system is in a quantum critical regime, cf. Ref. [86].[1] For small couplings, high temperatures or larger fields the spin is in the delocalized phase, where "delocalized" refers to delocalization on the Bloch sphere. Below we are concerned with properties of the system in the delocalized phase, that is, we assume temperatures to be sufficiently high and spin-bath coupling $g \ll 1$ to be sufficiently weak.

Shnirman and Makhlin utilized the Majorana representation for the spin-boson model (5.1) in Ref. [6], when the simple relations between spin and Majorana correlators (3.35) were established. The authors have found that the standard perturbative approach easily produces correct transverse spin correlators but fails to reproduce the longitudinal field-parallel correlator known from Bloch-Redfield theory. Particularly, the finite magnetization term was not obtained. Below, we recapitulate the Bloch-Redfield results and subsequently review the perturbative approach up to leading order in the self-energy within the Majorana representation. Upon constructing the dressed z-Majorana Green's function, we encounter the aforementioned long-time deficiency of the field-parallel spin correlator. The discussion motivates the next-to-leading order analysis and the path integral formulations in the main part of the chapter.

---

[1] We note that the authors of Ref. [104] also used the Majorana representation. There, the B-term in the Hamiltonian (5.7) was treated as perturbation, aiming at a perturbative RG in the vicinity of the localized state for sub- and super-Ohmic baths.

5.1.1. Spin Dynamics in the Bloch-Redfield Master Equation Technique

In the limit of weak dissipation the spin dynamics can be described by means of the phenomenological Bloch equations, which are well-known in the context of NMR (Nuclear Magnetic Relaxation) and discussed in many textbooks on the topic, e.g. Ref. [105]. The Bloch equations characterize the spin dynamics by two rates, Γ_1 and Γ_2. The dephasing rate Γ_2 describes the relaxation of the transverse spin components $\hat{S}_x$ and $\hat{S}_y$ to their equilibrium values, $\langle S_x \rangle = \langle S_y \rangle = 0$. The rate Γ_1 describes the relaxation of the longitudinal component $\hat{S}_z$ to its equilibrium value $\langle S_z \rangle = (1/2)\tanh B/(2T)$. In the present spin-boson model (5.1) the bath couples to the spin perpendicularly to the magnetic field axis, hence pure dephasing is absent and the simple relation $\Gamma_2 = \Gamma_1/2$ holds.

The Bloch equations for the spin-boson model can be derived from the Hamiltonian (5.1) using density matrix formalism. The time evolution of the full density matrix (spin and bath) is governed by the von Neumann equation. By tracing out the bath it is possible to derive the equation of motion for the reduced density matrix of the spin, sometimes referred to as Nakajima-Zwanzig equation, which can be regarded as a generalized master equation, cf. Refs. [1, 101, 103, 106, 107]. Then, the problem is typically simplified by so-called Markov and Born approximations, cf. Ref. [2]. In the Markov approximation memory effects of the bath are neglected, i.e., it is assumed that the bath relaxes on small timescales, much faster than the relevant timescales of the spin. To put it differently, the bath is assumed to be local in time. In the Born approximation one essentially assumes that the impact of the dynamic evolution of the system on the state of the bath is negligible. This is typically justified if the bath is reasonably large and the system-bath coupling is small. On the basis of such approximations one can obtain simple rate equations for the entries of the reduced spin density matrix, so-called Born-Markov master equations or Bloch-Redfield equations. For the derivation of Bloch-Redfield equations for the spin-boson model we refer to Refs. [101, 103] and references therein.

For later comparison, we briefly review the spin dynamics in the spin-boson model in two different limits, namely, the high-field limit $B \gg \Gamma_1$ and the low-field limit $B \ll \Gamma_1$, cf. Refs. [101, 103]. Within Bloch-Redfield theory, the relaxation rate Γ_1 and the dephasing rate Γ_2 are found to be

$$\Gamma_1 = 2\,\Gamma_2 = \frac{gB}{2}\coth\left(\frac{B}{2T}\right)\;. \tag{5.2}$$

In the high-field limit the spin performs coherent oscillations at frequencies $\sim B$. Correlations in transverse directions decay on the time scale $1/\Gamma_2$. From this one can conclude the shape of the symmetric, real-time correlation functions $C_{\alpha\alpha}^{(2)}(t,t') = \frac{1}{2}\langle\{S_\alpha(t), S_\alpha(t')\}\rangle$ in the frequency domain. In the high-field limit one finds

$$C_{xx}^{(2)}(\omega) \approx C_{yy}^{(2)}(\omega) \approx \frac{\Gamma_2}{4\left((\omega - B)^2 + \Gamma_2^2\right)} + \frac{\Gamma_2}{4\left((\omega + B)^2 + \Gamma_2^2\right)}\;. \tag{5.3}$$

The longitudinal correlation function $C_{zz}^{(2)}(\omega)$ consists of two parts, a Lorentzian of width Γ_1 and weight $(1 - 4\langle S_z \rangle^2)/2$ and a δ-function of weight $4\langle S_z \rangle^2$:

$$C_{zz}^{(2)}(\omega) = 2\pi\delta(\omega)\langle S_z \rangle^2 + \frac{\left(1 - 4\langle S_z \rangle^2\right)\Gamma_1}{2\left(\omega^2 + \Gamma_1^2\right)}\;. \tag{5.4}$$

In the low-field limit $B \ll \Gamma_1$ the spin shows overdamped dynamics. Eq. (5.4) holds, though the average $\langle S_z \rangle$ becomes negligibly small and $\Gamma_1 \approx gT$. The y-correlations are still governed by Γ_2. However, one finds that x-correlations are controlled by a different rate $\Gamma_< \approx B^2 / \Gamma_1$, which diminishes as temperature is increased. This behavior is recognized as the quantum watchdog (Zeno) effect, cf. Ref. [108]. That is, the bath, which couples to $\hat{S}_x$, suppresses transitions between the x-eigenstates by constantly monitoring the "x-fraction" of the spin state. As the time scale $1/\Gamma_>$ diverges for $T \to 0$, the effect can be interpreted as an indication of the quantum phase transition to the localized state, cf. Ref. [104].

The symmetric spin correlation functions $C^{(2)}_{\alpha\alpha}(\omega)$ can be translated to Majorana Green's functions by means of the simplified relations, cf. Refs. [5, 6], discussed in detail in Ch. 3. We recall Eq. (3.84):

$$C^{(2)}_{\alpha\alpha}(\omega) = \frac{i}{4} \left(G^R_{\alpha\alpha}(\omega) - G^A_{\alpha\alpha}(\omega) \right) \ . \tag{5.5}$$

Thus, the longitudinal correlator (5.4) yields the following anticipated result for the longitudinal retarded Majorana Green's function:

$$G^R_{zz,ant}(\omega) = \frac{A}{\omega + i0} + \frac{1 - A}{\omega + i\Gamma_1} \ . \tag{5.6}$$

with $A = 4\langle S^z \rangle^2 = \tanh^2 \frac{B}{2T}$. Similarly, the transverse retarded Majorana Green's functions can be obtained from Eqs. (5.3).

In a faithful approach to the dressed Majorana Green's functions one expects that the well-established Bloch-Redfield results, in particular (5.6), are reproduced. Below we compute the dressed Majorana Green's functions in standard perturbation theory, which turns out to produce the expected behavior for the transverse components but fails in the longitudinal case.

5.1.2. First-Order Perturbation Theory

Here we compute the self-energy of Majorana Green's functions to leading order in the coupling constant g. By means of the Dyson equation we construct the full Green's functions in order to compare with the results of Bloch-Redfield theory highlighted above. The results presented here have been obtained in Ref. [6].

For the discussion we recall the spin-boson Hamiltonian (5.1) in the Majorana representation (3.2),

$$H = H_0 + H_{int} \ , \qquad H_0 = -iB\,\hat{\eta}_x \hat{\eta}_y + H_B \ , \qquad H_{int} = -i\hat{\eta}_y \hat{\eta}_z\,\hat{X} \ . \tag{5.7}$$

The zeroth-order Hamiltonian contains the internal bath Hamiltonian and the magnetic field term. The field introduces a non-trivial matrix structure in spin space, included in the zeroth-order Majorana Green's functions $G_{f\alpha\beta}$, where $\alpha, \beta, \gamma \in \{x, y, z\}$. In frequency space the matrix-valued zeroth-order Green's functions $G^R_f(\epsilon)$ and $\mathcal{G}_f(i\epsilon_n)$ are given by

$$G^R_f(\epsilon) = \begin{pmatrix} \epsilon & iB & 0 \\ -iB & \epsilon & 0 \\ 0 & 0 & \epsilon \end{pmatrix}^{-1} \Bigg|_{\epsilon \to \epsilon + i0} \ , \qquad \mathcal{G}_f(i\epsilon_n) = \begin{pmatrix} \epsilon & iB & 0 \\ -iB & \epsilon & 0 \\ 0 & 0 & \epsilon \end{pmatrix}^{-1} \Bigg|_{\epsilon \to i\epsilon_n} \ , \tag{5.8}$$

with $\epsilon_n = (2n + 1)\pi T$, $n \in \mathbb{Z}$.

Figure 5.1.: First-order diagram for the Majorana self-energy. Solid and wavy lines represent Majorana propagators and bosonic bath propagators, respectively.

The interaction Hamiltonian H_{int} that couples Majoranas to the bath is treated perturbatively. The full Majorana Green's functions can be obtained through the Dyson equation $[\hat{G}]^{-1} = [\hat{G}_f]^{-1} - \hat{\Sigma}$, cf. Ref. [47], once the self-energy $\hat{\Sigma}$ is calculated within some approximation. In H_{int} only the y- and z-Majoranas are coupled to the bath, therefore the only non-zero entries of the self-energy matrix in spin space $\Sigma_{\alpha\beta}$ are $\Sigma_y \equiv \Sigma_{yy}$ and $\Sigma_z \equiv \Sigma_{zz}$ [2] As a consequence, the perturbative contributions to the self-energy only comprise $G_{fy} \equiv G_{fyy}$ and $G_{fz} \equiv G_{fzz}$, given by

$$G_{fy}^R(\epsilon) = \frac{1}{2}\left(\frac{1}{\epsilon - B + i0} + \frac{1}{\epsilon + B + i0}\right) , \qquad G_{fz}^R(\epsilon) = \frac{1}{\epsilon + i0} ,$$

$$G_{fy}^K(\epsilon) = \tanh\left(\frac{\epsilon}{2T}\right)\left(G_{fy}^R(\epsilon) - G_{fy}^A(\epsilon)\right) , \qquad G_{fz}^K(\epsilon) = 0 , \qquad (5.9)$$

and the bath correlator $\hat{\Pi}^{ab}(t,t') = \langle \mathcal{T}_K \check{X}^a(t)\check{X}^b(t')\rangle$. In the spectral representation, introduced for the Ohmic bath in Eq. (4.4), the Keldysh components of Π are given by

$$\Pi^{R/A}(\omega) = \int_{-\Lambda}^{\Lambda} \frac{dx}{i\pi}\frac{gx}{\omega + x \pm i0}, \qquad \Pi^K(\omega) = \coth\left(\frac{\omega}{2T}\right)\left(\Pi^R(\omega) - \Pi^A(\omega)\right) . \qquad (5.10)$$

The Matsubara form, cf. Eq. (4.6), equals to $\Pi(i\omega_m) = -i\Pi^{R/A}(\omega + i0 \to i\omega_m)$, with $\omega_m = 2m\pi T$ and $m \in \mathbb{Z}$. In the calculations below we make use of both Matsubara and Keldysh formalism. [3] Calculations have mostly been carried out within both techniques, but often the Matsubara expressions are more transparent for discussion.

The leading contribution to the self-energies are of first order in g and diagrammatically correspond to Fig. 5.1. Due to the structure of the vertex $\propto \hat{\eta}_y\hat{\eta}_z$, the y-component contains the z-Green's function,

$$^{(1)}\hat{\Sigma}_y^{ab}(\epsilon) = -\frac{1}{2}\int \frac{d\omega}{2\pi}\,\mathrm{Tr}\left\{\bar{\gamma}^a\hat{\Pi}(\epsilon + \omega)\bar{\gamma}^b\hat{G}_{fz}(\omega)\right\} , \qquad (5.11)$$

whereas the z-self-energy contains the y-Green's function

$$^{(1)}\hat{\Sigma}_z^{ab}(\epsilon) = -\frac{1}{2}\int \frac{d\omega}{2\pi}\,\mathrm{Tr}\left\{\bar{\gamma}^a\hat{\Pi}(\epsilon + \omega)\bar{\gamma}^b\hat{G}_{fy}(\omega)\right\} . \qquad (5.12)$$

---

[2] In other spin-boson models, where magnetic field $\boldsymbol{B}$ is not perpendicular to $\boldsymbol{X}$ of the bosonic bath, off-diagonal entries to the self-energy matrix appear.

[3] For the Majorana Green's function, the corresponding self-energy, and the bath correlator we use the standard Keldysh rotation, cf. Eqs. (4.53) or Ref. [47]:

$$\hat{G}_{\alpha\beta}(\epsilon) = \begin{pmatrix} G_{\alpha\beta}^K(\epsilon) & G_{\alpha\beta}^R(\epsilon) \\ G_{\alpha\beta}^A(\epsilon) & 0 \end{pmatrix}, \qquad \hat{\Sigma}_{\alpha\beta}(\epsilon) = \begin{pmatrix} 0 & \Sigma_{\alpha\beta}^A(\epsilon) \\ \Sigma_{\alpha\beta}^R(\epsilon) & \Sigma_{\alpha\beta}^K(\epsilon) \end{pmatrix}$$

$$\hat{\Pi}(\omega) = \begin{pmatrix} \Pi^K(\omega) & \Pi^R(\omega) \\ \Pi^A(\omega) & 0 \end{pmatrix}, \qquad \gamma^{cl} = \bar{\gamma}^q = \mathbb{1} , \qquad \gamma^q = \bar{\gamma}^{cl} = \tau_1 = \begin{pmatrix} 0 & 1 \\ 1 & 0 \end{pmatrix} .$$

Here the trace refers to the trace in Keldysh space. The imaginary part of the self-energy can be conveniently obtained by

$$\Gamma_\alpha(\epsilon) = -\text{Im}\Sigma_\alpha^R(\epsilon) = \frac{i}{2}\left(\Sigma_\alpha^R(\epsilon) - \Sigma_\alpha^A(\epsilon)\right) \ . \tag{5.13}$$

Having evaluated the traces in Keldysh space, the integrations are easily performed with the help of the δ-functions in Eqs. (5.10) and (3). The quantity Λ plays the role of a high-energy cutoff, thus we assume frequencies and magnetic field to be much smaller, $B, |\epsilon| \ll \Lambda$. The real part of the self-energy renormalizes the field B in the Green's functions, however, in the limit $g \ll 1$ this renormalization is small and can be neglected.

Transverse Dynamics

We first focus on the transverse y-component. From Eq. (5.13) one finds

$$\Gamma_y(\epsilon) = \frac{g\epsilon}{2}\coth\frac{\epsilon}{2T} \ . \tag{5.14}$$

By inversion of the submatrix x, y-part of the Dyson equation one obtains the retarded transverse Green's functions

$$G_x^R(\epsilon) = \frac{\epsilon + i\Gamma_y(\epsilon)}{\epsilon\left(\epsilon + i\Gamma_y(\epsilon)\right) - B^2} \ , \qquad G_y^R(\epsilon) = \frac{\epsilon}{\epsilon\left(\epsilon + i\Gamma_y(\epsilon)\right) - B^2} \ , \tag{5.15}$$

with poles at

$$\epsilon_{1/2} = -\frac{i\Gamma_y(\epsilon)}{2} \pm \sqrt{B^2 - \frac{\Gamma_y^2(\epsilon)}{4}} \ . \tag{5.16}$$

In the regions $\epsilon \sim \pm B$ the functions (5.15) have a Lorentzian resonance shape, their width given by the imaginary part of the poles:

$$\frac{\Gamma_y(B)}{2} = \frac{gB}{4}\coth\frac{B}{2T} = \Gamma_2 = \frac{\Gamma_1}{2} \ . \tag{5.17}$$

Thus we recover the standard dephasing rate Γ_2 in agreement with the Bloch-Redfield results (5.2) discussed above. In the high-field limit $B \gg \Gamma_2$ the results (5.15) correspond to the correlation functions given in Eqs. (5.3).

In the low-field limit $B < \Gamma_2$ the square root in (5.16) gets imaginary. One can then expand the square root and finds two diverging rates $\Gamma_>$ and $\Gamma_<$. The larger rate $\Gamma_>$ converges to the value (5.14) and describes the decay of the y-component in the low-field limit, at high temperatures $\Gamma_> = \Gamma_y(\epsilon) \sim gT$. The smaller rate $\Gamma_< \propto B^2/\Gamma_y(\epsilon) \sim B^2/(gT)$ is found to govern the decay of the x-component. Thus the dressed Majorana Green's functions (5.15) fully recover the results known from Bloch-Redfield theory as described in Subs. 5.1.1.

Longitudinal Dynamics

Now we turn to the longitudinal z-component. For the imaginary part (5.13) of the self-energy $^{(1)}\Sigma_z^R$ we find

$$\Gamma_z(\epsilon) = \frac{g}{4}\left((B+\epsilon)\coth\frac{B+\epsilon}{2T} + (B-\epsilon)\coth\frac{B-\epsilon}{2T} - 2B\tanh\frac{B}{2T}\right) \ . \tag{5.18}$$

In the small field limit $B \ll \epsilon$ and high temperatures we recover the thermal rate $\Gamma_z(\epsilon) \to gT$, similar to (5.14). For larger fields the peak of the Lorentzian in $G_z^R(\omega)$ is still situated at $\epsilon = 0$, which justifies to put $\epsilon \to 0$ in the expression above. Recognizing the relaxation rate $\Gamma_1 = gB/2 \coth B/(2T)$ and the factor $A = \tanh^2 \frac{B}{2T}$ introduced in Subs. 5.1.1 we find

$$\tilde{\Gamma}_1 \equiv \Gamma_z(\epsilon \to 0) = \Gamma_1 (1 - A) \ . \tag{5.19}$$

By means of the Dyson equation for the z-component we obtain the full z-Majorana Green's function

$$G_z^R(\epsilon) = \frac{1}{\epsilon + i\tilde{\Gamma}_1} \ . \tag{5.20}$$

The formula does not coincide with the well-known result (5.6) obtained in Bloch-Redfield theory. We address this issue in detail below. The discrepancy is the major motivation for the present chapter.

We remark that in the low-field limit and at high temperatures the leading-order perturbation theory is valid and yields the rate $\Gamma_y \approx \Gamma_z \approx gT$. This thermal rate governs the dynamics of the y- and z-Majoranas directly coupled to the bath, which is reminiscent of the Bose-Kondo model dynamics discussed in Ch. 4. There, through the isotropic spin-bath coupling, each Majorana is essentially coupled to two baths. In the spin-boson model considered here the y- and z-Majoranas are coupled to one bath, which explains the discrepancy of a factor of two between the limits above and the Korringa result Eq. (4.12), $\Gamma_K = 2gT$.

5.1.3. Discussion

Above we recapitulated the Bloch-Redfield solutions of the spin-boson model (5.1). We have reviewed the attempt in Ref. [6] to obtain these solutions within leading-order perturbation theory using the Majorana representation. The transverse Majorana Green's functions fully agree with the Bloch-Redfield results. We point out that the calculation was significantly simpler than any of those attempting to calculate the fermionic loop, underlining the benefit of the Majorana method, cf. Sec. 3.1 and Refs. [5, 6].

However, the result (5.20) for the longitudinal Majorana Green's function differs from the anticipated solution (5.6)

$$G_{z,ant}^R(\epsilon) = \frac{A}{\epsilon + i0} + \frac{1 - A}{\epsilon + i\Gamma_1} \ , \tag{5.21}$$

obtained in Bloch-Redfield theory. Thus we reproduce the problem noticed in Ref. [6]. The result (5.20) misses the first term in (5.21) describing the thermal magnetization average ($A \sim \langle S_z \rangle^2$) and does not produce the correct relaxation rate Γ_1. Instead of two Lorentzians (one with zero width and the other with width Γ_1) a single Lorentzian with width $\tilde{\Gamma}_1 = \Gamma_1 (1 - A)$ and unit weight was found.

One can observe that the solution (5.21) coincides with (5.20) in the limit $\epsilon \gg \Gamma_1$, cf. Ref. [6]. To do so we expand the two z-Green's functions around $\Gamma_1 \to 0$, consistent with the weak coupling limit $g \ll 1$,

$$G_{z,ant}^R(\epsilon) = \frac{1}{\epsilon + i0} - \frac{i(1 - A)\Gamma_1}{(\epsilon + i0)^2} - \frac{(1 - A)\Gamma_1^2}{(\epsilon + i0)^3} + \mathcal{O}(g^3) \ ,$$

$$G_z^R(\epsilon) = \frac{1}{\epsilon + i0} - \frac{i(1 - A)\Gamma_1}{(\epsilon + i0)^2} - \frac{(1 - A)^2\Gamma_1^2}{(\epsilon + i0)^3} + \mathcal{O}(g^3) \ .$$

Both expressions agree up to the first order in $\Gamma_1 \sim g$, discrepancies only arise in second order. This does not come as a surprise, since the self-energy, Eq. (5.12) and Fig. 5.1, has only been computed up to first order in g in the first place. Thus the failure of the diagrammatic calculation strongly suggests that the lowest-order approximation (5.12) for the longitudinal self-energy is insufficient, cf. Ref. [6].

The perturbative approach above fails to reproduce the longitudinal spin dynamics in the long-time limit. However, as we have shown in Ch. 3 the Majorana representation is a valid spin representation. Thus, one expects that the problem is resolved by computing the self-energy to higher orders in g, and that higher orders are crucial for an accurate description of the long-time limit. This provides the motivation for the second-order analysis in the next section.

5.2. Perturbative Approach to the Self-Energy in Second Order

Here we compute the second-order self-energy within the perturbative approach used above. Based on the Bloch-Redfield result (5.6) we can specify the expectations for the second-order self-energy calculation. To do so we introduce the anticipated self-energy $\Sigma_{z,ant}^R$ in terms of $G_{z,ant}^R(\epsilon) = (\epsilon - \Sigma_{z,ant}^R(\epsilon))^{-1}$. We then deduce the solution for $\Sigma_{z,ant}^R(\epsilon)$ from (5.6):

$$\Sigma_{z,ant}^R(\epsilon) = -i\frac{(1-A)\Gamma_1}{1 + \frac{iA\Gamma_1}{\epsilon}} = -i(1-A)\Gamma_1 - \frac{A(1-A)\Gamma_1^2}{\epsilon + iA\Gamma_1} \ . \tag{5.22}$$

In the first-order calculation above we found $^{(1)}\Sigma_z^R(\epsilon) = -i(1-A)\Gamma_1$, thus we observe the correspondence of the two in the limit $|\epsilon| \gg \Gamma_1$. We expand (5.22) in powers of g and obtain

$$\Sigma_{z,ant}^R(\epsilon) = -i(1-A)\Gamma_1 - \frac{A(1-A)\Gamma_1^2}{\epsilon} + \mathcal{O}(g^3) \ , \tag{5.23}$$

We recognize $A\Gamma_1/\epsilon$ as the expansion parameter, implying that the above series diverges for $\epsilon < A\Gamma_1$. From (5.23) we expect that the imaginary part of $^{(2)}\Sigma_z^R$ vanishes and that the real second-order self-energy is

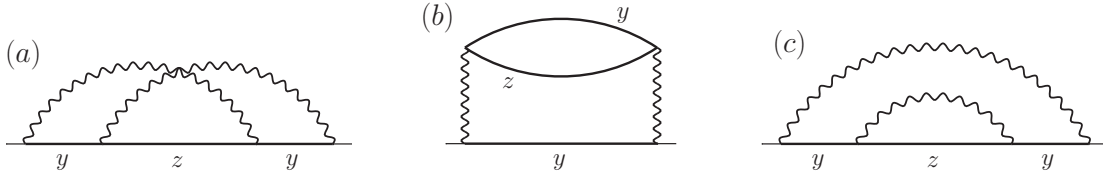$$^{(2)}\Sigma_z^R(\epsilon) = -\frac{A(1-A)\Gamma_1^2}{\epsilon} \ . \tag{5.24}$$

Below we find that this result is indeed produced in second-order perturbation theory, confirming the relevance of higher-order contributions in the long-time limit.

5.2.1. Second-Order Self-Energy: Matsubara Technique

In the perturbative expansion in $g \ll 1$ one finds three contributions to the second-order self-energy, which are shown in Fig. 5.2. The first order approximation in Subs. 5.1.2 yields accurate results for the transverse self-energy, therefore we concentrate on the longitudinal z-self-energy here. In the Matsubara technique we obtain for the first diagram (a)

$$^{(a)}\Sigma_z(\epsilon_n) = T^2 \sum_{\omega_1,\omega_2} \mathcal{G}_{fy}(\epsilon_n - \omega_1)\mathcal{G}_{fz}(\epsilon_n - \omega_1 - \omega_2)\mathcal{G}_{fy}(\epsilon_n - \omega_2)\Pi(\omega_1)\Pi(\omega_2) \ , \tag{5.25}$$

Figure 5.2.: Second-order diagrams for the self-energy Σ_z.

for the explicit form of the functions $\mathcal{G}$ and Π we refer to Subs. 5.1.2. The diagram (b) in Fig. 5.2 is given by

$$^{(b)}\Sigma_z(\epsilon_n) = T^2 \sum_{\omega_1,\omega_2} \mathcal{G}_{fy}(\epsilon_n - \omega_1)\mathcal{G}_{fz}(\omega_1 + \omega_2 - \epsilon_n)\mathcal{G}_{fy}(\epsilon_n - \omega_2)\Pi(\omega_1)\Pi(\omega_1) \ . \qquad (5.26)$$

Diagrams (a) and (b) strongly diverge ($\propto \Lambda^2$), but their sum diverges at most logarithmically. Indeed it can be written as

$$^{(ab)}\Sigma_z(\epsilon_n) = {}^{(a)}\Sigma_z(\epsilon_n) + {}^{(b)}\Sigma_z(\epsilon_n)$$

$$= -\frac{T^2}{2} \sum_{\omega_1,\omega_2} \mathcal{G}_{fy}(\epsilon_n - \omega_1)\mathcal{G}_{fz}(\epsilon_n - \omega_1 - \omega_2)\mathcal{G}_{fy}(\epsilon_n - \omega_2)$$

$$\times \left[\Pi(\omega_1) - \Pi(\omega_2)\right]^2 \ . \qquad (5.27)$$

This expression is evaluated with the help of Mathematica. Upon analytic continuation $i\epsilon_n \to \epsilon$ we find that the leading term in the limit $\epsilon \to 0$ diverges according to

$$^{(ab)}\Sigma_z(\epsilon) = -\frac{A(1-A)\Gamma_1^2}{\epsilon} \ . \qquad (5.28)$$

Thus we reproduce the second term of (5.23). We have also computed the third diagram (c) in Fig. 5.2 for Σ_z, however, the diagram does not lead to Γ_1/ϵ-like divergencies and can therefore be neglected as compared to the other two diagrams.

5.2.2. Second-Order Self-Energy: Keldysh Technique

Here we sketch the Keldysh approach to the second-order self-energy $^{(2)}\Sigma_z^R$. We present a framework for Keldysh calculations which is easily implemented in standard symbolic mathematical computation programs, e.g. Mathematica. To this end we make use of the notation defined in Subs. 3.2.3, $\check{\eta}_\alpha = (\eta_\alpha^{cl}, \eta_\alpha^q)$ etc. and matrices $\gamma^{cl} = \mathbb{1}$ and $\gamma^q = \tau_1$ (compare also the footnote on p. 79) For simplicity we drop the operator-hat, keeping in mind that Majorana η_α and bosonic X symbols are still operators as long as we do not switch to the path integral technique.

The perturbative expansion of time evolution operators in the interaction picture comprises the spin-bath interaction term (5.1) of the spin-boson model . The corresponding vertex

can be written in a compact form in the rotated Keldysh representation:

$$
-i\int_C dt\, H_{int}(t) = -\int_C dt\, X(t)\eta_y(t)\eta_z(t)
$$

$$
= -\frac{1}{\sqrt{2}}\int_{-\infty}^{\infty} dt\, \left(X^{cl}(t)[\check{\eta}_y(t)\gamma^q\check{\eta}_z(t)] + X^q(t)[\check{\eta}_y(t)\gamma^{cl}\check{\eta}_z(t)]\right)
$$

$$
= -\frac{1}{\sqrt{2}}\sum_a^{q,cl}\int_{-\infty}^{\infty} dt\, (\tau_1\check{X}(t))^a[\check{\eta}_y(t)\gamma^a\check{\eta}_z(t)] \;. \quad (5.29)
$$

From this vertex one can easily deduce the perturbative contributions within the Keldysh technique. The zeroth-order functions $\hat{G}_{f\alpha}(\epsilon)$ and Π can be found in Subs. 5.1.2.

The contribution corresponding to the first diagram (a) in Fig. 5.2 to the retarded self-energy $\Sigma^R = \Sigma^{q,cl}$ reads

$$
^{(a)}\Sigma_z^R(\epsilon) = \frac{1}{4}\sum_{a,b,c,d}^{q,cl}\int_{-\infty}^{\infty}\frac{d\omega_1 d\omega_2}{(2\pi)^2}\left(\gamma^a\hat{G}_{fy}(\omega_2)\gamma^b\hat{G}_{fz}(\omega_1+\omega_2)\gamma^c\hat{G}_{fy}(\omega_1+\epsilon)\gamma^d\right)^{q,cl}
$$

$$
\times\left(\tau_1\hat{\Pi}(\omega_2-\epsilon)\tau_1\right)^{ca}\left(\tau_1\hat{\Pi}(\omega_1)\tau_1\right)^{db}\;. \quad (5.30)
$$

The second diagram (b) contributes

$$
^{(b)}\Sigma_z^R(\epsilon) = -\frac{1}{4}\sum_{a,b,c,d}^{q,cl}\int_{-\infty}^{\infty}\frac{d\omega_1 d\omega_2}{(2\pi)^2}\,\text{Tr}\{\hat{G}_{fy}(\omega_2)\gamma^b\hat{G}_{fz}(\omega_1+\omega_2)\gamma^c\}\left(\gamma^a\hat{G}_{fy}(\omega_1+\epsilon)\gamma^d\right)^{q,cl}
$$

$$
\times\left(\tau_1\hat{\Pi}(\omega_1)\tau_1\right)^{ca}\left(\tau_1\hat{\Pi}(\omega_1)\tau_1\right)^{db}\;. \quad (5.31)
$$

We calculated the self-energies with the help of Mathematica. In the limit $\epsilon \to 0$ we obtain the divergent term $^{(2)}\Sigma_z^R = -A(1-A)\Gamma_1^2/\epsilon$, in agreement with the result obtained in the Matsubara technique and with the expected result (5.24). This again confirms that the two diagrams in Fig. 5.3 are responsible for the divergent term in the expansion (5.23).

For the transverse self-energy Σ_y we performed similar calculations in second order in g, which is also described by the diagrams in Fig. 5.2. In that case, we did not encounter the singular $1/\epsilon$-behavior. Therefore we conclude that the first-order results in Subs. 5.1.2 provide a valid approximation for the transverse self-energy at small spin-bath coupling.

In this section we reproduced the anticipated expression for the longitudinal self-energy (5.22) up to the second order in g. This shows that the discrepancy noticed in Ref. [6] is removed by accounting for higher order contributions to the self-energy of the longitudinal Majorana fermions. For a better understanding of this result we develop a path-integral description, which allows us to take advantage of the findings in Ch. 4.

5.3. Path-Integral Approach for the Spin-Boson Model

Here, along the lines of the discussion in Sec. 4.2, we develop a path integral approach for the spin-boson model (5.1). We derive the effective action of Σ-fields and analyze the saddle-point solution. In this framework we demonstrate that the diverging second-order contributions to the longitudinal self-energy can be interpreted in terms of fluctuations

around the saddle point. That is, fluctuations of the self-energy are important, in contrast to the Bose-Kondo model in Ch. 4.

In the Matsubara imaginary-time technique the partition function of the spin-boson model, $\mathcal{Z} = \int D[\dots] \exp[i\mathcal{S}]$, reads

$$\mathcal{Z} = \int D[X]D[\boldsymbol{\eta}] \exp\left\{ i\,\mathcal{S}_B + \int_0^\beta d\tau \left[-\frac{1}{2}\,\eta_\alpha(\tau)\,\partial_\tau \eta_\alpha(\tau) + iB\eta_x\eta_y + i\eta_y\eta_z\,X \right] \right\} \; . \quad (5.32)$$

Here $\mathcal{S}_B$ is the free bosonic action. The transformations below closely follow the approach for the Bose-Kondo model, we refer to Subs. 4.2.1 for details. The first step is to average over the fluctuations of X , yielding

$$\mathcal{Z} = \int D[\boldsymbol{\eta}] \exp\left\{ \int d\tau \left[-\frac{1}{2}\,\eta_\alpha(\tau)\,\partial_\tau\,\eta_\alpha(\tau) + i\,B\eta_x(\tau)\eta_y(\tau) \right] \right.$$
$$\left. -\frac{1}{2}\int d\tau d\tau'\,\Pi(\tau-\tau')\,\eta_y(\tau)\eta_z(\tau)\,\eta_y(\tau')\eta_z(\tau') \right\} \; , \quad (5.33)$$

In order to decouple the quartic Majorana-Majorana interaction we rearrange

$$i\mathcal{S}_{int}[\boldsymbol{\eta}] = -\frac{1}{2}\int d\tau d\tau'\,\Pi(\tau-\tau')\,\eta_y(\tau)\eta_z(\tau)\,\eta_y(\tau')\eta_z(\tau')$$
$$= \frac{1}{2}\int d\tau d\tau'\,\Pi(\tau-\tau')\,[\eta_y(\tau)\eta_y(\tau')]\,[\eta_z(\tau)\eta_z(\tau')] \; . \quad (5.34)$$

In contrast to the Bose-Kondo model in Subs. 4.2 the bath couples to η_y and η_z only. Thus, only two Hubbard-Stratonovich fields Σ_y and Σ_z (which inherit $\Sigma_\alpha(\tau,\tau') = -\Sigma_\alpha(\tau',\tau)$) are needed to employ the Hubbard-Stratonovich transformation. The new effective action reads

$$i\mathcal{S}[\boldsymbol{\eta},\boldsymbol{\Sigma}] = \frac{1}{2}\int d\tau d\tau'\,\eta_\alpha(\tau)\left(\mathcal{G}^{-1}\right)_{\alpha\beta}\eta_\beta(\tau') - \frac{1}{2}\int d\tau d\tau'\,\frac{\Sigma_y(\tau,\tau')\,\Sigma_z(\tau,\tau')}{\Pi(\tau-\tau')} \; . \quad (5.35)$$

The Majorana Green's function in (5.35) is

$$\mathcal{G}^{-1} = \begin{pmatrix} -\delta(\tau-\tau')\partial_{\tau'} & iB\delta(\tau-\tau') & 0 \\ -iB\delta(\tau-\tau') & -\delta(\tau-\tau')\partial_{\tau'} - \Sigma_y(\tau,\tau') & 0 \\ 0 & 0 & -\delta(\tau-\tau')\partial_{\tau'} - \Sigma_z(\tau,\tau') \end{pmatrix} \; . \quad (5.36)$$

The function $\Pi(\tau-\tau')$ (4.22) is positive and non-zero, the convergence of the Σ_α integrals can be established by appropriate choice of real and imaginary modes, cf. the discussion in Subs. 4.2.1. Finally, the effective action of the Σ-fields is obtained by integrating out the Majorana fields η_α,

$$i\mathcal{S}[\Sigma_\alpha] = \frac{1}{2}\mathrm{Tr}\log\left(\mathcal{G}^{-1}\right) - \frac{1}{2}\int d\tau d\tau'\,\frac{\Sigma_y(\tau,\tau')\,\Sigma_z(\tau,\tau')}{\Pi(\tau-\tau')} \; . \quad (5.37)$$

5.3.1. Saddle-Point Analysis

In close analogy to Subs. 4.2.2, a saddle-point solution $\Sigma_{0\alpha}$ is found by expanding $\Sigma_\alpha = \Sigma_{0\alpha} + \delta\Sigma_\alpha$ $(\alpha = y, z)$ around the saddle point and taking the linear order in $\delta\Sigma_\alpha$. Here we obtain, similar to (4.35),

$$\Sigma_{0y}(\tau-\tau') = \Pi(\tau-\tau')\mathcal{G}_{0z}(\tau-\tau') \; ,$$
$$\Sigma_{0z}(\tau-\tau') = \Pi(\tau-\tau')\mathcal{G}_{0y}(\tau-\tau') \; . \quad (5.38)$$

The equations are self-consistent in the sense that $\mathcal{G}_{0\alpha}$ are functionals of $\Sigma_{0\alpha}$ through the definition (5.36), where $\mathcal{G}$ and Σ have to be replaced by $\mathcal{G}_0$ and Σ_0, respectively.

For the analysis of the saddle-point solution we switch to the Keldysh version of the above equations, which was derived in Subs. 4.3.2. In order to keep Π in the numerator the Keldysh treatment relied on the Hubbard-Stratonovich fields $\hat{Q}$, thus the saddle-point equations simply read

$$\hat{Q}_{0y}(t - t') = \hat{G}_{0z}(t - t') \ ,$$
$$\hat{Q}_{0z}(t - t') = \hat{G}_{0y}(t - t') \ . \tag{5.39}$$

The self-energies $\Sigma_{0\alpha}$ at the saddle point are obtained through Eq. (4.55),

$$\hat{\Sigma}_{0\alpha}^{ab}(t - t') = -\frac{1}{2}\mathrm{Tr}\left\{\bar{\gamma}^a\hat{\Pi}(t - t')\bar{\gamma}^b\hat{Q}_{0\alpha}(t', t)\right\} \ , \tag{5.40}$$

which still allows to interpret fluctuations of Q-fields in terms of self-energy fluctuations. Substituting the saddle-point solutions $\hat{Q}_{0\alpha}$ into the self-energy and transforming to frequency space we obtain

$$\hat{\Sigma}_{0y}^{ab}(\epsilon) = -\frac{1}{2}\int\frac{d\omega}{2\pi}\,\mathrm{Tr}\left\{\bar{\gamma}^a\hat{\Pi}(\epsilon + \omega)\bar{\gamma}^b\hat{G}_{0z}(\omega)\right\} \ ,$$
$$\hat{\Sigma}_{0z}^{ab}(\epsilon) = -\frac{1}{2}\int\frac{d\omega}{2\pi}\,\mathrm{Tr}\left\{\bar{\gamma}^a\hat{\Pi}(\epsilon + \omega)\bar{\gamma}^b\hat{G}_{0y}(\omega)\right\} \ . \tag{5.41}$$

These equations look similar to the first-order results (5.11) and (5.12) obtained in Subs. 5.1.2. However, here the zeroth order Green's functions $\hat{G}_{f\alpha}$ are replaced by the saddle-point Green's functions $\hat{G}_{0\alpha}$, which are in turn related to the saddle-point self-energies by Dyson-like equations $\hat{G}_0^{-1} = \hat{G}_f^{-1} - \hat{\Sigma}_0$. This means that the Majorana self-energies have to be computed self-consistently.

In order to find the self-consistent formulas we use the usual iterative approach. We recalculate the self-energies (5.41) using the Green's function constructed from first-order self-energies (5.14) and (5.18),

$$G_y^R(\epsilon) = \frac{\epsilon}{\epsilon\left(\epsilon + i\Gamma_y(\epsilon)\right) - B^2} \ , \qquad G_z^R(\epsilon) = \frac{1}{\epsilon + i\Gamma_z(\epsilon)} \ , \tag{5.42}$$

instead of the a priori unknown saddle-point functions G_{0y}^R and G_{0z}^R. In the calculation it turns out that at small couplings the self-energy integrals in (5.41) are dominated by the same contributions which yielded the first-order results (5.14) and (5.18). This is the case in the limit $\epsilon \ll \Gamma_1$ as well as in the intermediate frequency range $\epsilon \lesssim B, T$. We conclude that the self-consistency does not change the first-order self-energy results considerably. Thus the Green's functions (5.42) constitute a proper approximation for the saddle-point Green's functions G_{0y}^R and G_{0z}^R. In the high-field limit $B \gg \Gamma_1$ we again obtain Lorentzian-like functions of widths given by $\Gamma_y(B)/2 \approx \Gamma_2$ and $\Gamma_z(0) \approx \tilde{\Gamma}_1 = (1 - A)\Gamma_1$.

Having obtained the longitudinal saddle-point solution $G_{0z}(\epsilon)$, we realize that this solution also fails to describe Bloch-Redfield results (5.6). Thus we expect that fluctuations around the saddle point are relevant, which are still to investigate.
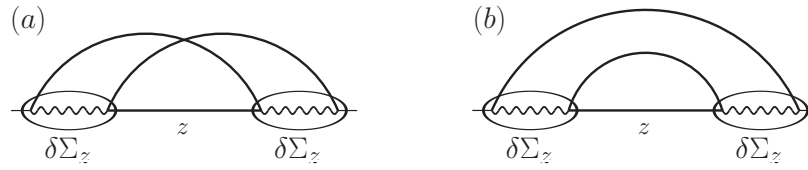
Figure 5.3.: Second-order diagrams that can be understood as fluctuations of the self-energy $\delta\Sigma_z$. These are the diagrams (a) and (b) of Fig. 5.2.

5.3.2. Role of the Fluctuations

The divergent second-order contributions to the longitudinal self-energy discussed in Sec. 5.2 are clearly not covered by the saddle-point solutions above. Here we interpret these contributions in terms of self-energy fluctuations $\delta\Sigma_y$ and $\delta\Sigma_z$. The action of fluctuations in the vicinity of the saddle point is derived by expanding the action (5.37) up to second order in fluctuations. In the more transparent Matsubara technique, similar to Eq. (4.39), the fluctuations are described by

$$i\mathcal{S}_{\delta\Sigma} = -\frac{1}{4}\sum_\alpha^{y,z}\int d\tau_1 d\tau_2 d\tau_3 d\tau_4\, \mathcal{G}_{0\alpha}(\tau_1-\tau_2)\, \delta\Sigma_\alpha(\tau_2,\tau_3)\, \mathcal{G}_{0\alpha}(\tau_3-\tau_4)\, \delta\Sigma_\alpha(\tau_4,\tau_1)$$
$$-\frac{1}{2}\int d\tau d\tau'\, \frac{\delta\Sigma_y(\tau,\tau')\,\delta\Sigma_z(\tau,\tau')}{\Pi(\tau-\tau')} \quad . \quad (5.43)$$

The first term above arises from the expansion of the trace-log term in (5.37).

Here we reanalyze the second-order self-energy diagrams shown in Fig. 5.2. The third diagram (c) is actually taken into account in the saddle-point calculation presented above. The first two diagrams of Fig. 5.2 correspond to fluctuations of the self-energy, arising from the first term in (5.43). This becomes evident if we redraw these diagrams as shown in Fig. 5.3. That is, we recognize that self-energy fluctuations are responsible for the divergence of the longitudinal self-energy Σ_z. The second-order calculations of the self-energy in Sec. 5.2 show that the saddle-point approximation is insufficient for the longitudinal spin component and that self-energy fluctuations are important.

We expect that a thorough investigation of the action (5.43) of self-energy fluctuations $\delta\Sigma_z$ is a complicated task, which is beyond the scope of this thesis. Hence it remains to be seen whether averaging of $\mathcal{G}_{0z}$ over fluctuations with the quadratic action (5.43) yields the correct long-time dynamics. This is not necessarily the case, since we can not rule out that higher terms in the trace-log expansion are relevant. However, below we develop a much simpler method to produce the correct long-time dynamics.

In the discussion of the zero-field Bose-Kondo model in Sec. 4.4 we pointed out that the purely off-diagonal[4] self-energy fluctuations do not affect the calculation of "parallel" spin correlation functions, i.e., correlators of only one spin component $\hat{S}_\alpha$. Here, this does not hold for $\hat{S}_z$, since the divergent second-order diagrams for Σ_z imply that the first term in (5.43) comprises a large diagonal term $\sim \delta\Sigma_z\delta\Sigma_z$. On the other hand, the analysis

---

[4]For the convenient choice $A_\alpha = 0$ of gauge fields, cf. Subs. 4.3.4

above shows that this is the only non-trivial component of fluctuations as compared to the Bose-Kondo model in Subs. 4.3.3. This observation motivates the arguments below.

5.4. Spin Correlators in the Spin-Boson Model

The insights above allow us to formulate a prescription for efficient calculation of a class of spin correlation functions of arbitrary order within the spin-boson model (5.1). In order to avoid divergences and the need to account for high-order contributions, one could essentially use the following approach: for calculation of a spin correlation function replace S_x with η_x, S_y with η_y, and S_z with $\eta_x\eta_y$. Thus, η_z is effectively avoided. Below we show that within this prescription spin correlation functions can be calculated using saddle-point Green's functions. Subsequently, we employ the method in order to recalculate the longitudinal two-spin correlator.

5.4.1. A Prescription for the Computation of Spin Correlators

In order to specify the prescription we propose here, we recall the Majorana representation (3.2) and the variant (3.24) thereof, [5]

$$S_x = -i\eta_y\eta_z , \quad S_y = -i\eta_z\eta_x , \quad S_z = -i\eta_x\eta_y , \tag{5.44}$$

$$S_x = \Theta\eta_x , \quad S_y = \Theta\eta_y , \quad S_z = \Theta\eta_z , \quad \{\Theta, \eta_\alpha\} = 0 , \quad \Theta^2 = \frac{1}{2} . \tag{5.45}$$

In order to avoid η_z in a spin correlation function $\langle S_{\alpha_1}(t_1) \dots S_{\alpha_N}(t_N)\rangle$ of arbitrary order, S_x is replaced by $\Theta\eta_x$, S_y by $\Theta\eta_y$ and S_z by $-i\eta_x\eta_y$. Then, by commuting Θ's one can make use of $\Theta^2 = \frac{1}{2}$ to annihilate any even numbers of Θ. Thus, any spin correlator comprising an overall even number of S_x and S_y corresponds to a Majorana correlator composed solely of η_x and η_y. At the same time the number of S_z is arbitrary.

Within the spin-boson model (5.1) Majorana correlators composed of only η_x and η_y can be efficiently calculated using the saddle-point solutions (5.38). To demonstrate that we consider the action (5.35) with sources ξ for the Majorana fermions:

$$i\mathcal{S} = \frac{1}{2}\boldsymbol{\eta}^T([\mathcal{G}_0]^{-1} - \delta\Sigma)\boldsymbol{\eta} - \frac{1}{2}\frac{\delta\Sigma_z\delta\Sigma_y}{\Pi} + \xi_x\eta_x + \xi_y\eta_y . \tag{5.46}$$

Here $\mathcal{G}_0$ is the Green's function at the saddle point, which can be obtained from (5.36) by replacing Σ by Σ_0. In this expression and below in this section we use sloppy notations implying proper time integrations. Integrating over the Majorana fermions, we find

$$i\mathcal{S} = \frac{1}{2}\operatorname{Tr}\log\left([\mathcal{G}_0]^{-1} - \delta\Sigma\right) - \frac{1}{2}\frac{\delta\Sigma_z\delta\Sigma_y}{\Pi} + \frac{1}{2}\boldsymbol{\xi}^T\left([\mathcal{G}_0]^{-1} - \delta\Sigma\right)^{-1}\boldsymbol{\xi} . \tag{5.47}$$

Since we are going to use only η_x and η_y, only the sources ξ_x and ξ_y will be relevant. In turn, this means that upon derivation with respect to the sources only the x- and y-components of $([\mathcal{G}_0]^{-1} - \delta\Sigma)$ will appear in the pre-exponential and will be averaged. These include only $\delta\Sigma_y$, but not $\delta\Sigma_z$.

---

[5]In this section we use the path integral formalism, i.e. Grassmann and Grassmann-composite variables instead of operators, cf. Section 3.2. The variables obey relations equivalent to the operator relations.

However, we can easily assess the importance of $\delta\Sigma_y$-fluctuations by looking at the propagator $\langle\delta\Sigma_y\delta\Sigma_y\rangle$. Expansion of the trace-log term to the second order gives

$$i\delta\mathcal{S} = \frac{1}{2}\begin{pmatrix} \delta\Sigma_y & \delta\Sigma_z \end{pmatrix}\begin{pmatrix} \mathcal{G}_{0y}\mathcal{G}_{0y} & \Pi^{-1} \\ \Pi^{-1} & \mathcal{G}_{0z}\mathcal{G}_{0z} \end{pmatrix}\begin{pmatrix} \delta\Sigma_y \\ \delta\Sigma_z \end{pmatrix} \tag{5.48}$$

In the analysis of fluctuations in the Bose-Kondo model in Subs. 4.2.3 and 4.3.3 we have shown that the kernel $\mathcal{G}_{0z}\mathcal{G}_z$ is negligibly small in the case $B = 0$. This observation applies here as well since B does not enter $\mathcal{G}_{0z}$ directly. If the 22-element of the matrix in (5.48) vanishes, the 11-element of the inverse matrix vanishes as well. The latter corresponds to the propagator $\langle\delta\Sigma_y\delta\Sigma_y\rangle$ of self-energy fluctuations $\delta\Sigma_y$, which can thus be neglected. As discussed above, only $\delta\Sigma_y$ can appear in the pre-exponential, hence we conclude that the fluctuations can be completely ignored. This proves the Wick theorem for the saddle-point Green functions.

To conclude, the recipe to calculate spin correlators in the spin-boson model works as follows: replace S_x with η_x, S_y with η_y and S_z with $\eta_x\eta_y$, utilize the above Wick theorem to contract η_x and η_y to obtain combinations of saddle-point Green's functions and then compute these expressions. This method is applicable to spin correlation functions of arbitrary order that include an even overall number of S_x and S_y.

5.4.2. Longitudinal Two-Spin Correlator

We demonstrate the method proposed above by means of the symmetric two-spin correlator $C_{zz}^{(2)}$. Using only η_x and η_y, i.e., $S_z = -i\eta_x\eta_y$, the correlator corresponds to

$$C_{zz}^{(2)}(t,t') = \frac{1}{2}\langle\mathcal{T}_K S_z^{cl}(t)S_z^{cl}(t')\rangle = -\frac{1}{4}\langle\mathcal{T}_K[\check{\eta}_x(t)\gamma^{cl}\check{\eta}_y(t)][\check{\eta}_x(t')\gamma^{cl}\check{\eta}_y(t')]\rangle \tag{5.49}$$

The existence of a Wick theorem for the saddle-point Green's functions means that vertex corrections to the simple loop are absent. Employing the Wick theorem on the symmetric correlator (5.49) one obtains three contributions by contracting the Majorana fields,

$$C_{zz}^{(2)}(t,t') = \frac{1}{4}\left[\left(G_{0xy}^K(0)\right)^2 - \text{Tr}\left\{\hat{G}_{0xy}(t-t')\hat{G}_{0xy}(t'-t)\right\}\right.$$
$$\left. + \text{Tr}\left\{\hat{G}_{0x}(t-t')\hat{G}_{0y}(t'-t)\right\}\right] , \tag{5.50}$$

depicted in Fig. 5.4. Transforming the above formula into frequency space we obtain

$$C_{zz}^{(2)}(\omega) = \frac{2\pi\delta(\omega)}{4}\left(\int\frac{d\Omega}{2\pi}\,G_{0xy}^K(\Omega)\right)^2 - \frac{1}{4}\int\frac{d\Omega}{2\pi}\,\text{Tr}\left\{\hat{G}_{0xy}(\Omega)\hat{G}_{0xy}(\Omega-\omega)\right\}$$
$$+ \frac{1}{4}\int\frac{d\Omega}{2\pi}\,\text{Tr}\left\{\hat{G}_{0x}(\Omega)\hat{G}_{0y}(\Omega-\omega)\right\} . \tag{5.51}$$

In order to perform the calculation we require the saddle-point Green's functions of Majorana fields η_x and η_y. The retarded functions can be obtained from the inverse Matsubara Green's function (5.36). For G_{0y}^R we can recall Eqs. (5.42), the full set of retarded functions
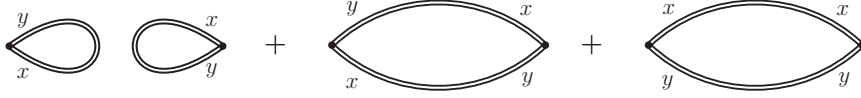
Figure 5.4.: The three contributions to the longitudinal z-spin correlator.

at the saddle point is given by

$$G_{0x}^R(\epsilon) = \frac{\epsilon + i\Gamma_y(\epsilon)}{\epsilon\,(\epsilon + i\Gamma_y(\epsilon)) - B^2} \;,\qquad G_{0y}^R(\epsilon) = \frac{\epsilon}{\epsilon\,(\epsilon + i\Gamma_y(\epsilon)) - B^2}$$

$$G_{0xy}^R(\epsilon) = \frac{-iB}{\epsilon\,(\epsilon + i\Gamma_y(\epsilon)) - B^2} \;,\qquad G_{0yx}^R(\epsilon) = -G_{0xy}^R(\epsilon) \;. \tag{5.52}$$

Corresponding advanced Green functions are obtained by complex conjugation. Keldysh Green functions follow from $G^K(\epsilon) = \tanh\frac{\epsilon}{2T}(G^R(\epsilon) - G^A(\epsilon))$. The rate $\Gamma_y(\epsilon)$ is the negative imaginary part $-\mathrm{Im}\Sigma_{0y}^R$ of the saddle-point self-energy (5.41). Due to the common denominator the above Green's functions are dominated by $|\epsilon| \sim B$. This justifies to use the approximation

$$\Gamma_y(\epsilon) \approx \Gamma_1 = \frac{gB}{2}\coth\frac{B}{2T} \tag{5.53}$$

within the saddle-point Green's functions, simplifying the calculation considerably. This also allows to replace $\tanh\frac{\epsilon}{2T}$ by $\pm\tanh\frac{B}{2T}$ in the Keldysh component.

We can now calculate the longitudinal spin correlator $C_{zz}^{(2)}(\omega)$ using the above introduced prescription, i.e., Eq. (5.51). Due to the denominator $(\epsilon\,(\epsilon + i\Gamma_1) - B^2)$ of Green's functions (5.52) the Ω-integrals in Eq. (5.51) are well-approximated by the poles with real part $|\Omega| \sim B$ and $|\Omega - \omega| \sim B$. As integrands decay fast enough for large Ω the integrals can be evaluated via residue theorem.

Let us first consider the low-field limit $B \ll \Gamma_1$. In this limit the off-diagonal Green's function can be neglected due to $\hat{G}_{0xy} \propto B$. The correlator $C_{zz}^{(2)}(\omega)$ is then obtained from the right-most diagram corresponding to the third term in Eq. (5.51), the result is

$$C_{zz}^{(2)}(\omega) \approx \frac{\Gamma_y}{2\left(\omega^2 + \Gamma_y^2\right)} \;, \tag{5.54}$$

where $\Gamma_y = gT$ is the thermal decay rate. In terms of Majorana Green's functions, cf. Eq. (3.84), the above result translates to $G_z^R(\omega) = (\omega + i\Gamma_y)^{-1}$. As expected, this coincides with the saddle-point result (5.42), since in the low-field limit $\Gamma_z = \tilde{\Gamma}_1 \approx gT$, cf. Eq. (5.18).

The more interesting case is the high-field limit $B \gg \omega, \Gamma_y$ where we expect to reproduce the well-known result (5.4). The squared G_{0xy}^K-term in (5.51), corresponding to the left-most bubble diagram in Fig. 5.4, yields a factor of $A = (\tanh\frac{B}{2T})^2 = 4\langle S_z\rangle^2$. In the high-field limit the second and third terms in (5.51), i.e., the two right-most diagrams in Fig. 5.4, both give rise to a Lorentzian of width $\Gamma_y(B) = \Gamma_1$. Thus we obtain

$$C_{zz}^{(2)}(\omega) = \frac{\pi\delta(\omega)A}{2} + \frac{(1-A)\,\Gamma_1}{2\left(\omega^2 + \Gamma_1^2\right)} \;, \tag{5.55}$$

which indeed coincides with (5.4) known from the Bloch-Redfield approach.

This demonstrates that the prescription proposed in Subs. 5.4.1 produces the correct longitudinal spin correlator and does not suffer from divergent self-energy fluctuations, in contrast to the approaches discussed in Subs. 5.1.2 and 5.3.1. In a similar way, i.e., by avoiding η_z, one can calculate longitudinal spin correlators of arbitrary order.

5.5. Conclusion

We have investigated the Ohmic version of the spin-boson model (5.1) within the Majorana representation, cf. Ch. 3. The first-order approximation for the self-energy captures several features of the spin dynamics but fails to reproduce the longitudinal dynamics in the long-time limit, as noticed first in Ref. [6]. By computing second-order contributions to the self-energy we have shown that the reason for the failure originates in divergencies in higher orders in perturbation theory. Within a path integral approach similar to the one developed in Ch. 4 we have shown that the the higher-order contributions can be interpreted in terms of fluctuations of the self-energy. Furthermore, the path-integral approach allowed us to suggest a prescription for efficient calculation of a class of spin correlators within the spin-boson model. This prescription enables for accurate results essentially by avoiding the use of the longitudinal Majorana fermion. A large class of spin correlation functions, represented in terms of the transverse Majorana fermions, can be easily evaluated using an effective Gaussian action, i.e., a Wick theorem. We have demonstrated that this method indeed yields the expected longitudinal spin correlations.

Using the above method, the effective action we have derived in Sec. 5.3 provides a sound framework for numerical analysis of spin correlation functions. This approach could be extended to sub-Ohmic environments. An extensive numerical analysis was done by Florens *et al.* in Ref. [86], within the Majorana representation but based on the perturbative approach. However, the analysis was carried out at zero temperature and in this limit all rates are infinitesimally small. Hence the discrepancy between the Bloch-Redfield and first-order results was not observed. In this regard our approach could be used to extend the results of Ref. [86] to finite temperatures.

In this chapter we have proposed a recipe that enables for efficient calculation of spin correlation functions within the spin-boson model specified by Eq. (5.1). In the preceding chapter we have developed a viable approach to spin correlators within the Bose-Kondo model. Both treatments utilize the Majorana method introduced in Ch. 3 and rely on similar path integral approaches. This illustrates the power and the flexibility of the method. Moreover, this suggests that similar approaches to other spin models are a promising candidate for future research.

6. Renormalization Group Approach for the Bose-Kondo Model

In this chapter the concept of renormalization group (RG) is applied to the sub-Ohmic Bose-Kondo model using the Majorana representation. RG approaches are efficient and powerful tools for the study of low-energy properties of physical models and system observables at low energy scales, e.g. low temperatures. Here we derive the RG flow equations for the couplings of the Bose-Kondo model. These equations have been obtained earlier by the authors of Refs. [3, 99], using the Abrikosov pseudofermion technique. We are interested in technical issues of the RG as well as of the two-loop calculations. The results confirm the known results and allow for a detailed comparison of the Majorana technique and the pseudofermion technique.

In Sec. 6.1 we give an introduction to the model, basic ideas of RG and the physical background. We review earlier results and the RG flow of the model. As a starting point to the RG, we present the dimensional analysis of the model action. In Sec. 6.2 we employ a Wilson-like RG framework, define vertex functions and calculate the corrections to the vertex up to two-loop order. As the standard Wilson framework turns out as unsuitable to derive the full RG flow equation, we present a modified scheme in Sec. 6.3. Finally, we compute the full RG equation up to two-loop order, check the renormalizability of the theory and provide a detailed comparison between the Majorana technique used in this work and the pseudofermion technique used in Refs. [3, 99].

6.1. Introduction

In this chapter we consider the Bose-Kondo model in the sub-Ohmic case and we allow for anisotropic coupling to the bath, i.e., in contrast to Ch. 4 the SU(2)-symmetry corresponding to spin-rotational invariance may be broken. Here we are not concerned with dynamical properties and high temperatures as in preceding chapters but rather in the effective behavior of the model at low energy scales, which is typically investigated using RG approaches. Central to such approaches is the concept of scale-dependent couplings g_α. It is therefore appropriate to include the g_α directly in the interaction Hamiltonian. The

Hamiltonian within the Majorana representation (3.2) is then given by[1]

$$H = H_B + \sqrt{g_x}\,\hat{X}_x \hat{S}_x + \sqrt{g_y}\,\hat{X}_y \hat{S}_y + \sqrt{g_z}\,\hat{X}_z \hat{S}_z$$
$$= H_B - \frac{i\sqrt{g_\alpha}}{2}\,\epsilon_{\alpha\beta\delta}\,\hat{X}_\alpha\,\hat{\eta}_\beta\,\hat{\eta}_\delta\ , \qquad \alpha,\beta,\delta \in \{x,y,z\}\ , \tag{6.1}$$

which includes the part H_B describing the bosonic bath. The bosonic bath is assumed to have a sub-Ohmic spectral density, defined as $\rho(|x|) = \Lambda^\varepsilon |x|^{(1-\varepsilon)}$ with $0 < \varepsilon < 1$, such that the Ohmic limit corresponds to $\varepsilon \to 0$. In imaginary time space the bosonic correlator is defined by $\langle \mathcal{T}_\tau \hat{X}_\alpha(\tau)\hat{X}_\beta(\tau')\rangle = \pi\delta_{\alpha\beta}\Pi(\tau - \tau')$. The high-energy cutoff Λ of the bath is conveniently implemented in $\Pi(i\omega_m)$ by the use of the spectral representation, cf. (4.4),

$$\Pi(i\omega_m) = \int\limits_{-\Lambda}^{\Lambda} dx\, \frac{\rho(|x|)\,\mathrm{sign}\,x}{x - i\omega_m}\ , \qquad \omega_m = 2\pi mT\ , \quad m \in \mathbb{Z}\ . \tag{6.2}$$

In the RG procedure below, the cutoff Λ will be reduced to a lower value Λ' by integrating out the bosonic modes in the energy shell between Λ' and Λ. Such a procedure is reasonable if one is interested in the physics on energy scales, e.g. temperature, much smaller than Λ. In such cases the RG provides a powerful tool to monitor the influence of the high-energy modes on the low-energy physics.

Some general features of the Bose-Kondo model have already been covered in the introductory Subsection 4.1.1, in particular the generic character of bosonic environments at weak coupling, cf. Ref. [2]. The sub-Ohmic version of the model allows for a range of values $0 < \varepsilon \lesssim 1$ and thus appears in manifold physical contexts. To mention some of them with exemplary references, these include Kondo lattice physics, Refs. [96, 99], spin glasses, Refs. [97, 98], cuprates, Ref. [109], or heavy-fermion compounds, cf. Ref. [3] and references therein. The sub-Ohmic Bose-Kondo model is particularly interesting since it displays a range of fixed points, a quantum phase transition and critical behavior.

The evolution of couplings g_α can be encoded in RG flow equations, that is, differential equations that describe the variation of couplings as the high-energy scale is lowered. The flow equations of the sub-Ohmic Bose-Kondo model have been obtained earlier and are briefly reviewed in Subs. 6.1.1. In Subs. 6.1.2 we introduce the action and provide the dimensional analysis of the model, which serves as an introduction to the subsequent full RG analysis within the Majorana representation.

6.1.1. RG Flow Equations

The Bose-Kondo model specified above displays rich flow equations with a number of small coupling fixed points. RG flow equations of the sub-Ohmic, anisotropic Bose-Kondo model have been worked out by Zaránd and Demler, Ref. [3], and Zhu and Si, Ref. [99]. Both groups of authors were concerned with the more general Bose-Fermi Kondo model, which additionally includes coupling to fermionic environments and thus also features the Kondo effect. Here, however, we are only interested in the purely bosonic case. The flow equation for the coupling g_x up to third order in g_α, as obtained in Refs. [3, 99], reads

$$\frac{dg_x}{dl} = \varepsilon g_x - g_x(g_y + g_z) + g_x^2\,(g_y + g_z)\ . \tag{6.3}$$

---

[1] The use of square roots $\sqrt{g_\alpha}$ here is convenient since only the square g_α will appear below. The definitions of g_α (g), $\hat{X}_\alpha$ and $\rho(|x|)$ in the present chapter differ from those in Ch. 4 and 5 for reasons of convenience. Eqs. (6.1) and (6.2) here compare with Eqs. (4.2) and (4.4).

The equations for g_y and g_z are obtained by cyclic permutation. These differential equations describe the variation of couplings as the high-energy scale is lowered. The lowering process is controlled by a parameter l and has to be stopped at the highest physical energy scale relevant to a specific setup. In the Ohmic limit $\varepsilon \to 0$, the right-hand sides are for sure negative and consequently all three couplings flow to zero. The sub-Ohmic exponent ε adds a positive term to the right-hand sides and thus plays a key role in the analysis of Eq. (6.3).

We briefly recapitulate some features from the elaborate discussion in Ref. [3], which applies to the case of small but finite values of ε. The model shows a rotational SU(2)-invariant fixed point at $g_x = g_y = g_z \equiv g \, (= \varepsilon/2)$, which is relevant in the context of antiferromagnetic transitions in cuprates, cf. Ref. [109]. This fixed point is unstable against spin anisotropy, e.g. for $\delta g = g_z - g_x > 0$. Another three fixed points of the type $g_x = g_y = \varepsilon$, $g_z = 0$ feature the XY-type symmetry, but they are also unstable against anisotropy. The only stable fixed points are of the Ising-type symmetry and are described by $g_z \to \infty$ while $g_x = g_y = 0$ and cyclic permutations thereof. The authors of Ref. [3] suggest that the anisotropic XY-type and Ising fixed points control the physics in magnetic heavy-fermion compounds.

The rich behavior of the Bose-Kondo model is of particular interest since the crossovers between the physics at the fixed points are examples of quantum phase transitions. That is, phase transitions that occur at zero temperature under variation of physical parameters like e.g. magnetic field or pressure. Systems which undergo quantum phase transitions exhibit different zero-temperature ground states depending on these physical parameters. As an example, the Bose-Kondo model shows a quantum phase transition from XY- to Ising-behavior, which is controlled by the SU(2)-symmetric fixed point and occurs below an energy scale $T^* \sim \Lambda g^{1/\varepsilon}$, cf. Ref. [3].

The RG equations for the Bose-Kondo model in Refs. [3, 99] were obtained by diagrammatic expansions in orders of small coupling accompanied by an ε-expansion. Both groups were using the Abrikosov pseudofermion technique. As we stated in Ch. 3, the pseudofermion representation suffers from unphysical states. It has to be guaranteed that the unphysical states don't affect the physical results. The authors of Refs. [3, 99] therefore need to introduce an artificial chemical potential μ_0 into the Hamiltonian, which is taken to infinity, $\mu_0 \to \infty$, at the end of the calculation. However, at intermediate stages of the calculations the chemical potential has to be kept finite and thus complicates the perturbative expansions. As we have elaborated in Subs. 3.1.2, the Majorana representation does not require such procedures, therefore we expect that the calculations are significantly simpler to perform. Our analysis below suggests that this is indeed the case.

6.1.2. Dimensional Analysis

Prior to the RG discussion we present the action of the Bose-Kondo model and the standard dimensional analysis of the terms in the action, as outlined in many textbooks, e.g. Ref. [94]. First, we recall the partition function (4.20) of the Bose-Kondo model from the discussion

in Ch. 4,

$$\mathcal{Z} = \int D[\boldsymbol{X}]D[\boldsymbol{\eta}] \exp\left\{ i\,\mathcal{S}_B + \frac{1}{2}\int\limits_0^{1/T} d\tau \left(-\eta_\alpha(\tau)\,\partial_\tau\eta_\alpha(\tau) + i\sqrt{g_\alpha}\,X_\alpha(\tau)\epsilon_{\alpha\beta\delta}\eta_\beta(\tau)\eta_\delta(\tau)\right)\right\}. \tag{6.4}$$

Here $\mathcal{S}_B = \mathcal{S}_B[\boldsymbol{X}]$ is the free bosonic action. For the RG analysis we prefer to integrate over the bosonic variables, cf. Subs. 4.2.1, which yields

$$\mathcal{Z} = \int D[\boldsymbol{\eta}] \exp\left\{ -\frac{1}{2}\int_0^{1/T} d\tau\,\eta_\alpha(\tau)\,\partial_\tau\,\eta_\alpha(\tau) \right.$$
$$\left. + \sum_{\boldsymbol{\alpha}} \frac{g_\alpha}{2}\int_0^{1/T} d\tau d\tau'\,\Pi(\tau - \tau')\,\eta_{\alpha'}(\tau)\,\eta_{\alpha'}(\tau')\,\eta_{\alpha''}(\tau)\,\eta_{\alpha''}(\tau') \right\}. \tag{6.5}$$

Here we define $\boldsymbol{\alpha} = \{\alpha, \alpha', \alpha''\}$ as a restricted set of spin indices. The sum over $\boldsymbol{\alpha}$ runs over values $\{\alpha, \alpha', \alpha''\} = \{x, y, x\}, \{y, z, x\}, \{z, x, y\}$. In Matsubara frequency space the action can be rewritten as

$$i\mathcal{S} = -\frac{T}{2}\sum_n \eta_\alpha^n(i\nu_n)\eta_\alpha^{-n} + \sum_{\boldsymbol{\alpha}} \frac{g_\alpha}{2}T^3 \sum_{n_i,k_i,m} \Pi_m\,\eta_{\alpha'}^{n_1}\,\eta_{\alpha'}^{k_1}\,\eta_{\alpha''}^{n_2}\,\eta_{\alpha''}^{k_2}\,\delta_{n_1+n_2+m}\delta_{k_1+k_2-m}, \tag{6.6}$$

with the shortcuts $\eta_\alpha^{n_1} = \eta_\alpha(i\nu_{n_1})$, $\Pi_m = \Pi(i\omega_m)$ and the notations ν_{n_i}, ν_{k_i} for fermionic and ω_m for bosonic Matsubara frequencies. The sums $\sum_{n_i}$ and $\sum_{k_i}$ thus run over odd numbers n_i, k_i while $\sum_m$ sums over even numbers. The form (6.6) will also be used for the calculations below.

As mentioned above, cf. Eq. (6.2), the bath correlator Π provides the cutoff Λ, which is the high-energy scale of interest with regard to the RG. Below we are aiming to integrate over bosonic high-energy modes in e.g. an energy shell from Λ/b to Λ with $b = e^l > 1$. For the naive dimensional analysis here one ignores interactions with these modes and simply replaces Λ by $\Lambda' = \Lambda/b$. One then asks for the consequences concerning the action (6.6). In principle, we could choose to alter any object O in the action by some factor $O' = b^d O$ under this modification of the theory. The exponent d is then said to be the naive scaling dimension or engineering dimension of the object O. Here we choose to keep temperature constant $T' = T$, i.e., temperature has scaling dimension zero. In turn, this applies to Matsubara frequencies as well. The engineering dimension of the Majorana fields is fixed by choosing one of the terms in the original action to be invariant. Choosing the first term in (6.6) to be the invariant one fixes the dimension of η_α to zero, since $(i\nu_n)$ is constant.

In the next step we turn to the second, quartic Majorana term in (6.6). Fields and temperature remain unchanged and for now there is no a priori reason to alter the couplings g_α. The idea of the procedure is to eliminate bosonic high-energy modes. To this end, we replace the integration boundaries $\pm\Lambda$ in the bosonic propagator (6.2) by the reduced scale $\pm\Lambda/b$. To then keep the overall form (6.2) of Π we have to add an additional factor of $b^{-\varepsilon}$ which has to be compensated for by b^ε, implying that Π has engineering dimension ε. [2] [3] Thus, the overall scaling dimension of the quartic Majorana term is ε. Within this

---

[2]The scaling dimension ε of Π originates from the bosonic fields X_α which have scaling dimension $\varepsilon/2$. At first glance this may remind the reader of the widely known notion of anomalous scaling dimension in the literature, cf. Ref. [94]. There, the bosonic engineering dimension does not contain $\varepsilon/2$, this factor only arises due to corrections through interaction and is therefore called anomalous. Here, however, the only assumption is that of a local theory and a sub-Ohmic form of the bosonic spectral function, which is sufficient to obtain $\varepsilon/2$ as an engineering dimension.

[3]There is another important difference between widely used RG discussions in the literature and the recent

simple analysis, this means that the term grows for $\varepsilon > 0$ if the cutoff is reduced. Therefore, this term is relevant in the RG sense. The growth according to b^ε can be included in the couplings g_α, which allows to recognize the positive εg_α term in the RG equation (6.3) to be associated with this growth.

The brief analysis here was naive because we ignored that the bosonic modes in the energy range $[\Lambda/b, \Lambda]$ interact with Majorana fields. This interaction in general changes the scaling behavior and is captured by the RG approach in the following sections. For example, Majorana propagators will get corrections due to the interaction, which may be captured by factors Z_α: $\mathcal{G}'_{f\alpha} = Z_\alpha \mathcal{G}_{f\alpha}$. In view of the RG equation (6.3) presented above and the connection $b = e^l$, one recognizes that corrections due to interaction with high-energy modes will add a negative part $-g_y - g_z$ to the scaling dimension of the interaction term. This is one of the terms which will be computed below.

6.2. RG Scheme and Calculations

In this section we employ the common condensed-matter RG scheme on the Bose-Kondo model within the Majorana representation. The scheme is similar to the standard Wilsonian RG and is described in many textbooks, e.g. Refs. [94, 110]. We present calculations of the corrections to the relevant quantities up to two-loop order The calculations allow us to derive the RG equations up to the second order in couplings g_α. The Wilson-like RG framework produces the RG equations to leading order in couplings g_α, but, as it turns out, fails to generate contributions to the RG equations from higher orders. We adopt a modified concept in Sec. 6.3, which yields the known second-order RG equations.

In order to simplify the calculations below, we introduce a slightly different but equivalent form of the action Eq. (6.5) of the Bose-Kondo model. The bosonic correlator Π, Eq. (6.2), includes a large constant part 2Λ, which would lead to highly divergent, though irrelevant contributions. To avoid these contributions we introduce

$$\tilde{\Pi}(i\omega_m) = \int_{-\Lambda}^{\Lambda} dx \frac{i\omega_m |x|^{-\varepsilon} \Lambda^\varepsilon}{x - i\omega_m} = \Pi(i\omega_m) - 2\Lambda \ . \tag{6.7}$$

The two versions Π and $\tilde{\Pi}$ differ only by the frequency-independent term 2Λ, which corresponds to a $\delta(\tau)$-term in imaginary time space in (6.5). Due to the property $\eta_\alpha(\tau)^2 = 0$ of Grassmann variables the additional term is zero, thus the action (6.6) is equivalent to

$$i\mathcal{S} = -\frac{T}{2} \sum_n \eta_\alpha^n \left(\mathcal{G}_{f\alpha}(i\nu_n)\right)^{-1} \eta_\alpha^{-n} + i\mathcal{S}_{int} \tag{6.8a}$$

$$i\mathcal{S}_{int} \equiv \sum_\alpha \frac{g_\alpha}{2} T^3 \sum_{n_i, k_i, m} \tilde{\Pi}_m \, \eta_{\alpha'}^{n_1} \eta_{\alpha'}^{k_1} \eta_{\alpha''}^{n_2} \eta_{\alpha''}^{k_2} \, \delta_{n_1+n_2+m} \delta_{k_1+k_2-m} \ , \tag{6.8b}$$

The above action of the Bose-Kondo model provides the basis for the calculations.

6.2.1. RG Scheme

Prior to the calculations, we now adapt a Wilson-like RG scheme, cf. Ref. [94]. The quartic interaction term $\mathcal{S}_{int}$ comprises the "fast" bosonic modes, i.e., the modes in a high-energy

theory. There are setups which introduce a finite ε into their theory for the only purpose of regularizing diverging integrals and performing ε-expansions. Although our recent theory benefits technically from this similarity, the primary purpose of our finite ε is to allow sub-Ohmic behavior of the bosonic bath, which is a purely physical motivation.

shell $[\Lambda/b, \Lambda]$ with $b > 1$, which we intend to eliminate. To do so, we split the bosonic correlator into parts, a "slow" part $\tilde{\Pi}^<$ and a "fast" part $\tilde{\Pi}^>$,

$$\tilde{\Pi}(i\omega_m) = \tilde{\Pi}^<(i\omega_m) + \tilde{\Pi}^>(i\omega_m) \ , \tag{6.9}$$

$$\tilde{\Pi}^>(i\omega_m) \equiv \left(\int_{-\Lambda}^{-\Lambda/b} + \int_{\Lambda/b}^{\Lambda} \right) dx \frac{i\omega_m |x|^{-\varepsilon} \Lambda^\varepsilon}{x - i\omega_m} \ . \tag{6.10}$$

Thus the fast part $\tilde{\Pi}^>$ is the one that characterizes the fast bosonic modes which are to be eliminated. In terms of the RG procedure described in Ref. [94], the first step of the RG process, "subdivision of field manifold", is implemented here by the above separation of $\tilde{\Pi}$ into a slow and a fast part. [4]

The second step of the RG process is to actually integrate out the fast part $\tilde{\Pi}^>$, cf. Ref. [94]. In view of the action (6.8b), the elimination of the fast part will clearly yield corrections to the bare terms in the action (6.8a) and possibly add new terms. A convenient way to monitor these corrections is to reformulate the action in terms of vertex functions $\Gamma^{(k)}$. For the bare action, i.e., the action at scale Λ, we introduce vertex functions as

$$\Gamma_\alpha^{(2)}(0) \equiv (\mathcal{G}_{f\alpha}(i\nu_n))^{-1} \ , \qquad \Gamma_\alpha^{(4)}(0) \equiv g_\alpha \ , \tag{6.11}$$

while all other bare vertex functions $\Gamma^{(k)}(0) = 0$ for $k \neq 2, 4$. The vertex function $\Gamma_\alpha^{(2)}$ corresponds to the inverse Majorana Green's function and $\Gamma_\alpha^{(4)}$ to the quartic Majorana-Majorana interaction vertex. The corrections which will arise in the process of eliminating $\tilde{\Pi}^>$ depend on the parameter b, which thus enters the vertex functions. To account for that we follow the standard definitions in the literature, introduce the logarithmic parameter $l = \log b$ and write $\Gamma_\alpha^{(k)}(l)$. In the limit $b \to 1$ it is then $l \to 0$ and one recovers the bare action with $\Gamma^{(k)}(l = 0)$.

To parametrize the corrections due to elimination of $\tilde{\Pi}^>$ we assume bare couplings to be small, $g_\alpha \ll 1$, and expand the corrections in orders of couplings. With regard to vertex functions the expansion in couplings corresponds to loop expansions, where each order of loops adds a factor of g_α. Here, the number of loops in a diagram is defined as the number of independent internal Matsubara frequency summations. Loop expansions are justified as long as the couplings remain small within the RG process. In the calculations below we compute the vertex functions up to two-loop order. For the inverse Green's function $\Gamma_\alpha^{(2)}$ this includes the diagrams

---

[4]We note that one can also develop a more standard Wilsonian RG concept that separates slow and fast fields, cf. Ref. [110], by the following procedure. Starting with the action (6.4), which depends on both Majorana and bosonic fields, one could integrate over Majorana fields to obtain an effective bosonic action. Bosonic variables X_α can then be separated into fast and slow fields $X_\alpha^>$ and $X_\alpha^<$, respectively, in consistence with the above separation of the bosonic correlator $\tilde{\Pi}$. One may then proceed along the lines of the Wilsonian RG scheme provided in textbooks, e.g. Ref. [110]. Naturally, we expect this procedure to yield results in agreement with the ones presented in this thesis.

$$-\frac{1}{2}\,\Gamma_\alpha^{(2)}(l) = \qquad + \qquad + \qquad$$

$$+ \qquad + \qquad + \quad \dots \qquad (6.12)$$

Here, internal straight lines correspond to the Majorana propagator $\mathcal{G}_\alpha$ and wiggled lines represent the fast part of the bosonic correlator $\tilde{\Pi}^>$. For the purpose of demonstration we also show the diagrams contributing to the vertex function $\Gamma_x^{(4)}$ up to one-loop order:

$$\frac{\tilde{\Pi}^<}{2}\,\Gamma_x^{(4)}(l) = \qquad + \qquad + \qquad$$

$$+ \qquad + \ \dots\ . \qquad (6.13)$$

We notice that in the scheme developed here the $\Gamma_\alpha^{(4)}$-vertices are accompanied by the slow part of the bosonic propagator $\tilde{\Pi}^<$. Having computed the vertex functions in the loop expansion up to some order, the $\Gamma_\alpha^{(k)}(l > 0)$ form a "corrected" action.

The third step of the RG process is to rescale the "corrected" action in order to allow for comparison with the initial action, cf. Ref. [94]. Due to corrections from the loop expansion, the inverse Green's functions $\Gamma_\alpha^{(2)}(l)$ differ from the initial ones. However, we want to keep the free Majorana term, the first term in (6.8a), invariant under the RG process. Thus we are forced to rescale the Majorana fields η_α in order to compensate for the "wrong" inverse Green's functions $\Gamma_\alpha^{(2)}$. To do so, one typically introduces renormalization factors $Z_\alpha(l)$ and rescales the fields $\eta_\alpha \to \sqrt{Z_\alpha}\,\eta_\alpha$ such that the renormalized inverse Green's functions $\Gamma_{\alpha R}^{(2)}$ equal the initial ones

$$\Gamma_{\alpha R}^{(2)} = Z_\alpha(l)\,\Gamma_\alpha^{(2)}(l) = (\mathcal{G}_\alpha(i\nu_n))^{-1}\ , \qquad (6.14)$$

which do not depend on l. Since $(\mathcal{G}_\alpha(i\nu_n))^{-1} = i\nu_n$ the factors Z_α can be obtained from $\Gamma_\alpha^{(2)}$ by

$$Z_\alpha(l) = i\nu_n \left(\Gamma_\alpha^{(2)}(l)\right)^{-1}\ . \qquad (6.15)$$

The rescaling of Majorana fields also affects the quartic Majorana-Majorana interaction term. To compensate for the rescaling one introduces the renormalized vertex functions $\Gamma_{\alpha R}^{(4)}$, which include the factors of Z_α arising from the rescaling of Majorana fields. The appropriate factors of Z_α are easily determined by the number of outer Majorana legs of the corresponding diagrams, cf. the diagrams in (6.13). Above that, the $\Gamma_{\alpha R}^{(4)}$ absorb the rescaling of the slow part $\tilde{\Pi}^<$ of the bosonic correlator. According to the dimensional
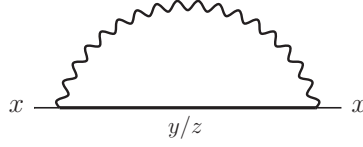
Figure 6.1.: One-loop contribution to the vertex function $\Gamma_x^{(2)}$ which generates the renormalization factor Z_x for $\mathcal{G}_x$.

analysis in Subs. 6.1.2 this adds another rescaling factor of $b^\varepsilon = e^{\varepsilon l}$. Altogether, the renormalized vertex functions $\Gamma_{\alpha R}^{(4)}$ are given by

$$\Gamma_{xR}^{(4)}(l) = e^{\varepsilon l} Z_y(l) Z_z(l) \, \Gamma_x^{(4)}(l) \ , \tag{6.16a}$$

$$\Gamma_{yR}^{(4)}(l) = e^{\varepsilon l} Z_z(l) Z_x(l) \, \Gamma_y^{(4)}(l) \ , \tag{6.16b}$$

$$\Gamma_{zR}^{(4)}(l) = e^{\varepsilon l} Z_x(l) Z_y(l) \, \Gamma_z^{(4)}(l) \ . \tag{6.16c}$$

The renormalized vertices act as couplings g'_α of the renormalized action and explicitly depend on initial couplings g_α. Thus the equation $g'_\alpha = \Gamma_{\alpha R}^{(4)}(g_\alpha)$ is a mapping between the couplings of the initial and the renormalized action. From this mapping one can derive differential equations for the couplings known as the Gell-Mann–Low or the RG equations, cf. Ref. [94]. In the limit of arbitrarily small values $l \to \delta l$ the difference between renormalized and bare coupling constant becomes arbitrarily small, motivating the definition of a differential $\frac{dg_\alpha}{dl}$ in terms of

$$\frac{dg_\alpha}{dl} = \lim_{\delta l \to 0} \frac{\Gamma_{\alpha R}^{(4)}(g_\beta, \delta l) - g_\alpha}{\delta l} \ . \tag{6.17}$$

As demonstrated in Subs. 6.1.1, these differential equations allow to read off parameter sets of $\{\varepsilon, g_x, g_y, g_z\}$ for which the couplings are left constant under the RG process. Such constant solutions are fixed points of the theory.

The computation of vertex functions up to two-loop order presented below enables us to derive the RG equations up to second order in g_α and to compare with the results of Refs. [3, 99]. First, we focus on the one-loop contributions to $\Gamma_\alpha^{(2)}$ and $\Gamma_\alpha^{(4)}$. Subsequently, we consider the two-loop contributions to the inverse Green's function $\Gamma_\alpha^{(2)}$ and to the vertex $\Gamma_\alpha^{(4)}$ separately. Details of the calculations can be found in Appendix A.
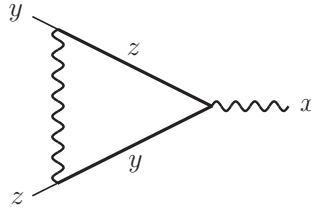
6.2.2. One-Loop Corrections

To begin with, we consider the one-loop contribution to $\Gamma_x^{(2)}$, the y- and z-components are obtained by cyclic permutation. As already displayed in (6.12), there is only one non-vanishing diagram in one-loop order, which is Fock-like diagram depicted in Fig. 6.1. In the calculation here and throughout the rest of the calculations we assume that the external frequencies are much smaller than the new cutoff scale: $\nu_n \ll \Lambda/b$. Expanding in the external frequency ν_n we find the contribution ($l = \log b$)

$$\Gamma_x^{(2)}(l) = i\nu_n \left(1 + (g_y + g_z) \, I_1(b) + \mathcal{O}(g_\alpha^2)\right) \ . \tag{6.18}$$

in terms of the integral

$$I_1(b) = \int_{\Lambda/b}^{\Lambda} dx \frac{\Lambda^\varepsilon}{x^{1+\varepsilon}} = \frac{b^\varepsilon - 1}{\varepsilon} = \frac{e^{\varepsilon l} - 1}{\varepsilon} \ . \tag{6.19}$$

Figure 6.2.: Relevant element for the one-loop contributions to the vertex.

Turning to the non-vanishing one-loop contributions to the vertex function $\Gamma_x^{(4)}$, we note that both diagrams in (6.13) contribute identically. That is, we can evaluate the element depicted in Fig. 6.2 and multiply by two. Again, outer Matsubara frequencies are neglected. Including the first diagram in (6.13) which corresponds to the bare coupling g_x, we find

$$\Gamma_x^{(4)}(l) = g_x \left(1 + 2 \, g_x I_1(b) + \mathcal{O}(g_\alpha^2) \right) \tag{6.20}$$

in one-loop order.

We note that there appear two other one-loop diagrams in the expansion of $\Gamma_x^{(4)}$ that however vanish. The first one is understood as the correction of the bosonic propagator, while the second one is the ladder-like diagram including two fast components $\tilde{\Pi}^>$. For details we refer to App. A where we show explicitly that these diagrams vanish.
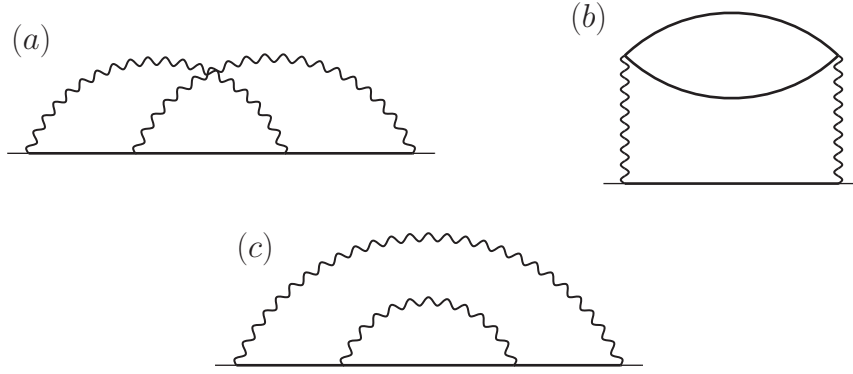
6.2.3. Two-Loop Corrections

Now we turn to corrections to the vertex functions $\Gamma_\alpha^{(2)}$ and $\Gamma_\alpha^{(4)}$ in two-loop order. Details of the calculations are given in App. A. Each loop includes one internal summation over Matsubara frequencies which is essentially evaluated by the use of residue theorem. The integrations arising from the spectral representation of $\tilde{\Pi}^>$, Eq. (6.10), have to be treated with care and will be discussed below. For now we prefer to introduce the integral $I_2(b)$ defined by

$$I_2(b) = \iint_{\Lambda/b}^{\Lambda} dxdy \frac{\Lambda^{2\varepsilon}}{x^\varepsilon y^\varepsilon (x+y)^2} = \iint_{1/b}^{1} \frac{dxdy}{x^\varepsilon y^\varepsilon (x+y)^2} \ . \tag{6.21}$$

The two-loop contributions can then be expressed in terms of integrals $I_1(b)$, Eq. (6.19), and $I_2(b)$.

We first concentrate on the two-loop contributions to the inverse Green's function $\Gamma_\alpha^{(2)}$. The three possible diagrams are depicted in Fig. 6.3. As we demonstrate explicitly in App. A.1.2 diagram (b) vanishes. The reason is that for finite bosonic frequencies ω_m the Matsubara sum in the Majorana loop in diagram (b) cancels, cf. Eq. (A.14), whereas at $\omega_m = 0$ the bosonic propagator (6.10) vanishes: $\tilde{\Pi}^>(i\omega_m = 0) = 0$. In the contributions

Figure 6.3.: Two-loop corrections to the inverse Majorana Green's function. Only diagrams (a) and (c) yield relevant contributions.

corresponding to diagrams (a) and (c) the sums of residues arising from the contour analysis of Matsubara sums, cf. Eqs. (A.13), were computed within the Mathematica program. We neglect outer frequencies and symmetrize the resulting expressions with respect to the integration variables. In terms of integrals $I_1(b)$ and $I_2(b)$ we find:

$$\Gamma_x^{(2,a)}(l) = i\nu_n \left(g_y^2 + g_z^2 \right) \left(I_2(b) + (I_1(b))^2 \right) , \tag{6.22a}$$

$$\Gamma_x^{(2,c)}(l) = -i\nu_n \left(g_y^2 + g_z^2 + g_x(g_y + g_z) \right) \left(I_2(b) + \frac{1}{2} (I_1(b))^2 \right) . \tag{6.22c}$$

Adding the two-loop corrections above to the full vertex function $\Gamma_x^{(2)}$ some terms cancel and we find

$$\Gamma_x^{(2)}(l) = i\nu_n \Big[1 + (g_y + g_z) I_1(b) - g_x(g_y + g_z) I_2(b)$$
$$+ \frac{1}{2} \left(g_y^2 + g_z^2 - g_x(g_y + g_z) \right) (I_1(b))^2 + \mathcal{O}(g_\alpha^3) \Big] . \tag{6.23}$$

Vertex functions $\Gamma_x^{(2)}$ and $\Gamma_x^{(2)}$ are easily obtained from (6.18) by cyclic permutation.

We proceed with the two-loop corrections to the vertex functions $\Gamma_\alpha^{(4)}$. Within the present approach based on the action (6.8b) two-loop contributions to the vertex function $\Gamma_x^{(4)}$ can be classified into vertex-like and ladder-like contributions. However, based on the fact that the ladder-like contributions vanish in one-loop order, cf. App. A.2.1, we conjecture that this type is not relevant here. For the discussion of vertex-like contributions, cf. Eq. (6.13), it is sufficient to consider one side of the four-Majorana vertex. We provide a more detailed discussion in App. (A.2).

There are eight different vertex-like contributions to the vertex function $\Gamma_x^{(4)}$, depicted in Fig. 6.4. Diagrams (g) and (h) include closed Majorana loops and thus vanish for the same reason as diagram (b) in Fig. 6.3 above, cf. Eq. (A.14). Again, we evaluated Matsubara sums of contributions (a) to (f) by complex analysis within Mathematica. In the limit of
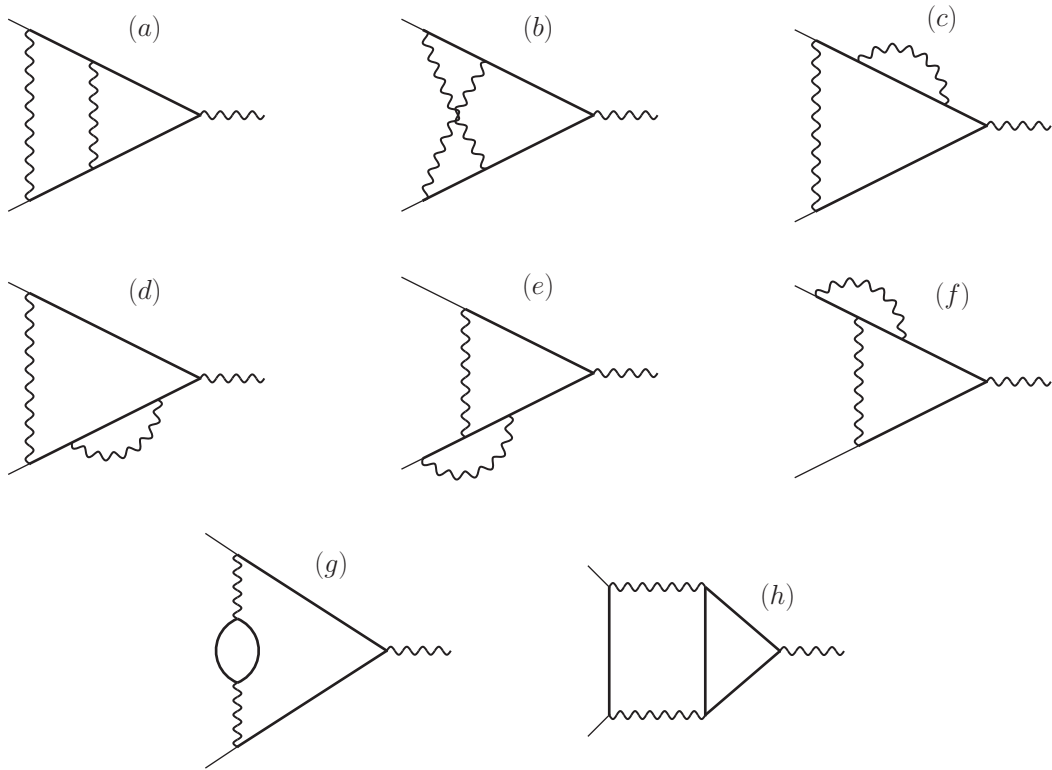
Figure 6.4.: Two-loop corrections to the vertex function $\Gamma_x^{(4)}$.

small outer frequencies, i.e., negligible in comparison to the reduced cutoff Λ/b, we obtain

$$(a): \qquad g_x^3 \left(I_1(b)\right)^2 - 2g_x^3 I_2(b) \;, \qquad\qquad (6.24a)$$

$$(b): \qquad 2\, g_x \left(g_x^2 - g_y g_z\right) I_2(b) \;, \qquad\qquad (6.24b)$$

$$(c)\text{ and }(d): \qquad -g_x^2(g_x + g_y)\left(I_1(b)\right)^2 \;, \qquad\qquad (6.24c)$$

$$(e)\text{ and }(f): \qquad g_x^3 \left(I_1(b)\right)^2 \;, \qquad\qquad (6.24d)$$

Here we used integrals $I_1(b) = (b^\varepsilon - 1)/\varepsilon$ and $I_2(b)$ defined in (6.21). Diagrams (c) and (d) as well as (e) and (f) yield identical results. Adding the two-loop contributions in Eqs. (6.24) to the vertex function $\Gamma_x^{(4)}$, Eq. (6.20), we obtain the two-loop result:

$$\Gamma_x^{(4)}(l) = g_x \left[1 + 2\, g_x I_1(b) - 2\, g_y g_z I_2(b) + \left(g_x^2 - g_x(g_y + g_z)\right)\left(I_1(b)\right)^2 + \mathcal{O}(g_\alpha^3)\right]. \quad (6.25)$$

Again, the y- and z-vertex functions can be obtained by cyclic permutation. The two-loop results for the two-Majorana vertex function, Eq. (6.23), and the four-Majorana vertex function above provide the starting point for the derivation of the RG equations for couplings g_α up to third order in g_α.

In order to achieve an improved understanding of the contributions Eqs. (6.22) and (6.24) of the two-loop diagrams, one can try to recombine one-loop diagrams into two-loop diagrams.

For example, consider the one-loop vertex diagram in Fig. 6.2, which yielded a factor of $g_x I_1$. This diagram contains three internal vertices. Replacing each of these three internal vertices by the one-loop vertex, one obtains the two-loop diagrams (a), (e) and (f) in Fig. 6.4, each including a factor of $(g_x I_1)^2$. In this way one can construct all non-vanishing two-loop diagrams except for diagram (b), which is special in this sense.

Furthermore, the above argument suggests that only two-loop contributions that include a term $\propto I_2$ yield "new" information as compared to the one-loop contributions. Indeed, we observe that only the diagrams (a) and (b) in Fig. 6.4 can contribute to the RG equation, since only linear contributions in $l = \log b$ will enter the RG equation. Expanding the integral I_1 in terms of l one notices that I_1 is at least linear, implying that its square is at least quadratic in l. Therefore, in view of Eqs. (6.24), the contributions (c) to (f) are quadratic in $\log b$ and thus do not enter the RG equation.

6.2.4. Discussion

The one-loop results for $\Gamma_\alpha^{(2)}$ and $\Gamma_\alpha^{(4)}$, Eqs. (6.18) and (6.20), allow us to derive the RG equations to the leading order in couplings g_α. Replacing $l \to \delta l$ in the integral (6.19) and expanding in small δl one finds $I_1(l) \approx \delta l$. To obtain the renormalized vertex $\Gamma_{xR}^{(4)}$ we first compute the renormalization factors Z_α, Eq. (6.15), from $\Gamma_\alpha^{(2)}$. Omitting terms of order $\mathcal{O}((g_\alpha \delta l)^2)$ we find

$$Z_x = 1 - (g_y + g_z)\,\delta l\ , \qquad Z_y = 1 - (g_x + g_z)\,\delta l\ , \qquad Z_y = 1 - (g_x + g_y)\,\delta l\ . \qquad (6.26)$$

The RG equation for g_x is then derived according to Eq. (6.17) from the rescaled vertex function $\Gamma_{xR}^{(4)}(g_\alpha, \delta l)$. We find

$$\frac{dg_x}{dl} = \varepsilon g_x - g_x(g_y + g_z)\ . \qquad (6.27)$$

Thus we recover the RG equation (6.3) to the lowest order in g_α as discussed in Subs. 6.1.1 of the introduction.

Starting from small but finite values of g_α and $g_x < \varepsilon$, Eq. (6.27) tells us that g_x can increase in the RG process. For example, for $g_x = g_y = g_z$ the coupling constants increase up to the value of ε. However, we only included the lowest order in g_α within a small coupling expansion. Hence, for moderate finite values of $0 < \varepsilon < 1$ the approximation breaks down before the coupling g_x actually reaches the value of ε, and Eq. (6.27) does no longer apply. Thus the range of applicability of Eq. (6.27) is limited to the regime $g_x, g_y, g_z, \varepsilon \ll 1$.

Unfortunately, the scheme discussed above fails to generate contributions to the RG equations from the two-loop corrections. Within this scheme, the RG equations have been obtained by replacing $l = \log b$ by a small quantity $\delta l \ll 1$ and expanding in this quantity up to linear order. We have shown that two-loop corrections to the vertex functions can be expressed in terms of integrals $(I_1)^2$ and I_2, cf. Eqs. (6.19) and (6.21), respectively. We recall

$$I_1(l) = \frac{e^{\varepsilon l} - 1}{\varepsilon}\ , \qquad I_2(l) = \iint_{e^{-l}}^{1} \frac{dx\,dy}{x^\varepsilon y^\varepsilon (x + y)^2}\ . \qquad (6.28)$$

Clearly, terms $\propto (I_1(\delta l))^2$ are at least quadratic in δl and thus do not add to the RG equation. However, in the limit $\delta l \ll 1$ one observes that the integral $I_2(\delta l)$ also becomes

quadratic in δl: $I_2(\delta l) \approx (\delta l)^2$. As a consequence, the two-loop order corrections do not change the RG equation within this scheme.

In the scheme we have developed in this section the RG step amounts to the integration over infinitesimal small shells $\sim \delta l$ in frequency space. It is known for a long time that similar RG schemes in momentum space, though quite successful in general, create problems in two-loop calculations, cf. Refs. [110, 111]. In particular, as reported in Ref. [112] for the one-dimensional case, two-loop contributions vanish if all internal momenta reside in the infinitesimal outer shell. This is strongly reminiscent of the problem we have observed above.

There are strategies that either circumvent or completely avoid the above-mentioned problems, cf. Refs. [110, 113]. So-called functional renormalization group methods introduce smooth cutoff functions to deal with the problem. Quantum-field-theoretical RG methods widely used in high-energy physics are based on a fundamentally different logic and thus fully avoid such problems. This method was employed in Refs. [3, 99] to derive the RG equations for the Bose-Kondo model using Abrikosov pseudofermions. In Ref. [112] the problem is circumvented by careful analysis of internal momenta over several RG steps. In this way linear contributions in $l = \log b$ are generated which then appear in the RG equation. However, it is unclear whether such a strategy can be successfully implemented in the present case. Rather, we resort to a different and, as we think, simpler strategy below.

6.3. Analysis of the Two-Loop RG calculations

In this section we present a modified version of the RG scheme, which enables us to determine the RG flow equations of couplings g_α to next-to-leading order. It turns out that our results agree with earlier results obtained in the Abrikosov pseudofermion technique, Refs. [3, 99]. Subsequently, we use the results of the two-loop calculations in order to show that the theory is indeed renormalizable. Finally, we use our results to provide a detailed comparison to previous works, i.e., a comparison between the Majorana and the pseudofermion techniques.

6.3.1. Modified RG Scheme

To generate linear log terms from the integral I_2 we adapt the following strategy. We allow for intermediate values of $l = \log b$ such that the product $g_\alpha l$ can still be considered as small enough to justify the differential limit. We argue that this is a qualified approach in the weak coupling limit, i.e., as long as $g_\alpha l \ll 1$. Let us illustrate the approach by considering the integral I_2 in the limit $\varepsilon \to 0$. One then finds

$$I_2(l)|_{\varepsilon=0} = l + 2\log(1 + e^{-l}) - \log 4 . \tag{6.29}$$

Now, in the intermediate range $l \sim 10$ it is $e^{-l} \ll 1$ and thus the log term above is exponentially suppressed and can be neglected. As a result we are left with the linear term. This line of reasoning holds at finite ε as long as $\varepsilon \ll 1$. Expanding in small ε, we neglect factors of e^{-l} and higher orders in ε and approximate the integral I_2 by

$$I_2(l) = l + \varepsilon l(-\log 4 + l) - \log 4 + \mathcal{O}(\varepsilon^2)$$
$$\approx l . \tag{6.30}$$

The linear l-term in I_2 generates the wanted contributions to the RG equation from the two-loop results of vertex functions $\Gamma_\alpha^{(2)}$ and $\Gamma_\alpha^{(4)}$.

To obtain the RG equations within this modified scheme we introduce a modified version of the general RG equation (6.17). For intermediate values of the parameter l, as required by Eq. (6.30), the differential limit $\delta l \to 0$ is no longer justified. However, in the weak-coupling regime $g_\alpha \ll 1$ the relative change of the renormalized vertex $\Gamma_{\alpha R}^{(4)}$ is at most of order $(g_\alpha l) \ll 1$ even for intermediate values of l. We may therefore replace the differential parameter δl by $(g_\alpha l)$. To this end we divide the original RG equation (6.17) by g_α and replace $\delta l \to (g_\alpha l)$ on the right-hand side:[5]

$$\frac{1}{g_\alpha} \frac{dg_\alpha}{dl} = \lim_{(g_\alpha l) \to 0} \frac{\Gamma_{\alpha R}^{(4)}(g_\beta, l) - g_\alpha}{(g_\alpha l)} \ . \tag{6.31}$$

This modified RG equation (6.31) applies to moderate values of l, thus allowing to neglect orders of e^{-l} and to use the approximation (6.30). With regard to the two-loop results for the vertex functions, Eqs. (6.23) and (6.25), we checked that any order of l is accompanied by sufficiently high orders of g_α (or ε) in order to justify the differential limit $(g_\alpha l) \to 0$. However, we have to keep in mind that the RG equations obtained through (6.31) are restricted to the weak-coupling regime, i.e., $g_x, g_y, g_z, \varepsilon \ll 1$.

6.3.2. RG Flow Equations

To derive the RG equation we first need the renormalized vertices $\Gamma_{\alpha R}^{(4)}$. The renormalization factors Z_α are easily obtained from vertex functions $\Gamma_\alpha^{(2)}$ by Eq. (6.15). Using the two-loop result (6.23) the factor Z_x is found to be

$$\frac{1}{Z_x} = 1 + (g_y + g_z)\, I_1(l) - g_x(g_y + g_z)I_2(l) + \frac{1}{2}\left(g_y^2 + g_z^2 - g_x(g_y + g_z)\right)(I_1(l))^2$$
$$+ \mathcal{O}(g_\alpha^3) \ . \tag{6.32}$$

The renormalization factors Z_y and Z_z are obtained by cyclic permutation. We recall the renormalized vertex function $\Gamma_{\alpha R}^{(4)}$, Eq. (6.16a),

$$\Gamma_{xR}^{(4)}(l) = e^{\varepsilon l} Z_y(l) Z_z(l)\, \Gamma_x^{(4)}(l) \ . \tag{6.33}$$

Furthermore, we recall the two-loop result (6.25)

$$\Gamma_x^{(4)}(l) = g_x\left[1 + 2\, g_x I_1(l) - 2\, g_y g_z I_2(l) + \left(g_x^2 - g_x(g_y + g_z)\right)(I_1(l))^2 + \mathcal{O}(g_\alpha^3)\right] \ . \tag{6.34}$$

Now we apply the approximations $I_1(l) \approx l$ and $I_2(l) \approx l$ for the integrals, cf. Eqs. (6.28) and (6.30), and use the modified version Eq. (6.31) to obtain the RG equation. We divide by $(g_\alpha l)$, remove higher orders of by $(g_\alpha l) \to 0$ and find

$$\frac{1}{g_x} \frac{dg_x}{dl} = \varepsilon - (g_y + g_z) + g_x(g_y + g_z) \ . \tag{6.35}$$

This result (and cyclic permutations thereof) coincides with Eq. (6.3), which was obtained in Refs. [3, 99] within the Abrikosov pseudofermion representation. Thus our calculations within the Majorana representation confirm the known results.

---

[5]Eq. (6.31) can also be interpreted as a differential equation for $\log g_\alpha$.

6.3.3. Renormalizability

In the above RG equations the change of couplings is encapsulated in a differential form. In writing these equations one assumes that the initial value of Λ, the width of a single RG interval, as well as the total number of intervals are completely irrelevant. If all these assumptions are valid the theory is said to be renormalizable. The two-loop calculations allow us, on the level of the one-loop RG equation, to check if these strong assumptions are indeed justified in the present case.

First, we construct the change of the coupling g_x for a finite interval Δl according to the one-loop RG equation. For convenience we introduce β_α-functions by $\beta_\alpha \equiv \frac{dg_\alpha}{dl}$. The one-loop β-functions, e.g. $\beta_x^{(1)}$, are easily obtained from the one-loop RG equation (6.27):

$$\beta_x^{(1)} = -g_x \left(g_y + g_z - \varepsilon \right) \tag{6.36}$$

Note that these $\beta_\alpha^{(1)}$-functions, quadratic in g_α, do not explicitly depend on l. Still, as functions of g_α they can be understood as carrying an implicit l-dependence. According to the one-loop RG equation (6.27) the change in g_x in a finite interval Δl is

$$\Delta g_x = \frac{dg_x}{dl} \Delta l + \frac{1}{2} \frac{d^2 g_x}{dl^2} (\Delta l)^2 + \mathcal{O}((\Delta l)^3) \tag{6.37}$$

Using the definition of β-functions and the relation

$$\frac{d^2 g_x}{dl^2} = \sum_\alpha \beta_\alpha \frac{\partial \beta_x}{\partial g_\alpha} \tag{6.38}$$

we may rewrite Eq. (6.37) to

$$\Delta g_x = \beta_x^{(1)} \Delta l + \frac{1}{2} \sum_\alpha \beta_\alpha^{(1)} \frac{\partial \beta_x^{(1)}}{\partial g_\alpha} (\Delta l)^2 + \mathcal{O}((\Delta l)^3) \ . \tag{6.39}$$

As we have noted earlier, the renormalized vertex function $\Gamma_{xR}^{(4)}(l)$ is nothing but the new, modified coupling "$g_x(l)$", after an interval $l = \log b$ starting from Λ has been integrated out. Thus, the effective coupling changes by $\Gamma_{xR}^{(4)}(l) - g_x$ as compared to its initial value g_x. We may expand this change in orders of l:

$$\Gamma_{xR}^{(4)}(l) - g_x = \beta_x^{(2)} l + \frac{1}{2} \frac{d^2 \Gamma_{xR}^{(4)}}{dl^2} l^2 \ . \tag{6.40}$$

Here we recognized that the prefactor of the linear order in l corresponds to the two-loop β-function.

If our above assumptions are indeed correct, the Δl-dependence of Eq. (6.39) has to resemble the l-dependence of Eq. (6.40). That is, the prefactors of each order in l in the two-loop vertex expansion are expected to coincide with the prefactors of corresponding orders in Δl in Eq. (6.37). The prefactors of the linear terms, one- and two-loop β-functions, clearly coincide within the accuracy of the one-loop RG calculations. In order to compare the quadratic prefactors we first compute the quadratic prefactor in Eq. (6.39) which originates from the one-loop RG equation. Using Eq. (6.36) (and cyclic permutations thereof) we find

$$\frac{1}{2} \sum_\alpha \beta_\alpha^{(1)} \frac{\partial \beta_x^{(1)}}{\partial g_\alpha} = \frac{g_x}{2} \left((g_y + g_z)^2 + g_x(g_y + g_z) + 2g_y g_z - 3\varepsilon(g_y + g_z) + \varepsilon^2 \right)$$
$$+ \mathcal{O}(g_\alpha^4) \ . \tag{6.41}$$

With the help of the two-loop results Eqs. (6.32), (6.33) and (6.34), we compute the renormalized vertex $\Gamma^{(4)}_{xR}$. From this we obtain the quadratic prefactor in Eq. (6.40):

$$\frac{1}{2}\frac{d^2\Gamma^{(4)}_{xR}}{dl^2} = \frac{g_x}{2}\left((g_y + g_z)^2 + g_x(g_y + g_z) + 2g_yg_z - 3\varepsilon(g_y + g_z) + \varepsilon^2\right) + \mathcal{O}(g^4_\alpha) \qquad (6.42)$$

We observe that Eqs. (6.41) and (6.42) indeed coincide. This confirms that the above assumptions are indeed justified, i.e., the RG flow does not depend on the initial value Λ and on the choice of intervals. The theory is renormalizable.

6.3.4. Comparison to Pseudofermion Technique

We have mentioned earlier that the RG for the Bose-Kondo model (and the more general Bose-Fermi Kondo model) has been performed by Zhu and Si as well as Gergely and Zaránd in Refs. [3, 99], using the Abrikosov pseudofermion technique. Here we are aiming at a more detailed comparison of our results to the ones obtained in Ref. [3].

There are several differences between the Abrikosov pseudofermion technique and the Majorana representation used here. Within the pseudofermion case there is just one inverse Green's function, whereas here one has three of these, due to the three flavors of Majorana fermions. However, the spin structure of the vertex is more transparent in the Majorana technique, which allows for three types of boson-Majorana vertices of the form $\sqrt{g_x}X_x\eta_y\eta_z$. Within the pseudofermion technique there are, roughly speaking, four types of vertices, two of the longitudinal type which carry $\sqrt{g_z}$ and two of the transverse type which mix couplings $\sqrt{g_x}$ and $\sqrt{g_y}$. In contrast to the Majorana representation, the Abrikosov pseudofermion technique allows for straightforward generalization to larger spins.

The pseudofermion technique requires the use of an artificial chemical potential in order to handle unphysical fermionic states. The chemical potential has to be kept finite throughout calculations and thus complicates calculations as compared to the Majorana technique. As reported in Ref. [3], the chemical potential gets renormalized within the RG process by diverging frequency-independent corrections to the inverse pseudofermion Green's function. Within the Majorana technique there is no chemical potential. In consistence with that, the calculations of corrections to the inverse Majorana Green's function in Sec. 6.2 did not generate any constant chemical-potential-like terms.

We may compare the diagrams that contribute to the two-loop calculations in Sec. 6.2, Figs. 6.1-6.4, to the relevant pseudofermion diagrams in Refs. [3, 99]. Within the pseudofermion technique, additional pseudofermionic loops vanish in the limit of infinite chemical potential and thus do not appear in the diagrams of Refs. [3, 99]. In the calculations within the Majorana representation in Sec. 6.2 we have included Majorana-fermion loops and have found that contributions from such loops also vanish (cf. App. A). Apart from the closed-Majorana-loop diagrams, we have also included ladder-like diagrams in our discussion. As we have found in App. A.2.1 contributions from these ladder-like diagrams also vanish. The authors of Refs. [3, 99] used a quantum-field-theoretical RG framework, they thus had to include several additional diagrams originating from counterterms. Apart from these rather minor differences, both calculations basically include the same set of relevant diagrams.

For a comparison of the two-loop vertex function results we recall Eqs. (6.23) and (6.25). To this end it is sufficient to replace the integrals $I_1(l)$ and $I_2(l)$ by l and to omit terms

quadratic in l:

$$\Gamma_x^{(2)}(l) = i\nu_n \left[1 + (1 - g_x)(g_y + g_z)\, l + \mathcal{O}(l^2) \right]\ , \tag{6.43a}$$

$$\Gamma_x^{(4)}(l) = g_x \left[1 + 2\, (\, g_x - g_y g_z)\, l + \mathcal{O}(l^2) \right]\ . \tag{6.43b}$$

These two formulas can be compared to the inverse pseudofermion Green's function and the pseudofermion-boson vertex function, Eqs. (A1) and (A2) in Ref. [3], respectively. In contrast to Eq. (6.43b), the pseudofermion-boson vertex includes an additional log-independent term. Strikingly, the overall form of the linear log-terms in both vertex functions in Eq. (6.43) is significantly shorter and simpler than the pseudofermion vertex functions. We suggest that the reason for this rather big difference between the techniques is the simple structure of boson-Majorana vertices in comparison with boson-pseudofermion vertices.

Based on the extensive discussion above, we conclude that the Majorana technique is the more convenient technique to treat the Bose-Kondo model as compared to the Abrikosov pseudofermion technique. We suggest that this also applies to the more general case of the Bose-Fermi Kondo model considered in Refs. [3, 99], as well as other models. The only advantage of the pseudofermin technique is that it can be straightforwardly generalized to larger spins.

In addition to the derivation of RG equations for the Bose-Fermi Kondo model, the authors of Refs. [3, 99] discussed the RG flow diagrams including fixed points and associated energy scales. We have reviewed part of this discussion in Subs. 6.1.1, for the full discussions we refer to the original works. Moreover, Refs. [3, 99] included e.g. discussions of the susceptibility and its critical exponent for the SU(2)-invariant, the xy-symmetric as well as the Ising-symmetric phases of the model. In addition, a discussion of the relevance regarding experimental results was provided. These topics are beyond the present thesis, for more information we again refer to Refs. [3, 99].

6.4. Conclusion

In this chapter we have calculated the RG flow equations for the sub-Ohmic Bose-Kondo model. The RG equations have been obtained earlier by Zhu and Si, Ref. [99], as well as Zaránd and Demler, Ref. [3], using the Abrikosov pseudofermion technique. Thus the RG analysis of the Bose-Kondo model has provided a good opportunity for a detailed comparison of the pseudofermion technique and the Majorana technique.

In Sec. 6.2, we have employed a Wilson-like RG framework, in which the high-energy cutoff Λ is reduced to a new value Λ/b in the RG process. For the RG, we have used the Bose-Kondo action in the pure Majorana form, including a boson-mediated four-Majorana interaction term. This form of the action has been chosen to avoid divergencies in the RG calculations. Expanding in small couplings g_α and small sub-Ohmic ε, we have computed the corrections to the vertex functions up to two-loop order.

As it has turned out, the common Wilson-like RG framework is insufficient to obtain the full RG flow equation beyond the leading order in the couplings, i.e., beyond the one-loop contributions. We have presented a modified RG scheme in Sec. 6.3. The modified scheme has allowed us to derive the RG flow equation up to two-loop order in couplings

g_α. Our results coincide with the results obtained in Refs. [3, 99] and thus confirm the form of the RG equations for the Bose-Kondo model. By comparing quadratic terms in the logarithmic parameter, the two-loop calculations have allowed to demonstrate that the theory is renormalizable.

Based on the simpler structure of the Majorana representation and the simpler form of results we have concluded that the Majorana technique is more convenient for the analysis of the Bose-Kondo model than the Abrikosov pseudofermion technique. We suggest that this extends to other models and recommend the use of the Majorana representation for future applications, in particular in the context of local spin models.

7. Conclusion

In this thesis we demonstrated that the Majorana representation is a suitable method for the calculation of observables of spin systems. In particular, we showed that it is a powerful and efficient method for local spin-1/2 models in which the spin is coupled to bosonic environments. Below, we review the key aspects of the present work with special focus on the Majorana representation. We also include some suggestions for future applications.

We have seen that a major benefit of the Majorana representation is that it allows for efficient calculations of two-spin and even four-spin correlation functions. Both types of correlation functions play an important role in the analysis of noise measurements. Yet the concept of four-spin correlation functions is relatively unknown in literature. Thus we provided a detailed discussion of the experimental relevance of four-spin correlation functions in Ch. 2. We introduced the concept of noise of susceptibility on a general level and derived Wiener-Khinchin-like relations between a special four-spin correlation function and the experimentally accessible quantity. The Majorana representation and the approach presented in Ch. 4 enabled us to compute the four-spin correlator and thus the noise of susceptibility for a simple model of independent spins. Comparing with experiments, we confirmed that this simple model cannot account for the experimental observations in the context of $1/f$ flux noise in superconducting Josephson devices.

So far, the Majorana representation has not been widely used in literature. Reasons for that might be doubts about the validity of the representation, as well as the failure of the perturbative expansion as seen in Ref. [6]. In this thesis we resolved both of these issues. First, we explicitly demonstrated that the Majorana representation does not suffer from Hilbert space complications in Ch. 3. Though the Majorana Hilbert space is enlarged as compared to the original spin Hilbert space, this enlargement does not affect physical quantities. Second, concerning the long-time failure of the perturbative approach to the longitudinal-spin correlations in the spin-boson model, we showed in Ch. 5 that the failure originates from divergencies in higher-order contributions in perturbation theory. Moreover, we were able to provide an alternative approach which avoids these complications and thus fully resolves the issue. We demonstrated that this alternative approach indeed produces the correct longitudinal-spin correlations for the spin-boson model.

In general, the calculation of higher-spin correlation functions is a complicated task. In this work we showed that the Majorana representation is particularly useful in this context. There are several reasons for that. One main aspect is the simplified relations between spin and Majorana correlation functions discovered in Refs. [5, 6]. Based on a special property of the Majorana representation, these relations state that a two(four)-spin correlator

corresponds to a two(four)-Majorana correlator. In Ch. 3 we extended these relations to pairwise spin correlators of arbitrary order, thus even including different spins.

One of the major achievements of this work concerns the calculation of higher-spin correlations functions. Namely, we developed efficient approaches for the calculation of large classes of spin correlation functions for two types of dissipative spin models, the Bose-Kondo model in Ch. 4 and the spin-boson model in Ch. 5. Our approaches allow to obtain controlled perturbative results for a wide range of spin correlators. To this end, we employed a path-integral approach. Using Hubbard-Stratonovich transformations we derived new effective actions. We identified the saddle-point solutions for the Majorana Green's functions and analyzed the fluctuations around the saddle-points, which correspond to fluctuations of the self-energy. We found that the diagonal fluctuations are small and can be neglected. This, in turn, allowed us to formulate Wick-theorem like prescriptions for the controlled calculation of spin correlation functions using saddle-point Majorana Green's functions. For the case of the Bose-Kondo model the approach allows to efficiently compute even-order same-spin correlation functions, as an example we computed the four-spin correlation function relevant for noise of susceptibility. For the case of the spin-boson model, we showed that our approach allows for the efficient calculation of spin correlation functions that include an even number of transverse spin operators.

We demonstrated that the Majorana representation is a flexible tool that can be, to some extend, adjusted to the actual problem under consideration. In most cases, the simplified relations between spin and Majorana correlators clearly facilitate the calculations. However, the use of the simplified relations for the spin-boson model in Ref. [6] did produce incorrect results for the longitudinal-spin correlations in the long-time limit. In Ch. 5 we achieved to resolve the problem by mixing the original spin representation and the simplified relations. That is, within the Majorana representation one has the freedom to choose whether or not to use the simplified relations. We showed that this freedom can be efficiently utilized to suitably adjust an approach to the model and to the quantity of under consideration.

In comparison to other techniques, the Majorana representation largely turns out to be preferable. In contrast to other spin representations, the Majorana representation does not suffer from enlarged Hilbert spaces and does not require additional procedures to eliminate unphysical states. This is what we showed explicitly in Ch. 3, confirming earlier statements. Using bilinear spin representations for two-spin and higher-spin correlation functions, the treatment of outer spin vertices is in general complicated. The simplified relations in the Majorana representation provide a unique way to avoid such complications. Regarding the efficient methods for the computation of spin correlations functions we developed in Chs. 4 and 5, the superiority of the Majorana technique over other representations becomes even more obvious. In Ch. 5 we showed that the Majorana representation easily reproduces results known from Bloch-Redfield Master equation techniques. We provided a detailed comparison to the widely used Abrikosov pseudofermion representation in Ch. 6. In this chapter we reproduced the RG equations for the sub-Ohmic Bose-Kondo model. Our results confirmed earlier results obtained in Refs. [3, 99]. However, the calculations up to two-loop order allowed for a detailed comparison of the methods. We concluded that the calculations in the Majorana representation are significantly easier. We also found that the overall form of intermediate results in the Majorana representation were of simpler structure than those in the pseudofermion representation. We attributed the latter to the more transparent structure of interaction vertices in the Majorana representation.

Let us now give some suggestions for future applications of the Majorana representation. The path-integral approach developed in Ch. 4 was successfully applied to both the Bose-Kondo and the spin-boson model in the Ohmic case. This suggests that this rather successful approach can also be applied to other versions of local spin models, e.g., sub-Ohmic variants of the models, the finite-field case of the Bose-Kondo model as well as extensions of the spin-boson model. Spin-boson models that include a second bosonic bath or an additional magnetic field term parallel to the bath display rich dynamics and phase diagrams and are particularly relevant with regard to the phenomenon of decoherence in open quantum two-level systems. Many calculations were carried using the Keldysh technique, allowing for direct generalization to nonequilibrium or disorder situations, e.g., in spin glasses. The sub-Ohmic Bose-Kondo model is relevant in the context of spin glasses, which suggests to reanalyze the saddle-point solutions that we obtained in Ch. 4 for the sub-Ohmic case and out of equilibrium. Finally, the Majorana representation could also be applied to spin-lattice models. Several earlier works used the Majorana representation for spin lattices, in particular for the Kondo lattice. This suggests future use in this context.

To conclude, we showed that the Majorana representation is a valid, powerful and flexible tool for the treatment of spin-1/2 problems. In particular, it is a unique tool for efficient approaches to higher-spin correlation functions and it bears a range of advantages against other methods. We recommend the Majorana representation for future use.

Appendix

A. Calculations of Diagrams for the RG Approach to the Bose-Kondo model

Here we provide detailed calculations for the RG approach to the Bose-Kondo model in Chapter 6. First of all, we recall the partition function and the action (6.8) as introduced in Sec. 6.2:

$$\mathcal{Z} = \int D[\boldsymbol{\eta}] \exp \left\{ -\frac{T}{2} \sum_n \eta_\alpha^n \left(\mathcal{G}_{f\alpha}(i\nu_n) \right)^{-1} \eta_\alpha^{-n} + i\mathcal{S}_{int} \right\} \ , \tag{A.1a}$$

$$i\mathcal{S}_{int} = \sum_{\boldsymbol{\alpha}} \frac{g_\alpha}{2} T^3 \sum_m^b \sum_{n_i,k_i,m}^f \left(\tilde{\Pi}_m^> + \tilde{\Pi}_m^< \right) \eta_{\alpha'}^{n_1} \eta_{\alpha'}^{k_1} \eta_{\alpha''}^{n_2} \eta_{\alpha''}^{k_2} \, \delta_{n_1+n_2+m} \delta_{k_1+k_2-m} \ . \tag{A.1b}$$

Here and below we use subscript $m, m_{(i)}$ and superscripts $n, n_{(i)}, k, k_{(i)}$ as shortcuts for bosonic and fermionic Matsubara frequencies, respectively. By superscripts b and f on sigma signs we denoted explicitly that summation over ω_m includes bosonic while summation over ν_n and ν_k includes fermionic Matsubara frequencies. The b and f superscripts are dropped below. The sum over the vector $\boldsymbol{\alpha}$ of indices runs over values

$$\boldsymbol{\alpha} = \{\alpha, \alpha', \alpha''\} \in \{\{x,y,z\}, \{y,z,x\}, \{z,x,y\}\} \ . \tag{A.2}$$

The diagrammatic contributions to the loop expansion of vertex functions $\Gamma_\alpha^{(2)}$ and $\Gamma_\alpha^{(4)}$ can be constructed explicitly. This is achieved by expanding the exponential (A.1a) in orders of $\mathcal{S}_{int}$. Each term of this expansion generates diagrams that are obtained by suitable contraction of Majorana fields in loops including the fast part $\tilde{\Pi}^>$. According to the respective number of outer legs the irreducible diagrams are assigned to the loop expansion of one particular vertex function. In doing so, we have to take care about prefactors in the definitions of vertex functions, which is $-\frac{1}{2}$ for the inverse Green's function $\Gamma_\alpha^{(2)}$ and $\frac{1}{2} \tilde{\Pi}^<$ for the vertex $\Gamma_\alpha^{(4)}$, cf. Eqs. (6.12) and (6.13) in the main text. In adding the diagrams as corrections to the vertex function we appropriately reexponentiate the important terms of the expansion of the exponential (A.1a).

In order to draw the diagrams we use straight lines to represent Majorana propagators and wiggled lines to represent the fast part of the modified form of the bosonic propagator:

$$\alpha \underline{\hspace{1cm} \nu_n \hspace{1cm}} \beta \quad = -\delta_{\alpha\beta} \, \mathcal{G}_\alpha(i\nu_n) \ , \tag{A.3}$$

$$\alpha \sim\sim\sim^{\omega_m}\sim\sim\sim \beta \quad = \delta_{\alpha\beta} \, \tilde{\Pi}^>(i\omega_m) \ . \tag{A.4}$$

To provide the full information for the calculations below we recall the Matsubara Green's functions, $\mathcal{G}_\alpha(i\nu_n) = \mathcal{G}(i\nu_n) = (i\nu_n)^{-1}$ and the fast part of the bosonic propagator, Eq. (6.10),

$$\tilde{\Pi}^>(i\omega_m) = \left(\int_{\Lambda/b}^{\Lambda} + \int_{-\Lambda}^{-\Lambda/b} \right) dx \, \frac{i\omega_m |x|^{-\epsilon} \Lambda^\epsilon}{x - i\omega_m} \, . \tag{A.5}$$

The parameters l and b are related by $l = \log b$.

A.1. Loop Expansion of the Inverse Majorana Green's function

First, we calculate the contributions to the inverse Majorana Green's function $\Gamma_\alpha^{(2)}$ up to two-loop order. Contributions to the four-point Majorana vertex $\Gamma_\alpha^{(4)}$ are calculated subsequently.

A.1.1. One-Loop Order

In the expansion of the exponential of the quartic Majorana interaction (A.1b), the first term generates the Fock-like diagram depicted in Fig. A.1 which is the only one-loop contribution to the inverse Green's function $\Gamma_\alpha^{(2)}$. The term is

$$\sum_{\boldsymbol{\alpha}} \frac{g_\alpha}{2} T^3 \sum_m \sum_{n_i, k_i} \tilde{\Pi}_m^> \, \eta_{\alpha'}^{n_1} \, \eta_{\alpha'}^{k_1} \, \eta_{\alpha''}^{n_2} \, \eta_{\alpha''}^{k_2} \, \delta_{n_1+n_2+m} \delta_{k_1+k_2-m} \tag{A.6}$$
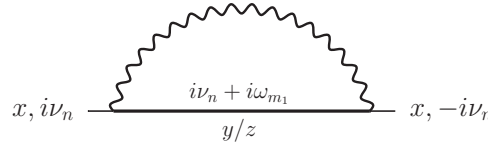
Figure A.1.: One-loop correction to the inverse x-Majorana Green's function. The internal Majorana propagator can have index y or z.

In order to obtain contributions to the x-component $\Gamma_x^{(2)}$ the two outer Majorana legs have to be η_x. Thus the internal Majorana index may be y or z, corresponding to vertices g_z and g_y, respectively. Omitting outer Majorana legs, the outer Matsubara sum and the prefactor $-\frac{1}{2}$ in (A.6), and contracting the remaining field variables, we find the contribution to $\Gamma_x^{(2)}$, i.e., the diagram in Fig. A.1:

$$(g_y + g_z) \left(-T \sum_m \tilde{\Pi}^>(i\omega_m) \mathcal{G}(i\nu_n + i\omega_m) \right) \, . \tag{A.7}$$

For large ω_m the above expression does not decay fast enough in order to evaluate the Matsubara sum via residue theorem. To use the residue theorem, we take advantage of the symmetry $\tilde{\Pi}(i\omega_m) = \tilde{\Pi}(-i\omega_m)$ and simultaneously replace $x \to -x$ in the integrand of $\tilde{\Pi}^>$.

In this way the integrand in brackets in expression (A.7) is transformed to

$$\frac{i\omega_m|x|^{-\epsilon}}{(x-i\omega_m)(i\omega_m+i\nu_n)} \rightarrow \frac{1}{2}\left(\frac{i\omega_m|x|^{-\epsilon}}{(x-i\omega_m)(i\omega_m+i\nu_n)} + \frac{-i\omega_m|-x|^{-\epsilon}}{(-x+i\omega_m)(-i\omega_m+i\nu_n)}\right)$$
$$= \frac{i\nu_n i\omega_m|x|^{-\epsilon}}{(x-i\omega_m)(i\omega_m+i\nu_n)(i\omega_m-i\nu_n)} \ , \quad \text{(A.8)}$$

which decays fast enough, i.e. quadratically, for $\omega_m \to \infty$ and enables to evaluate the Matsubara sum via the residue theorem. Thus we obtain

$$(g_y + g_z)i\nu_n \left(\int_{\Lambda/b}^{\Lambda} + \int_{-\Lambda}^{-\Lambda/b}\right) dx \frac{\Lambda^\varepsilon|x|^{-\varepsilon}\,x\coth\frac{x}{2T}}{(x^2-(i\nu_n)^2)} \ . \quad \text{(A.9)}$$

To perform the x-integral in $\tilde{\Pi}^>$ the outer frequency ν_n and temperature are assumed to be small, $\nu_n, T \ll \Lambda/b$. This approximation is correct up to logarithmic accuracy, i.e. corrections of order $\log(\nu_n/\Lambda)$. Introducing the integral

$$I_1(b) = \int_{\Lambda/b}^{\Lambda} dx \frac{\Lambda^\varepsilon}{x^{1+\varepsilon}} = \frac{b^\varepsilon-1}{\varepsilon} = \frac{e^{\varepsilon l}-1}{\varepsilon} \ , \quad \text{(A.10)}$$

the one-loop contribution (A.7), i.e. the Fock-like diagram in Fig. A.1 is evaluated to

$$(i\nu_n)(g_y + g_z)\,I_1(b) \ . \quad \text{(A.11)}$$

This is the result (6.18) given in the main text.

We note that Hartree-like bubble diagrams do not appear because vertices are off-diagonal in spin indices, $\alpha \neq \beta$, while Green's functions are diagonal $\mathcal{G}_{\alpha\beta} = 0$, as long as there is no external magnetic field. At finite magnetic field an expansion in the small field would yield a finite Hartree contribution to off-diagonal Majorana Green's functions.

A.1.2. Two-Loop Order

For the two-loop order corrections to the inverse Majorana Green's function $\Gamma_\alpha^{(2)}$ we consider the quadratic term $\propto (\tilde{\Pi}^>)^2$ in the expansion of the exponential of $\mathcal{S}_{int}$:

$$\sum_{\boldsymbol{\alpha},\boldsymbol{\beta}} \frac{g_\alpha g_\beta}{2^3} T^6 \sum_{m_i} \sum_{n_i,k_i} \tilde{\Pi}_{m_1}^> \eta_{\alpha'}^{n_1}\eta_{\alpha'}^{k_1}\eta_{\alpha''}^{n_2}\eta_{\alpha''}^{k_2} \, \tilde{\Pi}_{m_2}^> \, \eta_{\beta'}^{n_3}\eta_{\beta'}^{k_3}\eta_{\beta''}^{n_4}\eta_{\beta''}^{k_4}$$
$$\times \ \delta_{n_1+n_2+m_1}\delta_{k_1+k_2-m_1}\delta_{n_3+n_4+m_2}\delta_{k_3+k_4-m_2} \ , \quad \text{(A.12)}$$

Again, we compute the corrections to $\Gamma_x^{(2)}$, the y- and z-components follow from cyclic permutation of indices x, y, z. To get contributions to the inverse Majorana Green's function $\Gamma_x^{(2)}$ we need to contract six of eight Majorana fields in (A.12). There are essentially three possible ways to do the contractions, corresponding to three diagrams (a), (b) and (c) depicted in Fig. A.2.

Two Majorana fields have to be chosen as outer legs, one out of $\{n_{1/2}, k_{1/2}\}$ and another one out of $\{n_{3/4}, k_{3/4}\}$ in (A.12). Due to the restriction of spin combinations this adds a combinatorial factor of 4. Possible spin combinations for diagrams (a) and (b) are $\{\alpha, \alpha', \alpha''\} = \{\beta, \beta', \beta''\} = \{y, z, x\}$ and $= \{z, x, y\}$ yielding g_y^2 and g_z^2, respectively. In
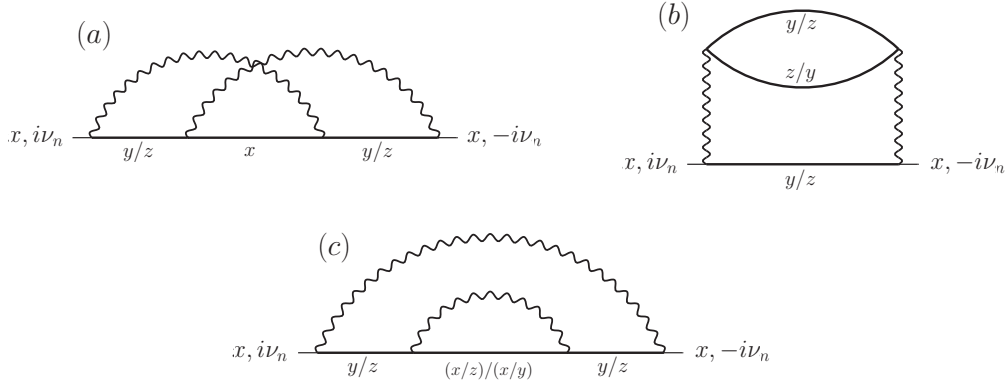
Figure A.2.: Two-loop contributions to renormalization of the Majorana propagator

diagram (c) the inner index may have any value differing from the intermediate index, in addition allowing for combinations $g_y g_x$ and $g_z g_x$. Thus, excluding the prefactor $-\frac{1}{2}$, the outer sum and outer legs, the contributions correspond to

$$(a): \quad -(g_y^2 + g_z^2)\, T^2 \sum_{m_1, m_2} \tilde{\Pi}_{m_1}^{>} \tilde{\Pi}_{m_2}^{>} \mathcal{G}(i\nu_n + i\omega_{m_1})$$

$$\times\, \mathcal{G}(i\nu_n + i\omega_{m_1} + i\omega_{m_2})\, \mathcal{G}(i\nu_n + i\omega_{m_2})\,, \quad \text{(A.13a)}$$

$$(b): \quad -(g_y^2 + g_z^2)\, T \sum_{m_1} \left(\tilde{\Pi}_{m_1}^{>}\right)^2 \mathcal{G}(i\nu_n + i\omega_{m_1})$$

$$\times\, T \sum_{m_2} \mathcal{G}(i\nu_n + i\omega_{m_1} + i\omega_{m_2})\, \mathcal{G}(i\nu_n + i\omega_{m_2}) \quad \text{(A.13b)}$$

and

$$(c): \quad -\left(g_y(g_x + g_y) + g_z(g_x + g_z)\right) T \sum_{m_1} \tilde{\Pi}_{m_1}^{>} \mathcal{G}(i\nu_n + i\omega_{m_1})\, \mathcal{G}(i\nu_n + i\omega_{m_1})$$

$$\times\, T \sum_{m_2} \tilde{\Pi}_{m_2}^{>} \mathcal{G}(i\nu_n + i\omega_{m_1} + i\omega_{m_2})\,. \quad \text{(A.13c)}$$

We first consider diagram (b). For $\omega_{m_1} = 0$ the function $\tilde{\Pi}^{>}(i\omega_{m_1})$ vanishes, cf. Eq. (A.5). Evaluating the sum over bosonic Matsubara frequencies ω_{m_2} at finite ω_{m_1} one finds

$$T \sum_{m_2} \mathcal{G}(i\nu_n + i\omega_{m_1} + i\omega_{m_2})\, \mathcal{G}(i\nu_n + i\omega_{m_2})$$

$$\stackrel{i\omega_{m_2} \to z}{=} -\oint \frac{dz}{2\pi i} \frac{n_B(z)}{(z + i\nu_n + i\omega_{m_1})(z + i\nu_n)}$$

$$= \frac{1}{2}\left(\frac{1}{-i\omega_{m_1}} + \frac{1}{i\omega_{m_1}}\right) = 0\,. \quad \text{(A.14)}$$

Thus we conclude that the (b)-contribution vanishes. We note that in the case of finite magnetic field B the poles of $\mathcal{G}_y$ are shifted, the difference in (A.14) won't cancel and diagram (b) yields a finite contribution.

Now we turn to the contributions (a) and (c), denoted by $\Gamma_x^{(2,a)}$ and $\Gamma_x^{(2,c)}$. We computed the Matsubara sums over ω_{m_1} and ω_{m_2} in (A.13a) and (A.13c) using residue theorem and performed the summation over residues with the help of Mathematica. In expanding the resulting expressions in small outer frequencies, $\nu_n \ll \Lambda/b$ we find that the lowest order is linear in ν_n, and drop higher orders. To simplify the integrals arising from the spectral representation of $\tilde{\Pi}^>$, Eq. (A.5), we take advantage of the symmetric integration around zero and introduce the integral

$$I_2(b) = \iint_{\Lambda/b}^{\Lambda} \frac{\Lambda^{2\varepsilon}dxdy}{x^\varepsilon y^\varepsilon (x+y)^2} = \iint_{1/b}^{1} \frac{dxdy}{x^\varepsilon y^\varepsilon (x+y)^2} \ . \tag{A.15}$$

In terms of $I_1(b)$, Eq. (A.10) and $I_2(b)$ we then find

$$\Gamma_x^{(2,a)}(l) = i\nu_n \left(g_y^2 + g_z^2 \right) (I_2(b) + I_1(b)) \ , \tag{A.16a}$$

$$\Gamma_x^{(2,c)}(l) = -i\nu_n \left(g_y^2 + g_z^2 + g_x(g_y + g_z) \right) \left(I_2(b) + \frac{1}{2} I_1(b) \right) \ , \tag{A.16c}$$

which are the results (6.22) in the main text. For the evaluation of the integral $I_2(b)$ we refer to the main text.

A.2. Loop Expansion of Four-Majorana Vertices

Now we turn to the diagrams which contribute to the four-point Majorana vertex $\Gamma_\alpha^{(4)}$. One can distinguish between two types of corrections to the four-point vertex. In the first type, the left and the right side of the four-point vertex in Fig. A.3 are "dressed" separately and remain connected merely by the slow part of the bosonic propagator $\tilde{\Pi}^<$. In the second type, the left-hand side and the right-hand side of the vertex become connected in a more complicated way, i.e., by two or more bosonic lines. The first and second type of contributions can be understood as vertex-like and ladder-like corrections, respectively. To begin with, we show that ladder-like contributions vanish. As a consequence, the important contributions are of the first type where it is sufficient to consider one side, either left or right, of the four-point vertex. The first-type corrections, which indeed turn out to be relevant, are computed subsequently.
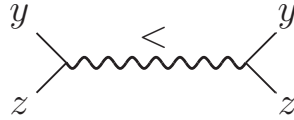
Figure A.3.: Bare four-point vertex $\frac{1}{2}\tilde{\Pi}^<\Gamma_x^{(4)}(0)$.

A.2.1. Ladder-Like Contributions

The quadratic term (A.12) in the expansion of the exponential of $i\mathcal{S}_{int}$ gives rise to ladder-like contributions of the type depicted in Fig. (A.4).

$$\sum_{\boldsymbol{\alpha},\boldsymbol{\beta}} \frac{g_\alpha g_\beta}{2^3} T^6 \sum_{m_i} \sum_{n_i,k_i} \tilde{\Pi}_{m_1} \eta_{\alpha'}^{n_1} \eta_{\alpha'}^{k_1} \eta_{\alpha''}^{n_2} \eta_{\alpha''}^{k_2} \tilde{\Pi}_{m_2} \eta_{\beta'}^{n_3} \eta_{\beta'}^{k_3} \eta_{\beta''}^{n_4} \eta_{\beta''}^{k_4}$$

$$\times \ \delta_{n_1+n_2+m_1}\delta_{k_1+k_2-m_1}\delta_{n_3+n_4+m_2}\delta_{k_3+k_4-m_2} \ , \tag{A.17}$$

Figure A.4.: Two pairs of ladder-like corrections to the four-Majorana vertex. The left pair has intermediate indeces y and z, whereas for the right pair the intermediate indeces have to be x.

There are always two ladder-like diagrams which cancel. As an example we consider the two diagrams depicted in Fig. A.4. Contracting four of the eight Majorana fields in (A.17) and excluding outer legs, sums and a factor of $\frac{1}{2}g_x$ one obtains

$$-2g_x T \sum_{m_1} \tilde{\Pi}^{>}(i\omega_{m_1})\tilde{\Pi}^{>}(-i\nu_n - i\nu_k - i\omega_{m_1})\mathcal{G}_z(i\nu_n + i\omega_{m_1})$$

$$\times \left(\mathcal{G}_y(i\omega_{m_1} + i\nu_n + i\omega_m) - \mathcal{G}_y(i\omega_{m_1} + i\nu_k - i\omega_m) \right) \quad \text{(A.18)}$$

Evaluating the Matsubara sum and taking the limit of vanishing outer fermionic frequencies ν_n and ν_k, one arrives at

$$2g_x T \Lambda^{2\varepsilon} \int dx \int dy \frac{i\omega_m}{|x|^{\varepsilon}|y|^{\varepsilon}(x+y)} \left(\frac{x\coth\frac{x}{2T}}{x^2 + \omega_m^2} - \frac{x\coth\frac{y}{2T}}{y^2 + \omega_m^2} \right) . \quad \text{(A.19)}$$

Due to the fact that the integration variables x and y can be interchanged the above term vanishes. In analogy to the pairs of diagrams depicted in Fig. A.4 a counterpart can be found for any ladder-like diagram. Thus all ladder-like contributions come in pairs which cancel each other.

In Fig. A.5 we have redrawn the left pair of ladder-like diagrams shown in Fig. A.4. In this form one recognizes that the second diagram can be obtained from the first be interchanging two of the outer legs. As outer frequencies can be neglected the two diagrams become equal up to a sign. This sign is due to the interchange of outer Majorana legs and provides the cause for the cancellation of the two diagrams.

Figure A.5.: These two ladder-like corrections to the four-Majorana vertex cancel.

So far we have only considered ladder-like contributions in one-loop order and have observed that such contributions cancel. In two-loop order a variety of ladder-like diagrams will arise. Based on the considerations above we suppose that ladder-like diagrams remain irrelevant in two-loop order. Thus the ladder-like contributions considered here are neglected in the remainder of this appendix as well as in the main part in Chap. 6.

A.2.2. Vertex-Like Contributions: One-Loop Order

Omitting the ladder-like contributions we proceed with the consideration of the relevant first-type contributions to the vertex functions $\Gamma_\alpha^{(4)}$. In the corresponding diagrams the left-hand side and the right-hand side three-point Majorana-boson vertices get dressed separately. Since outer frequencies are assumed to be much smaller than the reduced cutoff Λ/b it does not matter whether the left-hand or the right-hand side gets dressed. Thus, we only show diagrams with dressed left-hand vertices below.

Figure A.6.: One-loop contributions to the vertex function $\Gamma_x^{(4)}$.

The one-loop contributions to the vertex functions $\Gamma_\alpha^{(4)}$ are depicted in Fig. A.6. They are generated by the quadratic term in the expansion of the exponential of the interacting term (A.1b), namely from the term

$$2\sum_{\alpha,\beta}\frac{g_\alpha g_\beta}{2^3}\,T^6\sum_{m,m_1}\sum_{n_i,k_i}\tilde{\Pi}_m^<\,\eta_{\alpha'}^{n_1}\eta_{\alpha'}^{k_1}\eta_{\alpha''}^{n_2}\eta_{\alpha''}^{k_2}\,\tilde{\Pi}_{m_1}^>\,\eta_{\beta'}^{n_3}\eta_{\beta'}^{k_3}\eta_{\beta''}^{n_4}\eta_{\beta''}^{k_4}$$

$$\times\,\delta_{n_1+n_2+m}\delta_{k_1+k_2-m}\delta_{n_3+n_4+m_1}\delta_{k_3+k_4-m_1}\ ,\quad\text{(A.20)}$$

which includes both $\tilde{\Pi}^<$ and $\tilde{\Pi}^>$. The factor of two in (A.20) accounts for the fact that the mixed term occurs twice.

The right one of the diagrams in Fig. A.6 can be interpreted as a correction to the bosonic propagator $\tilde{\Pi}$. However, the diagram includes a loop of Majorana fermions. As we have shown in (A.14), the loop cancels at finite frequencies. In addition, the bosonic propagator vanishes at zero frequency. Thus, the right diagram does not contribute to the vertex function $\Gamma_\alpha^{(4)}$.

The type of diagrams depicted on the left in Fig. A.6 yield the relevant corrections to the vertex function $\Gamma_\alpha^{(4)}$. The diagrams can be obtained from (A.20) by appropriate contraction of four of the eight Majorana fields. To account for the second diagram that carries the dressed vertex on the right-hand side instead of the left-hand side of the bosonic propagator, we add another factor of 2. Excluding outer legs and outer sums as well as the prefactor $\tilde{\Pi}^<(i\omega_m)/2$ the contribution to the vertex function $\Gamma_\alpha^{(4)}$ reads

$$2g_x T\sum_{m_1}\tilde{\Pi}^>(i\omega_{m_1})\mathcal{G}(i\nu_n+i\omega_m+i\omega_{m_1})\mathcal{G}(i\nu_n+i\omega_{m_1})\qquad\text{(A.21)}$$

Again, the sum over Matsubara frequencies is readily evaluated using residue theorem. Neglecting the outer frequencies $i\nu_n$ and $i\omega_m$ and recalling $I_1(b)$ defined in Eq. (A.10) we find the one-loop formula for the vertex function $\Gamma_x^{(4)}$:

$$\Gamma_x^{(4)}(l) = g_x\left(1+2\,g_x I_1(b)+\mathcal{O}(g_\alpha^2)\right)\qquad\text{(A.22)}$$

This result corresponds to Eq. (6.20) given in the main text. The y- and z-components follow from $\Gamma_x^{(4)}$ through cyclic permutation.

A.2.3. Two-Loop Order

To construct the two-loop contributions to the vertex function $\Gamma_x^{(4)}$ we consider the cubic term in the expansion of the exponential of the interaction term (A.1b). The relevant terms include products of the form $\tilde{\Pi}^<(\tilde{\Pi}^>)^2$, which occur in three possible combinations:

$$\frac{3}{3!} \sum_{\boldsymbol{\alpha}_i} \frac{g_{\alpha_1} g_{\alpha_2} g_{\alpha_3}}{2^3} T^9 \sum_{m,m_i} \sum_{n_i,k_i} \tilde{\Pi}_m^< \eta_{\alpha_1'}^{n_1} \eta_{\alpha_1'}^{k_1} \eta_{\alpha_1''}^{n_2} \eta_{\alpha_1''}^{k_2} \tilde{\Pi}_{m_1}^> \eta_{\alpha_2'}^{n_3} \eta_{\alpha_2'}^{k_3} \eta_{\alpha_2''}^{n_4} \eta_{\alpha_2''}^{k_4} \tilde{\Pi}_{m_2}^> \eta_{\alpha_3'}^{n_5} \eta_{\alpha_3'}^{k_5} \eta_{\alpha_3''}^{n_6} \eta_{\alpha_3''}^{k_6}$$

$$\times \; \delta_{n_1+n_2+m} \delta_{k_1+k_2-m} \delta_{n_3+n_4+m_1} \delta_{k_3+k_4-m_1} \delta_{n_5+n_6+m_2} \delta_{k_5+k_6-m_2} \; . \quad \text{(A.23)}$$

On recognizes that there are eight possible types of contributions, depicted in Figure A.7. All contributions acquire a combination factor of 5! canceling the corresponding prefactor in (A.23).
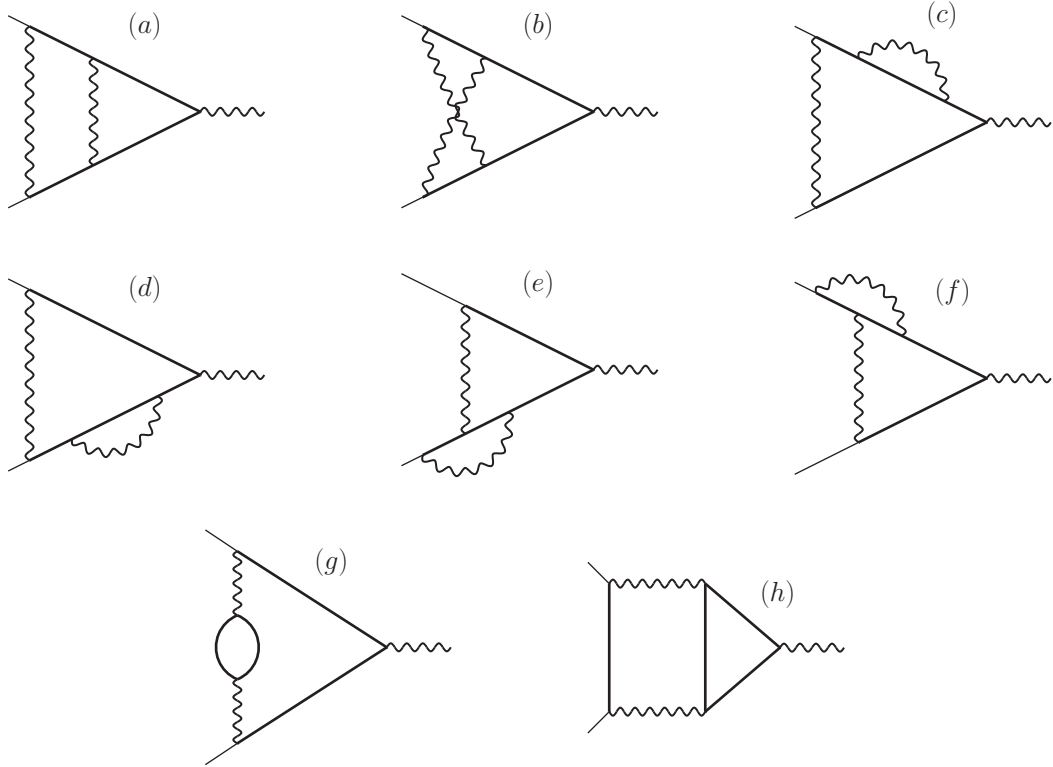
Figure A.7.: Two-loop corrections to the vertex function $\Gamma_x^{(4)}$.

We recognize that diagram (g) in Fig. A.7 includes a closed Majorana loop and thus vanishes according to Eq. (A.14). Upon evaluation of Matsubara sums, it turns out that the closed three-point Majorana loop in diagram (h) also vanishes. Thus, diagrams (g) and (h) do not contribute to the vertex function.

To keep the discussion short, we drop the details of the calculations of the remaining six

diagrams (a) to (f). Rather, omitting the prefactor $\tilde{\Pi}^</2$ we directly give the contributions to the vertex function $\Gamma_x^{(4)}$ in integral form:

$$(a): \quad 2g_x^3 \iint_{\Lambda/b}^{\Lambda} dxdy \frac{\Lambda^{2\epsilon}}{x^\epsilon y^\epsilon} \left(\frac{-1}{(x+y)^2} + \frac{1}{2xy} \right) \; , \tag{A.24}$$

$$(b): \quad 2g_x \left(g_x^2 - g_y g_z \right) \iint_{\Lambda/b}^{\Lambda} dxdy \frac{\Lambda^{2\epsilon}}{x^\epsilon y^\epsilon} \left(\frac{1}{(x+y)^2} \right) \; , \tag{A.25}$$

$$(c): \quad -2g_x^2 (g_x + g_y) \iint_{\Lambda/b}^{\Lambda} dxdy \frac{\Lambda^{2\epsilon}}{x^\epsilon y^\epsilon} \left(\frac{1}{2xy} \right) \; , \tag{A.26}$$

$$(d): \quad -2g_x^2 (g_x + g_z) \iint_{\Lambda/b}^{\Lambda} dxdy \frac{\Lambda^{2\epsilon}}{x^\epsilon y^\epsilon} \left(\frac{1}{2xy} \right) \; , \tag{A.27}$$

$$(e): \quad 2g_x^3 \iint_{\Lambda/b}^{\Lambda} dxdy \frac{\Lambda^{2\epsilon}}{x^\epsilon y^\epsilon} \left(\frac{1}{2xy} \right) \; , \tag{A.28}$$

$$(f): \quad 2g_x^3 \iint_{\Lambda/b}^{\Lambda} dxdy \frac{\Lambda^{2\epsilon}}{x^\epsilon y^\epsilon} \left(\frac{1}{2xy} \right) \; . \tag{A.29}$$

With the use of integrals I_1 and I_2, Eqs. (A.10) and (A.15), we can reexpress the above results as

$$(a): \quad g_x^3 \left(I_1(b) \right)^2 - 2g_x^3 I_2(b) \; , \tag{A.30}$$

$$(b): \quad 2g_x \left(g_x^2 - g_y g_z \right) I_2(b) \; , \tag{A.31}$$

$$(c): \quad -g_x^2 (g_x + g_y) \left(I_1(b) \right)^2 \; , \tag{A.32}$$

$$(d): \quad -g_x^2 (g_x + g_z) \left(I_1(b) \right)^2) \; , \tag{A.33}$$

$$(e): \quad g_x^3 \left(I_1(b) \right)^2 \; , \tag{A.34}$$

$$(f): \quad g_x^3 \left(I_1(b) \right)^2 \; . \tag{A.35}$$

These are the results given in Eqs. (6.24) in the main text. For the analysis of these results we refer to Secs. 6.2 and 6.3 of the main text.

Bibliography

[1] Shnirman, A., Makhlin, Y. & Schön, G. Noise and decoherence in quantum two-level systems. *Physica Scripta* **2002**, 147 (2002). URL `http://stacks.iop.org/1402-4896/2002/i=T102/a=024`. (see pp. 1, 76, 77).

[2] Schlosshauer, M. *Decoherence and the quantum to classical transition.* The frontiers collection (Springer, Berlin, 2008), corr. 3. print. edn. (see pp. 1, 50, 51, 76, 77, 94).

[3] Zaránd, G. & Demler, E. Quantum phase transitions in the Bose-Fermi Kondo model. *Phys. Rev. B* **66**, 024427 (2002). URL `http://link.aps.org/doi/10.1103/PhysRevB.66.024427`. (see pp. 2, 50, 93, 94, 95, 100, 105, 106, 108, 109, 110, 112).

[4] Frésard, R., Kroha, J. & Wölfle, P. The pseudoparticle approach to strongly correlated electron systems. In *Strongly Correlated Systems*, 65–101 (Springer, 2012). (see pp. 2, 30).

[5] Mao, W., Coleman, P., Hooley, C. & Langreth, D. Spin dynamics from Majorana fermions. *Phys. Rev. Lett.* **91**, 207203 (2003). URL `http://link.aps.org/doi/10.1103/PhysRevLett.91.207203`. (see pp. 2, 3, 30, 35, 36, 46, 47, 78, 81, 111).

[6] Shnirman, A. & Makhlin, Y. Spin-spin correlators in the Majorana representation. *Phys. Rev. Lett.* **91**, 207204 (2003). URL `http://link.aps.org/doi/10.1103/PhysRevLett.91.207204`. (see pp. 3, 31, 32, 35, 36, 37, 47, 75, 76, 78, 81, 82, 84, 91, 111, 112).

[7] Martin, J. L. Generalized classical dynamics, and the 'classical analogue' of a Fermi oscillator. *Proc. R. Soc. London A* **251**, 536–542 (1959). URL `http://rspa.royalsocietypublishing.org/content/251/1267/536.abstract`. (see pp. 3, 30, 31, 38).

[8] Feng, S., Lee, P. A. & Stone, A. D. Sensitivity of the conductance of a disordered metal to the motion of a single atom: Implications for 1f noise. *Phys. Rev. Lett.* **56**, 1960–1963 (1986). URL `http://link.aps.org/doi/10.1103/PhysRevLett.56.1960`. (see p. 8).

[9] Wellstood, F. C., Urbina, C. & Clarke, J. Low-frequency noise in dc superconducting quantum interference devices below 1 K. *Applied Physics Letters* **50**, 772–774 (1987). URL `http://link.aip.org/link/?APL/50/772/1`. (see pp. 8, 22).

[10] Yoshihara, F., Harrabi, K., Niskanen, A. O., Nakamura, Y. & Tsai, J. S. Decoherence of Flux Qubits due to $1/f$ Flux Noise. *Phys. Rev. Lett.* **97**, 167001 (2006). (see p. 8).

[11] Kakuyanagi, K., Meno, T., Saito, S., Nakano, H., Semba, K., Takayanagi, H., Deppe, F. & Shnirman, A. Dephasing of a Superconducting Flux Qubit. *Phys. Rev. Lett.* **98**, 047004 (2007). (see p. 8).

[12] Bialczak, R. C., McDermott, R., Ansmann, M., Hofheinz, M., Katz, N., Lucero, E., Neeley, M., O'Connell, A. D., Wang, H., Cleland, A. N. & Martinis, J. M. 1/f flux noise in Josephson phase qubits. *Phys. Rev. Lett.* **99**, 187006 (2007). (see pp. 8, 22, 25, 50).

[13] McDermott, R. Materials Origins of Decoherence in Superconducting Qubits. *Applied Superconductivity, IEEE Transactions on* **19**, 2–13 (2009). (see pp. 8, 9, 22, 23, 50).

[14] Lanting, T., Berkley, A. J., Bumble, B., Bunyk, P., Fung, A., Johansson, J., Kaul, A., Kleinsasser, A., Ladizinsky, E., Maibaum, F., Harris, R., Johnson, M. W., Tolkacheva, E. & Amin, M. H. S. Geometrical dependence of the low-frequency noise in superconducting flux qubits. *Phys. Rev. B* **79**, 060509 (2009). (see p. 8).

[15] Yoshihara, F., Nakamura, Y. & Tsai, J. S. Correlated flux noise and decoherence in two inductively coupled flux qubits. *Phys. Rev. B* **81**, 132502 (2010). URL http://link.aps.org/doi/10.1103/PhysRevB.81.132502. (see p. 8).

[16] Wellstood, F., Urbina, C. & Clarke, J. Role of geometry on the color of flux noise in dc SQUIDs. *Applied Superconductivity, IEEE Transactions on* **21**, 856–859 (2011). (see p. 8).

[17] Gustavsson, S., Bylander, J., Yan, F., Oliver, W. D., Yoshihara, F. & Nakamura, Y. Noise correlations in a flux qubit with tunable tunnel coupling. *Phys. Rev. B* **84**, 014525 (2011). URL http://link.aps.org/doi/10.1103/PhysRevB.84.014525. (see p. 8).

[18] Drung, D., Beyer, J., Storm, J., Peters, M. & Schurig, T. Investigation of low-frequency excess flux noise in dc SQUIDs at mk temperatures. *Applied Superconductivity, IEEE Transactions on* **21**, 340–344 (2011). (see pp. 8, 22).

[19] Anton, S. M., Müller, C., Birenbaum, J. S., O'Kelley, S. R., Fefferman, A. D., Golubev, D. S., Hilton, G. C., Cho, H.-M., Irwin, K. D., Wellstood, F. C., Schön, G., Shnirman, A. & Clarke, J. Pure dephasing in flux qubits due to flux noise with spectral density scaling as $1/f^\alpha$. *Phys. Rev. B* **85**, 224505 (2012). URL http://link.aps.org/doi/10.1103/PhysRevB.85.224505. (see pp. 8, 22).

[20] Sank, D., Barends, R., Bialczak, R. C., Chen, Y., Kelly, J., Lenander, M., Lucero, E., Mariantoni, M., Megrant, A., Neeley, M., O'Malley, P. J. J., Vainsencher, A., Wang, H., Wenner, J., White, T. C., Yamamoto, T., Yin, Y., Cleland, A. N. & Martinis, J. M. Flux noise probed with real time qubit tomography in a Josephson phase qubit. *Phys. Rev. Lett.* **109**, 067001 (2012). URL http://link.aps.org/doi/10.1103/PhysRevLett.109.067001. (see p. 8).

[21] Lanting, T., Amin, M. H., Berkley, A. J., Rich, C., Chen, S.-F., LaForest, S. & de Sousa, R. Evidence for temperature-dependent spin diffusion as a mechanism of intrinsic flux noise in SQUIDs. *Phys. Rev. B* **89**, 014503 (2014). URL `http://link.aps.org/doi/10.1103/PhysRevB.89.014503`. (see p. 8).

[22] Divincenzo, D. P. The Physical Implementation of Quantum Computation. *Fortschr. Phys.* **48**, 771–783 (2000). URL `http://dx.doi.org/10.1002/1521-3978(200009)48:9/112-E`. (see p. 8).

[23] Koch, R. H., DiVincenzo, D. P. & Clarke, J. Model for $1/f$ flux noise in SQUIDs and qubits. *Phys. Rev. Lett.* **98**, 267003 (2007). (see pp. 8, 23).

[24] Faoro, L. & Ioffe, L. B. Microscopic origin of low-frequency flux noise in Josephson circuits. *Phys. Rev. Lett.* **100**, 227005 (2008). (see p. 8).

[25] Choi, S., Lee, D.-H., Louie, S. G. & Clarke, J. Localization of Metal-Induced Gap States at the Metal-Insulator Interface: Origin of Flux Noise in SQUIDs and Superconducting Qubits. *Phys. Rev. Lett.* **103**, 197001 (2009). (see p. 8).

[26] Faoro, L., Ioffe, L. & Kitaev, A. Dissipationless dynamics of randomly coupled spins at high temperatures. *Phys. Rev. B* **86**, 134414 (2012). URL `http://link.aps.org/doi/10.1103/PhysRevB.86.134414`. (see pp. 8, 22).

[27] Sendelbach, S., Hover, D., Kittel, A., Mück, M., Martinis, J. M. & McDermott, R. Magnetism in SQUIDs at millikelvin temperatures. *Phys. Rev. Lett.* **100**, 227006 (2008). (see pp. 8, 22).

[28] Bluhm, H., Bert, J. A., Koshnick, N. C., Huber, M. E. & Moler, K. A. Spinlike Susceptibility of Metallic and Insulating Thin Films at Low Temperature. *Phys. Rev. Lett.* **103**, 026805 (2009). (see pp. 8, 22).

[29] Sendelbach, S., Hover, D., Mück, M. & McDermott, R. Complex inductance, excess noise, and surface magnetism in dc SQUIDs. *Phys. Rev. Lett.* **103**, 117001 (2009). (see pp. 8, 9, 12, 13, 16, 18, 21, 22, 24, 27, 28, 72).

[30] Dutta, P. & Horn, P. M. Low-frequency fluctuations in solids: $1/f$ noise. *Rev. Mod. Phys.* **53**, 497–516 (1981). URL `http://link.aps.org/doi/10.1103/RevModPhys.53.497`. (see pp. 8, 9, 22).

[31] Hooge, F. 1/f noise is no surface effect. *Physics Letters A* **29**, 139 – 140 (1969). URL `http://www.sciencedirect.com/science/article/pii/0375960169900760`. (see p. 9).

[32] Hooge, F. N. 1/f noise. *Physica B+C* **83**, 14 – 23 (1976). URL `http://www.sciencedirect.com/science/article/pii/0378436376900899`. (see p. 9).

[33] Voss, R. F. & Clarke, J. 1/f noise from systems in thermal equilibrium. *Phys. Rev. Lett.* **36**, 42–45 (1976). URL `http://link.aps.org/doi/10.1103/PhysRevLett.36.42`. (see pp. 9, 10, 13).

[34] Voss, R. F. & Clarke, J. Flicker (1/f) noise: Equilibrium temperature and resistance fluctuations. *Phys. Rev. B* **13**, 556–573 (1976). URL `http://link.aps.org/doi/10.1103/PhysRevB.13.556`. (see pp. 9, 13).

[35] Kogan, S. M. *Electronic noise and fluctuations in solids* (Cambridge University Press, Cambridge, 1996), 1. publ. edn. (see pp. 9, 10, 11, 12, 13, 14, 16).

[36] Beck, H. G. E. & Spruit, W. P. 1/f noise in the variance of Johnson noise. *J. Appl. Phys.* **49**, 3384–3385 (1978). (see pp. 9, 11).

[37] Restle, P. J., Hamilton, R. J., Weissman, M. B. & Love, M. S. Non-Gaussian effects in 1/ *f* noise in small silicon-on-sapphire resistors. *Phys. Rev. B* **31**, 2254–2262 (1985). URL `http://link.aps.org/doi/10.1103/PhysRevB.31.2254`. (see p. 9).

[38] Weissman, M. B. 1/*f* noise and other slow, nonexponential kinetics in condensed matter. *Rev. Mod. Phys.* **60**, 537–571 (1988). (see pp. 9, 11, 22, 23, 27).

[39] Weissman, M. B. What is a spin glass? A glimpse via mesoscopic noise. *Rev. Mod. Phys.* **65**, 829–839 (1993). (see pp. 9, 11, 22, 27).

[40] Chen, Z. & Yu, C. C. Comparison of Ising spin glass noise to flux and inductance noise in SQUIDs. *Phys. Rev. Lett.* **104**, 247204 (2010). URL `http://link.aps.org/doi/10.1103/PhysRevLett.104.247204`. (see pp. 9, 25).

[41] De, A. Ising-Glauber spin cluster model for temperature-dependent magnetization noise in SQUIDs. *Phys. Rev. Lett.* **113**, 217002 (2014). URL `http://link.aps.org/doi/10.1103/PhysRevLett.113.217002`. (see p. 9).

[42] Seidler, G. T. & Solin, S. A. Non-Gaussian 1/f noise: Experimental optimization and separation of high-order amplitude and phase correlations. *Phys. Rev. B* **53**, 9753–9759 (1996). (see pp. 10, 11).

[43] Blanter, Y. M. & Büttiker, M. Shot noise in mesoscopic conductors. *Phys. Rep.* **336**, 1 − 166 (2000). URL `http://www.sciencedirect.com/science/article/pii/S0370157399001234`. (see pp. 12, 13).

[44] Büttiker, M. Scattering theory of current and intensity noise correlations in conductors and wave guides. *Phys. Rev. B* **46**, 12485–12507 (1992). URL `http://link.aps.org/doi/10.1103/PhysRevB.46.12485`. (see p. 13).

[45] Lesovik, G. B. & Loosen, R. Negative excess noise in quantum conductors. *Z. Phys. B* **91**, 531 (1993). (see p. 13).

[46] Mahan, G. D. *Many-Particle Physics* (Plenum, New York, N.Y., 1993), 2nd edn. (see pp. 14, 29, 38).

[47] Kamenev, A. *Field theory of non-equilibrium systems* (Cambridge Univ. Press, Cambridge [u.a.], 2011), 1. publ. edn. (see pp. 14, 42, 43, 51, 52, 56, 61, 63, 79).

[48] Binosi, D. & Theußl, L. JaxoDraw: A graphical user interface for drawing Feynman

diagrams. *Computer Physics Communications* **161**, 76 – 86 (2004). URL `http://www.sciencedirect.com/science/article/pii/S0010465504002115`. (see p. 19).

[49] Slichter, D. H., Vijay, R., Weber, S. J., Boutin, S., Boissonneault, M., Gambetta, J. M., Blais, A. & Siddiqi, I. Measurement-induced qubit state mixing in circuit QED from up-converted dephasing noise. *Phys. Rev. Lett.* **109**, 153601 (2012). URL `http://link.aps.org/doi/10.1103/PhysRevLett.109.153601`. (see p. 22).

[50] Harris, R., Johnson, M. W., Han, S., Berkley, A. J., Johansson, J., Bunyk, P., Ladizinsky, E., Govorkov, S., Thom, M. C., Uchaikin, S., Bumble, B., Fung, A., Kaul, A., Kleinsasser, A., Amin, M. H. S. & Averin, D. V. Probing Noise in Flux Qubits via Macroscopic Resonant Tunneling. *Phys. Rev. Lett.* **101**, 117003 (2008). URL `http://link.aps.org/doi/10.1103/PhysRevLett.101.117003`. (see p. 22).

[51] Lanting, T., Amin, M. H. S., Johnson, M. W., Altomare, F., Berkley, A. J., Gildert, S., Harris, R., Johansson, J., Bunyk, P., Ladizinsky, E., Tolkacheva, E. & Averin, D. V. Probing high-frequency noise with macroscopic resonant tunneling. *Phys. Rev. B* **83**, 180502 (2011). URL `http://link.aps.org/doi/10.1103/PhysRevB.83.180502`. (see p. 22).

[52] Anton, S. M. & Clarke, J. Measurements of flux noise in a large variety of Nb-AlOx-Nb SQUIDs produced at MIT-LL and NIST. *private communication* (2012). (see pp. 23, 25, 26).

[53] Anton, S. M., Birenbaum, J. S., O'Kelley, S. R., Bolkhovsky, V., Braje, D. A., Fitch, G., Neeley, M., Hilton, G. C., Cho, H.-M., Irwin, K. D., Wellstood, F. C., Oliver, W. D., Shnirman, A. & Clarke, J. Magnetic flux noise in dc SQUIDs: Temperature and geometry dependence. *Phys. Rev. Lett.* **110**, 147002 (2013). URL `http://link.aps.org/doi/10.1103/PhysRevLett.110.147002`. (see pp. 25, 27).

[54] Anton, S. M. *Magnetic flux noise in SQUIDs and qubits*. Ph.D. thesis (2013). Copyright - Copyright ProQuest, UMI Dissertations Publishing 2013. (see pp. 25, 27).

[55] Nguyen, A. K. & Girvin, S. M. Non-Gaussian Noise in Quantum Spin Glasses and Interacting Two-Level Systems. *Phys. Rev. Lett.* **87**, 127205 (2001). URL `http://link.aps.org/doi/10.1103/PhysRevLett.87.127205`. (see p. 25).

[56] LaForest, S. & de Sousa, R. Flux-vector model of spin noise in superconducting circuits: Electron versus nuclear spins and role of phase transition. *Phys. Rev. B* **92**, 054502 (2015). URL `http://link.aps.org/doi/10.1103/PhysRevB.92.054502`. (see p. 25).

[57] Atalaya, J., Clarke, J., Schön, G. & Shnirman, A. Flux $1/f^\alpha$ noise in two-dimensional Heisenberg spin glasses: Effects of weak anisotropic interactions. *Phys. Rev. B* **90**, 014206 (2014). URL `http://link.aps.org/doi/10.1103/PhysRevB.90.014206`. (see p. 27).

[58] Vieira, V. R. New field theoretical method for spin 1/2. *Physica A: Statistical Me-*

chanics and its Applications **115**, 58 – 84 (1982). URL `http://www.sciencedirect.com/science/article/pii/0378437182901285`. (see pp. 30, 38).

[59] Tsvelik, A. M. *Quantum field theory in condensed matter physics* (Cambridge University Press, Cambridge, 1996). (see pp. 30, 31, 32, 37, 38).

[60] Jordan, P. & Wigner, E. Über das Paulische Äquivalenzverbot. *Zeitschrift für Physik* **47**, 631–651 (1928). URL `http://dx.doi.org/10.1007/BF01331938`. (see p. 30).

[61] Holstein, T. & Primakoff, H. Field dependence of the intrinsic domain magnetization of a ferromagnet. *Phys. Rev.* **58**, 1098–1113 (1940). URL `http://link.aps.org/doi/10.1103/PhysRev.58.1098`. (see p. 30).

[62] Kenan, R. P. Perturbation expansion for the magnetization of the spin ½ antiferromagnet. *Journal of Applied Physics* **37**, 1453–1454 (1966). URL `http://scitation.aip.org/content/aip/journal/jap/37/3/10.1063/1.1708512`. (see pp. 30, 31, 32).

[63] Spencer, H. J. & Doniach, S. Low-temperature anomaly of electron-spin resonance in dilute alloys. *Phys. Rev. Lett.* **18**, 994–997 (1967). URL `http://link.aps.org/doi/10.1103/PhysRevLett.18.994`. (see pp. 30, 31, 32).

[64] Popov, V. & Fedotov, S. The functional-integration method and diagram technique for spin systems. *JETP* **67**, 535 (1988). (see p. 30).

[65] Schwinger, J. On angular momentum. In Biederharn, L. & van Dam, H. (eds.) *Quantum Theory of Angular Momentum*, 229 (Academic Press, New York, 1965). (see p. 30).

[66] Arovas, D. P. & Auerbach, A. Functional integral theories of low-dimensional quantum Heisenberg models. *Phys. Rev. B* **38**, 316–332 (1988). (see p. 30).

[67] Read, N. & Sachdev, S. Large-N expansion for frustrated quantum antiferromagnets. *Phys. Rev. Lett.* **66**, 1773–1776 (1991). URL `http://link.aps.org/doi/10.1103/PhysRevLett.66.1773`. (see p. 30).

[68] Wang, F. Schwinger boson mean field theories of spin liquid states on a honeycomb lattice: Projective symmetry group analysis and critical field theory. *Phys. Rev. B* **82**, 024419 (2010). URL `http://link.aps.org/doi/10.1103/PhysRevB.82.024419`. (see p. 30).

[69] Affleck, I., Zou, Z., Hsu, T. & Anderson, P. W. SU(2) gauge symmetry of the large-u limit of the Hubbard model. *Phys. Rev. B* **38**, 745–747 (1988). (see p. 30).

[70] Marston, J. B. & Affleck, I. Large-n limit of the Hubbard-Heisenberg model. *Phys. Rev. B* **39**, 11538–11558 (1989). URL `http://link.aps.org/doi/10.1103/PhysRevB.39.11538`. (see p. 30).

[71] Andrei, N. & Coleman, P. Cooper instability in the presence of a spin liquid. *Phys.*

Rev. Lett. **62**, 595–598 (1989). (see p. 30).

[72] Dagotto, E., Fradkin, E. & Moreo, A. SU(2) gauge invariance and order parameters in strongly coupled electronic systems. *Phys. Rev. B* **38**, 2926–2929 (1988). URL `http://link.aps.org/doi/10.1103/PhysRevB.38.2926`. (see p. 30).

[73] Wen, X. G. Mean-field theory of spin-liquid states with finite energy gap and topological orders. *Phys. Rev. B* **44**, 2664–2672 (1991). URL `http://link.aps.org/doi/10.1103/PhysRevB.44.2664`. (see p. 30).

[74] Burnell, F. J. & Nayak, C. SU(2) slave fermion solution of the Kitaev honeycomb lattice model. *Phys. Rev. B* **84**, 125125 (2011). URL `http://link.aps.org/doi/10.1103/PhysRevB.84.125125`. (see p. 30).

[75] Fradkin, E. Jordan-Wigner transformation for quantum-spin systems in two dimensions and fractional statistics. *Phys. Rev. Lett.* **63**, 322–325 (1989). URL `http://link.aps.org/doi/10.1103/PhysRevLett.63.322`. (see p. 30).

[76] Huerta, L. & Zanelli, J. Bose-Fermi transformation in three-dimensional space. *Phys. Rev. Lett.* **71**, 3622–3624 (1993). URL `http://link.aps.org/doi/10.1103/PhysRevLett.71.3622`. (see p. 30).

[77] Vieira, V. R. Kondo lattice: Renormalization study using a new pseudofermion representation. *Phys. Rev. B* **23**, 6043–6054 (1981). URL `http://link.aps.org/doi/10.1103/PhysRevB.23.6043`. (see pp. 30, 38, 41).

[78] Tsvelik, A. M. New fermionic description of quantum spin liquid state. *Phys. Rev. Lett.* **69**, 2142–2144 (1992). URL `http://link.aps.org/doi/10.1103/PhysRevLett.69.2142`. (see pp. 30, 32).

[79] Coleman, P., Miranda, E. & Tsvelik, A. Possible realization of odd-frequency pairing in heavy fermion compounds. *Phys. Rev. Lett.* **70**, 2960–2963 (1993). URL `http://link.aps.org/doi/10.1103/PhysRevLett.70.2960`. (see p. 30).

[80] Nilsson, J. Fermionic representations of the Kondo lattice model. *Phys. Rev. B* **83**, 235103 (2011). URL `http://link.aps.org/doi/10.1103/PhysRevB.83.235103`. (see pp. 30, 35).

[81] Nilsson, J. & Bazzanella, M. Majorana fermion description of the Kondo lattice: Variational and path integral approach. *Phys. Rev. B* **88**, 045112 (2013). URL `http://link.aps.org/doi/10.1103/PhysRevB.88.045112`. (see pp. 30, 38, 39).

[82] Shastry, B. S. & Sen, D. Majorana fermion representation for an antiferromagnetic spin-chain. *Phys. Rev. B* **55**, 2988–2994 (1997). URL `http://link.aps.org/doi/10.1103/PhysRevB.55.2988`. (see pp. 30, 31, 32).

[83] Coleman, P., Ioffe, L. B. & Tsvelik, A. M. Simple formulation of the two-channel Kondo model. *Phys. Rev. B* **52**, 6611–6627 (1995). URL `http://link.aps.org/doi/10.1103/PhysRevB.52.6611`. (see pp. 30, 35, 37, 38).

[84] Cabrera Cano, M. & Florens, S. Magnetotransport in the Kondo model with ferromagnetic exchange interaction. *Phys. Rev. B* **88**, 035104 (2013). URL `http://link.aps.org/doi/10.1103/PhysRevB.88.035104`. (see pp. 30, 38).

[85] Sedrakyan, T. A. & Galitski, V. M. Majorana path integral for nonequilibrium dynamics of two-level systems. *Phys. Rev. B* **83**, 134303 (2011). URL `http://link.aps.org/doi/10.1103/PhysRevB.83.134303`. (see pp. 31, 38).

[86] Florens, S., Freyn, A., Venturelli, D. & Narayanan, R. Dissipative spin dynamics near a quantum critical point: Numerical renormalization group and Majorana diagrammatics. *Phys. Rev. B* **84**, 155110 (2011). URL `http://link.aps.org/doi/10.1103/PhysRevB.84.155110`. (see pp. 31, 75, 76, 91).

[87] Biswas, R. R., Fu, L., Laumann, C. R. & Sachdev, S. SU(2)-invariant spin liquids on the triangular lattice with spinful Majorana excitations. *Phys. Rev. B* **83**, 245131 (2011). URL `http://link.aps.org/doi/10.1103/PhysRevB.83.245131`. (see p. 31).

[88] Herfurth, T., Streib, S. & Kopietz, P. Majorana spin liquid and dimensional reduction in Cs_2CuCl_4. *Phys. Rev. B* **88**, 174404 (2013). URL `http://link.aps.org/doi/10.1103/PhysRevB.88.174404`. (see p. 31).

[89] Casalbuoni, R. The classical mechanics for Bose-Fermi systems. *Il Nuovo Cimento A (1965-1970)* **33**, 389–431 (1976). URL `http://dx.doi.org/10.1007/BF02729860`. (see p. 31).

[90] Berezin, F. & Marinov, M. Particle spin dynamics as the Grassmann variant of classical mechanics. *Annals of Physics* **104**, 336 – 362 (1977). (see pp. 31, 32, 38, 58).

[91] Spencer, H. J. Theory of $s-d$ scattering in dilute magnetic alloys with spin-1/2 impurities. *Phys. Rev.* **171**, 515–530 (1968). URL `http://link.aps.org/doi/10.1103/PhysRev.171.515`. (see pp. 31, 32, 35).

[92] Bastianelli, F. & Nieuwenhuizen, P. v. *Path integrals and anomalies in curved space.* Cambridge monographs on mathematical physics (Cambridge University Press, Cambridge, 2009). (see pp. 32, 39).

[93] Bänsch, H. Majorana spin representation in comparison to other fermionic and bosonic spin representations. Bachelor thesis (2014). Supervised by Prof. A. Shnirman. (see p. 32).

[94] Altland, A. & Simons, B. *Condensed Matter Field Theory* (Cambridge University Press, 2010), second edn. (see pp. 38, 40, 42, 51, 52, 54, 55, 56, 58, 95, 96, 97, 98, 99, 100).

[95] de Boer, J., Peeters, B., Skenderis, K. & van Nieuwenhuizen, P. Loop calculations in quantum mechanical non-linear sigma models with fermions and applications to anomalies. *Nuclear Physics B* **459**, 631 – 692 (1996). URL `http://www.sciencedirect.com/science/article/pii/0550321395005935`. (see p. 39).

[96] Sengupta, A. M. Spin in a fluctuating field: The Bose(+Fermi) Kondo models. *Phys. Rev. B* **61**, 4041–4043 (2000). URL `http://link.aps.org/doi/10.1103/PhysRevB.61.4041`. (see pp. 50, 74, 94).

[97] Georges, A., Parcollet, O. & Sachdev, S. Mean field theory of a quantum Heisenberg spin glass. *Phys. Rev. Lett.* **85**, 840–843 (2000). URL `http://link.aps.org/doi/10.1103/PhysRevLett.85.840`. (see pp. 50, 74, 94).

[98] Georges, A., Parcollet, O. & Sachdev, S. Quantum fluctuations of a nearly critical Heisenberg spin glass. *Phys. Rev. B* **63**, 134406 (2001). URL `http://link.aps.org/doi/10.1103/PhysRevB.63.134406`. (see pp. 50, 74, 94).

[99] Zhu, L. & Si, Q. Critical local-moment fluctuations in the Bose-Fermi Kondo model. *Phys. Rev. B* **66**, 024426 (2002). URL `http://link.aps.org/doi/10.1103/PhysRevB.66.024426`. (see pp. 50, 93, 94, 95, 100, 105, 106, 108, 109, 110, 112).

[100] Caldeira, A. O., Castro Neto, A. H. & Oliveira de Carvalho, T. Dissipative quantum systems modeled by a two-level-reservoir coupling. *Phys. Rev. B* **48**, 13974–13976 (1993). URL `http://link.aps.org/doi/10.1103/PhysRevB.48.13974`. (see p. 50).

[101] Leggett, A. J., Chakravarty, S., Dorsey, A. T., Fisher, M. P. A., Garg, A. & Zwerger, W. Dynamics of the dissipative two-state system. *Rev. Mod. Phys.* **59**, 1–85 (1987). URL `http://link.aps.org/doi/10.1103/RevModPhys.59.1`. (see pp. 50, 76, 77).

[102] Paaske, J., Rosch, A., Kroha, J. & Wölfle, P. Nonequilibrium transport through a Kondo dot in a magnetic field: Decoherence effects. *Phys. Rev. B* **70**, 155301 (2004). (see pp. 50, 56).

[103] Makhlin, Y., Schön, G. & Shnirman, A. Dissipative effects in Josephson qubits. *Chemical Physics* **296**, 315 – 324 (2004). URL `http://www.sciencedirect.com/science/article/pii/S0301010403004981`. The Spin-Boson Problem: From Electron Transfer to Quantum Computing ... to the 60th Birthday of Professor Ulrich Weiss. (see pp. 76, 77).

[104] Florens, S., Venturelli, D. & Narayanan, R. Quantum phase transition in the spin-boson model. In Chandra, A. K., Das, A. & Chakrabarti, B. K. (eds.) *Quantum Quenching, Annealing and Computation*, vol. 802 of *Lecture Notes in Physics*, 145–162 (Springer Berlin Heidelberg, 2010). URL `http://dx.doi.org/10.1007/978-3-642-11470-0_6`. (see pp. 76, 78).

[105] Slichter, C. P. *Principles of magnetic resonance.* Springer series in solid state sciences ; 1 (Springer, Berlin, 1992), 3., enlarged and updated ed., corr. 2. pr. edn. (see p. 77).

[106] Bloch, F. Generalized theory of relaxation. *Phys. Rev.* **105**, 1206–1222 (1957). (see p. 77).

[107] Redfield, A. On the theory of relaxation processes. *IBM Journal of Research and*

Development **1**, 19–31 (1957). (see p. 77).

[108] Misra, B. & Sudarshan, E. C. G. The Zeno's paradox in quantum theory. *Journal of Mathematical Physics* **18**, 756–763 (1977). (see p. 78).

[109] Vojta, M., Buragohain, C. & Sachdev, S. Quantum impurity dynamics in two-dimensional antiferromagnets and superconductors. *Phys. Rev. B* **61**, 15152–15184 (2000). URL `http://link.aps.org/doi/10.1103/PhysRevB.61.15152`. (see pp. 94, 95).

[110] Kopietz, P., Bartosch, L. & Schütz, F. *Introduction to the functional renormalization group* (Springer, Berlin; Heidelberg, 2010). URL `http://d-nb.info/997432764/04`. (see pp. 97, 98, 105).

[111] Wilson, K. G. & Kogut, J. The renormalization group and the ϵ expansion. *Physics Reports* **12**, 75 – 199 (1974). URL `http://www.sciencedirect.com/science/article/pii/0370157374900234`. (see p. 105).

[112] Bourbonnais, C., Guay, B. & Wortis, R. *Renormalization Group Technique for Quasi-One-Dimensional Interacting Fermion Systems at Finite Temperature.* CRM Series in Mathematical Physics (Springer New York, 2004). URL `http://dx.doi.org/10.1007/0-387-21717-7_3`. (see p. 105).

[113] Zinn-Justin, J. *Phase transitions and renormalization group* (Oxford University Press, 2007). (see p. 105).

Acknowledgments

LIST OF PUBLICATIONS

Pablo Schad, Alexander Shnirman, Yurij Makhlin

Using Majorana spin-1/2 representation for the spin-boson model

arXiv:1510.05838 [cond-mat.mes-hall], to appear in Phys. Rev. B

Pablo Schad, Yurij Makhlin, Boris N. Narozhny, Gerd Schön, and Alexander Shnirman

Majorana representation for dissipative spin systems

Annals of Physics, Volume 361, October 2015, Pages 401–422, DOI: 10.1016/j.aop.2015.07.006, available online 14 July 2015

Pablo Schad, Boris N. Narozhny, Gerd Schön, and Alexander Shnirman

Nonequilibrium spin noise and noise of susceptibility

Phys. Rev. B 90, 205419, published 17 November 2014, DOI: 10.1103/PhysRevB.90.205419